VAN ROSSUM RAADGEVENDE INGENIEURS

Soil-Structure Interaction Modelling of High-Rise Building Settlements due to Compressible Soil Layers below Foundation Level.

I. (Illona) Hartman

TU Delft

CRUX

Delft University of Technology

MSc Thesis

Soil-Structure Interaction Modelling of High-Rise Building Settlements due to Compressible Soil Layers below Foundation Level

I. (Illona) Hartman

4395956

In partial fulfilment of the requirements for the degree of

Master of Science in Civil Engineering (Geotechnical Engineering)

Defended publicly on January 12, 2023

Supervisor:	Dr. Ir. K. G. (Ken) Gavin	-	TU Delft
Thesis committee:	Dr. Ir. M. (Mandy) Korff	-	TU Delft
	Ir. R. (Roy) Crielaard	-	TU Delft
	Ing. F. K. (Korneel) de Jong	-	CRUX Engineering BV
	Ir. A. S. (Bram) Teeuwen	-	Van Rossum Raadgevende Ingenieurs BV


TU Delft
Delft
University of
Technology


CRUX


VAN
RAADGEVENDE
INGENIEURS
ROSSUM

Abstract

In the field of structural and geotechnical engineering, a uniform approach to predict and model foundation settlements during the design phase of a high-rise building appears to be missing. In the Netherlands, pile foundations of tower structures underlain by compressible soil layers are challenging to model due to different stiffness and load distribution effects. As a result, the Dutch building code currently used for foundation design, the NEN9997-1, does not include realistic soil-structure interaction (SSI) effects. Instead, the NEN defines a simplified approach for high-rise buildings as the sum of two types of foundation settlements: individual pile head settlements (s_1) and pile group settlements (s_2) due to compressible layers below pile tip level.

Numerical models were used in this thesis to predict the individual contribution of different soil layers to measured subsidence of tower structures. By running several simulations using Tomlinson's load spread method and the new embedded beam formulation (EB-I) in Plaxis 3D, it was found that approximately **65%** of the total (s_2) settlements are caused by the compression of clay layers below foundation level. Moreover, the effects of different pile factors (α_s, α_p) on the load distribution (more pile shaft resistance versus base resistance) from superstructure to subsurface were investigated. This research concluded that updated pile factors - in accordance with recent pile load tests on the *Maasvlakte* (Gavin, 2020) - influenced the predicted and modelled pile head settlements (s_1) slightly for a Fundex 560 pile. Nonetheless, the change in load distribution due to different pile factors did not affect the vertical effective stresses or resulting (s_2) settlements at depth.

Further, to accomplish a more uniform modelling approach for high-rise building settlements, this thesis provides insights for an automated soil-structure interaction *mattress* methodology as illustrated in Figure 1. A model verification is proposed for the mattress model approach using finite element software commonly used by geotechnical (Plaxis 3D) and structural engineers (SCIA Engineer) in daily practice. In essence, it is based on a simplified (s_2) settlement analysis from Plaxis 3D (step 1) and mattress fit model in SCIA Engineer (step 2) consisting of multiple springs with linear stiffness ($k_{bedding}$) connected by a plate (E_{plate}) and a simplified surface load on top. The surface load represents the *quasi-permanent* building loads. An apparent limitation of the Plaxis 3D model (step 1) was the missing building stiffness or load redistribution within the superstructure due to differential settlements over time. However, a modelling discrepancy of only **1%** was found for both the peak and differential settlements between SCIA Engineer (step 3) and Plaxis 3D (step 4) for a theoretical, symmetric high-rise building of 69 m in the North of Amsterdam. Thus, a model verification was accomplished by comparing the settlements from Plaxis 3D with the building on top of EB-I embedded beams (step 4) to the deformations of the fitted mattress model ($k_{bedding} + E_{plate}$) representing the compressible soils underneath the structure in SCIA Engineer (step 3). Altogether, this thesis provides a solid foundation towards a more universal design methodology between multiple stakeholders while including SSI effects for settlement predictions of high-rise buildings in daily practice.

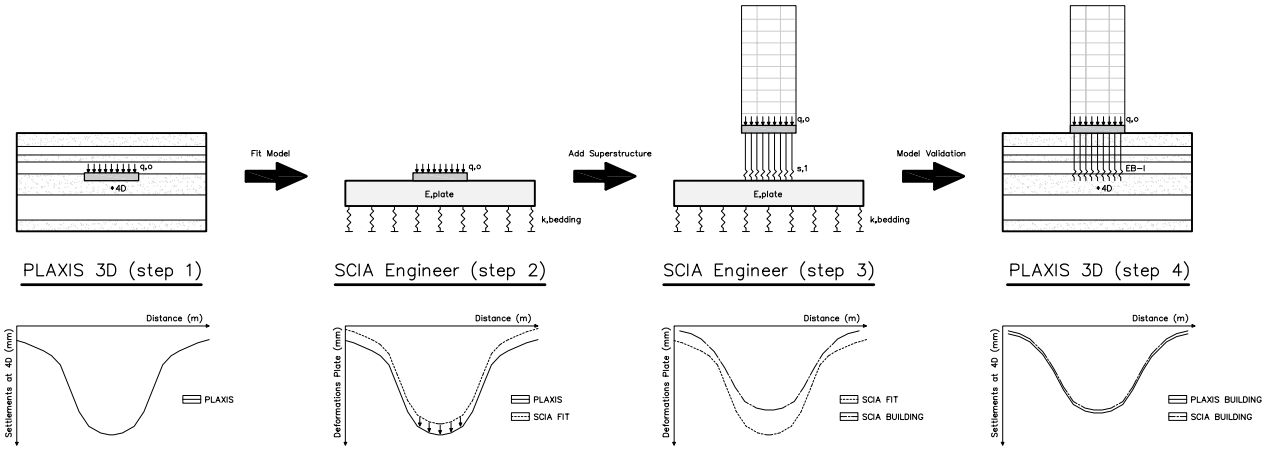

Figure 1: Proposed design flow for verification of soil-structure interaction modelling in Plaxis 3D and SCIA. (See Figure D.4 in Appendix D for an enlarged version)

Preface & Acknowledgements

This thesis report is created as partial fulfilment of my MSc Civil Engineering degree at the Department of Civil Engineering and Geosciences at the Delft University of Technology (TU Delft). The focus of my thesis was to minimise the gap between structural and geotechnical engineering during the design process of a high-rise building foundation in soft soil conditions. In particular, the research goal of this thesis was to propose and validate a simple soil-structure interaction (SSI) modelling approach between both disciplines to determine differential foundation settlements. The meta goal remains to publish an article in a national paper, so the first steps towards a more uniform and automated design methodology can be implemented among Dutch designers and engineers of high-rise structures. The research was conducted at TU Delft in tight collaboration with the knowledgeable geotechnical engineers of CRUX Engineering BV (CRUX) in Delft (and Amsterdam) and the sophisticated structural engineers of Van Rossum Raadgevende Ingenieurs BV (VRI) in Rotterdam (and Amsterdam). I want to thank my committee chair and members for joining me on this soil-structure interaction roller coaster ride and providing me with the opportunity to research my two main interests within civil engineering; foundation systems and sustainable building design. Notably, I want to thank the following committee members for their helpful supervision to complete my thesis:

- **Dr. Ir. K. G. (Ken) Gavin** for your critical view on contemporary pile design methods and providing new approaches regarding individual pile settlements to contribute to the scientific relevance of this thesis,
- **Dr. Ir. M. (Mandy) Korff** for your mental support and sharing your knowledge on pile group settlements,
- **Ir. R. (Roy) Crielaard** for your insights on building stiffness and automation of the design flow,
- **Ing. F. K. (Korneel) de Jong** for weekly meetings and assistance on Plaxis 3D and geotechnical engineering,
- **Ir. A. S. (Bram) Teeuwen** for weekly meetings and assistance on SCIA Engineer and structural engineering.

Furthermore, I want to thank **Dr. R. B. J. (Ronald) Brinkgreve**, my classmates, and my helpful colleagues at CRUX and VRI for their additional assistance on software, programming, and foundation design methods. I also want to express my gratitude towards my boyfriend, parents, family, and friends across the globe for their ongoing support. I am looking back to a very unique student experience that started in 2014 at TU Eindhoven as an architecture student and ended 8.5 years later at TU Delft after 5 incredible years as a student(-atlete) at Ohio University (B.S. Civil Engineering, Cum Laude) and Virginia Tech (first year M.S.) in the United States!

(Ir.) Illona Hartman
Delft, December 23, 2022.

Contents

List of Abbreviations

API application programming interface

BIM building information modelling

CEMS CRUX Engineering MicroServices BV

CRS constant rate of strain

CPT cone penetration test

CRUX CRUX Engineering BV

DL dead loads

DOF degrees of freedom

EB-I new embedded beam formulation

FEM finite element model

FoS factor of safety

GL ground level

GWL ground water level

HSS hardening soil small strain stiffness model

HS hardening soil model

InSAR interferometric synthetic aperture radar

LE linear elastic model

LL live loads

MC Mohr-Coulomb

MPM material point method

MV2 Maasvlakte 2

NC normally consolidated

OC overconsolidated

OCR over-consolidation ratio

OWT offshore wind turbines

SCIA SCIA Engineer

SLS serviceability limit state

SSM soft soil model

SSCM soft soil creep model

SSI soil-structure interaction

UCF underwater concrete floor

ULS ultimate limit state

VRI Van Rossum Raadgevende Ingenieurs BV

WL wind loads

PD prescribed displacements

PLT pile load test

PTL pile tip level

List of Nomenclature

Roman Symbols

A	=	Cross-sectional area (of a pile)	-	[m^2]
A_{4D}	=	Projected total area of the load four diameters below PTL under 45° load spread	-	[m^2]
A_b	=	Cross-sectional area of pile base (or toe)	-	[m^2]
A_{shaft}	=	Cross-sectional area of pile shaft	-	[m^2]
B	=	Width of pile group	-	[m]
C_α	=	Secondary compression (= creep) coefficient	-	[-]
c_i	=	Cohesion of interface elements (in Plaxis)	-	[kN/m^2]
C_p	=	Koppejan's compression index	-	[-]
c_{soil}	=	Cohesion of soil (in Plaxis)	-	[kN/m^2]
c'	=	Cohesion of soil (drained)	-	[kN/m^2]
CR	=	Bjerrum's compression ratio	-	[-]
D	=	Pile diameter (largest)	-	[mm]
D_{eq}	=	Pile diameter (base)	-	[mm]
d_{eq}	=	Pile diameter (shaft)	-	[mm]
D_{pos}	=	Distance from top of positive shaft friction to pile tip	-	[m]
D_{tom}	=	Depth at 2/3 of D_{pos} from top of positive shaft friction to pile tip	-	[m]
E	=	Young's modulus (or stiffness) of material	-	[N/m^2]
EA	=	Stiffness (of a pile's cross-section)	-	[kN]
$E_{ea;gem}$	=	Average stiffness of the layers 4D below PTL	-	[MPa]
E_{plate}	=	Stiffness of 1 m plate in mattress model representing deep soil compression	-	[N/m^2]
F_{foot}	=	Output for base resistance (spring) of embedded beam in Plaxis	-	[kN]
F_{fund}	=	Sum of individual pile loads	-	[kN]
F_{max}	=	Input for ultimate base resistance of embedded beam in Plaxis	-	[kN]
FoS	=	Factor of Safety	-	[-]
$F_{s,tot}$	=	Total axial load acting on (individual) piles	-	[kN]
$F_{s,tot,k}$	=	Characteristic axial load acting on (individual) piles ($= 0.7 \cdot F_{s,tot}$)	-	[kN]
$F_{shaft,neg}$	=	Negative skin friction	-	[kN]
G	=	Dead loads (in NEN)	-	[kN]
I_{avg}	=	Average moment of inertia of embedded beam in Plaxis	-	[kg/m^2]
K_0^{NC}	=	Stress ratio σ'_{xx} / σ'_{yy} in primary 1D compression	-	[-]
$k_{bedding}$	=	Stiffness of linear springs in mattress model representing deep soil compression	-	[N/m]
K_{foot}	=	Stiffness matrix at foot of embedded beam in Plaxis	-	[kN/m]
$k_{v,1}$	=	Spring constant or pile stiffness representing s_1 settlements	-	[MN/m]
L_{pile}	=	Length of (embedded) pile	-	[m]
L_s	=	Length of positive shaft friction along embedded pile (group)	-	[m]
M	=	K_0^{NC} related parameter (in Plaxis)	-	[-]
m^*	=	Dimensionless factor based on foundation geometry	-	[-]
N	=	Output for axial force of pile (in Plaxis)	-	[kN]
N	=	Number of piles in pile group	-	[-]
p^{ref}	=	Reference pressure (100 kPa)	-	[kPa]
Q	=	Live loads (in NEN)	-	[kN]
$q_{b0.1}$	=	Base resistance mobilised at 10% of D ($= q_{b;max}$)	-	[MPa]
q_c	=	Cone end resistance (from CPT)	-	[MPa]

Q_{total}	=	Total bearing capacity of pile group	-	[kN]
Q_w	=	Wind loads (in NEN)	-	[kN]
$q_{w;verd}$	=	Wind (suction) acting as lateral load on building	-	[kN/m^2]
R_{base}	=	Base capacity of a single pile	-	[kN]
R_{eq}	=	Equivalent pile radius of embedded beam in Plaxis	-	[m]
R_{inter}	=	Interface reduction factor in Plaxis	-	[-]
R_{max}	=	Ultimate bearing capacity of embedded beam in Plaxis	-	[kN]
RR	=	Bjerrum's re-compression ratio	-	[-]
R_{shaft}	=	Shaft capacity of a single pile	-	[kN]
R_{total}	=	Total bearing capacity of a single pile	-	[kN]
s	=	Pile shape reduction factor	-	[-]
$\mathbf{s}_1$	=	Pile head settlement = pile tip settlement (s_b) + elastic compression (s_{el})	-	[mm]
$\mathbf{s}_2$	=	Settlement of layers 4D below pile tip	-	[mm]
s_b	=	Pile tip settlement	-	[mm]
s_{el}	=	Linear elastic compression of pile	-	[mm]
T_{bot}	=	Input for (maximum) linear shaft friction of embedded beam (bottom) in Plaxis	-	[kN/m]
t_c	=	Total construction time (for gradual loading)	-	[days]
T_{max}	=	Input for (multi-)linear shaft friction of embedded beam in Plaxis	-	[kN/m]
t_s	=	Shear force in axial direction of embedded beam in Plaxis	-	[kN/m]
T_{skin}	=	Output for skin friction of the embedded interface element in Plaxis	-	[kN/m]
t_{skin}	=	Skin traction of the embedded interface element in Plaxis	-	[kN]
T_{top}	=	Input for (minimum) linear shaft friction of embedded beam (top) in Plaxis	-	[kN/m]
u_{rel}	=	Relative displacement vector of the embedded interface element in Plaxis	-	[m]
u_z	=	Deformation in z-direction (= absolute settlements)	-	[mm]
w	=	Distance between ground level and pile tip (for $1.5 \cdot w$ model domain)	-	[m]
w_{pp}	=	Pile tip settlement (Vesic, 1977)	-	[mm]
w_{ps}	=	Pile shaft displacement (Vesic, 1977)	-	[mm]
w_s	=	Pile axial deformation (Vesic, 1977)	-	[mm]

Greek Symbols

α_i	=	Interaction factor (Fleming et al., 2009)	-	[-]
α_p	=	Pile type reduction factor (base resistance)	-	[-]
α_s	=	Pile type reduction factor (shaft resistance)	-	[-]
β	=	Pile tip reduction factor	-	[-]
$\Delta\sigma'_v$	=	Change in vertical effective stress	-	[kPa]
$\dot{\epsilon}$	=	Initial strain rate	-	[%]
η_g	=	Efficiency of a pile group	-	[%]
κ^*	=	Modified swelling index (secondary)	-	[-]
λ^*	=	Modified compression index (primary)	-	[-]
μ^*	=	Modified compression index (creep)	-	[-]
ν	=	Poisson's ratio	-	[-]
ν_{ur}	=	Poisson's ratio for unloadig	-	[-]
ξ	=	Reduction factor based on the number of CPT's	-	[-]
σ'_p	=	Pre-consolidation pressure (or yield stress)	-	[kPa]
σ'_v	=	Vertical effective stress (= σ'_z)	-	[kPa]
σ'_{v0}	=	Initial vertical effective stress (= σ'_{z0})	-	[kPa]
$\sigma'_{v;4D}$	=	Vertical effective stress due to F_{fund} acting on A_{4D}	-	[kPa]
τ_f	=	Unit shaft or shear resistance (= $q_{s;max;z}$)	-	[kN/m^2]
ϕ_i	=	Friction angle of interface elements (in Plaxis)	-	[°]
ϕ_{soil}	=	Friction angle of the soil (in Plaxis)	-	[°]
ϕ'	=	Friction angle of the soil (drained)	-	[°]
ψ	=	Dilation angle of soil	-	[°]
ψ	=	*Momentaan factor*, reduction factor for live loads in load combinations	-	[-]
ψ_0	=	Reduction factor for characteristic live loads in load combinations	-	[-]
ψ_1	=	Reduction factor for frequent live loads in load combinations	-	[-]
ψ_2	=	Reduction factor for quasi-permanent live loads in load combinations	-	[-]

List of Figures

List of Tables

Chapter 1

Introduction

The goal of this thesis project is to provide insights on how to establish a new and more universal design procedure in which a simple, numerical soil modelling approach could be developed for interactive use by geotechnical and structural engineers. This new modelling approach should allow for the effects of (differential) settlements caused by compressible soil layer(s) beneath the foundation level of a high-rise building structure. Using this new method and model, the aim is to reduce time and costs while improving the flexibility associated with the current, often iterative and/or over-conservative approach during the design phase of a high-rise building in the Netherlands. Overall, this research will aim to fulfill the next steps in the contemporary design methodology of modelling soil-structure interaction between several engineering stakeholders. Examples of topics to be discussed in this thesis are:

- Proper modelling of soil and pile (group) behaviour in Plaxis 3D,
- Underlying settlement mechanisms contributing to measured high-rise building subsidence,
- Implementation of a more realistic building stiffness in a soil model,
- Fitting of settlement results from a 3D geotechnical model (in Plaxis) to a 2D model (in SCIA) for structural engineers.

Accomplishing those kind of improvements can lead to a new, integral design methodology for high-rise building structures within a specified bandwidth for a range of building loads (to be) constructed in deep, compressible soil layers.

This first chapter includes the research approach of this thesis. Using the initial research proposal as a first guideline, Chapter 1 therefore emphasizes on the problem statement associated with the research topic along with the relevance of the research, the goals and challenges, the research questions to be investigated, the methodology, and the scope of the research.

1.1 Background Information

For many centuries, the low-rise brickwork was a main feature of Dutch architecture alongside rows of windmills and *polders*. However, since the start of the industrial revolution and the development of the elevator, high-rise building structures were constructed extensively in the lowlands. For instance, Brassinga and van Tol (1991) describe the *Witte Huis* in Rotterdam as one of the very first high-rise building structures made of (eleven stories of) masonry in the Netherlands. The 43 m tall building was constructed in 1898 and founded on timber piles (in the Pleistocene sand layer). Moreover, Andeweg and Koopman (2007) describe the production methods and technologies used for the first high-rise buildings constructed after 1946 in the Netherlands. During WWII, over 500,000 Dutch houses were demolished, resulting in an excessive housing demand due to repatriation of soldiers (from Indonesia). From 1946 till 2000, over 6.6 million new dwellings were built (55% after 1965) in outskirts of large cities as part of parallel or perpendicular apartment building blocks. Since the early sixties, most of these apartments were identified as high-rise apartment blocks. Furthermore, the new Building Code of 1965 pleaded for more spacious living standards. A development in larger spans for concrete floor slabs allowed structural engineers to design bigger floor plans. Simultaneously, gas extraction in the north of the Netherlands conceded central heating. Those changes lead to relatively comfortable high-rise apartment blocks containing hundreds of (85 m^2) homes, see Figure 1.1. On average, the blocks designed in the sixties and seventies were ten stories tall ($\approx$ 30 m) with flat rooftops. The blocks were often constructed with the use of in-situ concrete building systems invented by the Dutch architect Willem Greve, whose method was based on the reuse of bombed concrete building materials (i.e., *korrelbeton*). Due to the low bearing capacity of peat and clay soils underneath these apartment blocks in the north and west of the Netherlands, the first high-rise buildings were built on post-war concrete piles, which was in contrast with the pre-war timber piles based on sleeve friction (Andeweg & Koopman, 2007).

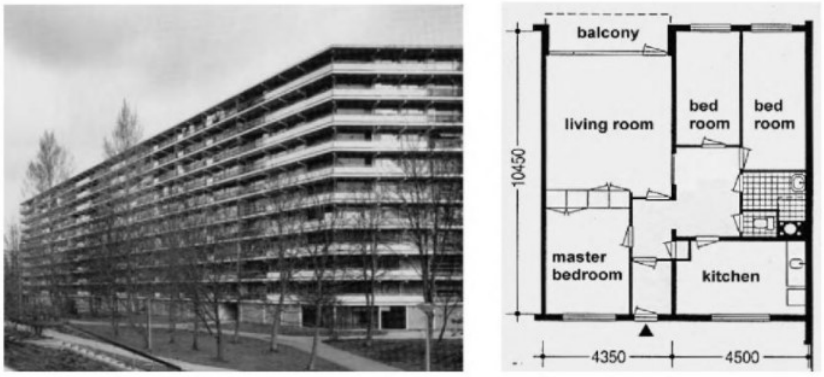

Figure 1.1: Typical facade (left) and floor plan (right) of post-war high-rise building blocks from the sixties (Andeweg & Koopman, 2007).

Considering the progressively increasing housing demand in the Netherlands of the current 21^{st} century, the main step forward is to focus on building vertically according to Boomen (2016), Modder (2016), and Van Wessel (2016, March 4). Furthermore, Camu (2019) describes the social relevancy of high-rise buildings as discussed at the 2019 conference *Hollandse Hoogbouw* organised by *Vastgoedjournaal* and *Stichting Hoogbouw*. At the time of the conference in 2019, the Netherlands had over 202 high-rise buildings (defined by a height of 70 m or more) and plans to construct another 70 towers before 2025 from which 80% will consist of dwellings. The municipality of The Hague is especially fond of high-rise buildings as a population growth of 4,000 - 5,000 people within city limits is expected by 2040, which translates to a need of 10,000 more dwellings. According to Michel Duinmayer from the Dutch Ministry of Infrastructure and Water Management, high-rise buildings go

hand in hand with sustainability and mobility challenges. He therefore advocates an integral design (method) when it comes down to constructing new towers. Examples of those projects to be built are The Windweel in Rotterdam or The Dutch Mountain in Eindhoven, which have already received much international attention emphasizing the need for integral design projects. The quality of such ambitious building projects are assessed by the *Hoogbouw Effect Rapportage* (HER) and regulated by the city's license department (Camu, 2019).

Settlement Analysis in Daily Practice (after 2000)

A large portion of the current Dutch population and high-rise buildings are situated in *De Randstad* of the Netherlands, which includes 4 out of 5 major cities of the provinces North- and South-Holland. The southern part of the Randstad (i.e., Rotterdam) is underlain by the Kreftenheye formation, which is derived from fluvial deposits stemming from the Rhine river, one of the three major cross-border river systems draining into the North Sea after flowing through the Netherlands and other countries. The deep, compressible clay layers in Amsterdam (see Figure 1.2) differ from the Kreftenheye formation in Rotterdam due to its geological history. In Amsterdam, located in the northern part of the Randstad, the clay layers originate from marine (Eem formation) and glacial times (Drenthe formation). The deepest Pleistocene sand layer found below the deep clay layers in the Randstad (see Figure 1.2) has measured cone resistances of 15-30 MPa while the shallower layer (at depths 20-25 m) ranges from 15-60 MPa (Gavin, 2020).

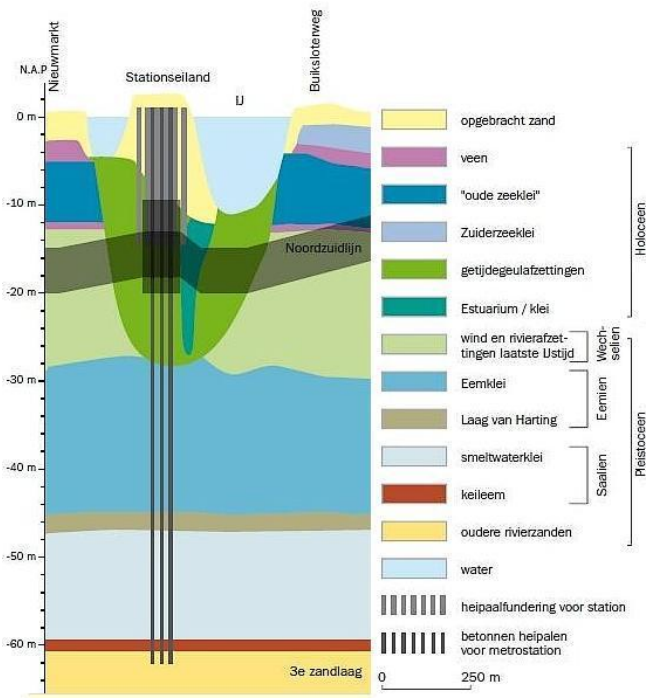

Figure 1.2: Typical soil profile for Amsterdam near central train station (De Gans, 2011).

For a long time, high-rise apartment blocks in the Netherlands were built on the shallower sand layer and (resulting) settlements were not considered for the design of (high-rise) buildings. However, building heights have increased rapidly and towers are now dominating the skyline of the major Dutch cities. As a result, foundations in the Randstad of the Netherlands were designed to rest on the deeper Pleistocene sand layers. A period of settlement discussion had begun, especially the effect of deep clay layers at a depth of 40 m below ground level (GL) and whether these layers are still considered compressible. For instance, Hoefsloot and Wiersema (2020) emphasize the importance of the compression of deep clay layers, especially for deeper piles

in contemporary foundation design of increasing tower heights. Along with several other engineers in the Netherlands, Hoefsloot and Wiersema (2020), Schippers et al. (2021), and Schippers and Broekens (2022) claim that those deep, overconsolidated (OC) clay layers are still compressible under large dead loads associated with tall towers ($\geq$ 70 m) over a long period of time (50+ years). On the other hand, Gavin (2021) and Ter Steege (2022), among others, call for an updated pile design using lower pile (tip) factors. For current pile factors in the Eurocode 7 (2005), they predict that buildings are settling due to failure of piles (by overestimating the pile tip resistance) or creep of the deeper Pleistocene sand layers. For aforementioned reasons, the author believes that both hypothesis regarding settlement mechanisms should be considered for settlement analysis of high-rise building structures instead of contributing predicted settlements to the deep clay layers below pile tip level (PTL) only.

One of the first settlement prediction analyses for those type of heavy structures in the Netherlands was recorded by Visser and Gutter (1999). They declare that the construction of high-rise building foundations at the first or second Plesitocene sand layer in Amsterdam result in consolidation settlements of deep lay layers, which govern the type of foundation system. Visser and Gutter (1999) investigated the settlement behaviour of a (Drenthe) clay layer (NAP - 40 m / 50 m) below the second, Pleistocene sand layer using the load distribution theory of Boussinesq and settlement approach of Terzaghi-Koppejan in Plaxis 6.3 (2D) for the *Breitnertoren* in Amsterdam. Using Boussinesq, the stiffness of the foundation or soil layers were not included and the load distribution follows an elastic half space starting from GL while assuming linear elastic soil behaviour. In reality, soil shows non-linear behaviour and the stiffness of foundation structure at the excavation depth as well as PTL should be considered due to the fact that piles and slab for the foundation system of the Breitnertoren are connected at the top. The foundation stiffness is therefore a function of the number of piles and thickness of the slab. As a result of the applied building loads and stiffnes of the foundation, the settlement trough shows a slight sagging curve similar to the shape of a sink (see Figure 1.3 below). Furthermore, Visser and Gutter (1999) concluded that a dilation between the high-rise and low-rise part of the building led to 60% less rotation and settlement of the tower. However, differential settlements between the two parts increased by 50%.

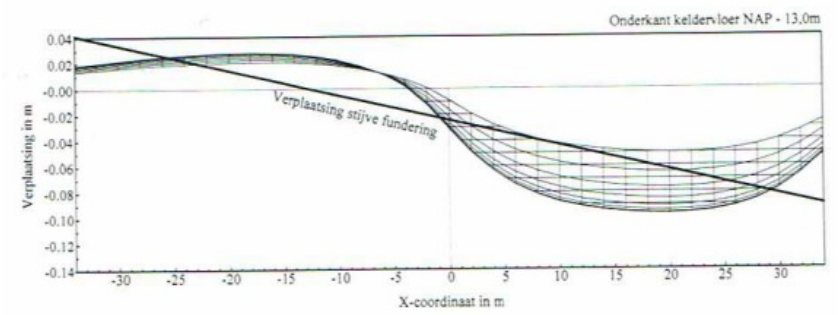

Figure 1.3: Typical settlement trough and consequent displacement for a stiff high-rise building foundation (Visser & Gutter, 1999).

In order to model (deep) clay layers in Plaxis, an elastic soft soil model (SSM) was used along with a linear-elastic perfectly-plastic Mohr-Coulomb (MC) model for the drained, granular layers. The SSM is an alternative to the Koppejan equation and describes a correlation between the compression of the soil and the logarithm of the applied load: the stiffness depends linearly on the mean effective stress under both loading and unloading conditions. The SSM makes use of the model parameters λ^* and κ^*, which are based on the Poisson's ratio for unloading and reloading. Thus, the modified compression index, λ^*, is described by the settlement behaviour after reaching the maximum stress under loading conditions while the modified swelling index, κ^*, describes the behaviour due to heave or reloading, see Eq. 1.1.

$$\lambda^* = \frac{1}{C'_p} \quad \text{and} \quad \kappa^* = \frac{1-\nu_{ur}}{1+\nu_{ur}} \cdot \frac{3}{C_p} \tag{1.1}$$

where, C_p is a compression index and ν_{ur} the Poisson's ratio for unloading. Instead of modelling sheet pile walls as part of the deep excavation, Visser and Gutter (1999) used large cohesion values for the soil elements of the mesh surrounding the excavation For a better comparison with Omegam's ZETBK! results, high stiffness values (i.e., 16,000 kN/m^2) were chosen for the soil layers below PTL (= foundation level) whereas low stiffness values (i.e., 1,000 kN/m^2) were selected for the layers above the foundation level. As a result, the effect of the soil stiffness above foundation level on the stress distribution below pile tip could be neglected. Subsequently, Visser and Gutter (1999) verified a translation of Koppejan's compression parameters to Plaxis' SSM parameters.

Furthermore, Visser and Gutter (1999) investigated the effect of the stiffness of the foundation and the arching effect of the soil layers by running a ternary of analyses. In the first case, a negligible stiffness (i.e., 1,000 kN/m^2) for the soil layers above the deep clay layer was chosen to model zero arching effect of the drained layers and an elastic foundation structure. In another case, the expected stiffness of the soil layers were used - especially for the sandy soils - to model a consequential arching effect with an elastic foundation structure. In the last case, the same soil stiffness as the latter scenario were used, but this time a stiff foundation structure (containing a 1.5 m thick concrete floor) was modelled by multiplying the EI-value with an arbitrary factor of 10. For the third scenario, the analysis showed minimal settlements (11 mm) at the top of the deep clay layer whilst more remarkable settlements (55 mm) were computed for the first scenario without considering the foundation stiffness and arching or creep effect of the soils. Thus, a stiffer foundation and including the arching effect of granular soil layers on top of the deep clay layer result in less settlements of a high-rise building structure (Visser & Gutter, 1999).

Recent Improvements of Settlement Analysis for High-Rise Buildings

Roughly ten years ago, structural engineers started calculating and modelling differential settlements (for high-rise buildings) on a larger and more detailed scale. Modelling of settlements was first approached by the use of prescribed displacements (PD) in structural analysis software as part of an iterative process with geotechnical engineers using separate models for the subsurface. In 2018, structural engineers of VRI proposed a new modelling approach, the *mattress* model, in an attempt to overcome the iterative process of determining consolidation settlements due to deep clay layers below PTL (Van der Sluis, 2017)[1]. This preliminary SSI model will be further explained in Section 2.1.3 after an overview of contemporary methodologies used by different engineering companies in the Netherlands. This thesis will focus on improving the current state of practice to provide insights about streamlining the process between structural and geotechnical engineers nation- or even worldwide regarding foundation settlements of high-rise buildings.

A more recent attempt to increase the accuracy of settlement analysis was performed by Hoefsloot and Wiersema (2020) for three case studies in Rotterdam. A common uncertainty in high-rise building design is the availability of settlement measurements to validate time-dependent settlement models, so Hoefsloot and Wiersema researched the technology of interferometric synthetic aperture radar (InSAR) to fill the monitoring gap. With the use of InSAR data and a mathematical algorithm, vertical displacements can be determined within an accuracy of 1-2 mm. Those displacements are commonly shown as circles on imagery of high-rise

[1] Internal document from VRI, no public access.

building rooftops and follow a downwards linear trend (see Figure 1.4). Note that the sinusoidal graph indicates seasonal effects due to the expansion of building materials in warmer periods of the year and shrinkage under colder temperatures.

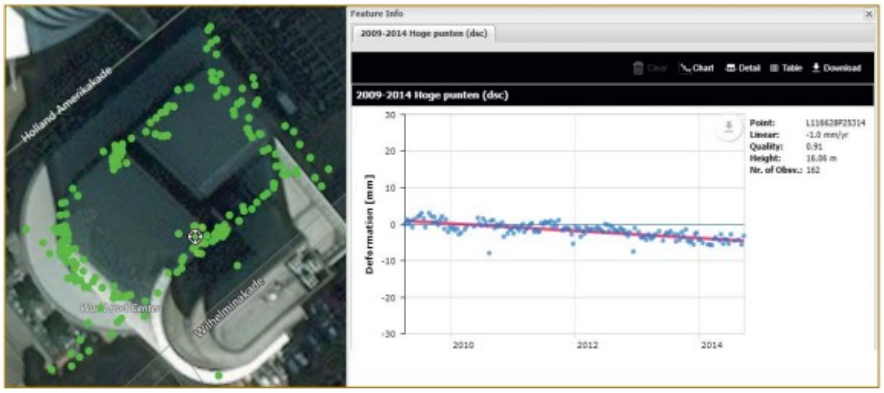

Figure 1.4: An example of vertical displacement for the World Port Centre (120 m) provided by InSAR data (Hoefsloot & Wiersema, 2020).

In order to compute the compression of deep clay layers, a load distribution procedure should first be selected. Hoefsloot and Wiersema (2020) used a method for which the permanent load acts as a surface load on the total area of the pile group at PTL or slightly above. Constitutive models such as isotach models (i.e., NEN-Bjerrum isotach or A,B,C-isotach model) were used to represent soil behaviour of the (*Kedichem*) clay layers. Isotach models appear to be most realistic for small load steps and minor changes in vertical stress as long as a realistic strain rate is used. The initial strain rate, $\dot{\epsilon}$, is inversely proportional to the over-consolidation ratio (OCR) without load steps - as illustrated by Bjerrum's correlation in Eq. 1.2 - and can be calibrated by the use of InSAR data.

$$\dot{\epsilon} = \frac{C_\alpha}{\ln(10)} \cdot OCR^{\frac{-(CR-RR)}{C_\alpha}} \tag{1.2}$$

where, CR is the compression ratio, RR is the re-compression ratio, and C_α is the secondary compression coefficient of the clayey soil found by laboratory experiments such as the constant rate of strain (CRS) test. After an initial strain rate is determined, the rate of autonomous subsidence (without any applied building loads) can be found by multiplying the total thickness of the clay layers by the calculated strain rate. Note that a larger OCR results in a smaller subsidence rate. Ultimately, it was concluded that settlement calculations based on calibrated model parameters (in D-Settlement) using InSAR correspond well with measured data and can be used to predict future settlement curves (Hoefsloot & Wiersema, 2020).

In addition, to further elaborate on the significance of this research, InSAR data was requested for several towers in Amsterdam and Rotterdam. The team of SkyGeo (2022) made InSAR data accessible for the settlements of the Breitnertoren in Amsterdam, the tower used in the predictions by Visser and Gutter (1999). Figure 1.5 on the next page shows the settlement rate recorded by ascending TerraSAR-X high resolution ("PS Hoge Punten") for the period of 2009 − 2017. See Appendix D for more satellite data that can be used as additional model and prediction validation in future research.

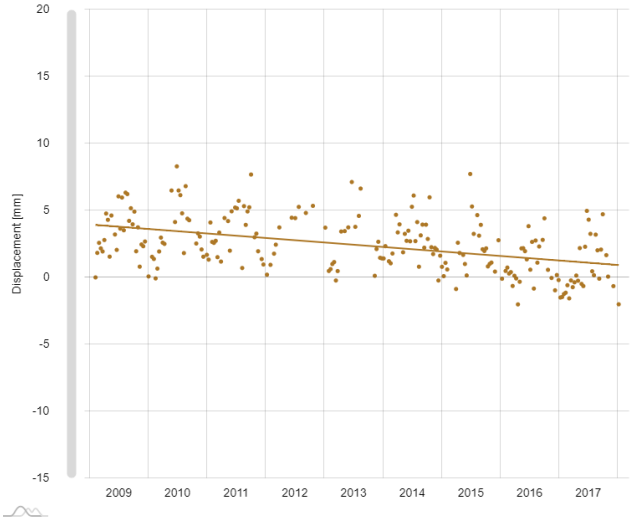

Figure 1.5: Vertical displacement data for the Breitnertoren in Amsterdam provided by InSAR data (SkyGeo, 2022).

Proposed Improvements by Other MSc Thesis Research

On top of research by practitioners and researchers, recent thesis research was performed by several MSc students on improving the SSI settlement analysis of high-rise buildings in soft soils. An improvement was proposed by Frissen (2020), who focused on implementing load redistribution effects on foundations in soft soils caused by SSI mechanisms and how this phenomenon affects differential settlement calculations of high-rise buildings. Consequently, Frissen (2020) improved the modelling of SSI effects in Plaxis 3D by implementing the behaviour of a single pile using embedded beams as well as implementing part of the bending stiffness of the superstructure for a pile group (see Section 2.1.1 for a more extensive summary). He claimed that an integral design method from an early stage of the design process between structural and geotechnical engineers is crucial to success. Using such integration, appropriate load redistribution by the soil and soil sub-grade reactions can lead to the possibility of linking geotechnical and structural models (Frissen, 2020).

In addition, Odijk (2017) looked into the structural behaviour of a high-rise building on compressible soils (in Rotterdam). He claimed that settlements due to the deep, compressible soil layer (Kedichem clay) result in an increase of internal forces in the superstructure, especially for high-rise buildings considering the large weight of the structure acting on a relatively small (foundation) area underground. A structural software, SCIA Engineer (SCIA), was used to model the superstructure of a case study whereas a soil settlement program (D-Settlement) was used to calculate the compression of the deep clay layer. In SCIA, similar to the prescribed displacement (PD) method, stiff spring elements were used to model the resulting deformations as forces acting on the structural elements. Odijk (2017) concluded that iterations between both software packages were needed to more accurately model SSI. Due to the calculated settlements in D-Settlement, a change of force flow in the superstructure (in SCIA) influences the load distribution to the foundation. Iteration should ideally show convergence of the settlement trough and consequent structural forces for the final design of a high-rise building. During one of the 2D calculations in SCIA, Odijk (2017) found a 15% increase of normal forces within columns (at the edges of a building) when soil settlements - due to the deep clay layer - were included in the structural model as stiff springs. Furthermore, Odijk (2017) investigated several structural aspects that may influence the differential settlements of a high-rise building on compressible soils. Using the CoolTower in Rotterdam as a case study, it was determined that the stiffness of the tower's facade influences the structural behaviour (due to load redistribution) the most (Odijk, 2017).

1.2 Problem Statement

Current methods for foundation engineering described in design codes, such as the NEN9997-1 or Eurocode 7, do not incorporate SSI effects (Eurocode 7, 2005). On top of that, the gap between geotechnical and structural engineers within a collaborative, building information modelling (BIM) design of a high-rise building structure is still prominent during its design and modelling phase. Currently, a uniform approach or design procedure between geotechnical and structural engineers in the Netherlands is missing, which makes the assessment of (differential) settlements a tedious job for a 21^{st} century state-of-the-art industry and often leads to additional, over-conservative forces within a building structure. According to the NEN9997-1 (2017), foundation settlements in the Netherlands are divided in two different terms; s_1 and s_2. Consequently, settlements of the top of a piled foundation are defined by the sum of those two settlement terms. The first type of settlement is described as "settlement at the top of an individual pile based on the results of mobilised pile-load displacement curves (NEN9997-1 section 7.6.4.2(e)) and field test results (i.e., a pile load test (PLT))", which is a function of the pile tip resistance, mobilised shaft friction, and the soil below an individual pile over a distance of four times its diameter, D. The settlement of soil layers below this foundation level are part of the s_2 settlements. This type of settlement is then defined by "settlement as a result of the compression of soil layers below pile tip level", which includes the immediate settlements (of sand), consolidation settlements (of clay), and creep settlements. In current design approaches, s_1 settlements are often computed analytically while s_2 settlements are determined by the use of extensive numerical models.

To include SSI effects, a variety of slow and costly iterative approaches have been used in different numerical models and finite element model (FEM) software to calculate (differential) settlements at different times during construction and the life cycle of a structure. This phased assessment is necessary to include the time dependent rate of consolidation and creep of soft soils in structural design analyses. Those phenomena in soft soils are described by (the dissipation of) excess pore water pressures over time and the time-dependent restructuring of the soil. Experience of CRUX (see Figure D.3) showed that deep, compressible soil layers below foundation level (i.e., Eem and/or Drenthe clay in Amsterdam, Kedichem clay in Rotterdam) between the second and third Pleistocene sand layers in the west of the Netherlands (see Figure 1.6)[1] have a significant influence on the total settlements of high-rise building projects. These type of soils compress gradually when exposed to large building loads. Interaction between piles in a group also depend on the load, however, the percentage of SSI effects is higher for lower load levels (Gavin, 2021). As a consequence, considerable changes of vertical effective stress within soil layers initiate settlements of a structure at the surface and below sub-grade. Uniform settlements do not necessarily cause issues for the building, however, the load distribution from the structure to the soil is not uniform, resulting in differential settlements instead: one part of the structure may deform more than another part while potentially exceeding the serviceability limit state (SLS) requirements of the building design. As an assessment guideline, SLS is commonly defined by rotation restrictions in design codes (Schoenmakers, 2020)[1], such as 1:600 for high-rise building structures. Nowadays, the safety class of a high-rise building of 70 m or lower is defined by CC2 in structural codes whereas CC3 is used for towers larger than 70 m. For this research, it will be interesting to investigate high-rise buildings on the edge of safety classes CC2 and CC3 as those result in the largest predicted soil settlements.

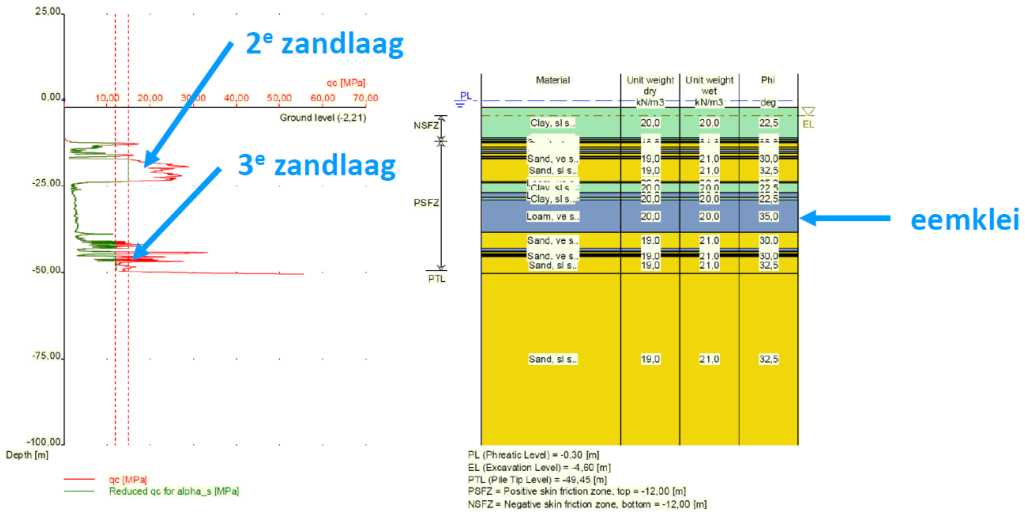

Figure 1.6: Representative soil profile for Amsterdam illustrating the depth of the compressible layer (*eemklei*) in between the two Pleistocene sand layers (*zandlaag*) as was used in the software D-Foundation by VRI & CRUX for the *Sluishuis* project in eastern Amsterdam (Schoenmakers, 2020).

In this research project, the existing gap between geotechnical and structural engineering processes will be investigated by explaining current design methods and providing insight to propose a new SSI methodology to optimise the design process of a high-rise building from a geotechnical as well as a structural perspective. As a starting point, design methods to implement settlements by structural engineers and geotechnical engineers will be thoroughly reviewed and explained during the literature review of the research process (in Section 2.1). In the current state of practice, soil settlements from geotechnical models are often added to structural models as PD - *opgelegde vervormingen* in Dutch - to the top of the foundation piles. Using PD, SSI is then managed by running several iterations of structural and geotechnical models subsequently to pursue convergence of the deformation results and consequent load redistributions, see Figure 1.7. After a preliminary design, building loads are first illustrated as a plan view with surface loads and shared with a geotechnical engineer who uses the loads as inputs for their geotechnical model. The building stiffness was normally not implemented in the geotechnical model, however, new procedures have been explored in which the building is modelled as an infinitely stiff plate and an elastic plate to define the boundary conditions of the realistic building stiffness. Two scenarios of s_2 settlement curves are then produced (by Plaxis 3D) and send back to the structural engineer who investigates the influence of the settlements on the force flow within the superstructure. Ideally, new building loads due to load redistribution (from the core to the edges of the building) within the superstructure and foundation will then be send back to the geotechnical engineer to restart the design loop. In the author's opinion, this loop should instead be streamlined to an integrated *geo-structural engineering pipeline* for a pre-defined bandwidth of loads while critically investigating both geotechnical and structural (model) assumptions and limitations. Hypothetically, this could be achieved by three different approaches: **1)** Simplifying a probabilistic approach using current models and many (load) variations, **2)** linking current models through a programming language, and **3)** creating one model in an integral software package.

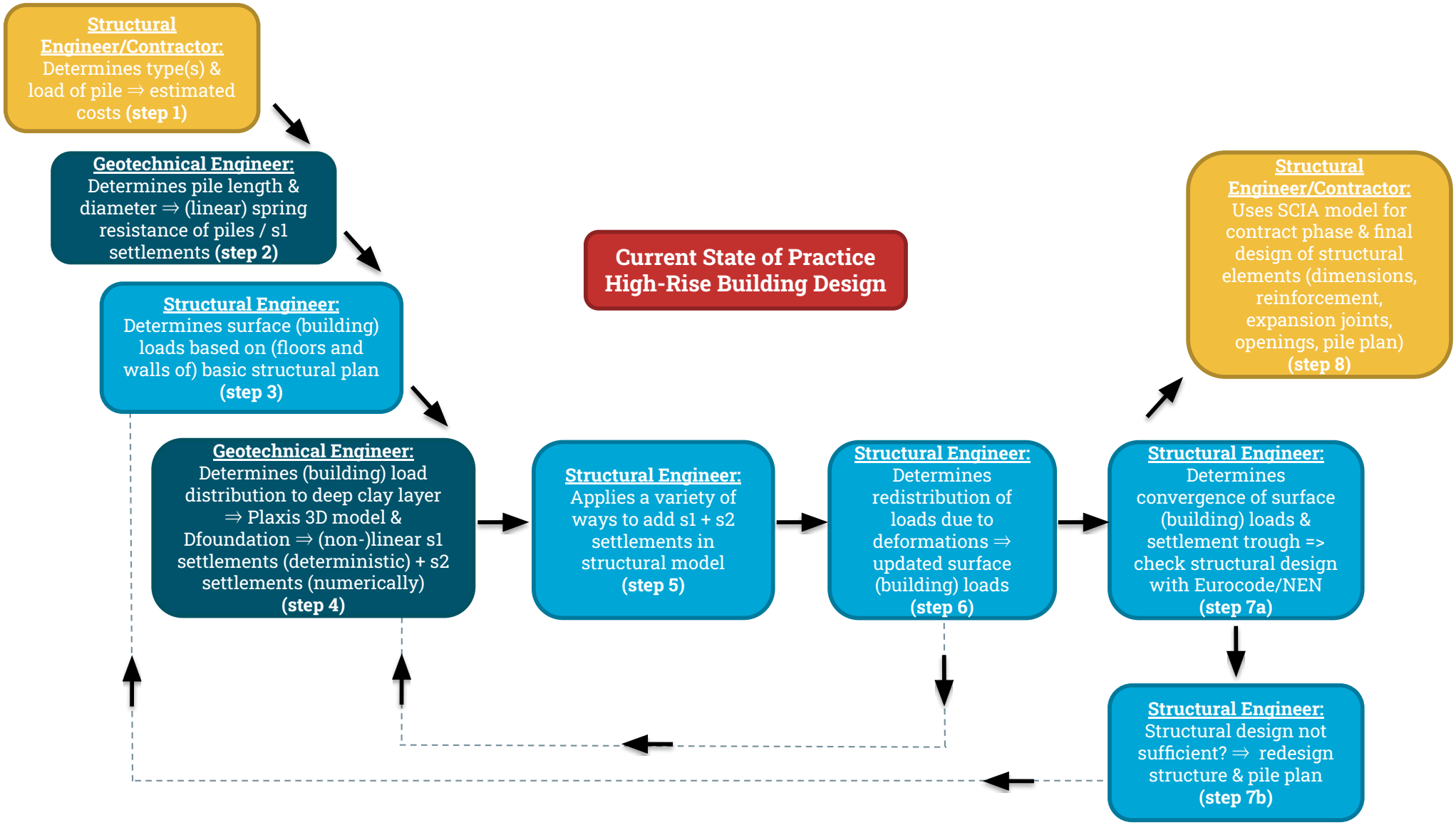

Figure 1.7: Current iterative design approach between geotechnical and structural engineers.

1.2.1 Ambiguity of Pile Factors and Pile Type Behaviour

Due to recent findings of ongoing pile load tests on the *Maasvlakte* near the Port of Rotterdam in the Netherlands, a discussion on the NEN alpha factors and general pile behaviour of common piles has been provoked since the start of the project in October 2019. According to Gavin (2020), the α_p values from the NEN are some of the largest among Europe by not incorporating factors such as residual stresses, soil ageing, pile roughness, plugging, and cyclic shear stresses due to installation of the pile. On the other hand, the NEN does include some safety factors with regards to the q_c values, which are limited to 12 - 15 MPa based on the thickness of the soil layer (12 MPa for $\leq$ 1 m, 15 MPa for $\geq$ 1 m) using the popular Koppejan averaging technique for the cone penetration test (CPT). An over-conservative limit considering the Pleistocene sand layers in the Netherlands have measured cone end resistances, q_c, between 20 and 80 MPa (Gavin, 2020).

As of now, using PLT data from the Maasvlakte 2 (MV2) in Rotterdam (applied to the *Limelette* site in Belgium for actual, measured q_c values) result in much lower α_p values for some of the commonly used screw piles (i.e., Fundex, Tubex) for high-rise buildings in the Netherlands, see Table 1.1. Using lower pile factors for the base resistance of this type of pile results in load-settlement behaviour closer to partial displacement piles (type 2) instead of the currently used soil displacement piles (type 1) as illustrated by the NEN normalised load-displacement curves (see Figure 2.1). Based on Ter Steege (2022), the screwing motion of Fundex and Tubex piles during installation reduce adhesion of clay and cause grain crushing of sand, which reduce the radial stresses on the pile. Based on this newly introduced hypothesis, it is a possibility that settlement measurements of high-rise buildings are caused by failure or increased creep of the piles instead of or next to the compression of the Eem clay (or Drenthe/Kedichem clay) layers due to the NEN's use of higher α_p values and overpredicition of the base resistance of piles. In order to test these assumptions regarding settlement mechanisms, two more sub-research questions on pile behaviour and settlement mechanisms are introduced to find insights on how to improve the current methods used in daily practice. Thus, Section 2.2 will elaborate on pile foundation design, Section 2.3 will emphasize on settlement theories and Section 3.1 will apply these theories to realistic high-rise building loads acting on a typical soil profile in Amsterdam. On top of that, an attempt of a more realistic, numerical soil and PLT in Plaxis 3D will be made to provide more insight on representative soil behaviour of Eem clay and pile behaviour of a Fundex pile (as part of a pile group) in FEM.

Table 1.1: Summary of pile factors & characteristics from the NEN and recent *Maasvlakte* (MV2) pile load tests applied to the *Limelette* site in Belgium for a Fundex 560 pile (Ter Steege, 2022).

Pile Type	**Installation Method**	**NEN9997 Pile Properties**	**Updated Pile Properties**
Screw pile with lost foot	Soil displacement Grout injection (reduced friction) In-situ concrete, Withdrawn steel casing, Lost foot	$\alpha_s = 0.009$, $\alpha_p = 0.63$, $s = 1.0$, $\beta = 1.0$ Type 1 curve, Chamfered q_c	$\alpha_s = 0.011$, $\alpha_p = 0.35$, $s = 1.0$, $\beta = 1.0$, Type 2 curve, Measured q_c

1.3 Relevance of the Research

In the author's opinion, high-rise buildings can be the foundation of a more sophisticated and sustainable built environment and may serve as a convenient way of providing safe housing in densely populated areas such as Amsterdam or Rotterdam. However, the subsoil conditions in *De Randstad* serve as a fundamental challenge for high-rise structures as large building loads are believed to result in compression of the deep, soft soil layers. Modelling soft soil layers underneath the foundation level as part of an interactive, integral design methodology between a geotechnical and structural engineer will lead to a less conservative structural design by a better prediction of the resulting settlements and deformations. As explained in the problem statement (see Section 1.2), both an engineering and scientific gap (Section 1.2.1) are visible in the Dutch, contemporary design methodology since an integral SSI design procedure for numerical, high-rise building models appears to be missing.

1.3.1 Social Relevance

First of all, closing the scientific gap will contribute to the global engineering expertise by comparing high-rise design methods used abroad with similar subsoil conditions (i.e., Frankfurt, Mexico City, Chicago, Singapore, Stockholm, etc.) to the newly proposed and validated model in this research for the Netherlands. Examples of integral design models and methods can also be found outside the civil engineering field, such as in offshore engineering. For offshore wind turbines (OWT), Skau (2018) addresses the necessity to include the geotechnical discipline in the design process for cost and material reduction by the use of macro element modelling. Skau et al. (2018) concluded that modelling the stiffness of the foundation resulted in more accurate results in comparison to field data. The author believes that following a similar, integral design approach for high-rise building structures can lead to a more optimised construction. Thus, this research will help to understand current integral design methods within and outside a civil engineering framework and simultaneously tweak existing methods for high-rise buildings in Dutch subsoil conditions to better interpret and estimate settlement curves for use in structural design.

1.3.2 Scientific Relevance

To make sure the research to be conducted will be of high academic quality, updated pile factors from recent pile load tests will be used along with a parametric investigation of the newly proposed integral modelling approach. The parametric study will include a sensitivity analysis of the geotechnical and structural input parameters. Variations such as different pile factors and types, load (re)distributions to the clay layers, the number of piles, spacing between piles, and/or group effects will be considered along with an investigation whether a simplified model is sufficient and in which cases or boundary conditions it is not. The effects of mesh density on pile spacing and number of piles will be investigated as part of a literature review (see Abdel-Azim et al. (2020) for piled raft foundations in Frankfurt) instead of a thorough numerical investigation as the computation time using embedded beam models can involve several hours or even days. In addition, settlement data can be gathered from municipal databases and extended with satellite data (InSAR monitoring) shown in Appendix D. As future recommendation, the settlement data should be evaluated thoroughly to understand the mechanisms causing the subsidence of the surroundings as well as (differential) settlements due to applied building loads.

1.3.3 Engineering & Design Relevance

Second of all, closing the gap in practice will lead to a better understanding between structural and geotechnical engineers in a daily framework. By performing this research, the language spoken by the geotechnical engineer will be better understood by the structural engineer and vice versa (Figure 1.8). In the current practice, a variety of design methods and models are used. When a more uniform method is implemented among Dutch designers, it is clear from the start of the project how the geotechnical design can be integrated early in the process to benefit from the site investigation and modelling of soil behaviour. This will result in more accurate dimensions of a building structure to help reduce the footprint of the built environment along with a reduction in costs and time by skipping tedious, iterative design approaches. For the future, it is extremely important to reduce CO_2 emissions and strive for climate neutral designs. The author believes an integrated model can help reach those climate goals and impose a sustainable, integral high-rise building design method in the Netherlands. Finally, streamlining the current process (as was explained by Figure 1.7 in Section 1.2) will help understand and critically check underlying assumptions of contemporary structural models used in practice that make use of settlements as prescribed displacements (PD) or a simplified soil model (i.e., VRI's mattress model approach) underneath a structure as will be thoroughly explained in Section 2.1.2. Thus, this thesis will explain simplified theories applied in FEM that can be improved and automatised to make current design methodologies less conservative and more uniform among Dutch designers and engineers.

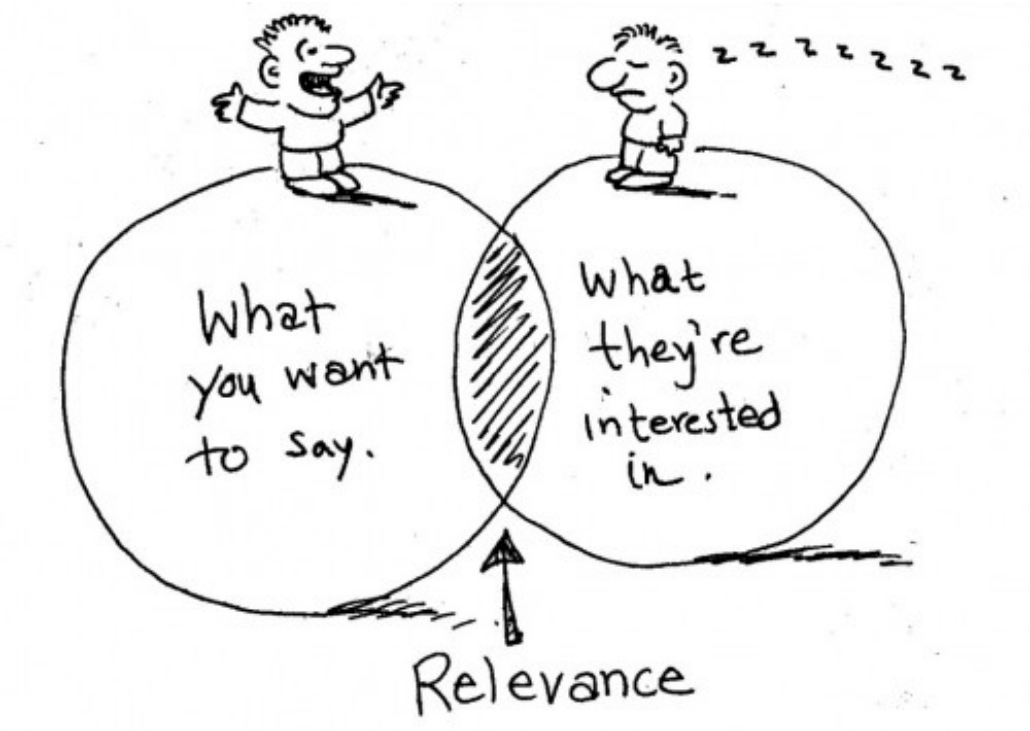

Figure 1.8: The narrow scope of relevancy, illustrated by Saga Briggs (2014).

1.4 Goals & Challenges of the Research

As explained, the overarching goal of this research will aim to close the scientific and practical design gap as well as the gap between academia and practice for structural and geotechnical engineering with regards to foundation settlement analysis.

1.4.1 Meta Goal

To contribute to a solution for the formulated problem statement while satisfying both scientific and design relevancy, a meta and a research goal are defined along with the challenges and how to overcome these to achieve the goals. The meta goal of the problem statement is as follows:

"To establish a more universal design procedure at a national level in which a simple, numerical soil modelling approach will be developed and validated for interactive use by geotechnical and structural engineers to include the effects of settlements caused by compressible soil layers beneath the foundation level."

1.4.2 Research Goal

The research cannot answer the meta goal alone, but will serve as a better understanding of current design methods for high-rise building structures in soft soils and will propose an improved, less conservative, integral modelling approach. During this process, the following research goal will be embraced:

"To propose an updated design methodology regarding foundation settlements using a simplified, integral modelling approach, which reduces time and costs while improving the flexibility associated with the current, iterative approach during the design phase of a high-rise building structure in soft soil conditions."

1.4.3 Expected Challenges

One of the major challenges will be accessibility to high quality settlement data for a high-rise building in deep, compressible soil deposits (that both CRUX and VRI have worked on) for validation of the current and, or new design method. Extensive data will be necessary to improve the scientific relevance of the research by understanding the underlying mechanisms causing the (autonomous) settlement of the GL, soil subsidence due to cyclic loads (i.e., fluctuations in ground water level (GWL) or wind), and consolidation/creep settlements of the (deep) soils due to the applied building loads. Nonetheless, it should be understood that even a high quality data set may have to be corrected due to monitoring nuisance and is not a perfect one-on-one representation of reality. To conquer this challenge, satellite data (i.e., InSAR monitoring) has been requested at SkyGeo (2022) for areas in Amsterdam and Rotterdam to collect more settlement data determined by the reflection of high-rise building roofs over time through the use of existing algorithms.

Another major challenge to overcome is to master two different disciplines in a timely matter to better understand SSI problems and associated modelling software; a geotechnical software (i.e., Plaxis 3D) and a structural software (i.e, SCIA). The above-mentioned software is most likely to be used in this research as it is commonly used by engineers in the Netherlands (and abroad). Understanding these software packages will help close the current (design) gap without having to teach employees (yet) how to use new software packages.

1.5 Research Questions

The meta and research goal, as described in Sections 1.4.1 and 1.4.2, can be attained by answering the following main and sub-research questions.

1.5.1 Main Research Question

"What integral design methodology can be followed by a geotechnical engineer to develop a joint, soil-structure interaction model that can be operated by a structural engineer to design a high-rise building structure in soft soil conditions?"

1.5.2 Sub-Research Questions

Below follow two sub-research questions subdivided by smaller topics in sub-sections to better understand the current practice (Q1), how to verify this method (Q2), and how to compare the improved method with daily practice (in future research):

(I) **Question 1:** What is the current design practice between a geotechnical and a structural engineer to determine the foundation settlements of a high-rise building (in the Netherlands)?

(a) Dutch design procedures [**Section 2.1**],

(b) Structural loads and loading conditions for high-rise buildings [**Sections 2.2.1 & 2.2.2**],

(c) Pile (group) capacity analysis [**Sections 2.2.3 & 2.2.4**],

(d) Settlements of individual pile (s_1) and pile group (s_2) [**Section 2.3**],

(e) Material linearity and constitutive models [**Section 2.4**],

(f) Building stiffness [**Section 2.5**],

(g) Numerical modelling (parameters) of soil-structure interaction in FEM [**Appendices B.1 & C.1**].

(II) **Question 2:** What is the error margin of the current design practice and is it possible to streamline it by safely eliminating the iterative process between geotechnical and structural models while maintaining realistic SSI effects?

(a) Hand calculation comparison with FEM [**Sections 3.1.1 & 3.1.2**],

(b) Pile (group) response under high-rise building loads [**Section 3.1.3 & 3.1.5**],

(c) Settlement mechanisms [**Section 3.1.4**],

(d) Set-up and verification of current, simple SSI approach [**Section 3.2**],

(e) Set-up of complex SSI approach based on multiple modelling scenarios [**Appendix B.2.1**].

1.6 Research Methodology & Report Structure

In pursuance of seeking answers for the research questions to close the existing gap (as defined in Section 1.2), a variety of research steps should be followed as part of the methodology to formulate a solution within the scientific and practical relevance. Below follows the anticipated research structure in which the research questions (as described in Section 1.5.2) constitute the workflow:

(i) **Phase 1a:** Performing a literature review on contemporary (integral) design methods for foundation settlement analysis of high-rise building structures in the Netherlands: structural (building) load conditions, pile (group) capacity, chosen constitutive & material models, building stiffness, and other model parameters (along with practicing tutorials in Plaxis 3D and SCIA).
↪ *This phase seeks to find answers for* ***research question 1*** *in Chapter 2.*

(ii) **Phase 1b:** Understanding and practicing current, iterative design method(s) and inputs of numerical models in the Netherlands between a geotechnical and structural engineer (based on the NEN/Eurocode).
↪ *This phase seeks to find answers for* ***research question 1*** *in Chapter 2.*

(iii) **Phase 2a:** Creating and verifying a simple soil-structure interaction model (in Plaxis 3D) for a pile (group) and soil test (in Plaxis' SoilTest facility).
↪ *This phase seeks to find answers for* ***research question 2*** *in the first part of Chapter 3.*

(iv) **Phase 2b:** Creating and verifying a simple soil-structure interaction model (in SCIA) for a theoretical, symmetric tower design.
↪ *This phase seeks to find answers for* ***research question 2*** *in the second part of Chapter 3.*

(v) **Phase 3:** Summarising numerical results and sensitivity analysis in a discussion to highlight the possibilities (of automation) and limitations of the model approach regarding the scientific and design relevance of the research.
↪ *This phase seeks to find an answer for the* ***main question*** *in Chapter 4.*

(vi) **Phase 4:** Finish writing of report and prepare for final presentation defense of MSc thesis.
↪ *This phase seeks to complete my* ***MSc Civil Engineering****.*

The research methodology is based on a typical FEM modelling process as described by Figure 1.9. In this research, the problem statement (i.e., how to better predict and model long-term settlements interactively between multiple stakeholders) and the evidence (i.e., measured settlements of high-rise buildings over time) drive the (new) numerical modelling approach between a geotechnical and structural engineer. The conceptual model definition will take place in (phase 1 of) the research process, followed by the model development (phase 2a), verification (phase 2b) and validation (phase 3) to be able to use the model in practice (phase 4).

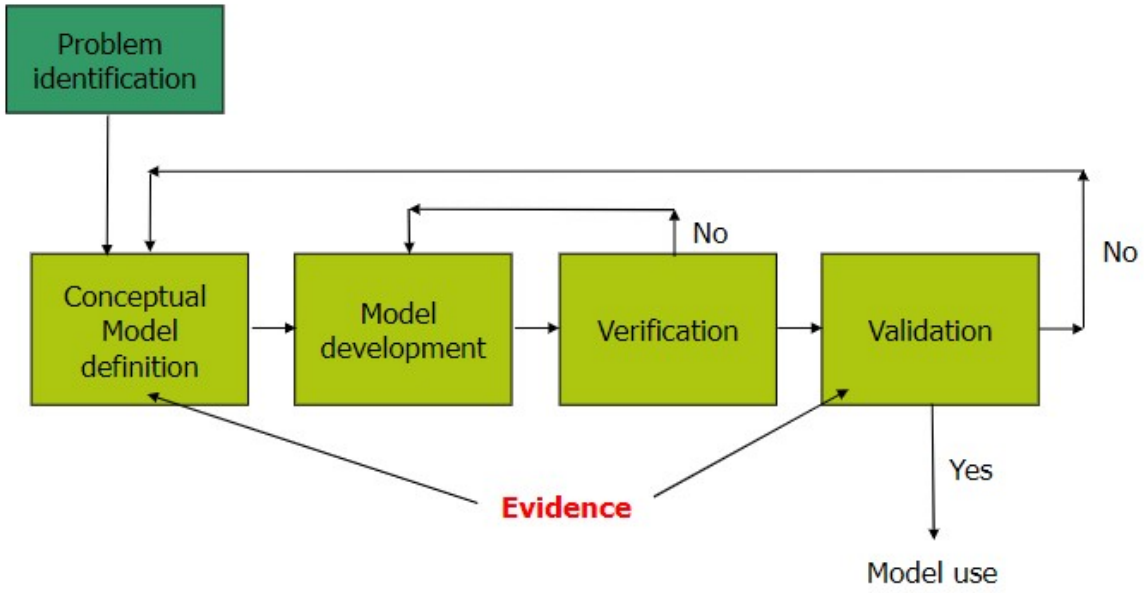

Figure 1.9: Typical process of (numerical) modelling (Van den Eijnden, 2022).

In conclusion, the research methodology and resulting report structure - based on the described research phases on the previous page - are summarised in Figure 1.10 below:

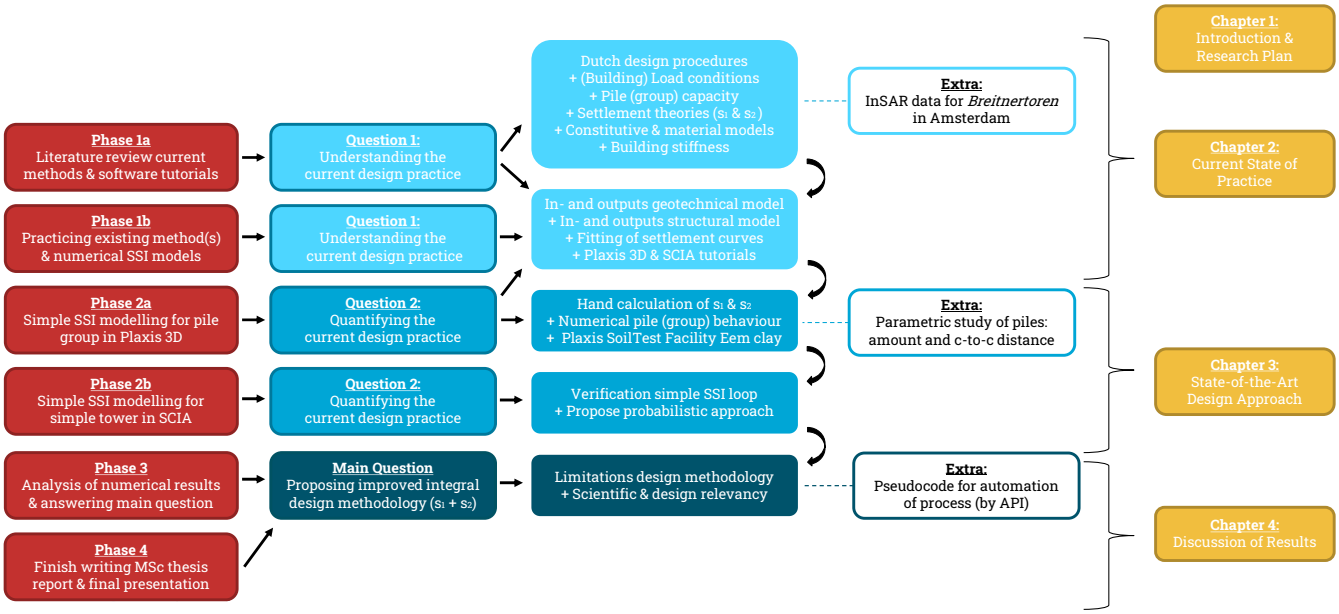

Figure 1.10: Proposed research methodology and report structure after approval of research proposal by MSc thesis committee.

1.7 Scope of the Research

In order to develop and validate a simple, interactive SSI modelling approach in the time span of a 40 ECTS MSc thesis (9-10 months) at TU Delft, decisions should be made regarding the scope of the research. For those reasons, the following topics **will not** be thoroughly investigated in this research report:

- Installation effects or different types/materials of piles; (concrete) displacement piles will be used when a distinction is needed as Tubex or Fundex (displacement) piles are commonly used in the Netherlands.
- Pile load tests or determination of p-z curves; load displacement (mobilisation) curves of the NEN9997-1 will be used to determine the s_1 settlements for the structural model.
- Negative skin friction or residual loads; the focus of the pile capacity will be on base and shaft resistance.
- Tension piles; the focus will be on compression piles as building loads are larger than pore pressures.
- Experimental tests for soil input parameters of constitutive models; a parameter set (representative for Amsterdam or Rotterdam) will be provided by the experience database of CRUX.
- Complex constitutive models not commonly used in practice (i.e., SHANSEP, hypo-plastic); a short list of common material models (i.e., Hardening Soil, Soft Soil Creep, Small Strain, etc.) will be made and compared to determine which ones are representative for soil profiles in the Netherlands.
- Incorporating complex numerical techniques such as the material point method (MPM).
- Modelling of different load distributions to the deeper clay layers; only the Tomlinson procedure is used as this method is generally selected by CRUX. However, the literature review does investigate certain (limitations of) other approaches.
- Structural safety classes; CC2 is used for the structural loads of a high-rise building ($\leq$ 70 m) along with CC3 ($\geq$ 70 m) in accordance with the NEN9990 (or Eurocode 0).
- The effect of lateral loads on piles and resulting deflection; wind loads will only be considered for one of the three extreme (ultimate limit state (ULS)) structural loading conditions added to a high-rise building structure in accordance with the NEN9990.
- Statistics behind model parameters, CRUX' soil parameters database, structural safety factors, or grouping of CPT's; NEN9990, NEN9991, NEN9997-1, and engineering judgement will be used.

Chapter 2

Literature Review of Current State of Practice

This chapter will seek to find an answer for the first research question:

Question 1:

"What is the current design practice between a geotechnical engineer and a structural engineer to determine the foundation settlements of a high-rise building (in the Netherlands)?"

Hypothesis 1:

It is expected that the current design process contains several iterations for the stress-dependent settlement solution to converge in both geotechnical and structural numerical models. Furthermore, a variety of different modelling approaches most likely define the Dutch market and in most methods a uniform, integrated SSI design approach between both disciplines is expected to be missing.

Several different topics are expected to influence the settlement analysis and will therefore be included in the literature review. Examples of these topics are:

1. Dutch design codes,
2. Structural loads and loading conditions for high-rise buildings,
3. Pile (group) capacity,
4. Settlements of an individual pile (s_1) and pile group (s_2),
5. Constitutive models and material linearity,
6. Building stiffness,
7. Numerical modelling (parameters) for SSI.

2.1 Contemporary Soil-Structure Interaction Design Approaches

To better understand the current state of practice, this section provides an overview of several design methods between geotechnical and structural engineering companies commonly used in the Netherlands as elaboration on the design loop presented in Figure 1.7 in Section 1.2. The section will end with a description of the current design methodology using a mattress model approach in an attempt to include SSI effects without iterations between structural and geotechnical engineer.

In the Netherlands, the *Omgevingswet* specifies what an engineer needs to deliver to the contractor and project developer for the project to be approved by the municipality as a safe and responsible design. For instance, the Omgevingswet (2018) requires a monitoring plan to determine the reference measurements (for settlements) and the maximum allowable settlements, rotations, and vibrations of the proposed building project and its surrounding structures. In practice, (s_2) settlement analysis are often neglected during the pre-design phase, but such an analyses is required during the final design phase of a high-rise building project and can have a significant influence on the feasibility of a project. Approximately, the final design phase includes steps 4 until the start of the construction phase (step 7, 8) as was described by Figure 1.7.

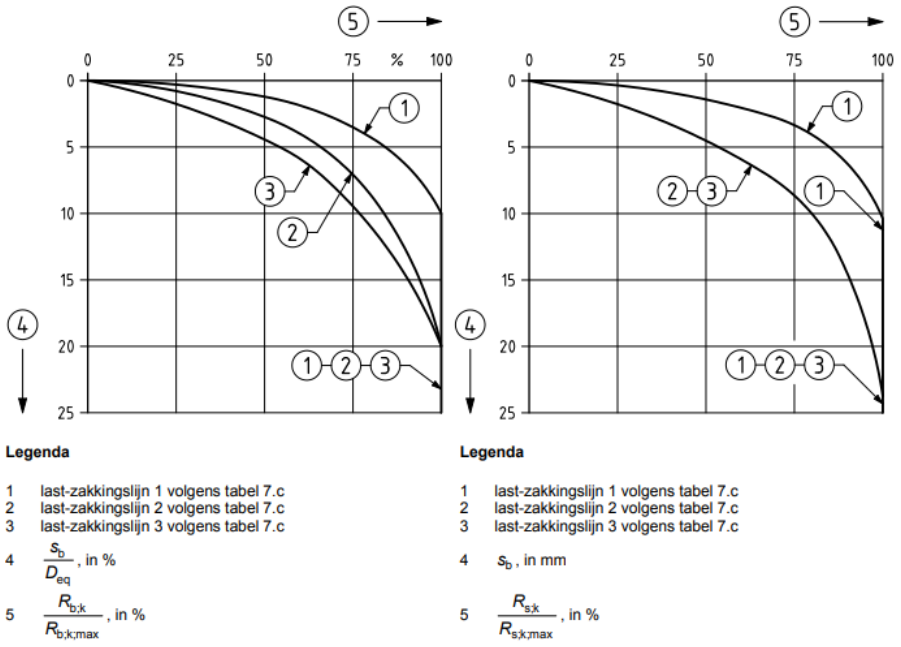

Figure 2.1: Load settlement curves from the NEN9997-1 for mobilised base resistance (left) and mobilised shaft resistance (right) for different types of piles (Eurocode 7 (2005), Figure 7.n) .

As part of the pre-design phase (see steps 1-3 in Figure 1.7), the axial load ($F_{s,tot}$) acting on the (individual) piles is calculated by the structural engineer based on some simple ULS calculations including the dead loads and the permanent part of the live loads. The latter is defined by the *momentaan factor* (ψ) and based on the type of building (i.e., offices or residential), which will be better explained in Section 2.2.1. The type of pile, corresponding stiffness (EA), and installation method is chosen based on the load, sub-soil conditions (often according to CPT data), and vibration or noise restrictions of the surroundings (in collaboration with the contractor and pile supplier). Note that a literature study describing the types of piles and foundation systems used in the Netherlands for high-rise buildings will be summarised in Section 2.2.3. The pile information is then send to the geotechnical engineer (step 2) who determines the foundation level and corresponding pile

length and diameter to carry the axial load. This results in the bearing capacity of the pile (R_{total}), see Section 2.2.4 for a more detailed pile resistance calculation. Based on the load settlement curves in the NEN9997-1 (see Figure 2.1 on the previous page) and the choice of pile (types 1, 2, and 3), the s_b settlement of the pile is often calculated at 70% of the characteristic shaft or base capacity ($F_{s,tot,k}$) by the geotechnical engineer. This percentage of the ULS axial load ($F_{s,tot}$) is used as a first estimate of the SLS load which still falls in the linear range of the pile stiffness response, see the x-axis in Figure 2.1. A stiffness value above 70% of the load would be closer to the plastic behaviour of the pile. The resulting pile tip settlement (s_b) along with the linear elastic compression of the pile itself (s_{el}) is transferred to a spring stiffness ($k_{v,1}$) using Eq 2.1 below:

$$k_{v,1} = F_{s,tot,k}/(s_b + s_{el}) \tag{2.1}$$

Note that the s_1 settlements of the piles are defined by the addition of s_b and s_{el} and a more detailed settlement definition and analysis will follow in Section 2.3. When the bearing capacity of the pile exceeds the axial load with a certain safety factor higher than 1.0, the design is considered safe and the $k_{v,1}$ stiffness is used by the structural engineer in numerical models (i.e., SCIA). To be more conservative due to many uncertainties (in soil and material parameters), it is common in practice to work with partial factors in the ranges of 1.2 - 1.5 instead. Generally, an upper limit regarding uncertainty in soil parameters is determined by multiplying the stiffness values by $\sqrt{2}$ and dividing by $\sqrt{2}$ for a lower limit respectively. To conclude the pre-design phase, the structural engineer determines the surface loads (step 3) based on simple SLS calculations, which can be used by a geotechnical engineer as input for numerical models (i.e., Plaxis 3D) to determine the s_2 settlements (step 4) of the deep soil layers below pile tip. This is currently done in a variety of ways as will be explained by the following sub-section. Including s_2 settlements in structural FEM models is important as those time-dependent deformations can lead to large shear forces, among other mechanisms, in (shear) walls of a high-rise building structure.

2.1.1 An Overview of Geotechnical Engineering Procedures in the Netherlands

This sub-section provides a summary of the design methods used by CRUX (and other geotechnical engineers) for determining time-dependent (s_2) settlements for pile groups of high-rise buildings in soft soils (see step 4 in Figure 1.7). The methods are described with Amsterdam as reference, where compressible soils (Eem clay and Drenthe clay) are found between the second and third sand layer. In the north of Amsterdam, the foundation level is often the second (Pleistocene) sand layer. In the southern part of Amsterdam (i.e., *De Zuidas*), deep clay layers are no longer found in representative soil profiles and therefore follow a slightly different design methodology for deep foundation systems.

First of all, the domain size of the model is important to accurately model settlement effects of soft soils. The initial depth of the subsurface model is defined by the PTL. When the pile tip is constructed in the second sand layer, the bearing layer underneath the deep clay layer (= the third sand layer in Amsterdam) should have a minimum thickness of 20 m below PTL in Plaxis and modelled with the use of the hardening soil small strain stiffness model (HSS). The total depth of the vertical model dimension can then be estimated by $1.5 \cdot w$, where w is the GL minus the PTL in metres (see Figure 2.2)[1]. Furthermore, the width and length of the model domain are defined by adding (at least) the width of the structure (i.e., foundation slab) in each direction (x and y). This results in an influence zone described by 45 degrees from the bottom of the domain.

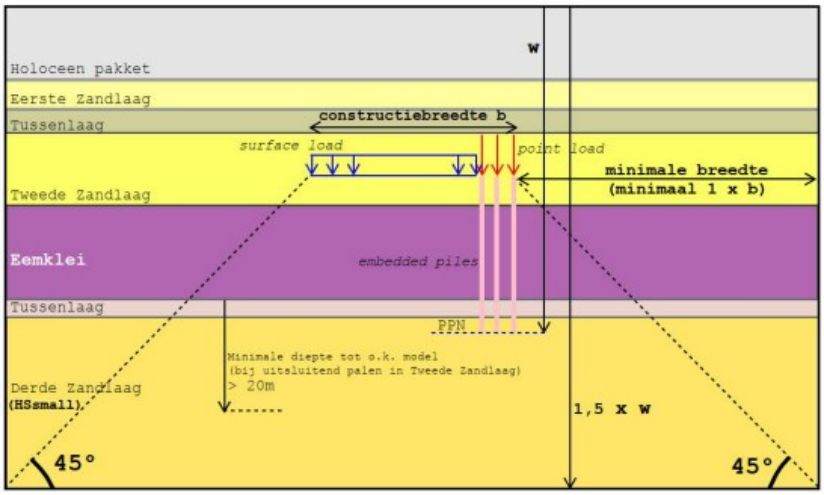

Figure 2.2: Model dimensions in Plaxis 3D based on foundation level (De Jong & De Koning, 2021).

The optimised model depth for the soft soil creep model (SSCM) is verified by calculating the change in vertical effective stress due to the (largest) applied building load. Ideally, the bottom of the model domain lays within the stress reduction zone of 10% - 20% change in stress, $\Delta\sigma'_v$, with regards to the initial vertical effective stress, σ'_{v0}. This is in accordance with the NEN9997-1 and will be further described in Section 2.3. For more realistic (and smaller) settlements due to the small strain stiffness response of deep clay layers, De Jong and De Koning (2021)[1] at CRUX model those compressible layers below the specified stress reduction zone (where $\Delta\sigma'_v \leq 20\% \cdot \sigma'_{v0}$) with the use of HSS parameters instead of the SSCM. The SSCM model parameters used for the Eem or Drenthe clays above the 20% stress reduction limit are based on laboratory tests of specific reference projects. Resulting Isotach parameters (a, b, c) can be modified to the required input for Plaxis using Eq. 2.2 below:

$$\lambda^* = b \quad , \quad \kappa^* = 2a \quad \text{and} \quad \mu^* = c \tag{2.2}$$

where, λ^* describes the primary (consolidation) settlement, κ^* defines the secondary (consolidation) settlement, and the μ^* includes the creep settlement. A collection of parameters for Eem or Drenthe clay can be found in the experience database of CRUX, which is used in combination with laboratory results due to significant disturbance during sampling of deep (clayey) soils. According to the database, the lower limit of the OCR for those type of clays is often 1.5 whereas the upper limit goes to 2.5. The OCR for the SSCM, however, also includes ageing effects in accordance with Den Haan (2008) and the upper limit is therefore approximated as 3.5. This OCR_2 value is defined by Eq. 3.7 to include the ageing effect of the clay layer:

$$OCR_2 = OCR^{\frac{\lambda^*}{\lambda^* - \kappa^*}} \tag{2.3}$$

An OCR of 1.0 or higher means that the deep, 'soft soils' are OC and behave relatively stiff until the new applied building load ($\Delta\sigma'_v$) exceeds the pre-consolidation pressure (σ'_p) or maximum past pressure. Again, the HSS constitutive model (instead of the SSCM) is used to take into account the strain-dependent stiffness response of the deeper clay layers from the depth where the change in strain becomes less than 20%. Using

[1] Internal document from CRUX, no public access.

this approach, the (stiffer) bottom part of the clay layer contributes less to the settlement, which is in line with shallow foundations as described by article 6.6.2 of the NEN9997-1 (Chortis et al., 2021)[1].

Load Spread Methods

The building loads provided by the structural engineer are commonly modelled as a surface load without considering the stiffness of the structure and this method is therefore lacking actual SSI effects. The determination of the building loads will be described shortly in Section 2.1.2 and an extensive elaboration of this topic will follow in Section 2.2. Modelling the applied building load (minus the pore water pressures in case of a basement) in Plaxis can be done in several ways. The most common method (by CRUX) is Tomlinson's equivalent raft approach. This procedure assumes the load is fully carried by shaft or base capacity of the pile with a load spread of 1 in 4 starting at the top of the bearing layer until a depth of 2/3 times D_{pos}. For friction piles in clayey soils (Figure 2.3a), D_{pos} is taken from GL while no load spread is assumed for end-bearing piles resting on bedrock (Figure 2.3c). The foundation level in Amsterdam is often in the second sand layer, for which D_{pos} is defined by the top of the positive shaft friction or distance between the top of the bearing layer - often the first sand layer - and the bottom of the piles (= PTL) in the second sand layer, see Figure 2.3b. In the north of Amsterdam, the PTL is often around 25 m below GL. Occasionally, CRUX makes a distinction in Plaxis between the load distribution due to shaft friction and the load transfer to the pile toe to correspond better with the NEN9997-1 method for s_1 settlements of an individual pile. Consequently, the shaft capacity (R_{shaft}) percentage of the total pile capacity (R_{total}) or building load is modelled as a surface load at Tomlinson's level (= D_{tom}), while the base capacity (R_{base}) percentage of the total pile capacity is modelled as surface load at PTL (see Figure B.20 in Appendix B.2.1). Thus, one building load will be modelled as two separate surface loads at different depths in Plaxis 3D. Section 2.2.4 will elaborate more on a pile capacity analysis of a single pile and that of a pile group for common foundation systems of high-rise buildings.

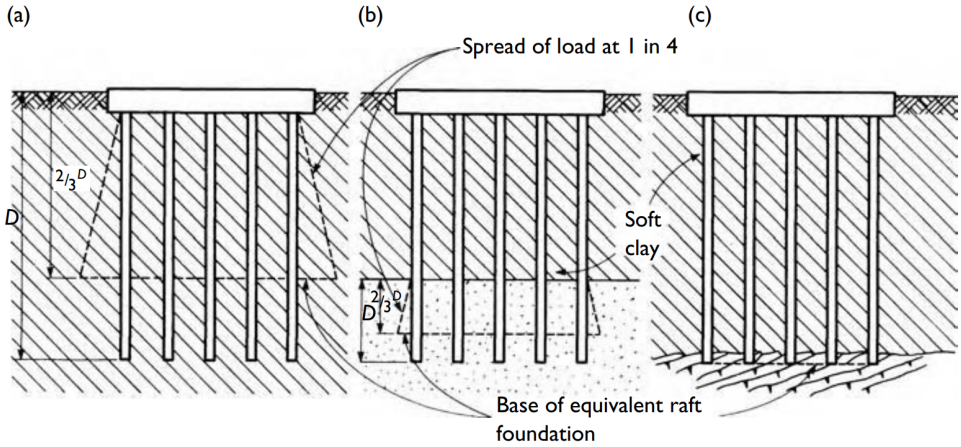

Figure 2.3: Schematic visualisation of Tomlinson load distribution procedure (Tomlinson & Woodward, 2008).

Embedded Beam & Volume Pile Methods

In an attempt to include SSI effects and to take advantage of a combined model for both s_1 settlements (due to individual pile stiffness) and s_2 (due to deep soil layers) in Plaxis 3D, a different method was investigated by Frissen (2020). The superstructure was modelled in Plaxis 3D along with a stiff plate slightly above GL, which is connected to piles modelled in Plaxis 3D as line elements with embedded beams as material model.

The embedded beam model should first be fitted against analytical software (i.e., D-foundations) or pile load tests for correct use of the (multi-)linear shaft capacity (T_{max}), base resistance (F_{max}), and calculated linear pile stiffness ($k_{v,1}$ and/or s_1) in Plaxis. Thus, the ultimate bearing capacity (R_{max}) of the embedded beam pile (see Figure 2.4) is an input and not a result of the FEM analyses. Note that the ultimate bearing capacity input should be the maximum the pile can hold and is not the mobilised capacity under a certain load. The maximum base resistance, F_{max}, is then further defined by Brinkgreve (2021) as the "maximum force allowed at the foot of the embedded beam" and the interaction between the base of the pile and the soil is modelled by a linear elastic perfectly plastic interface element, K_{foot}, see Figure 2.5a. When the base resistance is fully mobilised, plastic behaviour will occur and the output of the embedded beam (F_{foot}) equals the maximum base resistance: $F_{foot} = F_{max}$. However, in Dutch soils, the shaft capacity often mobilises first before reaching the maximum capacity of the toe. Hence, the total bearing capacity of the embedded beam is defined by Eq. 2.4, for which T_{top} and T_{bot} can be replaced by a multi-linear skin resistance (T_{max}) using curves for shaft resistance (in kN/m) based on the analytical solution for pile capacity:

$$R_{total} = 1/2 \cdot (T_{top} + T_{bot}) \cdot L_{pile} + F_{max} \tag{2.4}$$

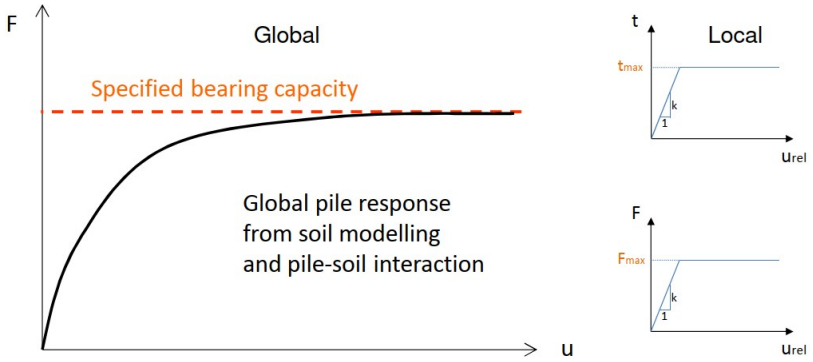

Figure 2.4: User specified bearing capacity versus modelled SSI and pile behaviour (Brinkgreve, 2014).

In essence, the embedded beam model is an improvement (or simplification) of the volume pile. A volume pile in Plaxis exists of continuum finite elements defined by a linear elastic model (LE) under "soil and interfaces" containing the properties of the pile (i.e., Young's Modulus, Poisson's ratio, and unit weight of concrete). The surface of the volume pile is connected with the soil layers by modelled (negative) interface elements containing the parameter R_{inter} to take into account the relative movement due to adhesion and friction between the volume pile and the surrounding soil. Brinkgreve (2021) defines the interface reduction factor (R_{inter}) as the relationship between "the strength of the interfaces to the strength of the soil" according to the following equations:

$$c_i = R_{inter} \cdot c_{soil} \qquad \text{and} \qquad tan(\phi_i) = R_{inter} \cdot tan(\phi_{soil}) \tag{2.5}$$

When the interface reduction factor falls below 1.0, a reduced interface friction is modelled meaning that the interface cohesion (c_i) is lower than the soil's cohesion (c_{soil}) and friction angle (ϕ_{soil}) surrounding the pile. Since the volume pile is defined by volumetric soil elements, it is not possible to directly retrieve the axial force (N) of the pile in Plaxis 3D Output. To overcome this issue, a beam element can be modelled at the axis of the volume pile containing a Young's Modulus 10^6 times lower than that of the volume pile (Dao, 2011).

The volume pile may work as a good method for individual piles or small pile groups, however, according to Frissen (2020) and CRUX, the numerical model becomes unstable and complex for large pile groups as this method requires small soil elements resulting in high computational demand. The embedded beam model requires less computation cost as the mesh of the FEM does not need to be altered for the pile locations. The embedded pile was first formulated by Sadek and Shahrour (2004) and later improved by Engin and Brinkgreve (2009), Tschuchnigg (2013), Turello et al. (2016) and Smulders (2018). More recent, Granitzer and Tschuchnigg (2021) have validated the new embedded beam formulation (EB-I) by Turello et al. (2016) with interaction surfaces, which allows the spread of non-linear SSI effects over the integration points at the physical interaction surface instead of over the pile's axis. The latter is not yet available in the user interface of commercial software, however, EB-I can be switched on by a toggle in Plaxis[2]. In general, the embedded beam has been developed as a beam which can cross any volume element (i.e., 10-node tetrahedral soil elements) in Plaxis and consists of (real) beam nodes containing 6 degrees of freedom (DOF) for translation and rotation in x, y, z direction and (virtual) interface nodes containing 3 DOF's for translation only, see Figure 2.5b (Brinkgreve, 2014). The shaft and base of the pile fall within an elastic region similar to the pile's diameter (D) and the soil stress points within this region are forced to behave elastically, see Figure 2.5c.

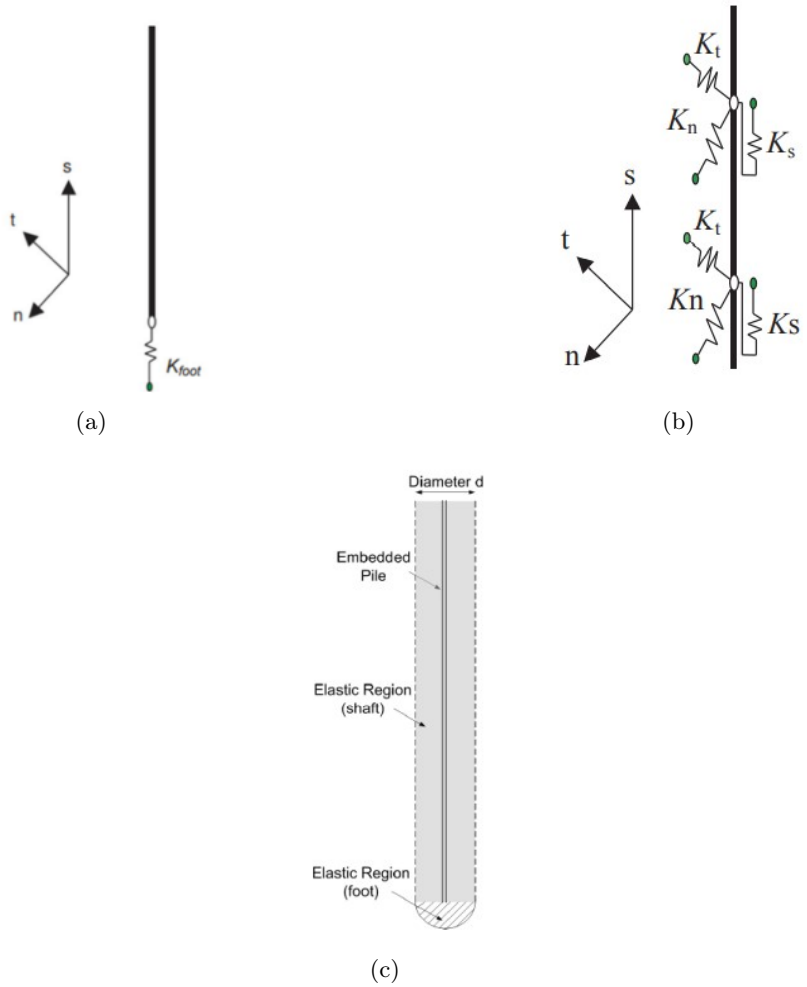

Figure 2.5: Stiffness of the interface elements a) at the toe, b) at the skin, and c) at soil stress points of the embedded beam element in Plaxis 3D (Brinkgreve, 2021).

[2]Create an empty text file called "NEW_EMBEDDED_BEAM" in the Program Files folder of Plaxis 2D or 3D.

Therefore, the shear force along the embedded beam in axial direction (t_s) should be lower than T_{max} within the elastic region, otherwise plastic behaviour will occur ($T_{max} \leq t_s$). The diameter of the elastic region was first introduced by Engin and Brinkgreve (2009) for the new embedded beam formulation (EB-I) to reduce mesh sensitivity and is described by Eq. 2.6 and 2.7:

$$R_{eq} = \{\sqrt{\frac{A}{\pi}}, \sqrt{\frac{2 \cdot I_{avg}}{A}}\} \tag{2.6}$$

where,

$$I_{avg} = \frac{I_2 + I_3}{2} \tag{2.7}$$

Note that R_{eq} is defined as the equivalent pile radius, A as the cross-sectional area of the pile, ϕ_i as the friction angle of the interface elements, c_i as the cohesion of the interface elements, I_{avg} as the average moment of inertia for the pile, and I_2 and I_3 as moment of inertia of the pile perpendicular to the pile axis.

Thus, next to the force at the foot (F_{foot}) and axial force in the pile (N), Plaxis also calculates the material stiffness of the embedded interface element in the global coordinate system (T_{skin}). The latter is described by Brinkgreve (2021) as a function of the skin traction increment (t_{skin}) and the difference in the increment of the soil displacement and beam displacement (u_{rel}): T_{skin}=t_{skin}/u_{rel}. Interaction is created by integrating between a pair of nodes, one as part of the soil element and the other of the beam element.

Using the embedded beam method, load redistribution within the superstructure and load spread to the subsurface can be modelled more accurately. This design methodology can be preferred over the load spread method when a project includes multiple, overlapping building loads (due to a difference in building heights) and a variety of pile tip levels. Overlapping building loads using the surface load option (according to Tomlinson) in Plaxis would result in incorrect superposition of loads or numerical errors when the vertical distance between modelled surfaces is too small. However, using embedded beams in Plaxis 3D significantly increases the computation time from several hours to several days for complex structures. In addition, even the new formulation of the embedded beam (EB-I) tends to underestimate pile tip resistance slightly (see Figure 2.6) due to the connection with the mesh on top of neglecting installation effects for soil displacement piles.

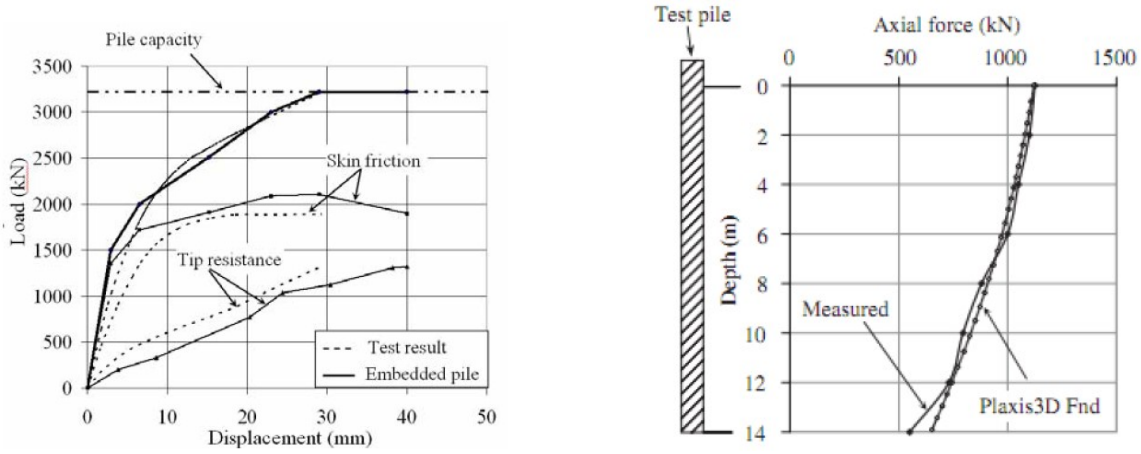

(a) Alzey Bridge.

(b) Amsterdam.

Figure 2.6: Embedded beam model verification using compression pile load tests performed at a) Alzey Bridge, and b) Amsterdam (Engin & Brinkgreve, 2009).

Construction & Consolidation Phases

For the phases in Plaxis for both methods used by CRUX, the applied building load is modelled as an instant load during the construction and initial consolidation phase, often at t = 1 day. For a more realistic consolidation settlement during construction, gradual loading can be applied where the applied load is linearly dependent on the estimated construction time. In this scenario, t is defined by t_c, which is the total construction time in months or even years. The choice of gradual loading results in less settlement prediction and is strongly correlated to the uncertainty in permeability which governs the progress of construction. The choice of construction stages should therefore always be communicated with the structural engineer, see Figure 2.7[1]. Other phases to model primary and secondary consolidation settlements can be defined by 2, 30 or 50 years, where the latter defines the total lifespan of the structure after construction is completed. Settlement results are retrieved at a depth of 4 times the diameter (D) of the pile below the actual PTL (not Tomlinson's level, denoted as D_{pos}) with a maximum of 4 m. This is in accordance with the 4D-8D Koppejan method described in NEN9997-1. Note that a finer mesh should be used directly below the largest building load and for the entire thickness of the deep clay layer(s).

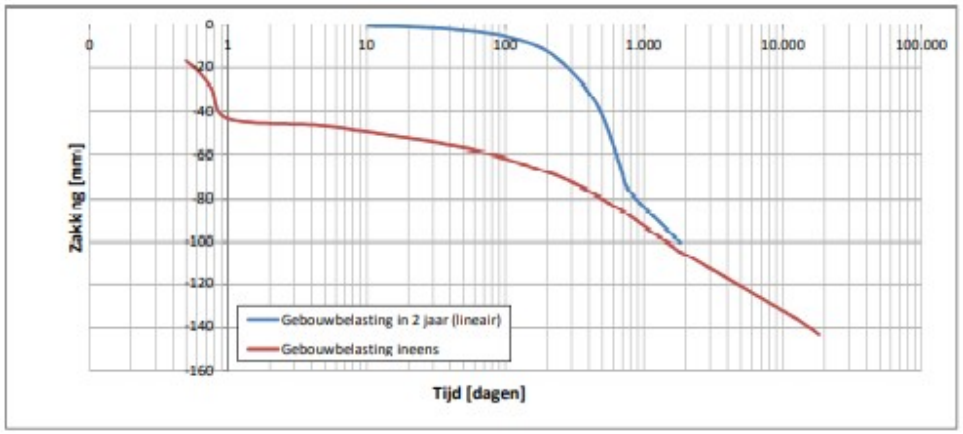

Figure 2.7: The effect of gradual loading (blue) and instant loading (red) on settlement curves (De Jong & De Koning, 2021).

At the end of the settlement analysis, it is important to take into account continuous creep settlements due to ageing (*autonome bodemdaling* in Dutch), which can be defined by μ^* and OCR_2 (for the SSCM) as explained previously. Unlike creep settlements, autonomous settlements are not influenced by the applied building load and resulting change in (effective) stresses. Based on settlement data by Omegam (at the *Noord-Zuidlijn* in northern Amsterdam), creep of the Eem or Drenthe clay are approximated as 0.3 mm per year up to values of 1 mm per year, which is in accordance with satellite data (for *IJburg* in eastern Amsterdam). The s_2 settlement results can be verified with the use of another experience database by CRUX, which includes plots of calculated s_2 settlements versus building loads for several high-rise building projects in the North of Amsterdam (see Figure D.3 in Appendix D). Based on this database, s_2 settlements can range from 80 mm to 170 mm for building loads between 180 kN/m^2 and 350 kN/m^2 for a tower structure of 70 m or lower (De Jong & De Koning, 2021)[1].

Other Geotechnical Methods

In addition to the methods used by CRUX, below follows a summary of modelling approaches used by other (geotechnical) organisations. For instance, both Schippers et al. (2021) and Schippers and Broekens (2022) from Geobest BV described the s_1 and s_2 settlement predictions used for the 215 m tall *Zalmhaventoren* currently being constructed and monitored in Rotterdam as the tallest residential tower in the Benelux.

Similar to Amsterdam, buildings in Rotterdam are often carried by piles with lengths of 25 - 30 m reaching the first Pleistocene sand layer underlain by varying sand and clay layers below a depth of NAP - 33 m. Even though the deep clay layers are considered highly OC due to a lower sea level in the last ice age, compression still occurs due to increased vertical effective stresses caused by building loads. Especially highly concentrated building loads due to high-rise buildings (around 150 m in height) can lead to consolidation settlements of 100 - 300 mm. When too large settlements (and resulting rotations) are predicted, the only solution would be to use piles till a depth of - 55 m below GL, which is underneath the compressible soil layers in Rotterdam (*Waalre* formation). Schippers et al. (2021) explain that the load distributed by shaft resistance in the first Pleistocene sand layer leads to increased vertical effective stresses acting on the compressible soil layers. This results in additional consolidation settlements and more mobilised shaft and toe resistance in the bottom part of the pile (in comparison to the top part). Thus, load redistribution over time leads to a force flow going from the first sand layer to the deep soil layers below PTL resulting in additional foundation settlements (s_2).

Schippers et al. (2021) used the pile factors for shaft and toe capacity listed in Table 7.c and 7.d in the NEN9997-1. Furthermore, they used an average pile diameter (D) based on the toe (D_{eq} = 962 mm) and shaft (d_{eq} = 762 mm) diameters. A representative point load of 10 MN was used for the s_1 static pile stiffness ($k_{v,1}$ = 270 MN/m) including elastic compression (s_{el}) of the pile itself. The pile head settlement (s_1) found by Plaxis 3D for an individual pile as embedded beam were lower than was predicted by D-Pilegroup. The pile group for the s_2 settlement prediction in Plaxis 3D was modelled as a group (consisting of 164 piles) with a concrete (foundation) plate of 38 x 40 x 2.5 m on top. The building load acting on this plate was modelled as a surface load equal to the SLS point load divided by the area of the foundation plate (= 428 kN/m^2). Schippers and Broekens (2022) also used a Plaxis 3D model with the same soil stratigraphy, but without any structural elements to determine an autonomous settlement of 0.65 mm/year. Ultimately, a settlement driven approach was used for the foundation design of the Zalmhaventoren in Rotterdam.

2.1.2 An Overview of Structural Engineering Procedures in the Netherlands

This sub-section provides a summary of a variety of design methods used by VRI (and other structural engineers in the Netherlands) on the implementation of time-dependent (s_2) settlements in FEM structural models of high-rise buildings in soft soil conditions (see step 5 in Figure 1.7). Considering also the different types of design methods from a geotechnical point of view as discussed above, enforcing one interactive methodology among Dutch engineers can lead to a more economical, sustainable, and time efficient high-rise building design process regarding foundation settlements. For instance, most structural engineers implement both s_1 along with s_2 settlements in FEM models. Pile head settlements (s_1) and deep foundation settlements (s_2) are often modelled as linear springs or prescribed displacements added to pin supports underneath a basic structural model including the building and its foundation plate or basement. However, as stated in the problem statement, soil behaviour is non-linear and the prescribed displacement method does not include any SSI effects leading to over-conservative shear forces in the superstructure. First, an explanation of this method will be provided in this sub-section, followed by an improved methodology (mattress model method) and finished by a brief description of other methods based on a literature review of Dutch structural design reports.

Prescribed Displacements Method

Prior to 2018, VRI (along with many other structural engineering firms) implemented settlements following the iterative design approach using a prescribed displacement (equal to the sum of s_1 and s_2). Prescribed displacements can be used to control the displacement (of pin supports) of structural elements. This was applied as a load case to each pile as a pin support in structural FEM models (i.e., SCIA) in a similar way as adding dead loads, live loads, and wind loads to the structure. Settlements are first calculated by a geotechnical engineer (based on building loads from the structural engineer) and visualised as a map with contour lines. Thereafter, the structural SCIA model is underlain by this settlement map and for each pile (or a group of piles) the corresponding s_2 settlement is determined and added as a point displacement & translation of support (Figure 2.8a). Instead, one can also choose to add a line displacement subjected to longitudinal (Figure 2.8b) or flexural strain instead (Figure 2.8c). If no iteration step is taken back to the geotechnical engineer, using the method of prescribed displacements does not include SSI effects and is therefore a conservative modelling approach. For example, the geotechnical engineer often does not include the stiffness of the building and thereby not the load distribution of the superstructure (= Greenfield conditions), which would normally decrease the amount of predicted settlement when included in the settlement analysis.

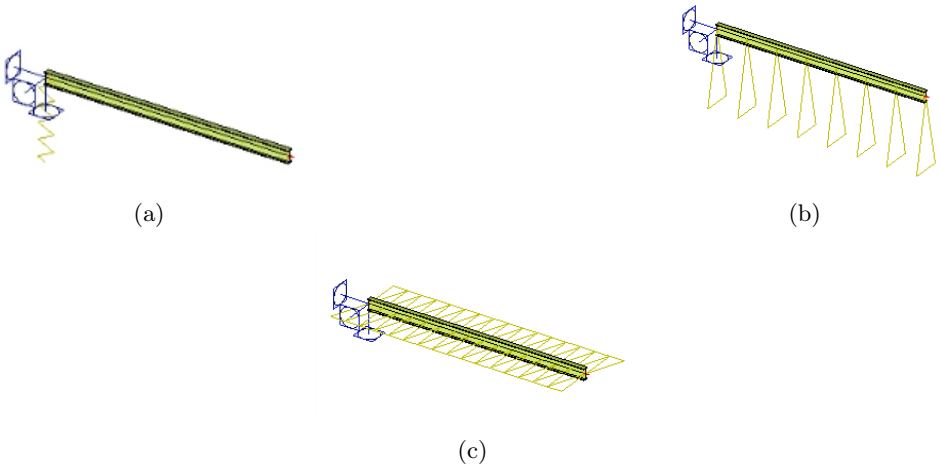

(a) (b)

(c)

Figure 2.8: Types of prescribed displacements in SCIA (for a beam element).

Mattress Model Method

In practice, the aforementioned iterative approach using prescribed displacements appeared unsatisfactory and too conservative, among other things, during the modelling process of the Galaxy Tower in Utrecht by VRI. Prior to construction in 2018 (Ballast Nedam, 2018), this method predicted massive deformations of the building structure. As a result, a new method was designed by VRI (Van der Sluis, 2017)[1]: a mattress model. The so called mattress model (in SCIA) resulted in more realistic settlements. The modelling approach is best described by a plate of 1 m thick with stiffness, E_{plate}, combined with linear springs containing stiffness, $k_{bedding}$, underneath the building's deep foundation, which is initially modelled as a Poulos model (1971) with linear springs ($k_{v,1}$) underneath the structure. The $k_{bedding}$ springs are often modelled as pin supports at a grid of 2 m x 2 m to keep the number of elements to a minimum. Altogether, the bottom plate and springs represent the deep, soft soil layer(s) and the bedding of those compressible layers beneath the PTL, see Figure 2.9. Bedding can be further defined as a spring constant correlating building loads to (s_2) soil settlements. Another goal of VRI's mattress model is to make the iterative process redundant, which results in a reduction of time and associated costs during the design phase of a project. Instead of endless 'ping-ponging' between structural and geotechnical engineers, the input parameters (E_{plate} & $k_{bedding}$) of the mattress model are manually changed (in SCIA) by the structural engineer as part of a deformation (u_z) fitting procedure (in Excel) with regards to the shape of the (preliminary) s_2 settlement curves generated by geotechnical engineers (in Plaxis), see Figures 2.10[1] and C.7.

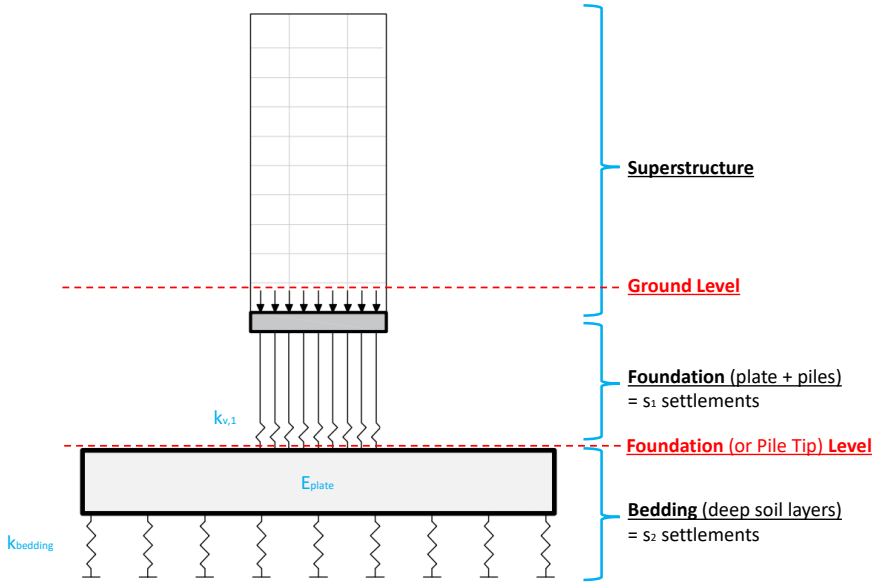

Figure 2.9: Schematic visualisation of VRI's mattress model for a pile foundation. The top row of springs ($k_{v,1}$) represent the (s_1 settlements of) piles, while the bottom row of springs ($k_{bedding}$) and the plate (E_{plate}) represent the (s_2 settlements of) deep, soft soils 4D below pile tip (after Van der Sluis (2017)).

When a satisfactory fit is achieved, the two (linear) model parameters are added back to a more advanced structural model to continue the structural analysis of the superstructure. Often, a variety of models is used based on the type of foundation. For instance, for a piled raft foundation, a model variant using stiff piles and flexible bedding can be used to determine the ULS pile loads. On the other hand, a variant with flexible piles and stiff bedding can be used to determine the maximum ULS vertical effective stress acting on the soil beneath the foundation. Largest settlements are expected for the model variant where the load is more concentrated in comparison with a model containing more load spread.

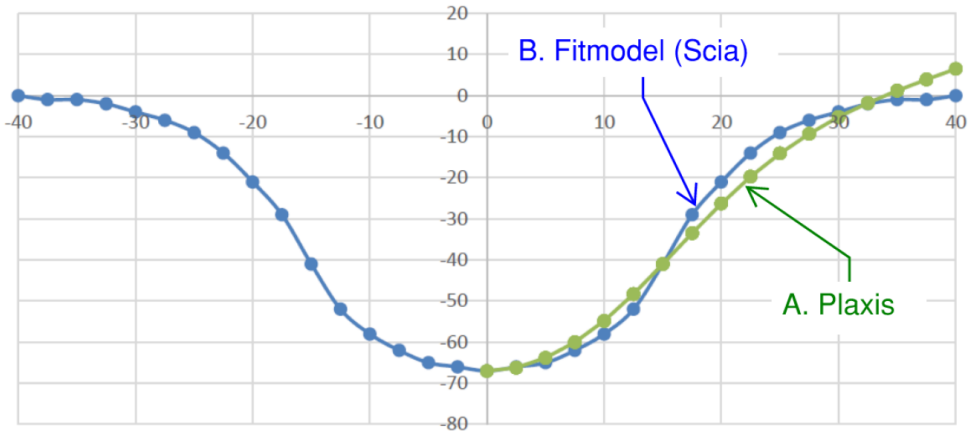

Figure 2.10: Example of u_z fitting between Plaxis and SCIA for a high-rise building (Bartels & van Gijn, 2020).

The SSI mattress modelling approach of VRI's structural engineers in SCIA now serves as a conservative (2D) simplification of a complicated soil model normally provided (through Plaxis 3D) by a geotechnical engineer. After its first use for the Galaxy Tower in 2018, the mattress model approach was used for many high-rise building design by VRI to model SSI of the s_2 settlements at four times the pile diameter (= 4D) below pile tip level (= PTL). In other words, a mattress model is a first attempt for a Plaxis embedded structural model to minimise iterations and include non-linear (SSI) effects. Nonetheless, scientific research of the relatively new mattress model conducted in this thesis can serve as a verification and optimisation tool to establish a less conservative, integral SSI modelling approach to ultimately be used uniformly at national level.

Other Structural Methods

Based on a literature review of Dutch structural design and forensic reports alongside confidential conversations with engineering companies, additional soil-structure interaction methodologies were investigated and the following conclusions were drawn:

1. Project X in Amsterdam: The structural engineer calculated building loads as point loads acting directly on the piles ⟶ pile stiffness was included twice (i.e., in Plaxis and SCIA) ⟶ too high settlements as prescribed displacements.
2. Project Y in Amsterdam: Rotation limits exceeded when settlement predictions were determined based on surface loads ⟶ instead used embedded beams with point loads in Plaxis and non-linear springs in structural model ⟶ load distribution due to (stiffness of) superstructure only included in structural model ⟶ iteration lead to sufficient rotation requirements.
3. Project Z in Amsterdam: s_2 settlement prediction based on surface loads and combined with s_1 as one spring in structural model in pre-design and final design phase ⟶ similar approach as VRI's mattress model ⟶ issues with the modelling approach and building load calculation ⟶ new analysis needed during construction phase.
4. Project *Breitnertoren* in Amsterdam: Building loads (250 kN/m^2) based on 85% of the ULS loads including the (28 m x 34 m) foundation plate, basement, superstructure, furniture, and dynamic loads minus pore water pressure at the bottom of the basement (NAP - 9.5 m) applied as surface load at pile tip level (NAP - 31.5 m) ⟶ load distribution of Boussinesq and settlement analysis of

Terzaghi-Buisman (Koppejan formulation) for a consolidation period of 10,000 days (= 30 years) using Omegam's ZETBK! 2.0 $\longrightarrow$ neglecting stiffness of soil layers and foundation while including excavation as surface unloading (-75 kN/m^2) $\longrightarrow$ maximum settlement of 102 mm determined at NAP - 40.5 m (= top of Drenthe clay) at the end of consolidation $\longrightarrow$ redone in Plaxis 6.3 (SSM + MC material models) using a circular foundation plate (R = 17.4 m) of 250 kN/m^2 (at NAP - 31.5 m) $\longrightarrow$ maximum settlement (at NAP - 40.5 m) of 105 mm without and 55 mm with plate stiffness (Visser & Gutter, 1999).

5. Project *Zalmhaventoren* in Rotterdam: Piles as embedded beams + concrete foundation plate + representative building load as surface load on top of the plate with piles $\longrightarrow$ load at pile tip level $\longrightarrow$ small changes in predicted and measured settlements caused by an asymmetric load distribution of the building and foundation due to a dominant wind direction (Schippers & Broekens, 2022).

In addition to the list above, Schippers et al. (2021) described the need of a dynamic spring stiffness for piles to capture the dynamic behaviour due to wind loads. The dynamic stiffness of the piles is part of the structural engineer's duty, but should still belong to the collaborative foundation design of the building as it includes interaction between superstructure and foundation. For instance, Schippers et al. (2021) looked into bi-linear pile behaviour including the static and dynamic stiffness and what length of the pile should be influenced by wind in the first place. For the influence zone of the pile by wind loads was defines up to a depth of NAP - 40 m, where the normal forces in the pile during loading, unloading, and reloading were relatively equal. However, this type of dynamic analysis (using D-Pilegroup) is not yet included in the NEN and goes beyond the scope of this research.

In order to improve the contemporary SSI design methodology (see following Section 2.1.3), a parametric study for s_1 settlements and a sensitivity analysis of s_2 settlements will be performed in Chapter 3 (Sections 3.1.3 and 3.1.5) for which the results will be summarised in Section 3.1.6. Afterwards, Chapter 3 (Section 3.2) will briefly discuss and compare a combination of aforementioned design methodologies to capture the different modelling approaches in a (s_2) settlement bandwidth for a faster, safer, and less conservative design process.

2.1.3 Soil-Structure Interaction Modelling

To sum up the first section of Chapter 2 and to test the hypothesis for the first research question, the following sub-section repeats the design steps taken during the generalised high-rise building process between geotechnical and structural engineers as summarised in Figure 2.17 at the end of this section. For steps 4 and 5, a combination of the detailed methods described in Sections 2.1.1 and 2.1.2 can be used to determine the final design.

Step 1:

Following the procedure thoroughly described at the start of Section 2.1, the first step of the design process results in the type (1, 2, or 3), stiffness (EA), and ULS load (in kN/m) of piles which is calculated by the structural engineer and shared with the geotechnical engineer. An example of ULS pile reactions using a simple SCIA model without mattress or redistribution of forces in the superstructure (due to soil settlements) is shown by Figure 2.11a.

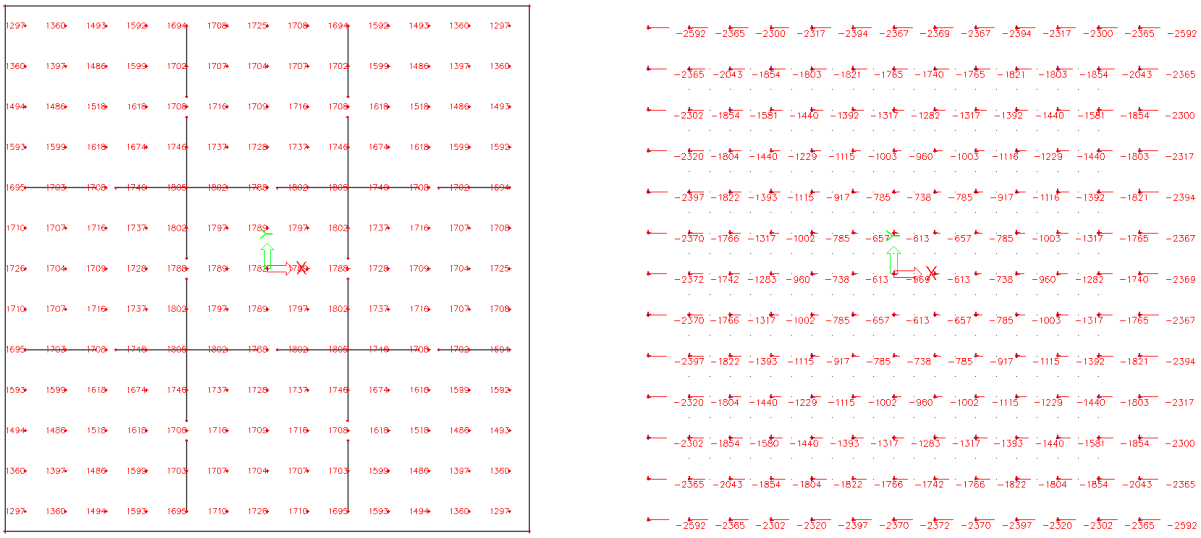

(a) **without** mattress model. (b) **with** mattress model.

Figure 2.11: **ULS** pile reactions in kN a) without, and b) with redistribution of forces in superstructure due to s_2 settlements as mattress model in SCIA. Figures C.3 - C.4 show an enlarged version of the SCIA results.

Step 2:

In the next step, using soil-structure interaction of piles, the geotechnical engineer determines the pile dimensions (diameter & length) and foundation level at which the individual or group bearing capacity exceeds the maximum pile load with a certain factor of safety. As a result, a table with multiple (linear) spring resistances of piles ($k_{v,1}$) representing s_1 settlements at 70% of the ULS load (or pile capacity) for different pile tips are send back to the structural engineer, see Table A.2 in Appendix A.4 for an example.

Step 3:

Next, the structural engineer determines the *quasi-permanent* SLS (surface) building loads based on the preliminary design of the structure including the weight of floors, walls and columns. This can be done with a simple hand-calculation or with the use of a SCIA model in which piles are modelled as pin supports having a (linear) spring resistance ($k_{v,1}$) as was determined by the geotechnical engineer in the previous step. The SLS building loads (in kN/m^2) can then be determined by dividing the calculated pile resultant force (kN) by the outer centre-to-centre distance of the piles (in m). The resulting surface loads are often presented to the geotechnical engineers as a plan view of the building, see Figure 2.12[1] for an example.

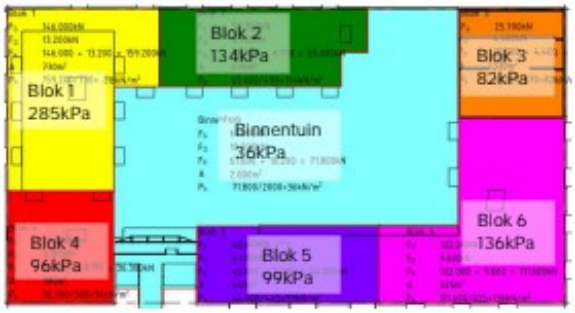

Figure 2.12: Building loads in kN/m^2 (or kPa) from a project in Amsterdam (Chortis et al., 2021).

Step 4:

Then, part of the building loads distributed to the deep soil layers below the foundation level and corresponding s_2 settlements are determined by the geotechnical engineer using Plaxis (3D). This is often done by embedded beams or (a variation on) the Tomlinson method, as was thoroughly explained in Section 2.1.1. Embedded beams require more computation time and cost, but can be beneficial and more accurate when a mix of foundation levels is required. At the end of this step, one horizontal cross-section (symmetric) or two (for an asymmetric tower) with u_z deformations at 4D below PTL are transferred from Plaxis to Excel as (s_2) settlement curves. Those settlement curves are send back to the structural engineer as input for SCIA.

Step 5:

The following step by the structural engineer can be divided in a methodology prior to 2018 using PD and another using a mattress model after 2018, as indicated by the blue arrows in Figure 2.17. Both methods were described in Section 2.1.2 and the main difference is defined by a design loop needed for the prescribed displacements method while this is optional for the mattress model method. This is where the research goal comes in, to improve the current methodology in such a way that this type of feedback loop to the geotechnical engineer becomes redundant. In essence, a structural engineer now models the piles as 2D beam elements and adds s_1 settlements as springs with $k_{v,1}$ at the bottom of the piles, see Figure 2.13, while the s_2 settlements are added as a SLS fitted mattress in the ULS SCIA model (Figure 2.13b). If the engineer decides to use PD, no individual piles are modelled and the s_2 settlements are added as as load case. Also, in this design step the geotechnical and structural engineer may reconsider a $k_{v,1}$ stiffness value beyond the elastic range ($\geq 70\%$) to run a non-linear analysis in SCIA instead of linear when this turns out better for the project to meet design criteria. For a non-linear analysis, piles are modelled as bi-linear springs, which is known as *aftoppen* in Dutch.

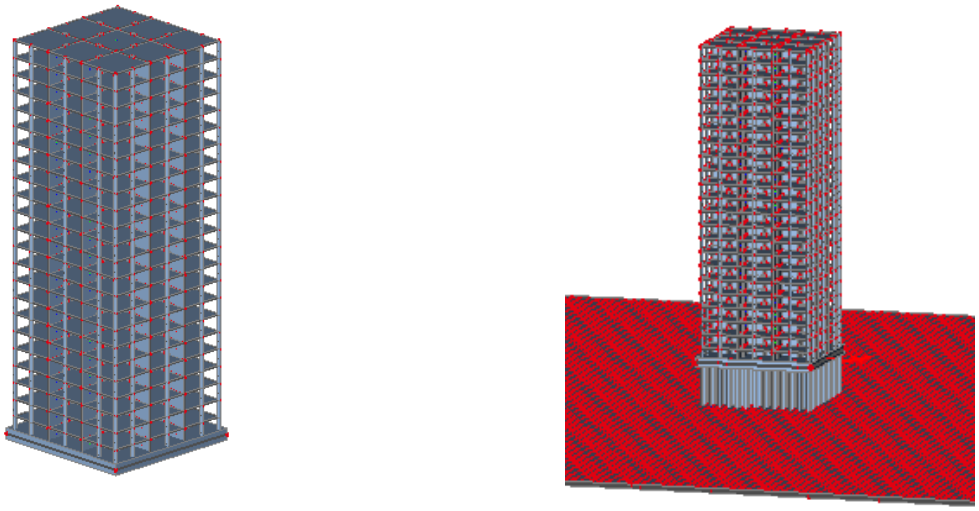

(a) basic model **without** mattress model.

(b) basic model **with** mattress (fit) model.

Figure 2.13: A theoretical example of a simple, symmetric tower structure in SCIA a) without, and b) with mattress model underneath basic building model.

Steps 6-8:

The final steps in the design process check if the resulting rotations of the (foundation of the) tower using the updated building loads (due to the predicted soil settlements) fall within the limits determined by building codes. If this does not satisfy, the process restarts as indicated by the dash lines in Figure 2.17. A feedback loop is less crucial for the mattress model method as it includes redistribution of forces resulting in a more realistic force flow towards the edges of the building instead of the center, see Figure 2.11b. Ideally, the redistributed forces would be split in zones of updated surface loads and still send back to the geotechnical engineer (in a plan view) to double check the s_2 settlements. A feedback loop for s_1 settlements appears insignificant as it may result only in millimeter differences, while s_2 could vary by centimeters due to the non-linear load-settlement response of soils below PTL.

In daily practice, the fitting of the E_{plate} and $k_{bedding}$ parameters of the mattress model is done in a separate FEM SCIA model only containing a plate of 1 m thick, linear springs underneath the plate and SLS quasi-permanent surface loads on top as a simplified version of Plaxis 3D embedded in SCIA. When a proper fit of u_z between the deformation of the 1 m plate from SCIA (Figure 2.14a) and the settlement curves 4D below foundation level from Plaxis 3D (Figure 2.14b) is found, the fitted parameters (E_{plate} and $k_{bedding}$) are added as mattress model (plate and linear springs) to the SCIA *Basismodel* with the entire structure and all ULS loading conditions including wind (Figure 2.15).

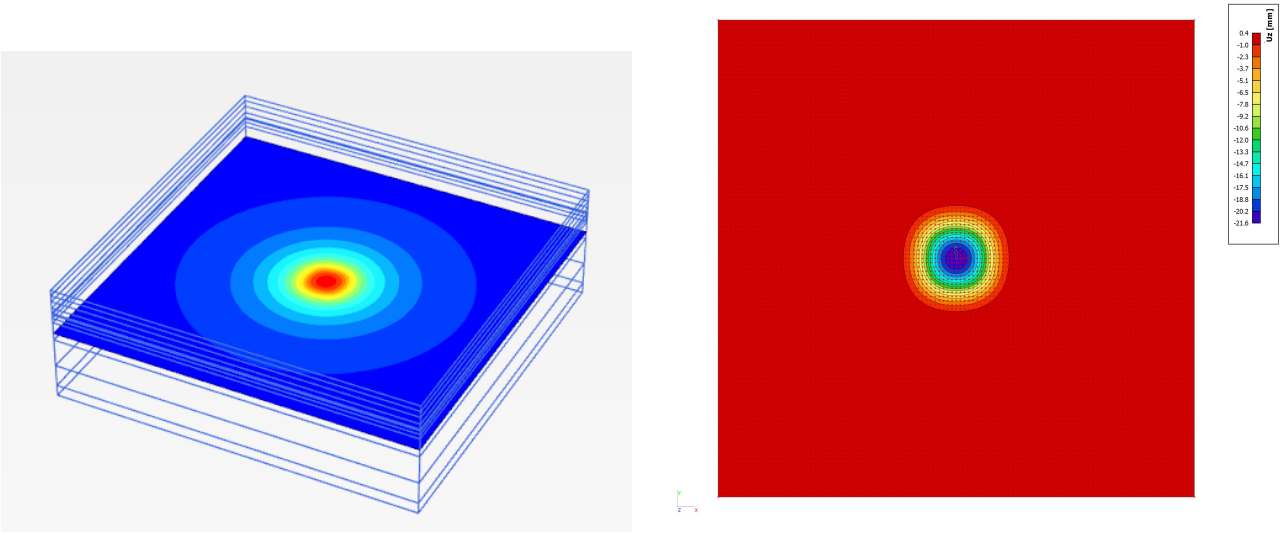

(a) **Plaxis 3D** deformations.

(b) **SCIA** deformations.

Figure 2.14: Deformations (u_z) of a) soil layers 4D below foundation level, and b) mattress model including load distribution to deep soil layers for s_2 settlements.

Simultaneously, an analysis with another ULS SCIA model without a mattress or s_2 settlements is run, see Figure 2.13a or *Basismodel* in Figure 2.15[1]. In short, the model without mattress represents the short-term loading conditions (without consolidation settlements) while the model with mattress symbolises long-term loading (with consolidation settlements). Both models are used by the structural engineer to manually check for each structural element in the superstructure what scenario (or SCIA model) governs. The structural element with the largest forces in SCIA governs and those forces are used for the final design of that specific element, which is often the SCIA model including s_2 settlements (as mattress model) and again emphasises the importance of this research in daily practice. Ultimately, the governing SCIA model results are used for the contract and final design phase of the high-rise building project. Based on the results from SCIA, structural plans are created by drafting software (i.e., Autodesk Revit or AutoCAD) for the final design phase. The plans are an important tool to communicate structural dimensions, reinforcement, expansion joints, opening sizes in floors and walls for installation and plumbing, and a finalised pile plan to the contractor.

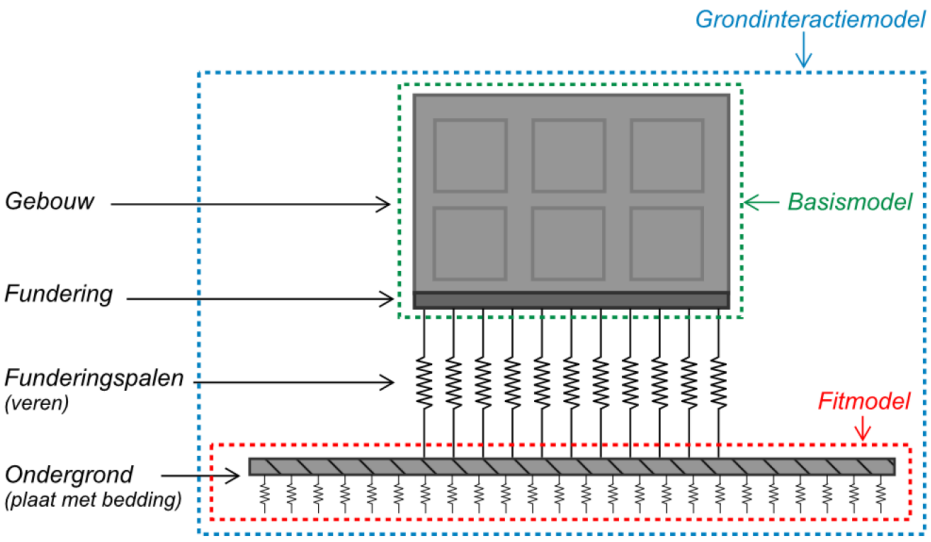

Figure 2.15: Mattress model approach (as SLS *fitmodel*) underneath basic building model in SCIA with all SLS and ULS load combinations (Bartels & van Gijn, 2020).

First Thoughts for Improvement

After thoroughly investigating and practicing the current design methodology including high-rise building settlements between two well-known and leading engineering companies in the Netherlands (Figure 2.16)[1], some first thoughts of potential improvements are listed below. Note that some of the improvements are already suggested in Figure 2.17 by the white boxes on the next page.

- How to make the methodology safer without having to iterate back to the geotechnical engineer, so the mattress model does not have to be fitted against SLS loads for extra safety?
- How to implement a realistic building stiffness in Plaxis 3D?
- What is the influence of pile spacing in D-foundations (geotechnical part step 2), Plaxis 3D (geotechnical part step 4) or SCIA (structural part step 5), and how can this be used in an updated design methodology to make safe changes in a pile plan without iterations?
- Is it possible to add an extra step (after step 6) as optimisation of the design process by adding the deformation results (u_z) of the mattress model as PD load case (instead of a plate with springs) to the basic ULS building model in SCIA? This may help to check the resulting forces for each structural element in one model that includes all SLS and ULS loading conditions for the final design.

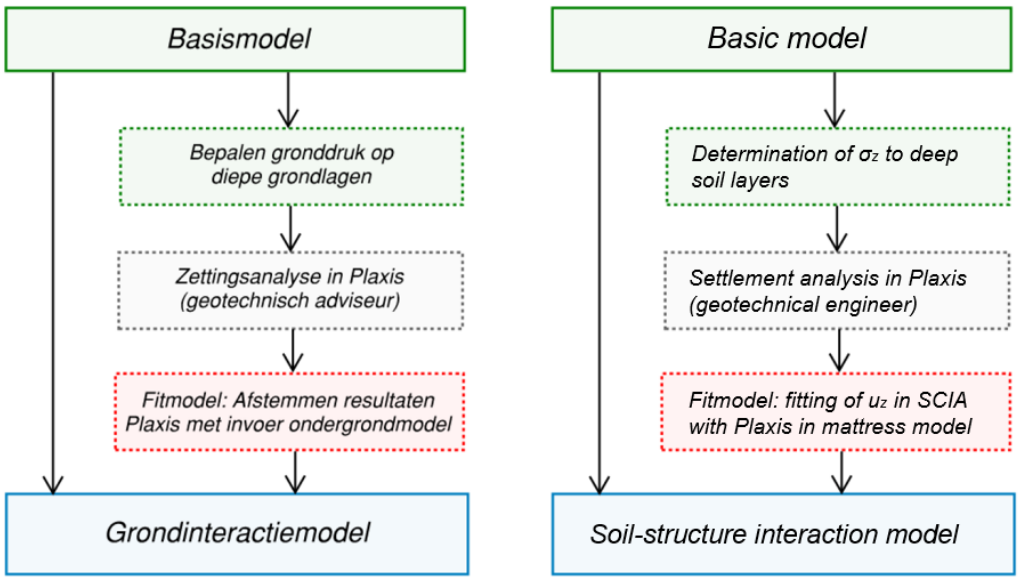

Figure 2.16: Simplified process of SSI mattress model in Dutch and English (Bartels & van Gijn, 2020).

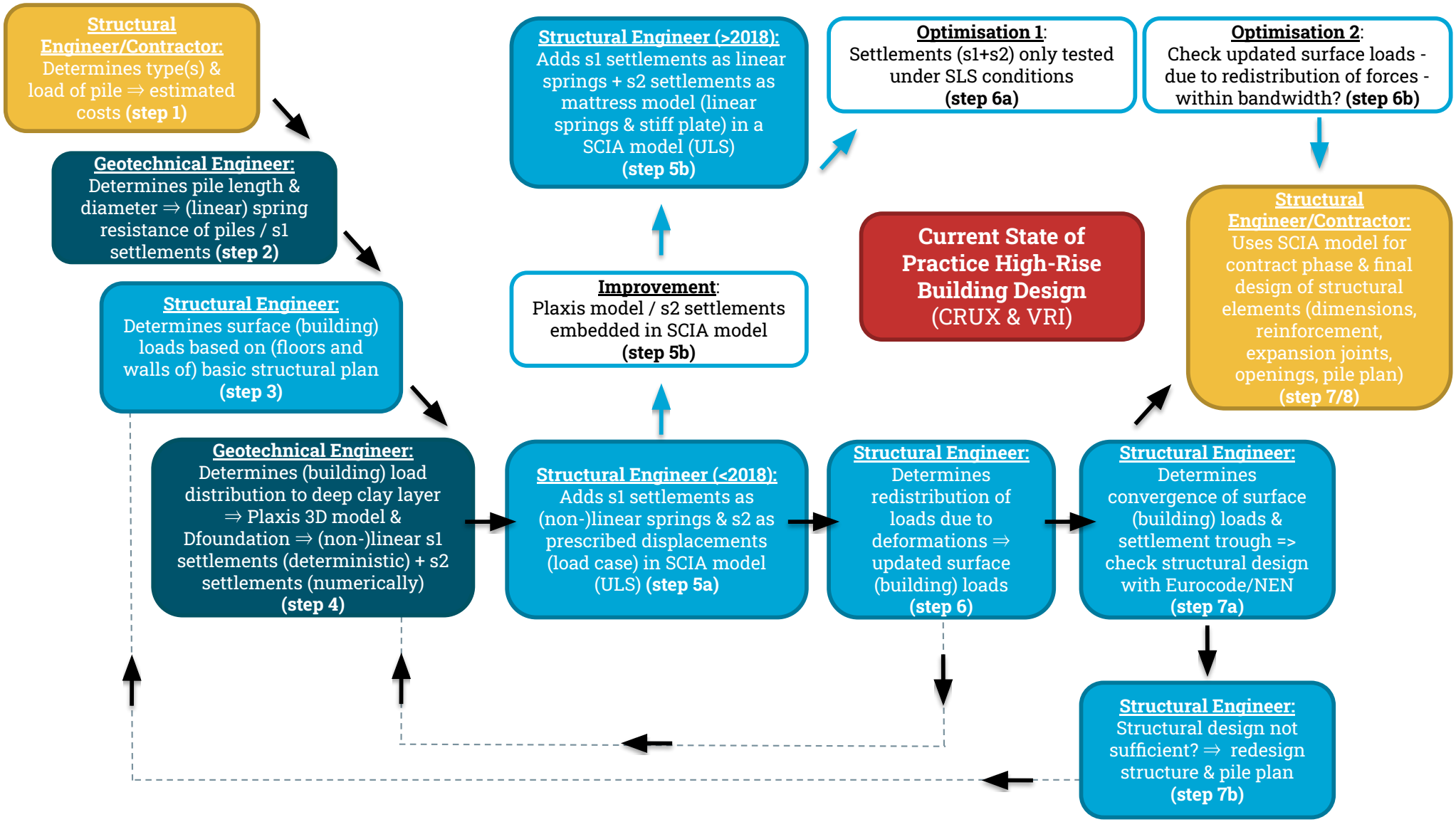

Figure 2.17: Old (black arrows) and current (blue arrows) design approach with proposed optimisation steps (white boxes) between geotechnical (CRUX) and structural (VRI) engineers.

2.2 Structural Loading Conditions according to Standard Codes

In structural engineering, a numerical analyses includes several loading conditions to test the stiffness and strength of a building. For high-rise building design (in SCIA), loading conditions can be divided in the following:

1. Structural load cases (*belastinggevallen* in Dutch)
2. Structural load combinations (*belasting combinaties*)
3. Structural load classes (*resultaatklasses*)

The most common load conditions in civil engineering are known as ULS (*rekenwaarde* in Dutch) and SLS (*representatieve waarde*). For settlement calculations, structural and geotechnical engineers should work with SLS values, which is often approximated by 70% of the ULS load, as was explained in Section 2.1. It is not necessary to take into account the full variable load, as it is very unlikely that every m^2 floor of a building is occupied at the same time. For a residential building, the ULS load should include the dead load and 40% of the live load (ψ_0), which should be checked by the structural engineer for the exact percentage. The final calculation or SLS load should include the ψ factor for the live loads to find the maximum (s_2) settlement due to the group effect of piles. The NEN makes a distinction between the following ψ factors for residential buildings:

1. $\psi_0 = 0.4$, used for the characteristic (= *karakteristieke*) load combinations
2. $\psi_1 = 0.5$, used for the frequent (= *frequente*) load combinations
3. $\psi_2 = 0.3$, used for the quasi-permanent (= *quasi permanente*) load combinations

Below follows an overview of the most common types of structural loads and corresponding partial factors for load combinations and classes in accordance with the NEN / Eurocode. Note that most of the partial factors depend on the function of the building (i.e., residences, offices, etc.) as it has an influence on the ψ factor and live loads, which affects both the SLS as ULS load combinations.

2.2.1 Structural Load Cases

In SCIA or other structural engineering software, the following structural load cases are often modelled:

1. Dead loads, denoted as G in the NEN
2. Live loads, denoted as Q in the NEN
3. Wind loads, denoted as Q_w in the NEN
4. *Optional: Prescribed displacements*

Prescribed displacements are an optional load case as this is only needed for structural models without an underlain mattress model to incorporate s_2 settlements. Below follows a short description of each type and common values for the type of load case. See Table C.3 in Appendix C for the exact load case inputs in SCIA.

Dead Loads (DL)

The dead loads (DL) can be described as the permanent load of a building which is always present during the lifetime of a structure. The DL can be subdivided in the following items:

1. Self weight of structure
2. Finishing works: screed & facade

When using SCIA, the self weight of the structure is calculated by the model itself once the direction is set to -Z. On the other hand, the screed (also known as a finishing floor on top of the structural floor) and facade loads need to be specified by the user as surface loads or line loads, respectively. Based on project properties chosen for this thesis, $\mathbf{1.4\ kN/m^2}$ is used for a screed (of 7 cm) and $\mathbf{3.0\ kN/m}$ for the facade of an average story height of 3 m.

Live Loads (LL)

The live loads (LL) can be described as building loads that vary over time and are related to the occupancy of the structure. The LL can be subdivided in the following items:

1. People & furniture
2. Partition walls

Based on standard codes, $\mathbf{1.75\ kN/m^2}$ is used for the movement of people and furniture while a surface load of $\mathbf{0.8\ kN/m^2}$ is used for partition walls. This results in a total live load of $\mathbf{2.55\ kN/m^2}$ acting on each floor of the high-rise structure.

Wind Loads (WL)

The wind loads (WL) can be described as a pressure and tensile force acting on a building due to wind coming from all directions. In SCIA, the wind directions are simplified to line loads acting on each story floor in X and Y components with each a negative and positive factor to model all directions. The value of the wind load is a function of the location and type of terrain for which the NEN distinguishes three types:

1. Urban (Category III)
2. Country (Category II)
3. Coastal (Category 0)

Often, a high-rise building in the Netherlands is considered to be constructed in a country terrain even though it is to be built within a city. This is because of the large heights of those type of buildings with respect to neighbouring structures. In addition to the location and type of terrain, the WLs are related to the tower height, see Tables C.5 and C.6 in Appendix C.1 for a typical WL calculation for a tower height of 69 m and a width of 24 m. For this symmetric geometry (see Section 3.2.1 for more details) in a country terrain (Category III) and coastal wind section (i.e., Zone II in Figure 2.18), the tower experiences (unfactored) wind loads

ranging from **2.20 kN/m** at the ground floor up to loads of **5.86 kN/m** near the roof for all four wind directions.

Verdeling van Nederland in drie windsnelheidsgebieden volgens figuur NB.1 uit NEN-EN 1991-1-4(NB).

Gebied I: Markermeer, Waddeneilanden en de provincie Noord-Holland ten noorden van de gemeenten Heemskerk, Uitgeest, Wormerland, Purmerend en Edam-Volendam;

Gebied II: Het resterende deel van de provincie Noord-Holland, de provincies Groningen, Friesland, Flevoland, Zuid-Holland en Zeeland;

Gebied III: Het resterende deel van Nederland.

Ter plaatse van de grenzen van de gebieden dient een continue overgang te worden aangenomen van 5 km vanaf de grenslijn afbouwend naar de grenslijn. Hanteer hierbij de winddrukwaarden (in Pa) uit de tabel 'Toetsingsdruk'.

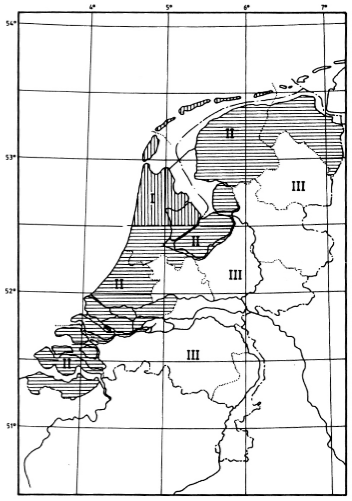

Figure 2.18: Wind sections in the Netherlands according to the NEN (Eurocode 7, 2005).

Prescribed Displacements (PD)

The PD load case can be described as displacements with a certain value that are enforced by the user, see Section 2.1.2. For instance, s_2 settlements fall under the type of displacements needed as an input for this load case. Due to time constraints, the scope of this research is limited to the s_2 mattress modelling approach only, so the use of PD to implement soil settlements in SCIA will not be further discussed in this chapter.

2.2.2 Structural Load Combinations & Classes

After assigning the type of loads to a structural model, a combination of loads are created to simulate different, extreme scenarios that the structure needs to be designed for. To model realistic loads, each combination contains partial factors (i.e., as ψ for LLs) as discussed above. Altogether, a structural model is required to be tested for at least the following combinations in accordance with the NEN:

- 7x SLS load combinations
- 10x ULS load combinations

See Table C.4 in Appendix C for the exact partial factors used for the 17 load combinations in SCIA.

Serviceability Limit State

As mentioned before, SLS load combinations consist of seven groups and are used to calculate the stiffness and displacements of a structure to ensure the building functions as intended. This thesis considers the following SLS load combinations in SCIA:

- 5x characteristic load combinations

- 1x frequent load combination
- 1x quasi-permanent load combination

For this thesis and (s_2) settlement analysis in general, the third load combination - the quasi-permanent load - is most important and considered most realistic due to the ψ_2 factor. In essence, the quasi-permanent load can be defined as follows:

$$Quasi - permanent = 1.0 \cdot \mathrm{DL} + \psi_2 \cdot \mathrm{LL} + 0 \cdot \mathrm{WL} = 1.0 \cdot \mathrm{DL} + 0.3 \cdot \mathrm{LL} \tag{2.8}$$

Thus, the load combination causing soil settlements is a function of the self weight & finishing works of a structure along with 30% of the live loads caused by the change of moving people, furniture, and partition walls inside a building at the same time. No WL is considered due to the short term condition of wind versus the long term condition of soil settlements.

Ultimate Limit State

In contrast with the SLS load combinations, ULS load combinations contain ten groups and are used to calculate the strength of a structure and the reinforcement needed to transfer maximum forces through structural elements down to the foundation (see Section 2.2.3) and load bearing soil layers. This thesis considers the following ULS load combinations in SCIA:

- 1x DL extreme load combination
- 1x LL extreme load combination
- 8x WL extreme load combinations

Considering the statistics behind partial factors recommended by Eurocode 7 (2005) are outside of the scope, this thesis will no further explain the background of different load combinations.

Load Classes

Once the load combinations are assigned in SCIA, the structural model gathers the combinations in two different classes:

- All 10x ULS load combinations
- All 7x SLS load combinations

In daily practice, the first load class (ULS) is used in SCIA to find the maximum force in the piles for the bearing capacity analysis of a pile group. The second load class (SLS) is used for s_1 settlements of an individual pile ($= k_{v,1}$) and s_2 settlements of a pile group. The bearing capacity calculations and settlement analysis as part of a piled foundation design will be explained in Sections 2.2.4 and 2.3 of this chapter.

2.2.3 Foundation Systems of High-Rise Buildings

Foundation systems for high-rise buildings generally fall under raft foundations, combined piled raft foundations, and piled foundations. The latter is the most common in the Netherlands due to Holocene soft soil deposits. The piles are needed to transfer the large loads from the superstructure down to the stronger, load-bearing sand layers. Due to the thick Holocene clay layers, piles in the Netherlands are often considered friction piles. Nonetheless, those type of piles are still called end-bearing in daily practice due to the large contribution of base resistance (in the Pleistocene sand layers). In other parts of the world, piles can be considered end-bearing piles as long as the piles transfer most of the load down to the bedrock.

Raft Foundation

In some parts of the world (i.e., Shanghai), the subsoil profile is strong and shallow enough to allow the use of only a shallow, raft foundation (see top of Figure 2.19) to transfer the load to bearing layers or almost directly to the bedrock underlying the top sand layers. An example of this type of foundation applied in the Netherlands is the *Witte Huis* in Rotterdam (Brassinga & van Tol, 1991). Another potential location for a (very thick) raft foundation could be explored in southern Amsterdam where the *Zuidas* is known for some large towers. The (deep) subsoil conditions at the Zuidas contain less clay and more sand in comparison to other parts of Amsterdam due to glacial periods reaching only the northern part of the city.

Piled Raft Foundation

Some parts of Europe (i.e., Frankfurt) and the Netherlands (i.e., Utrecht) contain more sand layers which allow for the use of a combined piled raft foundation, see bottom of Figure 2.19. Piles can transfer the load from the superstructure to the bearing layers, often the (second or third) Pleistocene sand layers. For instance, this system was used for the Galaxy tower in Utrecht (Van der Sluis, 2017)[1].

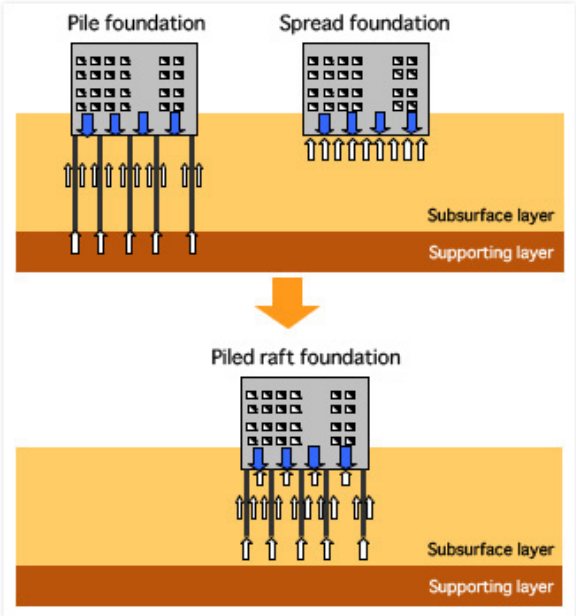

Figure 2.19: Different types of foundation systems for high-rise buildings (Abdelaziz, 2020).

Pile Foundation

In general, three types of piled foundations exist in the Netherlands in accordance with the NEN for load-settlement behaviour of a single pile:

1. **Type 1:** Soil displacement piles (*grondverdringend* in Dutch),
2. **Type 2:** Partial displacement piles (*weinig grondverdringend*),
3. **Type 3:** Non-displacement piles (*grondverwijderend*).

Besides the load-settlement behaviour of a pile, the type of pile chosen for a particular project heavily depends on the installation method and its effect on the surroundings (and environment) of the project, see Figure 2.20. Often, such as in urban areas, limitations are set on driving or hammering of piles due to noise pollution and the risk of vibrations, which favor non-displacement or screwed piles as an alternative solution over displacement piles. On top of that, the type of pile defines what type of load settlement curve (and corresponding stiffness behaviour) to choose in accordance with the NEN9997-1. The code distinguishes between type 1, type 2, and type 3 piles, which influences the expected (s_1) settlement of the design based on the applied load (see Figure 2.1). For this thesis, a short literature review was performed on the most common type of piles used in the Netherlands with regards to their applicability for high-rise buildings. A summary is shown by Table 2.1. It was concluded that the last three types of piles in the table (vibro, Fundex, and Tubex piles) are most applicable for contemporary towers. Driven concrete piles are also applicable for high-rise buildings, but are no longer used in densely populated areas due to disturbance. The piles are sometimes combined with an underwater concrete floor (UCF) and tension piles (such as GEWI bars and anchor bolts) for the uplift of the basement. Since compression loads are much larger than tensile loads for high-rise buildings, tension piles are not further considered in this thesis.

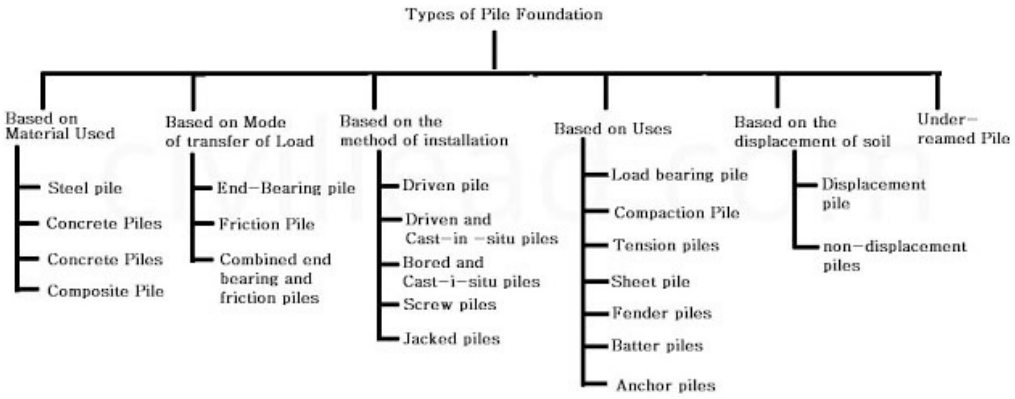

Figure 2.20: General distinction between types of pile foundation systems (Abdelaziz, 2020).

Table 2.1: Summary of piles commonly used in Dutch practice (Stichting Bouwresearch, 1995).

Type of Piles (English)	**Type of Piles (Dutch)**	**SSI Effects**	**Applicability High-Rise**	**Other Characteristics**	**Usage Period**
Driven timber pile	*Geheide houten paal*	Soil displacement pile (type 1)	Below GWL, **not applicable** for high-rise	Douglas fir, pine or larch wood, lengths of 20 m	1550 untill 1945 (Baas, 2001)
Driven (prefab) concrete pile	*Geheide (geprefabriceerde) betonnen paal*	Soil displacement pile (type 1)	Large compression forces, **less applicable** for high-rise	Prefabricated or in-situ, lengths of 35 m, bearing capacity of 3,500 kN	$>$ 1945 (Baas, 2001)
Bored concrete pile	*In de grond gevormde betonnen paal*	Non-displacement pile (type 3)	Very large compression forces, **applicable** for high-rise	Combined with bentonite, est. bearing capacity of 12,500 kN	$>$ 1930
Steel tube pile	*Stalen buispaal*	Soil displacement pile (type 1)	Tight workspace, renovations, **not applicable** for high-rise	Filled with concrete, lengths of 30 m, bearing capacity of 1,500-2,500 kN	$>$ 2000
Driven vibro pile	*Geheide vibro (combinatie) paal*	Soil displacement pile (type 1)	Deep building pits, excellent for tension and compression forces, **applicable** for high-rise	Filled with grout or concrete, often combined with UCF, bearing capacity of 3,500-5,000 kN	$>$ 1960
Screwed Fundex pile	*Geschroefde Fundex paal*	Soil displacement pile (type 1)	Large compressive & tensile strength, **very applicable** for high-rise	Filled with concrete, lengths of 35 - 40 m, est. bearing capacity of 2,500 kN	$>$ 1980
Screwed Tubex pile	*Geschroefde Tubex paal*	Soil displacement pile (type 1)	Large compressive & tensile strength, **very applicable** for high-rise (in soft soils)	Filled with concrete, lengths of 30 m, est. bearing capacity of 2,500 kN	$>$ 1980

2.2.4 Pile Capacity Analysis

In the Netherlands, the total bearing capacity (R_{total}) of a single pile (in kN) in accordance with the CPT based method is a function of the shaft capacity, the pile tip resistance, and the negative skin friction (see Eq. 2.9). The CPT was developed in the Netherlands in 1950's (Gavin, 2020) and many correlations exist between the cone end resistance, q_c, and the base and and shaft resistance of the pile using constant cone reduction factors (α_p, α_s):

$$R_{total} = R_{base} + R_{shaft,post} - F_{shaft,neg} \tag{2.9}$$

where,

$$R_{base} = \alpha_p \cdot q_c \cdot A_b \tag{2.10}$$

$$R_{shaft,pos} = L_s \cdot \pi \cdot d_s \cdot \Sigma\alpha_s \cdot q_c \tag{2.11}$$

The $\alpha_p \cdot q_c$ terms in Eq. 2.10 for the base resistance can be rewritten as $q_{b0.1}$, which is defined as the base resistance mobilised at a pile tip displacement equal to 10% of the pile diameter, D. The summed term in Eq. 2.11 can also be rewritten as the unit shaft or shear resistance, τ_f, along the length of the pile experiencing positive shaft friction (Gavin, 2020), see Eq. 2.12 and 2.13 below:

$$q_{b0.1} = \alpha_p \cdot q_c \tag{2.12}$$

$$\tau_f = \alpha_s \cdot q_c \tag{2.13}$$

In Dutch practice, the τ_f value in Eq. 2.13 can also be defined as $q_{s;max;z}$, while the $q_{b0.1}$ value in Eq. 2.12 is often replaced by $q_{b;max}$ in the NEN and obtained by Koppejan's CPT averaging technique described below:

$$q_{b;max} = \frac{1}{2} \cdot \alpha_s \cdot \beta \cdot s \cdot \left(\frac{q_{c;I;avg} + q_{c;II;avg}}{2} + q_{c;III;avg}\right) \tag{2.14}$$

Furthermore, A_b is the area of the pile toe, L_s is the length of the pile and d_s is the diameter of the pile shaft where SSI effects result in positive shaft friction. In this thesis it is chosen to neglect the effects of negative skin friction ($F_{shaft,neg}$) as this can be a whole study by itself (Jacobs, 2021) and is not relevant for deep foundation (s_2) settlements. According to Jacobs (2021), negative skin friction can be described as the downwards movement of soil over time due to reconsolidation of remolded soil, groundwater drawdown, or surcharge loading. This results in soil 'holding on' to an individual pile instead of vice versa (= positive skin friction increasing the shaft capacity). However, the effects are minimal for s_2 settlements of pile groups for high-rise buildings in Dutch soil conditions (Meinhardt & de Koning, 2021)[1] as the building load is much larger in comparison to the negative skin friction developed over time. Thus, for this research it is more interesting to look at the total bearing capacity of a pile group (Q_{total}), described by the following equations:

$$Q_{total} = Q_b + Q_s \tag{2.15}$$

where,

$$Q_b = q_{b;0.1} \cdot B^2 \tag{2.16}$$

$$Q_s = L_s \cdot 4 \cdot B \cdot \tau_f \tag{2.17}$$

The pile group dimensions, L_s and B, are illustrated by Figure 2.21 below:

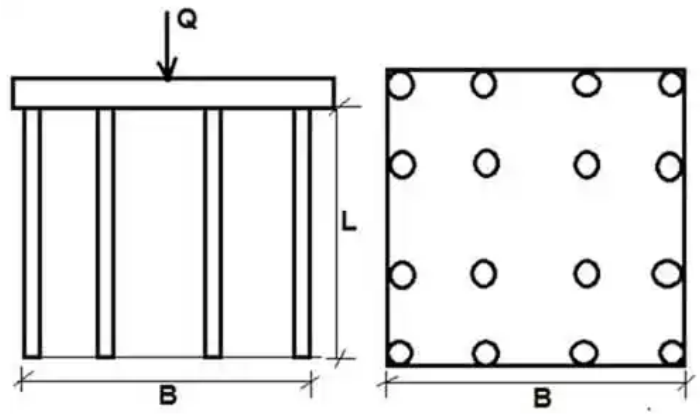

Figure 2.21: Basic set-up of a squared pile group (Abdelaziz, 2020).

In general, Q_{total} is a function of the sum of the individual bearing capacities in the pile group, which is influenced by the spacing between the individual piles. For instance, when the pile spacing for bored piles is less than $3 \cdot D$, the efficiency of the group's bearing capacity significantly reduces and a simple summation is no longer applicable. For driven piles, the efficiency even reduces when the center-to-center distance falls below $4 \cdot D$ due to different, soil displacement installation methods and consequent SSI effects. The efficiency of a pile group, η_g, is then described by:

$$\eta_g = \frac{Q_{total}}{N \cdot R_{total}} \cdot 100 \tag{2.18}$$

where N is the total number of piles in the pile group. In most cases, η_g is less than or equal to 1.0, meaning the piles behave more like a foundation block for the bearing capacity. On the other hand, the efficiency for settlement behaviour of pile groups is often above 1.0. This can be explained by the stiffer load-settlement response of a pile group in comparison to a single pile. Settlements due to group effects will be further explained in Section 2.3.2.

2.3 Settlement Analysis in Foundation Design

The most common settlement definitions in foundation design are described by s_1 and s_2 settlements:

1. $\mathbf{s_1}$ **settlements** = settlement at the top of an individual pile (= soil layers from GL − 4D below PTL)
   - $s_b + s_{el}$
   - pile tip settlement + elastic compression of pile
   - f (R_{shaft}, R_{base})
   - through deterministic analysis (i.e., D-Foundations (2022) or PileCore (2022))
   - ↪ added to structural FEM models as a spring stiffness ($k_{v,1}$)
2. $\mathbf{s_2}$ **settlements** = settlement of soil layers below foundation level (= 4D below PTL − $\Delta\sigma'_v \leq 20\% \cdot \sigma'_{v0}$)
   - elastic compression of sand + primary & secondary consolidation of clay + creep of soils
   - through numerical analysis (i.e., Plaxis 3D (Brinkgreve, 2014))
   - ↪ added to structural FEM models in a variety of ways

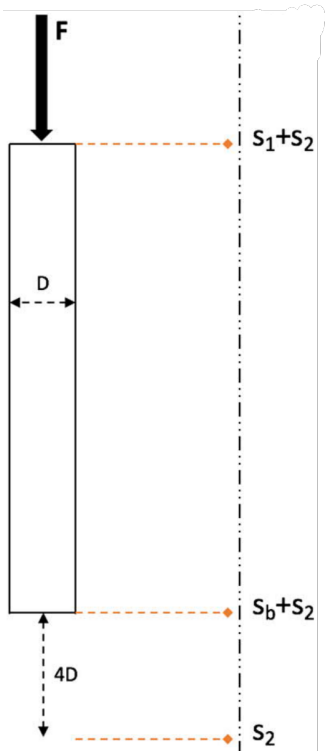

Figure 2.22: Settlement definitions due to pile group effects according to the NEN 9997-1 (Frissen, 2020).

It was clear from the problem statement of this thesis (Section 1.2) that settlements due to deep layers below the PTL - also called s_2 settlements - are determined interactively and result in decimeter differential settlements for buildings in comparison to only millimeter differences for s_1. This big difference can be explained by an increased stress bulb development when multiple piles are introduced within a certain pile spacing of one another (Meinhardt & de Koning, 2021), see Figure 2.23.

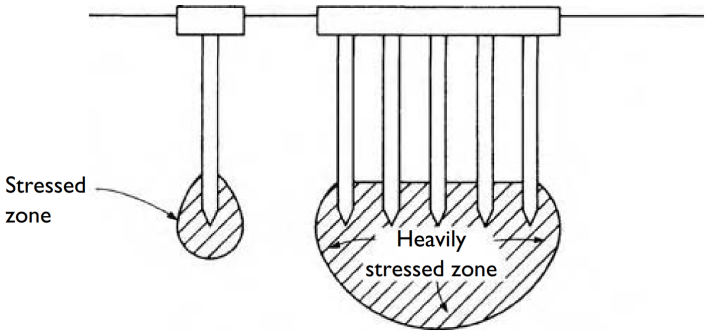

Figure 2.23: Stress distribution below single pile (left) and pile group (right) (Tomlinson & Woodward, 2008).

As mentioned in Section 2.1.1 and supported by Tomlinson and Woodward (2008), the deepest layers that should be considered for s_2 settlements (where $\Delta\sigma'_v \leq 20\% \cdot \sigma'_{v0}$) are visualised in Figure 2.24. Note that σ_z in this figure is the same as $\Delta\sigma'_v$ in this thesis report:

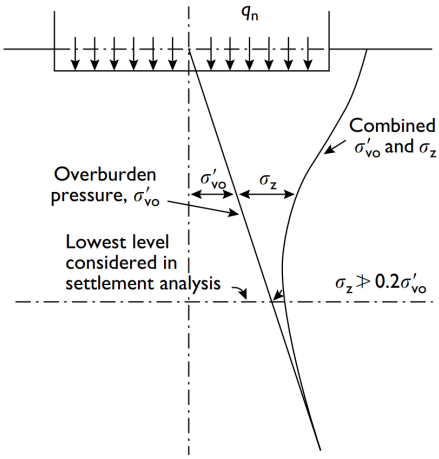

Figure 2.24: Zone of influence for pile group (s_2) settlements (Tomlinson & Woodward, 2008).

To better understand (the development of) foundation settlement analysis in FEM software, this section will elaborate on some of the earliest and most common non-numerical approaches for individual pile (Section 2.3.1) and pile group settlements (Section 2.3.2).

2.3.1 Settlement Analysis of Individual Piles (s_1)

The pile tip settlement (s_b) can be determined by the use of the load-displacement curves from the NEN9997 (see Figure 2.1) when the dimension of the pile's cross-section (D_{eq}) is known along with the applied ULS load ($F_{s,tot}$). Based on the pile's stiffness (AE), the elastic compression of the pile (s_{el}) is then found by:

$$s_{el} = \frac{F_{s,tot,k} \cdot L_{pile}}{E \cdot A_{shaft}} \tag{2.19}$$

Where $F_{s,tot,k}$ is 70% of the ULS load or total pile capacity, L is the length of the pile from pile head to pile tip, E is the stiffness of the pile (i.e., 20x10^9 N/m^2 for concrete, 200x10^9 N/m^2 for steel, and 3.6x10^9 N/m^2 for timber), and A_{shaft} is the cross-sectional area of the pile shaft.

The s_1 settlement of a single pile is then the summation of s_b and s_{el}. In literature, a variety of (semi-)empirical and analytical methods are described to determine the settlement of an individual pile. This thesis will briefly summarise the following two methods:

1. Empirical Method by Vesic (1977)
2. Analytical Method by Poulos & Davis (1968)

Empirical Method by Vesic

Empirical methods are often based on experience and test data rather than soil mechanic principles. For this reason, empirical methods are only applicable and trustworthy for similar situations as the test data or site. An example of a (semi-)empirical method is described by Vesic (1977). Vesic distinguishes the following three contributions to individual pile settlements:

1. Load transfer at the pile tip (w_{pp}),
2. Load transmitted along the pile shaft (w_{ps}),
3. Axial deformation (or elastic compression) of the pile shaft (w_s).

For the pile tip settlement (w_{pp}) and shaft displacement (w_{ps}), Vesic (1977) proposed the following correlations based on the empirical factors C_p and C_s, which can be found in literature tables (Vesic, 1977):

$$w_{pp} = \frac{C_p \cdot Q_p}{D \cdot q_0} \tag{2.20}$$

and

$$w_{ps} = \frac{C_s \cdot Q_s}{L_p \cdot q_0} \tag{2.21}$$

Where L_p is the pile length, D the pile's diameter, Q_p the base resistance, Q_s the shaft resistance and q_0 the ultimate point resistance. Note that w_s in Vesic's correlations is determined in a similar way as s_{el} discussed above (see Eq. 2.19) based on the NEN9997-1. The total settlement according to Vesic (1977) is then found by:

$$w_t = w_{pp} + w_{ps} + w_s \tag{2.22}$$

Analytical Method by Poulos & Davis

Another, more elaborated method to determine the s_1 settlements was proposed by Poulos and Davis (1968). Poulos and Davis (1968) divide the pile into uniformly loaded elements for which the base and shaft are decoupled, resulting in normal stresses acting on the base and shear stresses along the shaft. This method is based on theoretical soil mechanics principles and the theory of elasticity, making the method only applicable for linear elastic perfectly plastic materials. Considering soil deposits for foundation design often show inhomogeneity due to anisotropic behaviour, this method is not further discussed or applied in this thesis.

2.3.2 Settlement Analysis of Pile Groups (s_2)

Fleming et al. (2009) explain that the combined surface settlement profile of individual piles in a pile group under the same point load can be calculated with the use of an interaction factor. The interaction factor (α_i) is a function of the surface settlement profile for individual piles and the spacing of neighbouring piles. Based on this factor, additional settlements due to adjacent piles can be calculated.

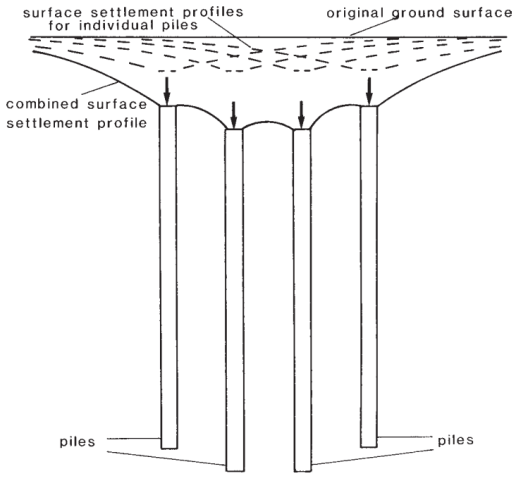

Figure 2.25: Principle of superposition for pile group settlement (profiles) under the same loading (Fleming et al., 2009).

In most high-rise building design, the foundation consists of pile groups with a cap or foundation plate on top. This part of the foundation structure then redistributes the load from the superstructure to the piles instead of equal point loads. For this reason, it is challenging to apply Fleming's analytical approach to a pile group of high-rise building structures. Many other approaches exist to predict the settlements of a pile group, however, this thesis will limit the literature review to the following approaches used in Dutch daily practice:

1. NEN9997-1 Method
2. Equivalent Raft Approach by Terzaghi and Peck
3. Equivalent Raft Approach by Tomlinson

NEN9997-1 Method

Section 7.6.4.2 of the NEN9997-1 proposes an analytical solution for the s_2 settlements of pile groups for which the spacing between the piles is less than ten times the pile diameter ($10 \cdot D$). If the foundation design meets those requirements, the group settlement can be found by Eq. 2.23. For pile foundations of a spacing equal or larger than 10D, $s_2 = 0$ may be implied.

$$s_2 = \frac{m^* \cdot \sigma'_{v;4D} \cdot 0.9 \cdot \sqrt{A_{4D}}}{E_{ea;gem}} \tag{2.23}$$

where,

$$\sigma'_{v;4D} = \frac{F_{fund}}{A_{4D}} \tag{2.24}$$

and,

$$E_{ea;gem} = factor \cdot q_c \tag{2.25}$$

where m^* is a dimensionless factor based on the geometry of the foundation (i.e., 0.95 for a square and 0.96 for a circular slab), $E_{ea;gem}$ is the average stiffness of the layers 4D below PTL, $\sigma'_{v;4D}$ is the vertical effective stress due to F_{fund} (= sum of individual pile loads) acting on A_{4D}, and A_{4D} is the projected total area of the load four diameters below PTL under a spread of 45°.

Since the dimensionless factor in Eq. 2.25 disappeared from the Eurocode 7 (2005), Frissen (2020) proposed a lower limit of 3.0 and an upper limit of 5.0 to predict a preliminary range of settlements based on the cone resistance q_c of the layers 4D below PTL. These factors are based on the Deltares user manual and previously used factors from the Eurocode.

However, this analytical method can only be performed for the elastic part of the bearing layer and does not include time-dependent behaviour such as creep or consolidation. Therefore, this method can be considered a first approximation of the settlement bandwidth, but is unreliable for final settlement predictions of soil stratigraphy including compressible layers beneath the foundation level.

Equivalent Raft Approach by Terzaghi & Peck VS Tomlinson

Prior to the load spread method proposed by Tomlinson, Terzaghi and Peck (1967) first analysed a simplified settlement approach for pile foundations, see Figure 2.26. Using the increased dimensions of the foundation area, the settlement (S) for both traditional methodologies can be computed with the use of Eq. 2.26.

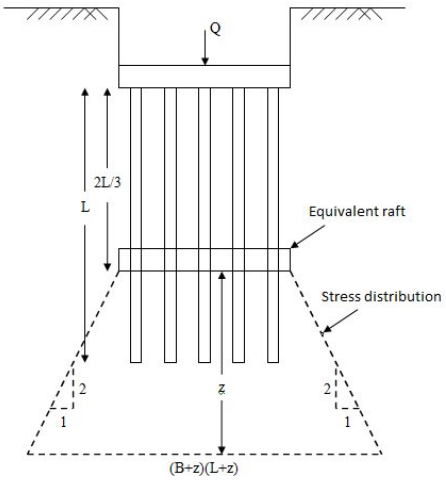

Figure 2.26: Equivalent raft approach according to Terzaghi and Peck (Terzaghi & Peck, 1967).

$$S = \frac{q \cdot B \cdot (1 - \nu^2)}{E_s} \cdot I \tag{2.26}$$

where, s is foundation settlement, q is the base pressure, B is the foundation width, ν is the Poisson's ratio of soil, E_s is the modulus of elasticity of underlain soil, and I is a coefficient which differs for a rigid square foundation (0.82) and flexible square foundation (0.95). Both methods assume that the pile foundation works as a block system with a triangular distribution of the shaft friction for which the centre of gravity is 2/3 from the top (1/3 from the bottom). This empirical value was validated by several case studies in the field where the foundation was designed with friction piles. For those reasons, both methods are most reliable for pile design dominated by shaft resistance over base resistance, which is the case for most of the high-rise buildings (being) constructed in Netherlands.

The main difference between both load spread methods is the assumption regarding the stress distribution above and below the equivalent raft approach. According to Yengar and Olgun (2017), Terzaghi and Peck predict 40% more settlements when compared to Tomlinson for the same problem geometry and load, see Figure 2.27. Terzaghi and Peck (1967) may be too conservative or Tomlinson and Woodward (2008) too favorable. Thus, careful application of the Tomlinson method should be considered in this thesis.

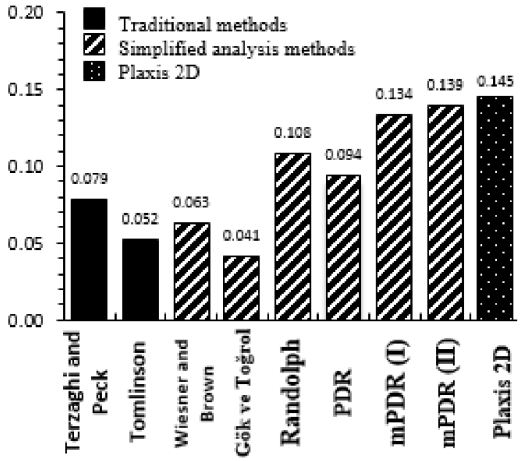

Figure 2.27: Comparison between traditional design methods and numerical methods (Yengar & Olgun, 2017).

In addition, the equivalent raft approach developed by Tomlinson and Woodward (2008) can be applied to pile groups in soft soil conditions or a bearing stratum underlain by soft soils, such as the soil stratigraphy typical for the Dutch deltaic area. In addition, Tomlinson can be modified for use in a layered stratum as shown in Figure 2.28. The latter is preferred over the method by Terzaghi and Peck.

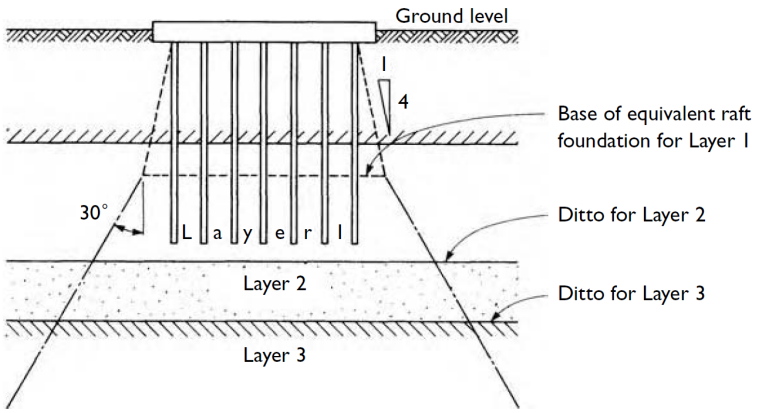

Figure 2.28: Load distribution based on Tomlinson's equivalent raft approach for a layered soil stratigraphy (Tomlinson & Woodward, 2008).

2.4 Common Constitutive & Material Models

Considering the compressible soils underneath the second Pleistocene sand layers (i.e., Eem, Drenthe, or Kedichem clays, etc.) are over-consolidated, this thesis aims to find more insight whether high-rise building loads result in consolidation settlements to test the main s_2 settlement assumption in daily practice. This will be done by running soil tests in Plaxis (see Section 3.1.4) with the use of constitutive models in FEM similar to the previous research performed by Hoefsloot and Wiersema (2020) for several towers in Rotterdam. Below follows a short summary of the compressibility of deep clay layers and the most common material models in Plaxis for their applicability of foundation settlement analysis.

2.4.1 Compressibility of Deep Clay Layers

In 2019, MOS Grondmechanica BV was able to obtain (undisturbed) samples of Eem clay at a depth of NAP -27.24 m in IJburg (eastern Amsterdam) and perform an oedometer laboratory experiment resulting in typical 1D compression test results, see Figure 2.29 below.

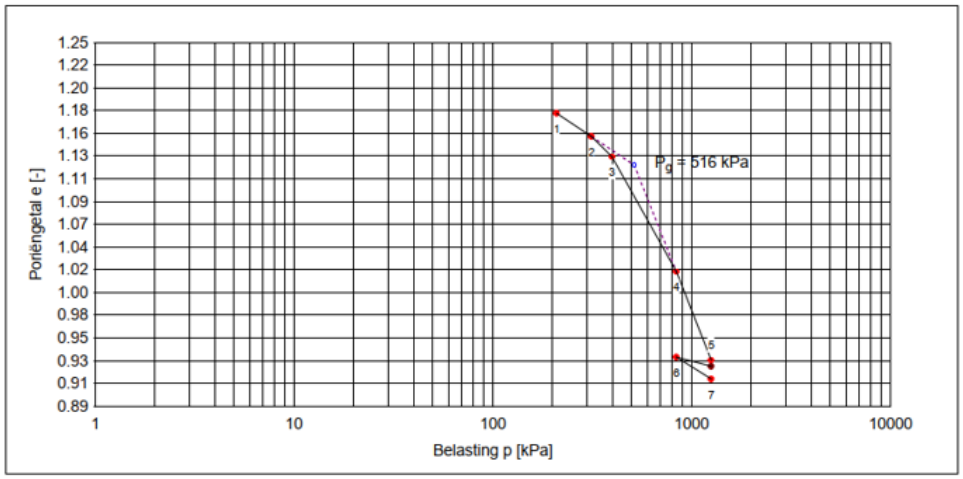

Figure 2.29: Compression tests performed by MOS Grondmechanica BV on Eem clay in Amsterdam.

Using seven load steps, they determined the following Bjerrum compressibility coefficients:

$$C_r = 0.103 \quad , \quad C_c = 0.428 \quad , \quad C_{sw} = 0.050 \quad \text{and} \quad C_\alpha = 0.0076 \tag{2.27}$$

According to international literature (Bjerrum), soils are considered soft when C_c/C_s falls in the range of 5 - 10. For this particular Eem clay sample, the ratio is $0.428/0.05 =$ **8.56** and is thus considered soft and compressible. See Figures A.5 and A.4 in Appendix A for the complete oedometer test results of this sample.

As mentioned above, Section 3.1.4 will elaborate more on the behaviour of Eem clay (in Plaxis). For this reason, below follows a short summary of the theory, model parameters, characteristics, and limitations of the constitutive models accessible in Plaxis 2D and 3D to describe the behaviour of cohesive (i.e., clayey) and cohesionless (i.e., sandy) soils under high-rise building loads in FEM. Note that this thesis only describes the models interesting for this research topic and a more extensive list can be found in the Plaxis manuals (Brinkgreve, 2021).

2.4.2 Soft Soil Model (SSM)

The soft soil model, also abbreviated as SSM, is applicable for near-normally consolidated clays, clayey silts, and peats with E_{oed} values between 1 and 4 MPa. According to Brinkgreve (2021), NC clays behave ten times softer than NC sands under 1D compression. For highly over-consolidated soils, SSM shows a stress state in which the horizontal stress (σ'_{xx}) is higher than the vertical stress (σ'_{yy}). Table 2.2 lists the main model parameters, for which the compression indices can be derived from oedometer results, see Figure 2.30.

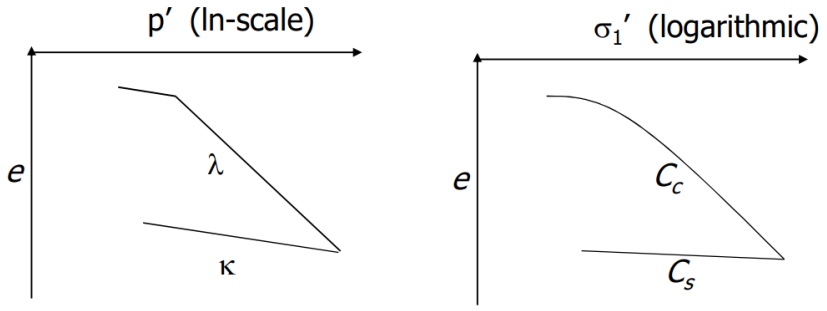

Figure 2.30: Compression parameters from oedometer test results versus soft soil theoretical model (Brinkgreve, 2020b).

Table 2.2: Model parameters and definitions for SSM (Brinkgreve, 2020b)

Symbol	Definition
λ^*	Modified compression index
κ^*	Modified swelling index
ν_{ur}	Poisson's ratio for unloading / reloading
c'	Cohesion
ϕ'	Friction angle
ψ	Dilation angle
K_0^{NC}	Stress ratio σ'_{xx} / σ'_{yy} in primary 1D compression
M	K_0^{NC} related parameter

Note that Plaxis uses Jaky's equation (1948) to approximate the stress ratio:

$$K_0^{NC} = 1 - sin(\phi') \tag{2.28}$$

The stress ratio, also known as lateral earth pressure coefficient, also influences the parameter M, which describes the slope of the critical state line in p-q plane. Parameter M can be approximated by:

$$M \approx 3.0 - 2.8 \cdot K_0^{NC} \tag{2.29}$$

In addition, the default value of 0.15 for ν_{ur} is advised by the Plaxis manual for both SSM and SSCM.

Characteristics of SSM (Brinkgreve, 2020a)

- Partially based on the Cam-Clay theory; plastic volumetric strain instead of void ratio,
- Not a Critical State model; can model dilatancy at failure,
- Logarithmic stress-strain relationship; stiffness linearly dependent on mean effective stress (p'),
- Cap hardening; generates plastic volumetric strain in primary compression,
- Elastoplastic behaviour in primary compression,
- Elastic behaviour in unloading and reloading,
- Memorizes the pre-consolidation pressure, σ'_p
- Stiffness is stress-dependent and stress-path dependent,
- M is a function of K_0^{NC} instead of ϕ,
- MC failure criterion.

Limitations of SSM (Brinkgreve, 2020a)

- Not applicable for other types of soil,
- Less suitable for non-compressive stress paths,
- Not recommended for excavations and pure unloading,
- Goes directly to final strength (no peak strength and softening),
- Deformation behaviour heavily depends on K_0^{NC},
- No secondary compression (creep),
- Isotropic model; no anisotropy.

2.4.3 Soft Soil Creep Model (SSCM)

The soft soil creep model, also known as SSCM, has similar characteristics as the SSM in Plaxis. However, SSCM includes time-dependent effects of soil soils such as creep or secondary compression, see Figure 2.31. For deep foundations of high-rise buildings, initially OC soil layers can reach a state of normally consolidated (NC) due to the effects of the newly introduced building loads. Such a softer response in soil behaviour can lead to additional creep settlements of soil layers below foundation level. For both 1D and 3D models, the SSCM includes elastic (Hooke's Law) and creep strains (viscoplastic flow rule): $d\epsilon^e$ and $d\epsilon^c$. In 3D, plastic strains according to MC failure criterion, $d\epsilon^p$, are also included in the division of strains, see Eq. 2.30.

$$d\epsilon = d\epsilon^e + d\epsilon^c + d\epsilon^p \tag{2.30}$$

Table 2.3 lists the main model parameters for which ϕ ranges from 20 to 30 degrees for soft clay under the assumptions of ≈ 0.2 for ν_{ur} and 1.0 for K_0 on average. For the stress ratio approximation it is assumed that

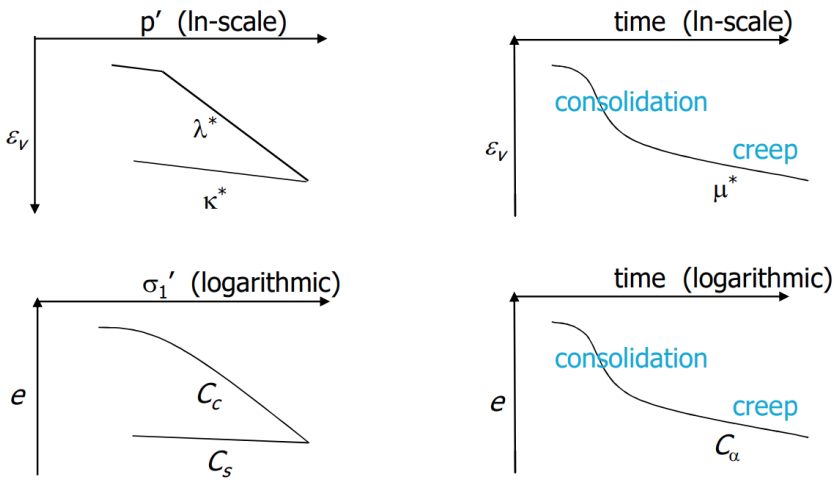

Figure 2.31: Compression parameters from oedometer test results versus soft soil theoretical model (Brinkgreve, 2020b).

during unloading the average stress state is an isotropic stress state, so $\sigma'_{xx} = \sigma'_{yy}$. Note that the SSCM generates creep strains as long as there is effective stress, which is generally dominated by initial stresses due to self weight in foundation design. Thus, deep clay layers modelled with the use of SSCM in Plaxis will creep even without additional loading and is heavily influenced by the initial OCR and λ^* / μ^*. For this reason, it is important to fit the OCR to the initial strain rate contributing to autonomous surface settlements (see Eq. 1.2).

Table 2.3: Model parameters and definitions for SSCM (Brinkgreve, 2020b)

Symbol	Definition
λ^*	Modified compression index
κ^*	Modified swelling index
μ^*	Modified creep index
ν_{ur}	Poisson's ratio for unloading / reloading
c'	Cohesion
ϕ'	Friction angle
ψ	Dilation angle
K_0^{NC}	Stress ratio σ'_{xx} / σ'_{yy} in primary 1D compression
M	K_0^{NC} related parameter

Characteristics of SSCM (Brinkgreve, 2020a)

- Stress-dependent stiffness (same as SSM),
- Elastic unloading/reloading (same as SSM),
- Distinction between primary loading and unloading-reloading (same as SSM),
- Memory of preloading (same as SSM),
- Irreversible volume strain upon primary loading (same as SSM),
- MC failure criterion (same as SSM),

- Elastic strains related to change in effective stress,
- Creep strains related to change in pre-consolidation stress,
- Secondary compression,
- Compression induced creep as well as shear induced creep,
- Irreversible strains by visco-plasticity instead of plasticity,
- Ageing of pre-consolidation pressure.

Limitations of SSCM (Brinkgreve, 2020a)

- Deformation strongly influenced by the M (or K_0^{NC}) parameter,
- Initial OCR influences initial creep strain rate and pre-consolidation stress,
- Creep and settlements unrealistic when stress state dominated by the initial stresses (due to self weight),
- Isotropic model; no anisotropy,
- No softening behaviour,
- Does not include structure (bonding).

2.4.4 Hardening Soil Model (HS)

The hardening soil model (HS) is a newer, non-linear model for both soft and stiff soils and is depth-dependent, which former models (i.e., LE, MC or Hyperbolic / Duncan-Chang) did not incorporate. The origin of this model is similar to the Hyperbolic model - also known as the Duncan-Chang model - which describes a hyperbolic function for the stress-strain behaviour under drained compression conditions in a triaxial test. However, the Hyperbolic model does not involve dilatancy. On top of that, the HS model is a double hardening model. A distinction can be made between two main types of hardening, for which the (yield) cap can expand due to plastic straining:

1. Shear (or friction) hardening; models irreversible strains (primary deviatoric loading),
2. Compaction hardening; models irreversible plastic strains (primary compression).

Shear hardening will continue until the maximum shear strength according to MC is reached and compaction hardening occurs in a similar way as the SSM. The HS model requires the input parameter m, which is 1.0 for soft soils simulating logarithmic compression behaviour. For sands, values between 0.5 and 1.0 are sufficient. Table 2.4 lists the main model parameters for HS, which are visualised for a drained triaxial and oedometer test in Figure 2.32. In addition, the default value of 0.2 for ν_{ur} is advised by the Plaxis manual for both the HS and HSS models.

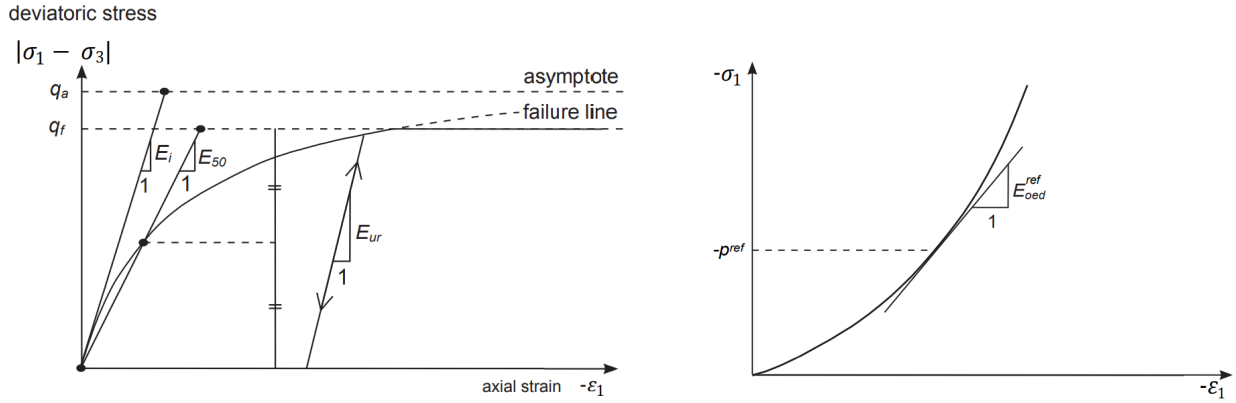

(a) Triaxial.

(b) Oedometer.

Figure 2.32: Stress-strain hyperbolic and stiffness HS parameters from a) drained triaxial, and b) oedometer tests (Brinkgreve, 2021)

Table 2.4: Model parameters and definitions for HS (Brinkgreve, 2020b)

Symbol	Definition
E_{50}^{ref}	Secant stiffness from triaxial test at reference pressure
E_{oed}^{ref}	Tangent stiffness from oedometer test at p^{ref}
E_{ur}^{ref}	Reference stiffness in unloading / reloading
m	Rate of stress dependency in stiffness behaviour
p^{ref}	Reference pressure (100 kPa)
ν_{ur}	Poisson's ratio in unloading / reloading
c'	Cohesion
ϕ'	Friction Angle (peak)
ψ	Dilation angle (peak)
R_f	Failure ratio q_f / q_a (i.e., 0.9 for Duncan-Chang)
K_0^{NC}	Stress ratio σ'_{xx} / σ'_{yy} in 1D primary compression
m	Power for stress-level dependency of stiffness

Characteristics of HS (Brinkgreve, 2020a)

- Stress (path) dependent stiffness according to a power law (m),
- Hyperbolic stress-strain relationship in axial compression,
- Plastic straining due to primary deviatoric loading (E_{50}^{ref}),
- Plastic straining due to primary compression (E_{oed}^{ref}),
- Elastic unloading / reloading (E_{ur}^{ref}),
- Memory of preconsolidation stress,
- Preferred for OC soils in comparison to MC model,
- Well suited for excavations,
- MC failure criterion

Limitations of HS (Brinkgreve, 2020a)

- No peak strength and softening,
- Immediate residual strength,
- No accumulation of strain or pore pressure in cyclic loading,
- Does not include creep behaviour,
- Isotropic model; no anisotropy,
- Difficulties with very soft soils ($E_{50}^{ref}/E_{oed}^{ref} > 2.0$).

2.4.5 Hardening Soil Small Strain Stiffness Model (HSS)

Similar to the HS model, the HSS model also depends on the depth and resulting vertical effective stresses acting on the soil. The main difference between the HS model and its updated version (the HSS model) is based on the very small range in which soil can be considered truly elastic. This is an important observation considering the HS model assumes elastic behaviour during unloading and reloading. In other words, the HS model may overestimate the soil's ability to recover from applied straining (Brinkgreve, 2021). In reality, soil stiffness decreases non-linearly with increasing strain (amplitude) due to plastic straining and should be accounted for in foundation design, see Figure 2.33. The HSS model includes this type of strain-dependent stiffness. Plastic strains can be modelled by strain hardening in both models and Brinkgreve (2021) defines very small strains as $\epsilon < 10^{-6}$. According to Brinkgreve (2020b), models without a strain-dependent stiffness (i.e., SSM, SSCM, and HS) may overestimate the width of the (s_2) settlement curve in foundation design of high-rise buildings. This is because the strains further away from the foundation are very small and the resulting settlements are over-predicted by the previously mentioned models.

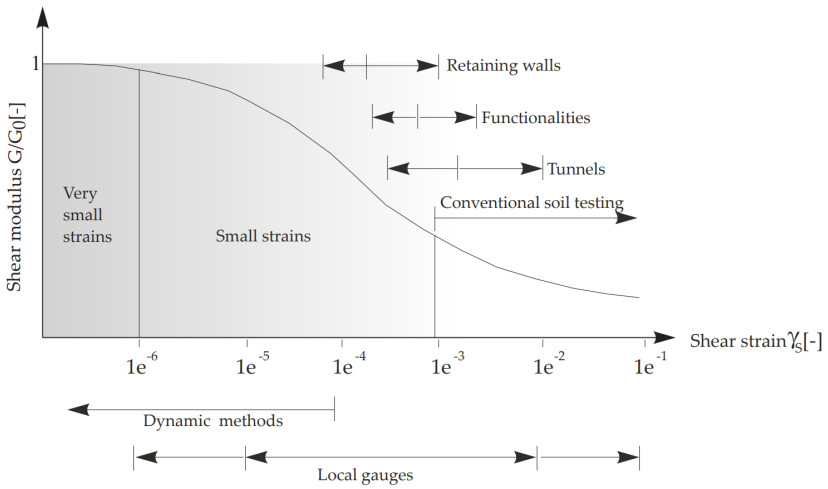

Figure 2.33: Characteristic S-shaped stiffness reduction curve and applicability for soils (Brinkgreve, 2020b).

Table 2.5 lists the main model parameters for HSS, which are visualised in Figure 2.34. Note that it involves the same parameters as the HS model in addition to the small-strain parameters G_0^{ref} and $\gamma_{0.7}$.

Table 2.5: Model parameters and definitions for HSS (Brinkgreve, 2020b)

Symbol	Definition
E_{50}^{ref}	Secant stiffness from triaxial test at reference pressure
E_{oed}^{ref}	Tangent stiffness from oedometer test at p^{ref}
E_{ur}^{ref}	Reference stiffness in unloading / reloading
G_0^{ref}	Initial or reference shear stiffness at small strains
$\gamma_{0.7}$	Shear strain at which G has reduced to 72.2%
m	Rate of stress dependency in stiffness behaviour
p^{ref}	Reference pressure (100 kPa)
ν_{ur}	Poisson's ratio in unloading / reloading
c'	Cohesion
ϕ'	Friction Angle
ψ	Dilation angle
R_f	Failure ratio q_f / q_a (i.e., 0.9 for Duncan-Chang)
K_0^{NC}	Stress ratio σ'_{xx} / σ'_{yy} in 1D primary compression
m	Power for stress-level dependency of stiffness

The two HSS small-strain parameters can be retrieved by the following equations and Hardin-Drnevich correlation:

$$G_0^{ref} = \frac{E_0^{ref}}{2(1+\nu_{ur})} \tag{2.31}$$

and,

$$\gamma_{0.7} = \frac{1}{9G_0} \cdot [2c'(1+cos(2\phi')) - \sigma'_1(1+K_0)sin(2\phi')] \tag{2.32}$$

Together, the two parameters describe the following hyperbolic formula as the base of this constitutive model:

$$G_s = \frac{G_0}{1+0.385\gamma/\gamma_{0.7}} \tag{2.33}$$

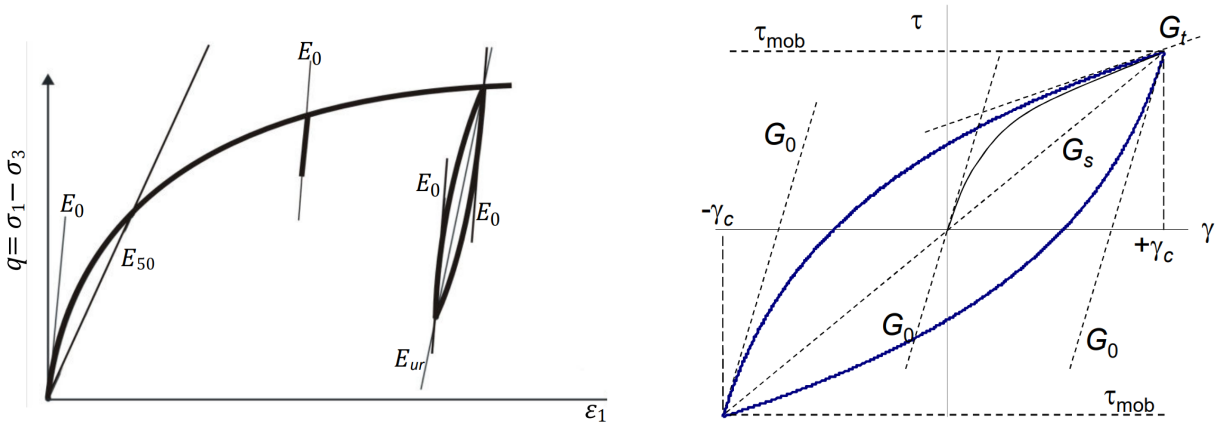

(a) Triaxial.

(b) Cyclic shear.

Figure 2.34: HSS stiffness parameters from a) a drained triaxial test, and b) a cyclic shear test (Brinkgreve, 2021)

Characteristics of HSS (Brinkgreve, 2020a)

- Stress dependent stiffness according to a power law; m (same as HS),
- Hyperbolic stress-strain relationship in axial compression (same as HS),
- Plastic straining due to primary deviatoric loading; E_{50}^{ref} (same as HS),
- Plastic straining due to primary compression; E_{oed}^{ref} (same as HS),
- Elastic unloading / reloading; E_{ur}^{ref} (same as HS),
- Memory of preconsolidation stress (same as HS),
- Preferred for OC soils in comparison to MC model (same as HS),
- MC failure criterion (same as HS),
- Well suited for vibrations, excavations, retaining walls and tunnel settlements,
- Large stiffness at small strain levels (using modulus reduction curve),
- Includes hysteresis; stiffness restarts at small-strain stiffness, G_0, at strain reversal (i.e., cyclic loading),
- Applicable for dynamic analysis; allows energy dissipation (enclosed by hysteresis loop) and damping.

Limitations of HSS (Brinkgreve, 2020a)

- No peak strength and softening,
- Immediate residual strength,
- Does not include creep behaviour,
- Isotropic model; no anisotropy,
- Difficulties with very soft soils ($E_{50}^{ref}/E_{oed}^{ref} > 2.0$).

2.5 Effects of Building Stiffness & Load Redistribution

Soil-structure interaction (SSI) of a building is a function of the behaviour of the superstructure as well as its foundation system and underlain soil deposits. Forces acting on the superstructure will be transferred down - through columns and walls - to the foundation and ultimately spreads to the subsurface by skin friction along the pile and base forces at the bottom of the piles. Over time, the resulting stresses and compression of the soil layers then affect the pile (group) behaviour and load transfer in the superstructure leading to a (re)distribution of forces. This SSI process will continue until a force equilibrium is reached.

The type of superstructure - or more specifically - the stiffness of the superstructure has been determined to have a significant effect on the building's SSI and settlements according to Breeveld (2013), Zoidi (2015), Odijk (2017), Frissen (2020), and others. Determining the building's stiffness without modelling the whole building's structural elements appears to be rather difficult. However, the settlement curves should always fall within two building stiffness extremes: 1) infinitely flexible, and 2) infinitely stiff. See Figure 2.35 below.

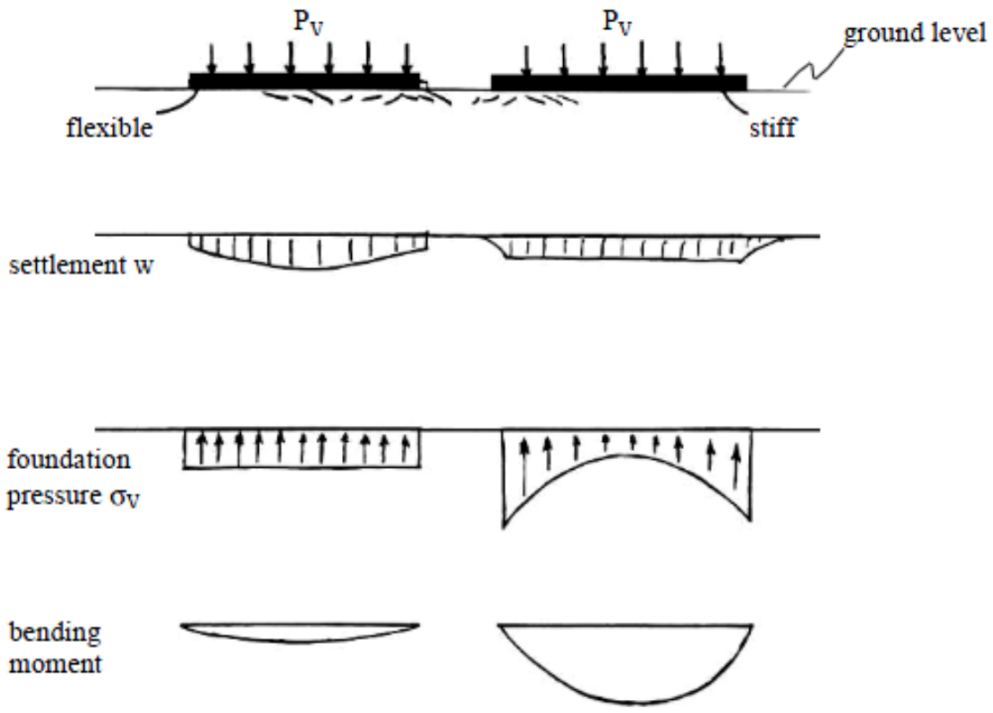

Figure 2.35: Effects of (building) stiffness on (differential) settlements (Zoidi, 2015).

In the scenario of a flexible building, one can see that the peak and resulting differential settlements (= difference between center and corner settlements) are larger in comparison to a stiff building. A flexible building will thus result in less redistribution of loads in the superstructure due to soil settlements. However, for the stiff building, the load will distribute along the elements towards the edges if the building as a function of the building stiffness and modulus of sub-grade reaction of the soils. As a result, the structural elements will settle uniformly (= less differential settlements), but the settlement effects on the surroundings are much larger for a stiffer building. For the stiffness scenarios in between the two extremes, a relative stiffness or stiffness ratio (k_r) can be determined based on the following formula (Breeveld, 2013):

$$k_r = \frac{Et^3}{12 \cdot E_s L^3} \tag{2.34}$$

where, E is the Young's Modulus of the slab, E_s is the stiffness of the soil(s), t is the thickness of the slab, and L is the length of the slab. For $k_r \leq 0.01$, the structure can be defined as flexible (scenario 1) while a structure with a $k_r \geq 0.1$ can be considered stiff (scenario 2). For structures within this range, a SSI calculation is deemed necessary. Stiffer elements within this type of building structure will attract a larger portion of the load resulting in higher bending moments and additional settlements in comparison to less stiff elements.

2.5.1 Modelling Building Stiffness in FEM

For aforementioned reasons, settlement predictions without (proper) modelling of building stiffness will result in more extreme (differential) settlements. Building stiffness is a function of the combined stiffness values of a building's structural elements and the interaction between those. For instance, Zoidi (2015) investigated several modelling approaches to include the (building) stiffness in Plaxis 3D. The research focused on *De Rotterdam* tower(s) in Rotterdam and concluded that the piles, foundation plate and cores of the building contributed to most of the building's overall stiffness. The stiffness of the columns was negligible, but was needed to distribute the loads correctly. However, Zoidi (2015) also considered computational costs and concluded that modelling the entire building in Plaxis resulted in too much computation time. Instead, Zoidi (2015) recommended modelling only the excavated basement (floor) along with the cores and columns of the building while applying only the dead load of the superstructure to the ground floor, see Figure 2.36.

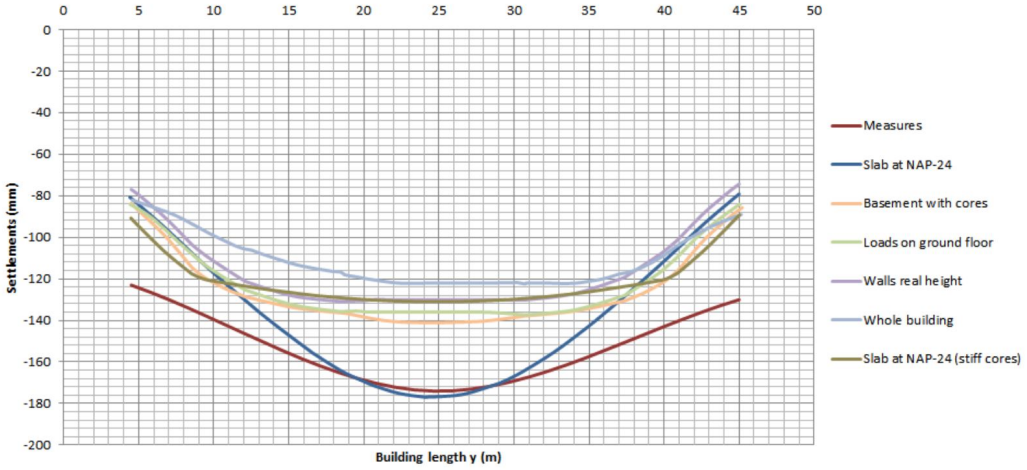

Figure 2.36: Settlements curves from Plaxis 3D versus measurements for *De Rotterdam* (Zoidi, 2015).

On top of that, the stiffness in x-direction is not equal to the y-direction for most high-rise buildings. To simplify the building stiffness in FEM, the SSI modelling in this thesis are limited to symmetric buildings only.

Building Stiffness in SCIA

The structural model in SCIA requires a stiffness input as the Young's Modulus (E) for each type of structural element. Structural elements are often split into the following types:

1. Foundation piles,
2. Foundation plate (or basement/ground floor),
3. Floors,
4. Walls,
5. Columns,
6. Lintels (above door or window openings).

The 1D structural elements can be assigned a specific cross-sectional area (based on a library), which is often done for the piles, columns and lintels in a separate menu in SCIA. On the other hand, thicknesses of floors, plates, and walls (2D structural elements) are specified in the structure tab. See Appendix C.1 for examples of material stiffness used in this thesis.

Building Stiffness in Plaxis 3D

The bending stiffness (EI) for a foundation plate in Plaxis can be calculated by multiplying the Young's modulus (E) of the material by the moment of inertia (I):

$$EI = E \cdot \frac{1}{12} \cdot b \cdot h^3 \tag{2.35}$$

where b is the in-plane width and h the height of the plate. The input can be retrieved from the structural model (in SCIA). The material model of the line columns in Plaxis are modelled as anchors for which the stiffness is determined by EA. See Appendix B.1 for examples of material stiffness used in this thesis.

The main difference of the material models for structural elements between Plaxis and SCIA are the units for the stiffness and weight. Furthermore, in Plaxis 3D the geometry of the element (i.e., thickness or diameter) is part of the material model while SCIA separates the geometry inputs from the material properties. Both FEM software results heavily depend on the mesh coarseness. For this reason, it is important to run a mesh optimisation beforehand and select the same mesh density for both FEM models in SCIA and Plaxis. For instance, a coarser mesh in SCIA will result in a much stiffer response of the individual structural elements, while a coarser mesh in Plaxis results in less compression of soil layers.

By trial-and-error in Plaxis 3D, it was found by the author that the weight of the structural elements in Plaxis do not result in the same DL as calculated by SCIA. Because of these findings, the materials models (shown in Tables B.10 and B.11) are updated with a unit weight, γ, of 0 kN/m^3 and replaced by an equivalent (surface) load representing the building weight in kN, kN/m, or kN/m^2 (kPa) for use in Sections 3.2 and Appendix B.2.1.

2.6 Conclusions Research Question 1

This chapter provided insight on the following items and consequent sub-research question 1 to better understand the contemporary design methodology:

Question 1:

"What is the current design practice between a geotechnical engineer and a structural engineer to determine the foundation settlements of a high-rise building (in the Netherlands)?"

As was expected, several geotechnical and structural modelling approaches are being used in daily practice to predict and model foundation settlements appropriately. In the author's opinion, the SSI mattress modelling approach is a better methodology (in comparison to prescribed displacements for instance), because it appears to be a good, first attempt to streamline the design process. The mattress model approach seems to allow structural engineers to get rid of the feedback loop to a geotechnical engineer once the mattress model underneath a structure (in SCIA) is fitted against the settlement results of the (Plaxis 3D) geotechnical model.

However, the current mattress modelling approach assumes linear behaviour of the soil and the s_2 settlement curve(s) computed by the geotechnical engineers do not take into account realistic pile (group) behaviour for s_1 settlements. On top of that, settlements and wind loads are currently used simultaneously in the total SCIA structural engineering model while the Plaxis 3D geotechnical model is lacking a realistic building stiffness or load redistribution within the superstructure.

For those reasons, the next chapter will focus on a parametric study and sensitivity analysis of input parameters to follow a probabilistic approach in coupling the SCIA and Plaxis numerical models based on several model scenarios in each software. This will help in determining the bandwidth and model uncertainty of the current SSI design methodology for high-rise building settlements, as is visualised in Figure 2.37 below.

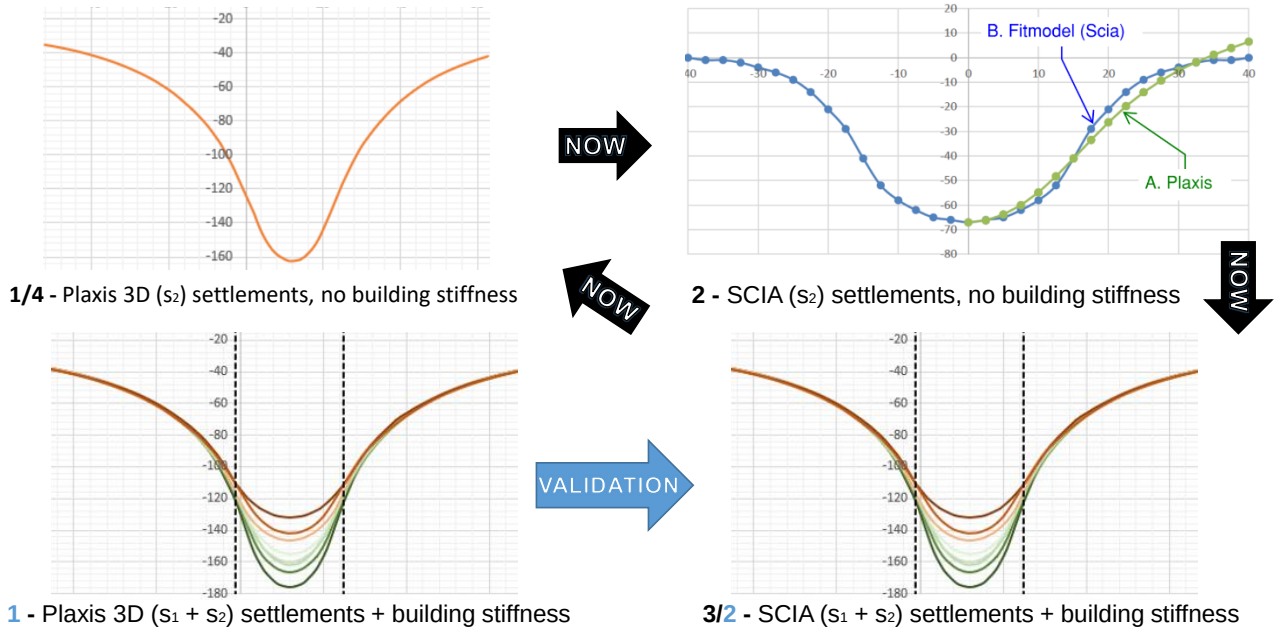

Figure 2.37: Current and proposed soil-structure interaction design methodology for foundation settlements.

Chapter 3

State-of-the-Art Design Approach

This chapter will seek to find an answer for the second research question:

Question 2:

"What is the error margin of the current design practice and is it possible to streamline it by safely eliminating the iterative process between geotechnical and structural models while maintaining realistic SSI effects?"

Hypothesis 1: From a geotechnical standpoint, verification of the current design approach could be achieved by investigating the sensitivity of the following: **1)** redefining the input for the soil parameters of currently used constitutive material models in Plaxis (i.e., SSCM and HSS) and/or load-settlement and stress-strain curves of extant models, **2)** understanding the limitations of currently used constitutive models and load distribution procedure to the deep soil layers, **3)** implementing non-linear soil behaviour by analysing different stiffness parameters, **4)** reconsidering a more realistic modelling approach of piles as bi-linear springs or adding in the stiffness of the building structure, and **5)** investigating the effects of different pile factors and pile design methods. Ultimately, a comprehensible translation of non-linear settlement curves as outputs of geotechnical models should be made accessible as an input with a certain bandwidth for structural models (i.e., mattress model), which can then be used as an interactive design tool for structural engineers without tedious iterations and infinite feedback loops during the design phase of a high-rise building structure.

Hypothesis 2: From a structural standpoint, the modelling approach can be tested by: **1)** analysing the current use of material linearity as a representation of soil and piles (as linear springs) to incorporate more realistic, non-linear soil and material behaviour without the loss of computational power and time, and **2)** listing assumptions and explaining limits of the current methodology for discussion in future recommendations.

3.1 Parametric Study of Soil and Pile (Group) Behaviour in FEM

Simple settlement approximations previously described in Chapter 2 for pile capacity (defining s_1) and load distribution procedures (defining s_2) are applied to a typical, piled foundation system (Fundex 560) in the Netherlands for a theoretical, symmetric tower to be constructed on a representative soil profile in the North of Amsterdam. The settlement approximations in this chapter are followed by a numerical pile load test and soil test under representative high-rise building loads (= 382 kPa or 1,302 kN) in Plaxis 3D. The latter is used primarily to check the stresses at pile tip level in the second Pleistocene sand layer and what portion of this stress will be distributed to the compressible clay layers underneath.

3.1.1 Approximation of s_1 Settlements

To better understand the pile behaviour of the most commonly used pile for high-rise buildings in the Netherlands, a first approximation for settlement of an individual pile (s_1) will be performed based on analytical methods described in Section 2.3. The s_1 and s_2 approximations will be performed separately for a Fundex 460/560 installed in a group of 169 piles with a center-to-center spacing of 24 m underneath a foundation plate of 26 m x 26 m. In order to use realistic, unfactored building loads, a simple and symmetric high-rise building with 23 floors is constructed in SCIA similar to the building shown in Figure 2.13 (Section 2.1.3). The resulting SLS pile loads for a pile group spaced 2 m apart is based on the dead loads of the building and quasi-permanent portion of the live loads as described in the SLS load combination described in Section 2.2.2. A more elaborate description of the SCIA model, load combinations, and problem geometry will be explained in Section 3.2.1 when the current SSI design loop (as described in Section 2.1.3) will be applied to this simple high-rise building structure. For the soil stratigraphy of this analysis, the fictive tower will be constructed in the North of Amsterdam. Figure 3.1 below shows the soil layers used to calculate the required PTL using D-Foundations and resulting bearing capacity (R_{total}) of the Fundex 460/560 pile.

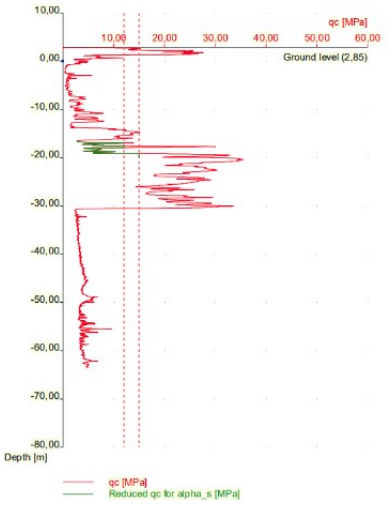

Tabel 1 Globale bodemopbouw

Nr.	Grondtype	B.k. laag [m NAP]
1	Ophooglaag, zand	+0,4 à 2,5
2	Samendrukbare lagen, lokaal op variabele dieptes doorsneden met zandige tussenlagen	-0,5
3	Siltige klei	-3,0
4	Hollandveen	-4,5
5	Wadafzetting klei	-5,0
6	Wadzand	-9,5
7	Hydrobiaklei	-12,5
8	Eerste Zandlaag	-13,5
9	Kleiige tussenlaag (Alleröd)	-16,5
10	Tweede Zandlaag	-19,0
11	Eemklei	-30,0
12	Drenthe klei	-48,0
13	Derde Zandlaag	-64,5

Figure 3.1: Average soil profile for North of Amsterdam provided by CRUX (De Jong & Meinhardt, 2021).

Firstly, the elastic compression (s_{el}) of the Fundex pile can be approximated with the use of Eq. 2.19. This was found to be $\approx$ **10 mm** based on a PTL of NAP - 23 m, GL of NAP + 2.85, shaft diameter (d_{eq}) of 460 mm, and Young's Modulus of concrete:

$$s_{el} = \frac{1,302 \cdot 10^3 N \cdot (23m + 2.85m)}{20 \cdot 10^9 N/m^2 \cdot \pi(\frac{0.460m}{2})^2} = 0.10m = 10mm \tag{3.1}$$

Secondly, using the normalised load-displacement curves in Figure 2.1 from the NEN9997-1 for a type 1 pile (current design approach) and type 2 pile (updated design approach by Gavin (2020)), the pile tip settlement (s_b) can determined. For a mobilised shaft friction ($= R_{s;k}/R_{s;k;max}$) of ≈ 0.35, values of **1 mm** and **3 mm** are found for a type 1 and type 2 pile, respectively. Note that these values are very small and for most scenarios in practice the s_b will be closer to 10 mm due to a smaller factor of safety (FoS). Adding the 1 mm and 3 mm to the computed s_{el} above, results in an approximate s_1 range of **11 mm - 13 mm** for a Fundex 460/560 under an SLS load of 1,302 kN.

3.1.2 Approximation of s_2 Settlements

Thirdly, the settlements due to the deep, compressible layers below foundation level (s_2) can be approximated using several analytical methods as described by the theory in Section 2.3.2. Based on the arguments made in this section, the NEN9997-1 method (see Eq. 2.23 - 2.25) is chosen to approximate the range of s_2 settlements for a pile group consisting of Fundex 460/560 piles:

$$A_{4D} = (24m + 2 \cdot (4 \cdot 0.560m))^2 = 811m^2 \tag{3.2}$$

$$F_{fund} = 169piles \cdot 1302kN = 220,038kNSS \tag{3.3}$$

$$\sigma'_{v;4D} = 220,038kN/811m^2 \approx 271kN/m^2 \tag{3.4}$$

Based on the CPT data presented in Figure 3.1, the average q_c for the Pleistocene sand layers between PTL and 4D below is $\approx$ 22 MPa. Based on the factors proposed by Frissen (2020) and explained in Section 2.3.2, the lower and upper limits for s_2 can be computed:

$$s_{2;lower} = \frac{0.95 \cdot 271kN/m^2 \cdot 0.9 \cdot \sqrt{689m^2}}{5.0 \cdot 22 \cdot 10^3 kPa} = 0.06m \approx 60mm \tag{3.5}$$

$$s_{2;upper} = \frac{0.95 \cdot 271kN/m^2 \cdot 0.9 \cdot \sqrt{689m^2}}{3.0 \cdot 22 \cdot 10^3 kPa} = 0.10m \approx 100mm \tag{3.6}$$

This results in a range of predicted s_2 settlements of **60 mm - 100 mm**. Adding both s_1 and s_2 settlements leads to an approximated, total settlement range of **71 mm - 113 mm** due to the applied building loads. Note that this approximation does not (properly) include the time-dependent consolidation and creep settlements of the compressible clay layers below PTL. Consolidation during the lifespan of a high-rise building structure as well as creep of soils (even after the lifespan) can lead to significant, additional settlements over time.

3.1.3 Pile Load Test in Plaxis 3D

According to Brinkgreve (2021), most pile analyses in Plaxis need to be performed in 3D and modelled with volume elements for most realistic SSI effects. However, a volume pile requires very small elements and therefore demands large computation costs (see Section 2.1.1). For those reasons, this thesis focuses on modelling a pile with use of the new embedded beam formulation (EB-I) only (Smulders, 2018). Furthermore, Frissen (2020) described how to properly fit an embedded beam model in Plaxis 3D (for both s_1 and s_2 settlements) using a pile capacity analysis in D-Foundations (2022), see Figure 3.2. For this thesis, the proposed procedure by Frissen using D-foundations is used for the bearing capacity input of an EB-I in Plaxis as well as PileCore (2022) - invented by CRUX Engineering MicroServices BV (CEMS) - and hand-calculations. This way, the user has the flexibility of changing q_c values and updated α and β pile factors in accordance with recent pile load tests at the Port of Rotterdam (Gavin, 2020) for Fundex and other types of screwed piles (Ter Steege, 2022). Note that the updated pile factors are named "Maasvlakte" (or "MV2") in the graphs while the current pile factors are denoted by "NEN". However, this thesis does not cover installation effects in Plaxis, so this research will not check whether the response is too soft (brown boxes in Figure 3.2) or reduce the interface reduction factor of the soil (R_{inter}) for grout injection or layer-dependent skin friction for EB-I models. Instead, R_{inter} values of 0.5 are used for the soft soils and 1.0 for the granular soils within the zone of positive shaft friction.

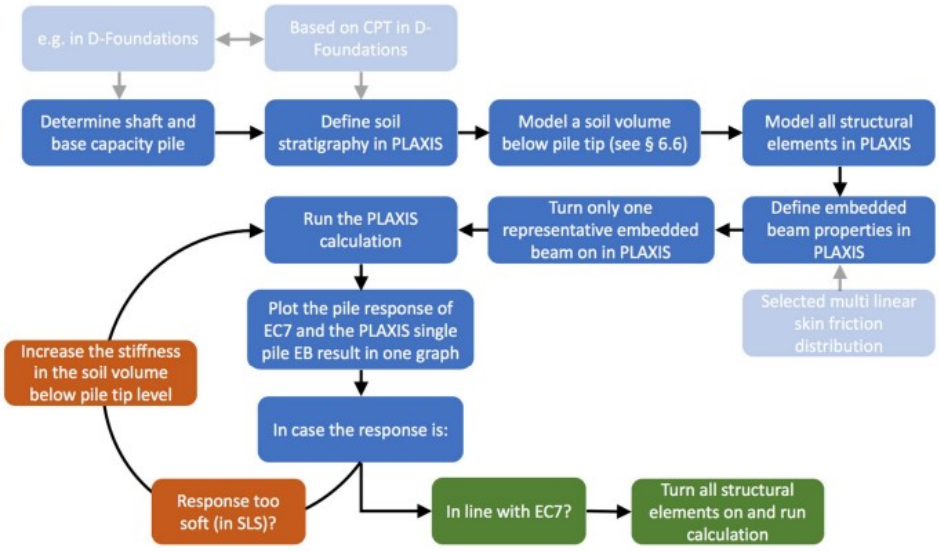

Figure 3.2: Fitting procedure of embedded beam piles in Plaxis 3D (Frissen, 2020).

To create a representative pile load test in Plaxis 3D, the average soil profile in northern Amsterdam is derived from 37 CPTs by engineering judgement, see Figure A.1 in Appendix A.1 for the most representative CPT. Since the pile calculation in both D-foundations as PileCore are based on only 1 CPT to simplify the analysis, the ξ factor should be set to 1.39. However, this thesis does not include proper grouping of CPT's nor should the inputs in Plaxis be reduced by any safety factors, so the factors are therefore overruled by 1.0.

Structural Response of Fundex 560

For a typical Amsterdam soil profile, as shown in Figure 3.1, positive shaft friction starts at the top of the first sand layer (= NAP - 13.5 m) and negative skin friction and an excavation depth are neglected, so the top of the ≈ 26 m pile corresponds with the GL (= NAP + 2.85 m). A bearing capacity and settlement calculation is done for a Fundex 460/560 pile (Table 3.1) using PileCore for the NEN and the updated design method in accordance with recent Maasvlakte data. For this numerical pile load test, the depth of the domain is limited to the top of the Eem clay layer (= NAP - 31 m) to only consider s_1 settlements. To investigate the effect of a larger (shaft) diameter, the same analysis is done for a Fundex 520/560 pile (Table 3.2). Both analysis are summarized in Figures 3.3 and 3.4. One can see that the total bearing capacity at PTL (= NAP - 23 m) is not affected by the type of load-settlement behaviour due to full mobilisation of the capacity at the bottom of the pile. However, the total shaft capacity of the NEN method might be underestimated by approximately 60% due to limits on the cone end resistance, q_c, as was experienced by PLTs at the *Maasvlakte* (Gavin, 2020).

Table 3.1: Summary of ultimate bearing capacity using D-foundations and PileCore for a Fundex 460/560 (at NAP - 23 m) behaving as a type 1 or type 2 pile with or without limits on q_c (under F = 1,302 kN).

NEN Load-Settlement Curve	**q_c limit (MPa)**	**Pile Factors (NEN or MV2)**	**Shaft Capacity (kN)**	**Base Capacity (kN)**	**Total Bearing Capacity (kN)**	**Pile Tip Settlement, s_b (mm)**	**Elastic Compression, s_{el} (mm)**	**Pile Stiffness, $k_{v,1}$ (kN/mm)**
1	12-15	$\alpha_s = 0.009$ $\alpha_p = 0.63$ $s = 1.0$ $\beta = 1.0$	1369	2751	4119	1.3	9.3	123
2	12-15	"..."	1369	2751	4119	4.0	9.3	98
1	No limit	$\alpha_s = 0.011$ $\alpha_p = 0.35$ $s = 1.0$, $\beta = 1.0$	2569	1528	4098	0.8	9.0	132
2	No limit	"..."	2569	1528	4098	3.0	9.0	108

Table 3.2: Summary of ultimate bearing capacity using D-foundations and PileCore for a Fundex 520/560 (at NAP - 23 m) behaving as a type 1 or type 2 pile with or without limits on q_c (under F = 1,302 kN).

NEN Load-Settlement Curve	**q_c limit (MPa)**	**Pile Factors (NEN)**	**Shaft Capacity (kN)**	**Base Capacity (kN)**	**Total Bearing Capacity (kN)**	**Pile Tip Settlement, s_b (mm)**	**Elastic Compression, s_{el} (mm)**	**Pile Stiffness, $k_{v,1}$ (kN/mm)**
1	12-15	$\alpha_s = 0.009$ $\alpha_p = 0.63$ $s = 1.0$ $\beta = 1.0$	1547	2751	4298	1.1	7.2	156
2	12-15	"..."	1547	2751	4298	3.6	7.2	120

To better understand the load distribution from the pile (tip) to deeper soil layers, a pile load test will be ran in Plaxis 3D for the new and updated design methods for a Fundex 460/560 (see row 1 and 4 in Table 3.1). The bearing capacity of a pile in Plaxis 3D is implemented by a multi-linear axial skin resistance ($= T_{skin}$) and the base resistance ($= F_{max}$) as inputs for the EB-I model with a diameter of 0.46 m, see Tables B.8 and B.7 in Appendix B.1. Note that T_{skin} in this model is defined as the maximum shaft capacity at pile tip level (divided by 0.5) over the distance of positive skin friction, so the triangular area underneath the resulting T_{skin} plot by Plaxis 3D equals the total shaft capacity of the pile. The resulting (normalised) load-displacement curves from Plaxis 3D are plotted and compared to both the predicted pile behaviour as well as the normalised curves from the NEN. See Figures 3.5, 3.6, and 3.7 on the next pages. As expected, one can see that a Fundex 560 with updated pile factors will result in less s_1 settlements due to the higher $k_{v,1}$ and stiffer behaviour of the pile past SLS. However, when compared to the normalised NEN load-displacement curves, the normalised base resistance for the updated pile factors follow the type 1 curve instead of the by Ter Steege (2022) expected type 2 behaviour. This could be due to the slightly higher α_s values in comparison to the NEN method. For a better comparison, the computed load-settlement curves should be compared with the measured pile load tests performed at the *Maasvlakte*.

Furthermore, the analysis show that different pile type behaviour does influence the s_1 settlement and corresponding pile stiffness, $k_{v,1}$, under the same SLS building load (= 1,302 kN), see Figure 3.3. Since $k_{v,1}$ is an important input parameter for the pile springs in the structural models in SCIA, the pile stiffness can be further investigated as a model variation in Section 3.2 (see Figure 3.42) and compared with the current $\sqrt{2}$ uncertainty range for a pile stiffness.

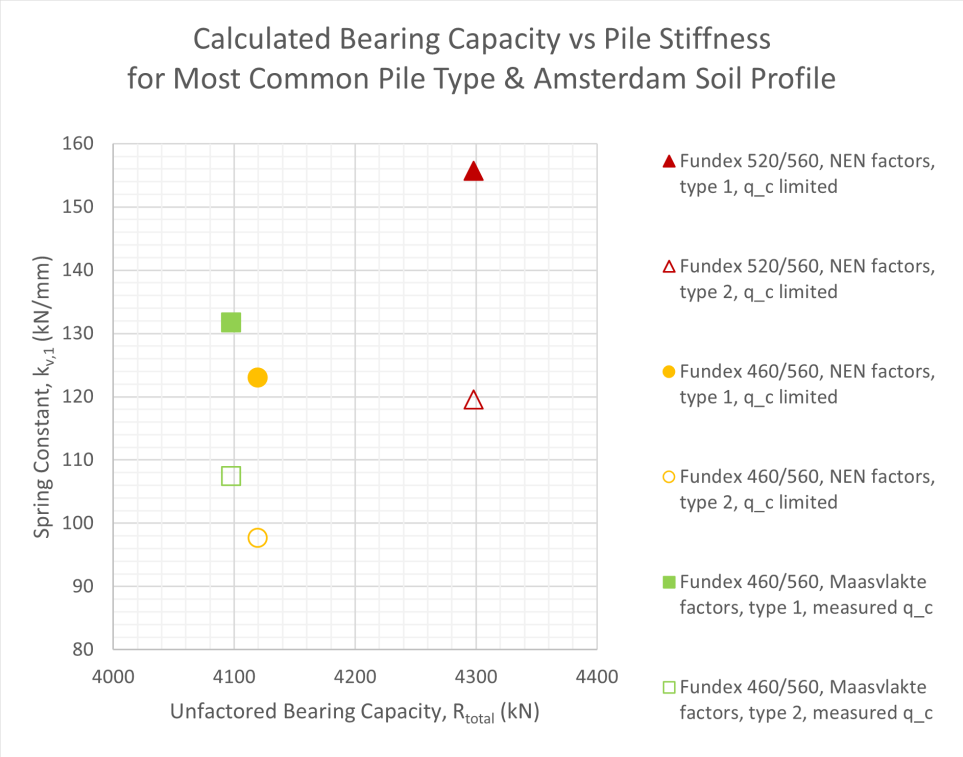

Figure 3.3: Results of PileCore bearing capacity calculations and pile stiffness for Fundex 560.

Moreover, Figure 3.4 shows the contribution of the shaft capacity on the y-axis and the base capacity on the x-axis for the unfactored, total capacity of a Fundex 460/560 and Fundex 520/560 for both design methods. This data set can be used to verify both the traditional Tomlinson equivalent raft approach and the updated

method (Figure B.20), which splits the total building load in the contribution of shaft and base resistance with respect to the total pile capacity. As was explained in Section 2.1.1, the updated method implements the percentage of the shaft capacity (R_{shaft}) of the total capacity (R_{ult}) as a surface load modelled at 2/3 of positive skin friction ($= D_{tom}$) while including a load spread of 1/4 from top positive skin friction ($= D_{pos}$). The remaining building load is then added as a surface load at PTL to represent the base contribution of a pile group.

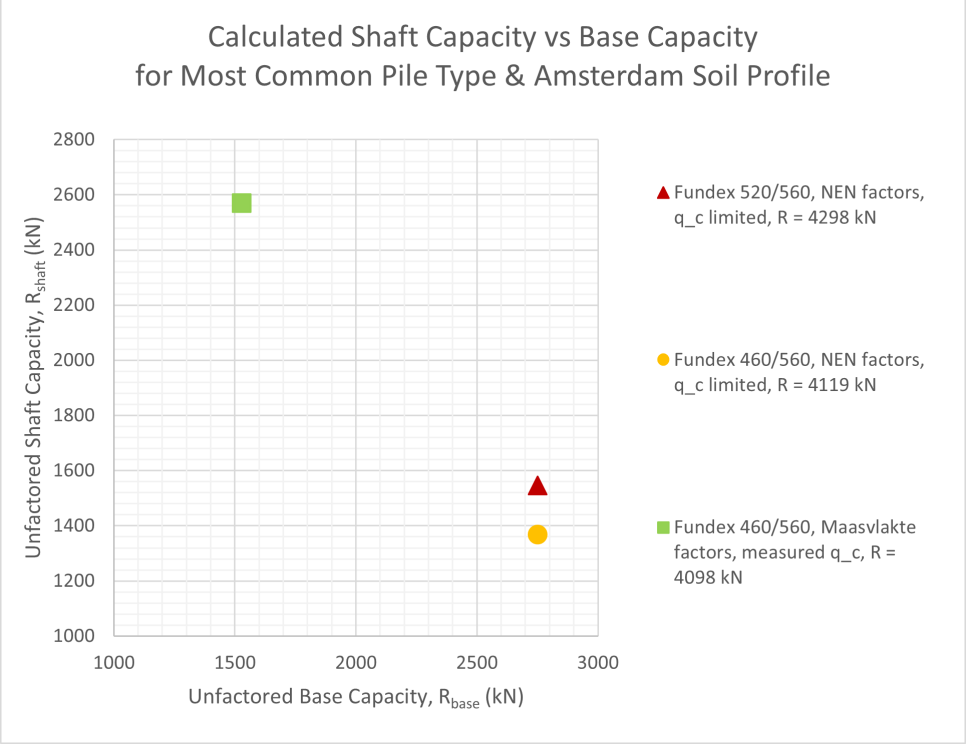

Figure 3.4: Results of PileCore bearing capacity calculations for Fundex 560.

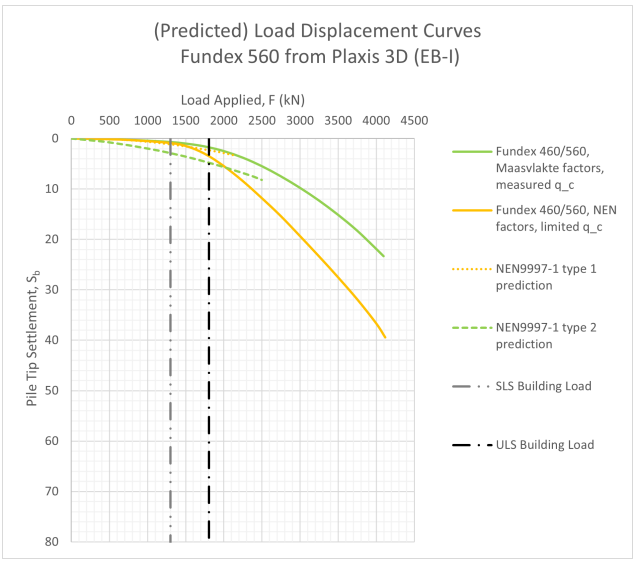

(a) Pile tip settlement.

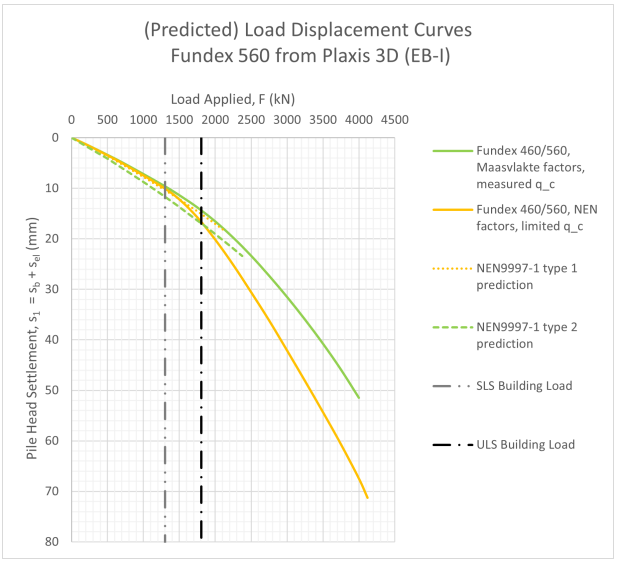

(b) Pile head settlement.

Figure 3.5: Plaxis 3D load settlement results and NEN predictions for Fundex 460/560.

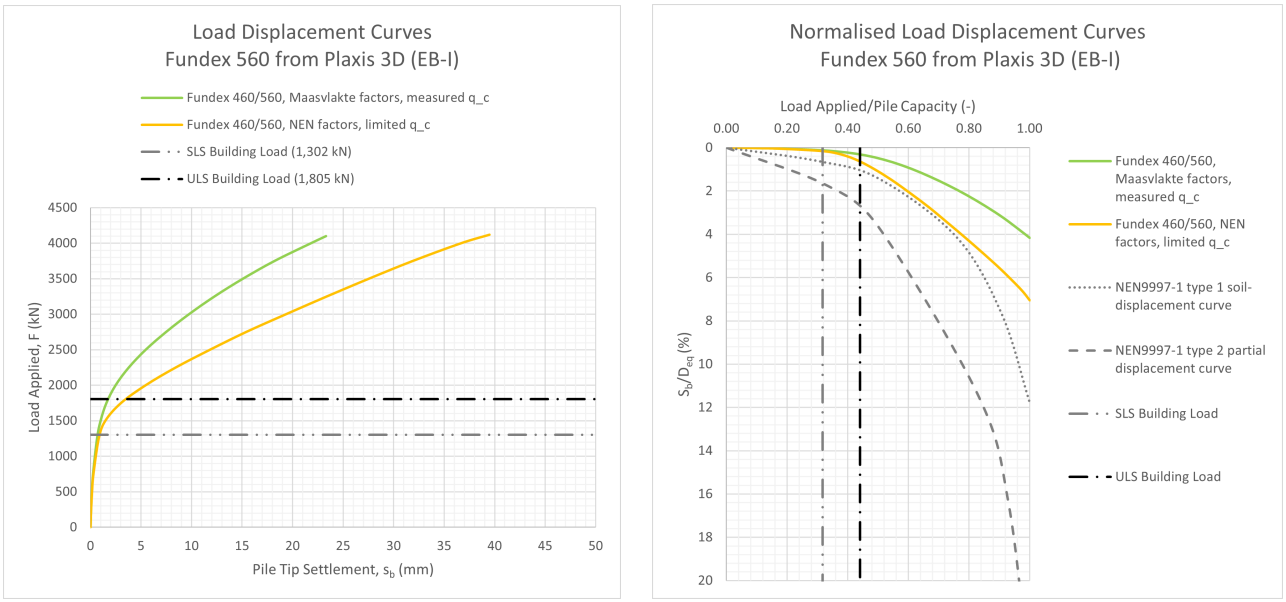

(a) Total load. (b) Normalised.

Figure 3.6: Plaxis 3D load settlement results for Fundex 460/560.

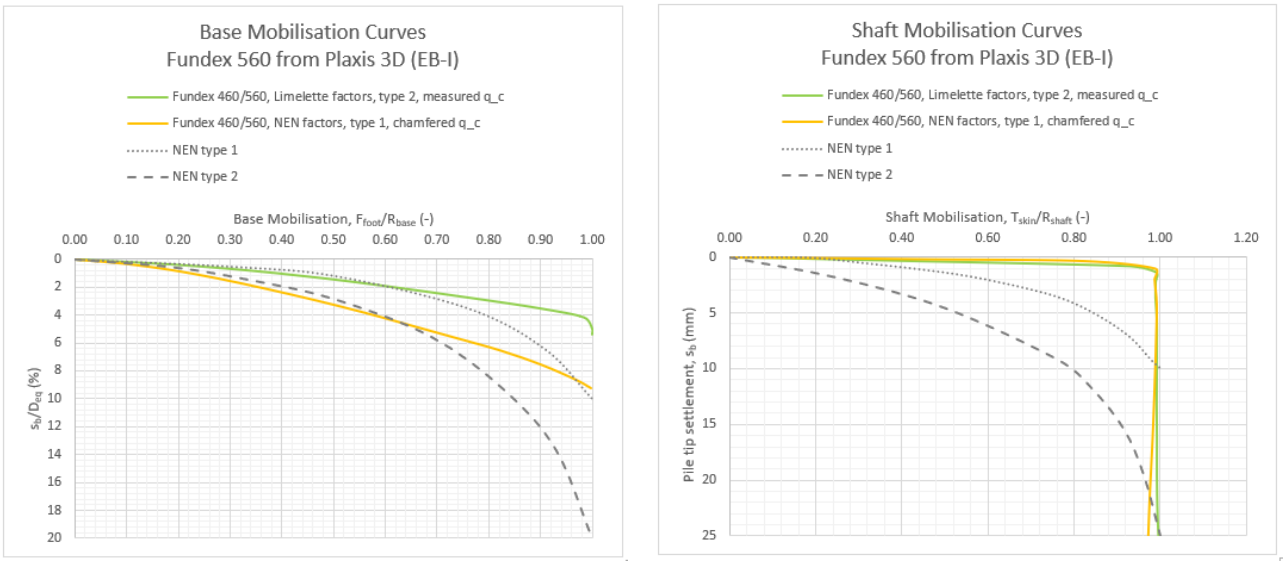

(a) Base. (b) Shaft.

Figure 3.7: Plaxis 3D mobilisation curves for Fundex 460/560.

For the remainder of this section, the focus will be on the response under SLS loading conditions - rather than the full loading response - for a Fundex 460/560 as this is the most realistic load combination (See Section 2.2.2) for (differential) settlement predictions. The calculated SLS load of 1,302 kN in SCIA for a simple tower seems much lower than the ultimate capacity of the individual pile ($\approx$ 4,000 kN), which is due to the partial factors γ_f of 1.2 and ξ of 1.39 used for a preliminary design in D-Foundations (see Tables A.2 - A.3 and Figures A.14 - A.17 in Appendix A.4) to determine the PTL. This thesis is inspired by the preliminary design report for a case study in northern Amsterdam for which the pile foundation was calculated and designed by CRUX and VRI. Without the partial factors, the FoS of the design is 3.2 while the design FoS is only 1.6 including the factors. Below, one can see the different responses of mobilised shaft capacity (T_{skin}) and

mobilised base resistance (F_{foot}) for the NEN method (Figures 3.8a and 3.9a) and the Maasvlakte pile factors (Figures 3.8b and 3.9b) calculated by Plaxis 3D (EB-I) under an SLS load 1,302 kN.

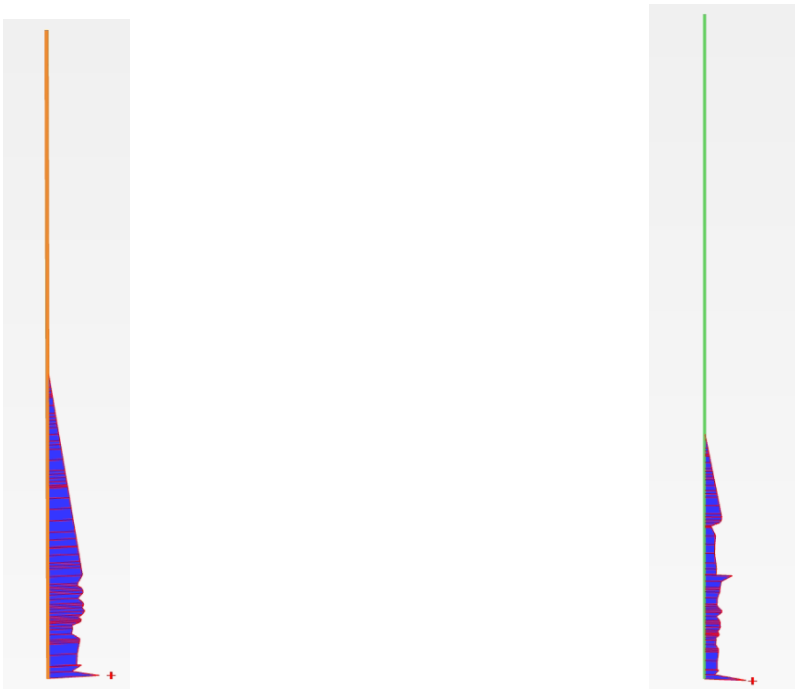

(a) NEN. (b) Maasvlakte.

Figure 3.8: Plaxis 3D shaft mobilisation (T_{skin}) at SLS loading (= 1,302 kN) for a Fundex 460/560 with a) NEN, and b) Maasvlakte pile factors.

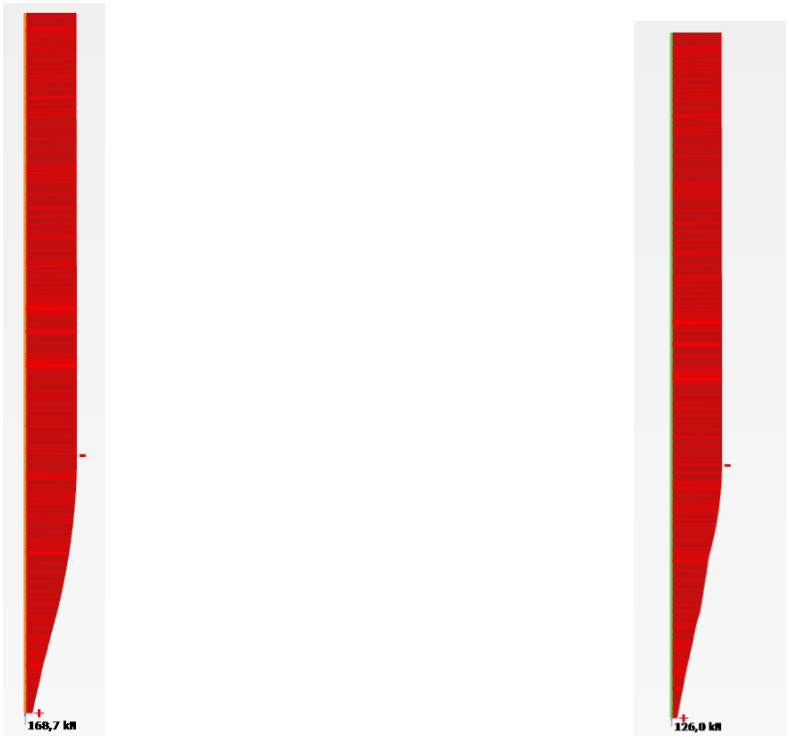

(a) NEN. (b) Maasvlakte.

Figure 3.9: Plaxis 3D base mobilisation (F_{foot}) at SLS loading (= 1,302 kN) for a Fundex 460/560 with a) NEN (= 169 kN), and b) Maasvlakte (= 126 kN) pile factors.

Stress Distribution below Fundex 560

For the current and updated pile design method in Plaxis 3D, the stresses at pile tip level and 4D below are summarised in Table 3.3. Using the calculated base resistance from Plaxis (F_{foot}) and a load spread distribution of 1 in 4 (30 degrees) from PTL, the resulting stress on the Eem clay layer range from **8 kPa** to **10 kPa** due to a single pile under an SLS load of 1,302 kN. According to the Plaxis 3D model, the effective stress equals **258 kPa** for the initial situation without pile and increases to **261 kPa** for the NEN pile factors and **260 kPa** for the Maasvlakte pile factors under the same load.

Table 3.3: Summary of stresses acting on the Eem clay layer based on 1 in 4 load spread for both bearing capacity methods under SLS load of F = 1,302 kN with a pile base area (A_{base}) of 0.246 m^2 at NAP - 23m.

Pile Type	F_{foot} **(kN)**	**Stress at pile tip due to load (kPa)**	**Stress 4D below pile tip due to load (kPa)**	**Stress on Eem Clay due to load (kPa)**	**Plaxis 3D: Initial effective stress on Eem Clay (kPa)**	**Plaxis 3D: Max. SLS effective stress on Eem Clay (kPa)**
NEN Fundex 460/560	169	685	76	10	258	261
MV2 Fundex 460/560	126	512	57	8	258	260

This translates to basically no change in vertical (effective) stresses on the Eem clay for either bearing capacity method, so one can conclude the Eem clay will not compress (much) due to 1 pile. One may also conclude Plaxis 3D uses a load distribution smaller than 1 in 4 as the hand calculations overestimated the load transferred from PTL (= NAP - 23 m) to the top of the Eem clay layer (= NAP - 31 m) by ≈ 6 kPa in comparison to the Plaxis σ'_{zz} results. See Figures 3.13 - 3.18 below for the 3D visuals created by Plaxis 3D for (the change in) vertical effective stress by both bearing capacity methods at different depths. Figure 3.10 shows the three horizontal and one vertical section used to compare the stresses between both methods. One can see that the stresses at PTL for the NEN method are ≈ 80 kPa higher than the MV2 method, see Figure 3.12. Based on the hand-calculations (Table 3.3), a much larger difference of 205 kPa was expected. A reason for the discrepancies could be that Plaxis 3D only allows one diameter for which the smaller shaft diameter (d_{eq}) was used. On top of that, Plaxis 3D shows an unexpected 'unloading' zone between the eight outer nodes of the plastic region and the center node at the base of the EB-I pile. For other depths, the difference is negligible.

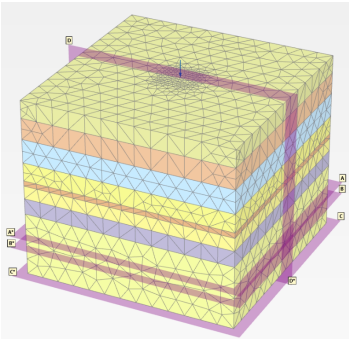

Figure 3.10: Plaxis 3D visualisation of soil layers, mesh, horizontal and vertical cross-sections.

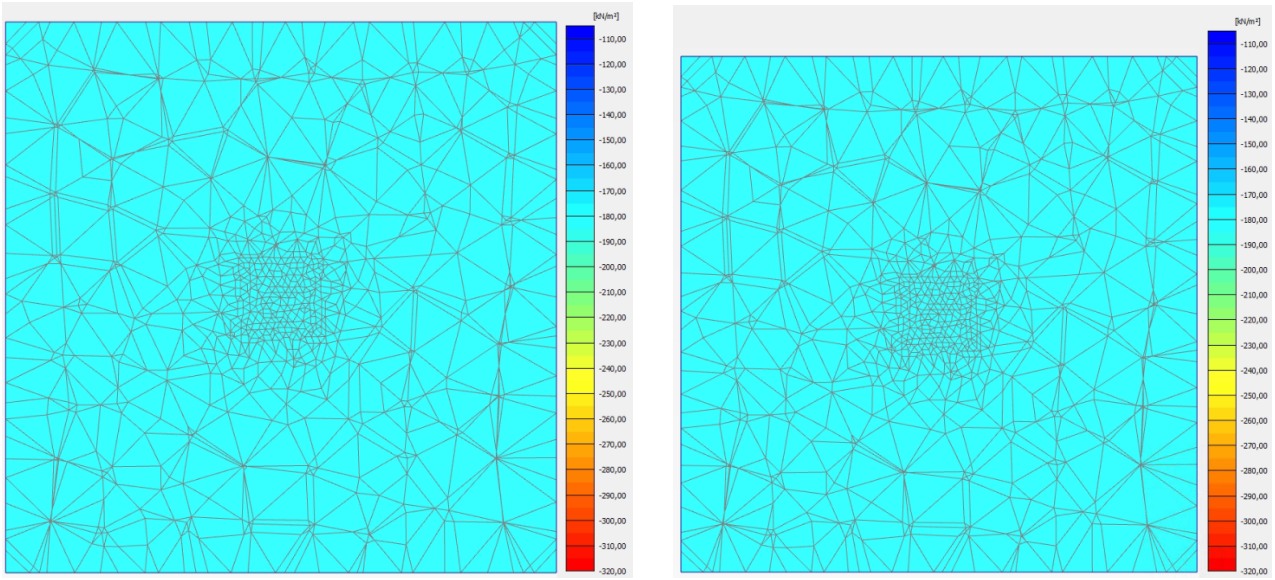

(a) NEN Method. (b) Maasvlakte Method.

Figure 3.11: Initial Cartesian effective stresses (σ'_{zz}) under K_0 conditions calculated at pile tip level (= NAP - 23 m) by Plaxis 3D for the a) NEN, and b) Maasvlakte bearing capacity methods.

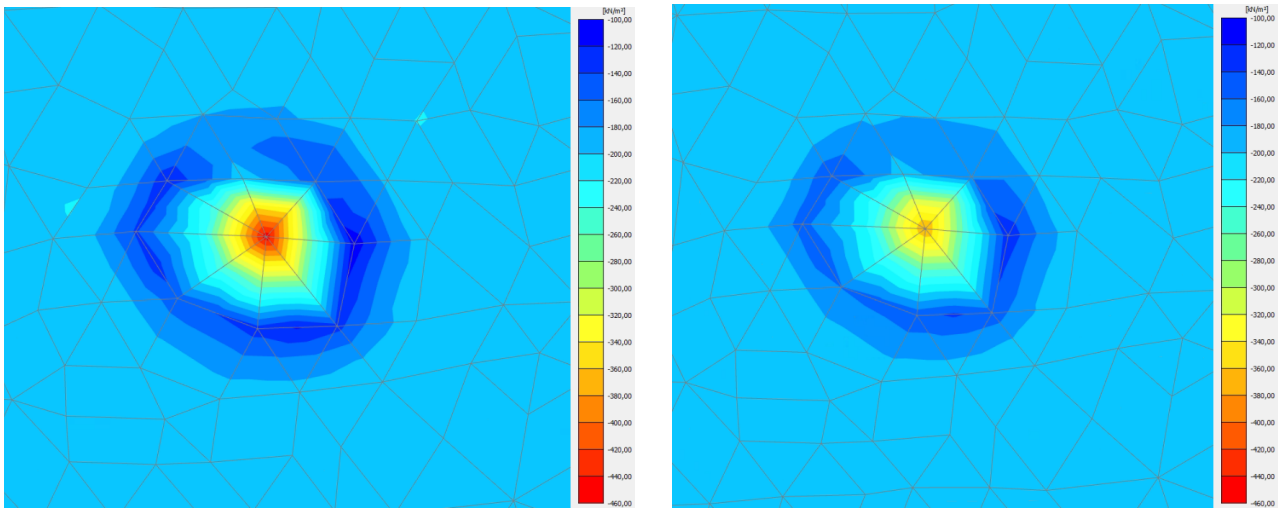

(a) NEN Method. (b) Maasvlakte Method.

Figure 3.12: Cartesian effective stresses (σ'_{zz}) under SLS load (= 1,302 kN) calculated at pile tip level (= NAP - 23 m) by Plaxis 3D for the a) NEN, and b) Maasvlakte bearing capacity methods 2 m around pile.

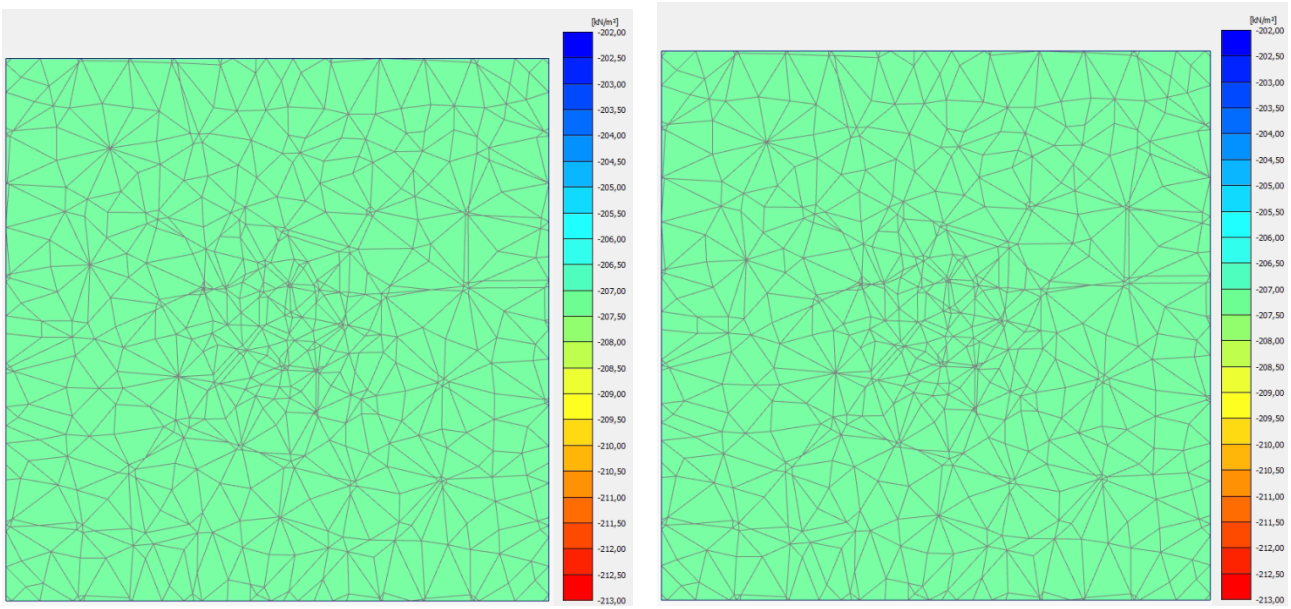

(a) NEN Method.

(b) Maasvlakte Method.

Figure 3.13: Initial Cartesian effective stresses (σ'_{zz}) under K_0 conditions calculated at 4D below pile tip level (= NAP - 25.24 m) by Plaxis 3D for the a) NEN, and b) Maasvlakte bearing capacity methods.

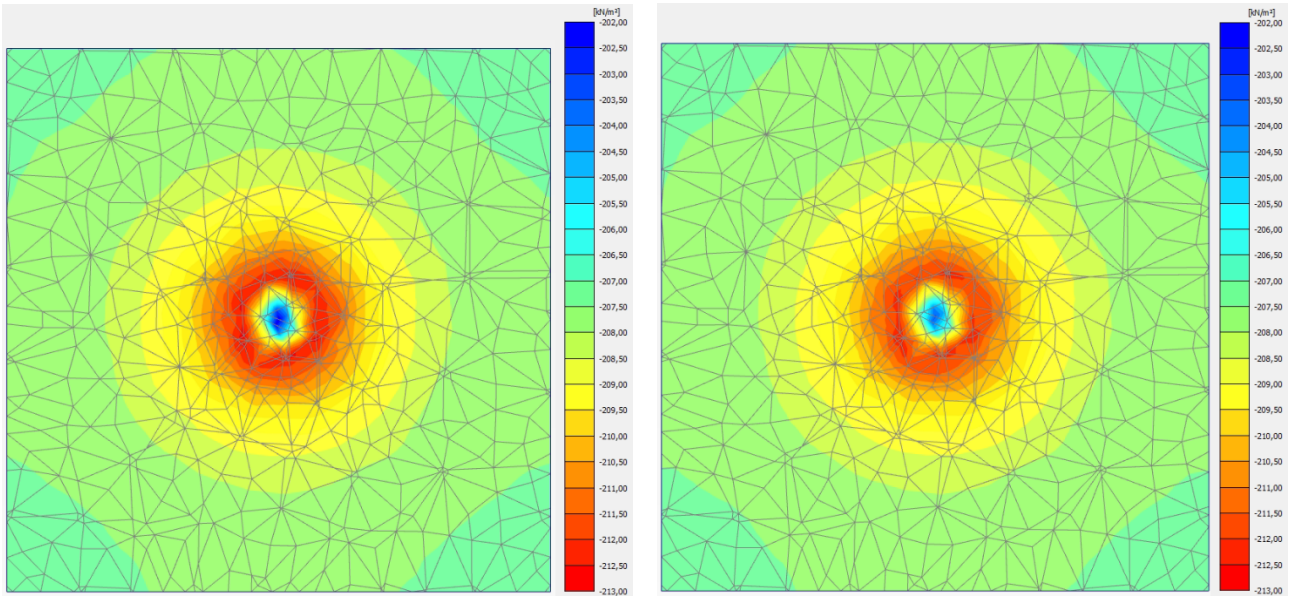

(a) NEN Method.

(b) Maasvlakte Method.

Figure 3.14: Cartesian effective stresses (σ'_{zz}) under SLS load (= 1,302 kN) calculated at 4D below pile tip level (= NAP - 25.24 m) by Plaxis 3D for the a) NEN, and b) Maasvlakte bearing capacity methods.

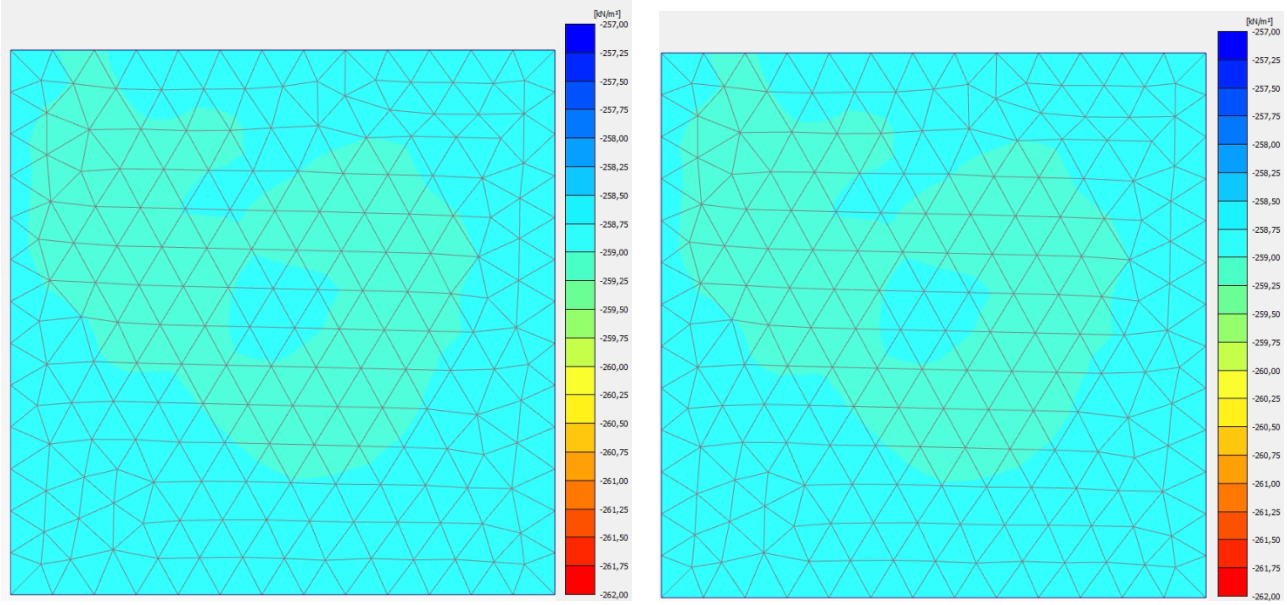

(a) NEN Method. (b) Maasvlakte Method.

Figure 3.15: Initial Cartesian effective stresses (σ'_{zz}) under K_0 conditions calculated at top of Eem clay (= NAP - 31 m) by Plaxis 3D for the a) NEN, and b) Maasvlakte bearing capacity methods.

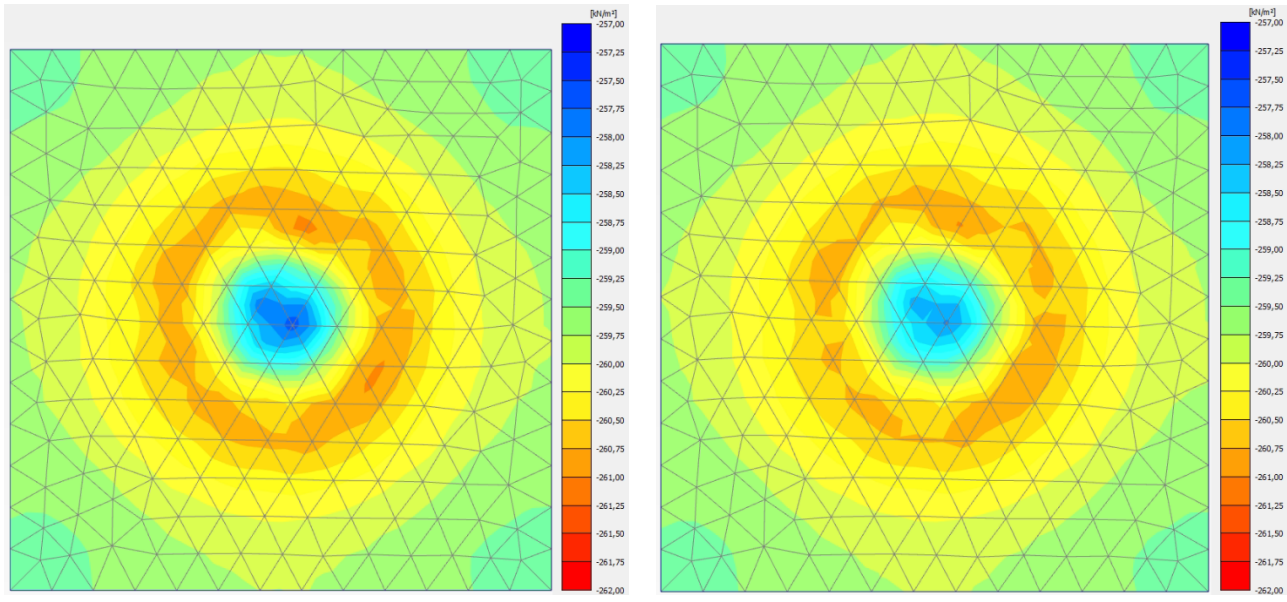

(a) NEN Method. (b) Maasvlakte Method.

Figure 3.16: Cartesian effective stresses (σ'_{zz}) under SLS load (= 1,302 kN) calculated at top of Eem clay (= NAP - 31 m) by Plaxis 3D for the a) NEN, and b) Maasvlakte bearing capacity methods.

The 'unloading' zone shown in Figures 3.13 - 3.18 for both bearing capacity methods was first thought to be the result of an increase in pore water pressures within the elastic zone of the EB-I. However, the excess pore water pressures (p_{excess}) across the entire depth are zero according to Plaxis 3D (see Figure B.4a in Appendix B.2). Instead, Plaxis 3D showed a rotation of principle stresses (Figure B.4b) outside the elastic zone of the EB-I due to possible arching effects and increased shear stress of the granular layers below PTL, which may cause the ring around the pile. The soil within this ring is pushed to the outside (Figure B.5b) resulting in an increase of volumetric strain (ϵ_v) of the soil (Figure B.5a) explaining the reduction in vertical effective stress

right below the center of the EB-I pile. Further research should investigate whether this hypothesis is correct as this 'squeezing phenomena' falls outside of the scope of this thesis. Subsequently, expected unloading zones are illustrated by the vertical cross-sections (see Figures 3.17 and 3.18) along parts of the shaft due to the elastic region around the EB-I in which soil is forced to behave elastically. This region should be ignored for conclusions regarding stresses caused by the Fundex 560 pile and transferred to the Eem clay.

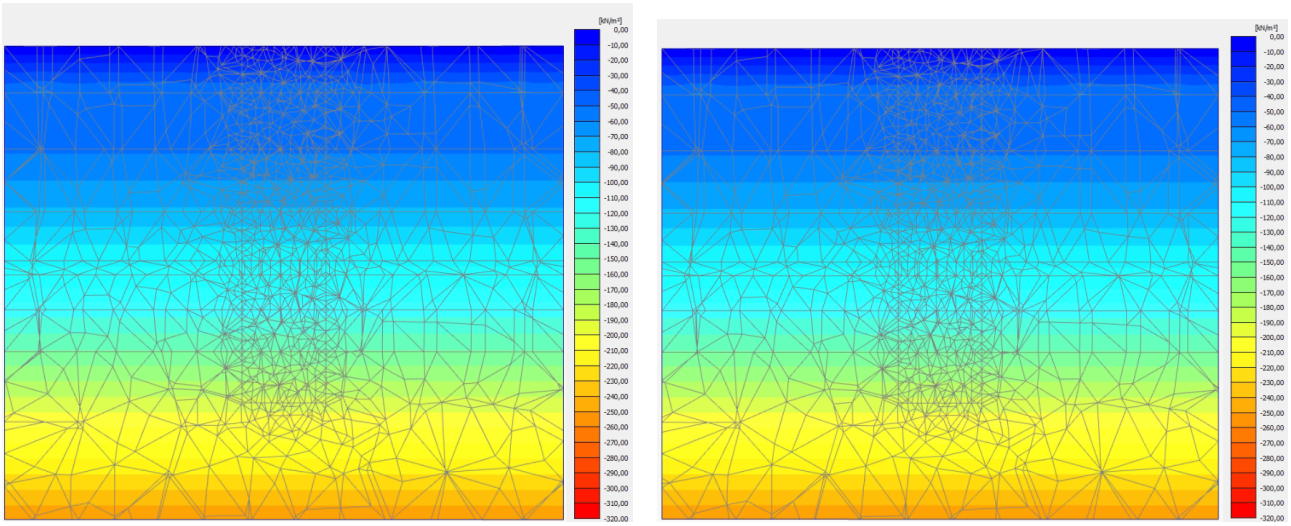

(a) NEN Method. (b) Maasvlakte Method.

Figure 3.17: Change in initial Cartesian effective stresses (σ'_{zz}) under K_0 conditions calculated for entire depth (= NAP + 2.85 m − NAP - 31 m) by Plaxis 3D for the a) NEN, and b) Maasvlakte bearing capacity methods.

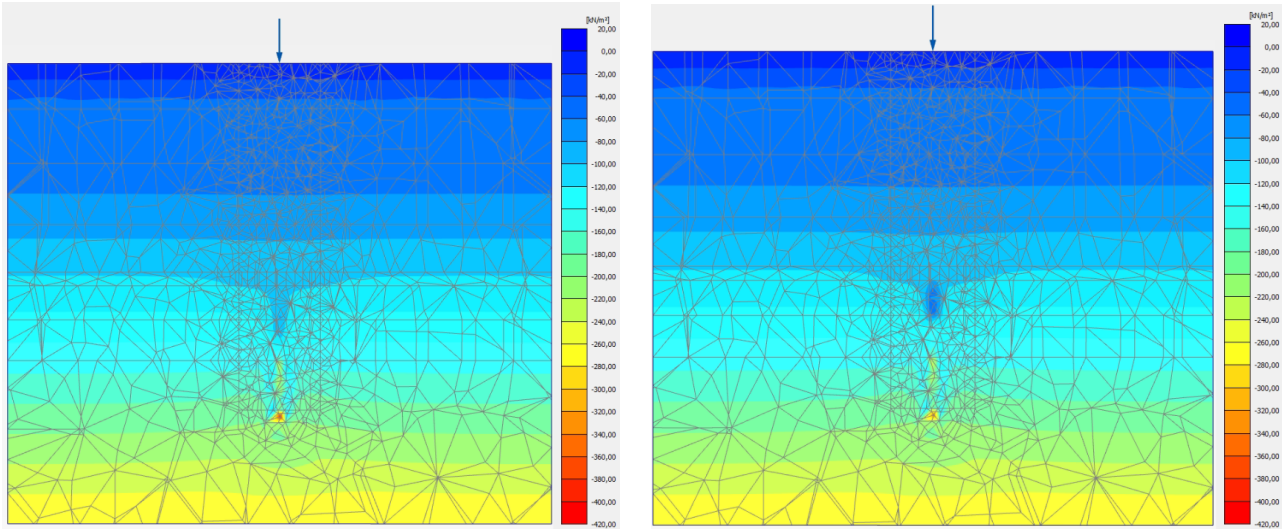

(a) NEN Method. (b) Maasvlakte Method.

Figure 3.18: Change in Cartesian effective stresses (σ'_{zz}) under SLS load (= 1,302 kN) calculated for entire depth (= NAP + 2.85 m − NAP - 31 m) by Plaxis 3D for the a) NEN, and b) Maasvlakte bearing capacity methods.

3.1.4 Soil Test in Plaxis 3D (SoilTest Facility)

To better understand and verify the constitutive models and soil parameters for the Eem clay (layer), the soil parameters from the CRUX database and direct oedometer tests performed by MOS for Eem clay will be tested in the SoilTest facility in Plaxis under the material models and compared with 1D oedometer (compression) laboratory results in Appendix A.2. In Plaxis' oedometer SoilTest, one can add phases including a duration (in days), number of calculation steps (i.e., 100), and a stress increment (in kN/m^2). A negative stress or load added to the sample means compression or loading, while positive means tension or unloading (Brinkgreve, 2021). In addition - for the HSS model specifically - the mobilised relative shear strength option is available to set the initial shear hardening contour. The HSS model parameters will not be tested in this thesis as it requires triaxial test data for the stiffness parameters (E_{50}, E_{ur}, G_0, and $\gamma_{0.7}$). When a satisfactory fit is achieved between Plaxis' SoilTest and MOS' lab tests, the soil profile used for the individual PLT will be extended with the compressible clay layers to a depth of $\approx$ NAP - 63 m. The (fitted) Plaxis SSCM parameters for the Eem clay will help investigate the 'real' soil response underneath pile groups for a foundation structure modelled as a plate with surface load and - more realistically - as embedded beams.

Eem Clay Soil Test (SSCM)

As discussed in Section 2.4.1, several compressibility lab tests (i.e., oedometer tests) have been performed on Eem clay samples from multiple locations in Amsterdam, mostly as part of the *Noord-Zuidlijn* subway project. See Figures A.4 - A.9 in Appendix A.2 for hand-selected tests with minimal sample disturbance for two locations in Amsterdam (East & North). The least sample disturbance was determined by comparing the reloading curve with the loading curve, which should have a similar gradient up to the pre-consolidation pressure, σ'_p. This yield point on the (virgin) curve is important to determine the OCR of the Eem clay, see Eq. 3.7, where σ'_{v_0} is the vertical effective stress in-situ. The latter is approximated by multiplying the depth of the sample by $\approx$ 8 kN/m^2, while σ'_p is taken from the NEN / Bjerrum oedometer test results (516 kPa, 579 kPa and 550 kPa respectively) shown in Figures A.5, A.7 and A.10 for three different Eem clay samples taken from two locations in Amsterdam.

$$OCR = \frac{\sigma'_p}{\sigma'_{v_0}} \tag{3.7}$$

Using Eq. 3.7, OCR values of **2.37** are calculated for the Eem clay sample taken at eastern Amsterdam and **2.02** and **1.64** for the two samples at northern Amsterdam. The OCR needed for the SSCM is defined as OCR_2 (see Section 2.1.1) and includes an ageing effect of the layer, which can be calculated by Eq. 2.3 to calibrate the autonomous surface subsidence (Den Haan, 2008). This results in OCR_2 values of **5.27** (East), **2.62** (North #1), and **2.07** (North #2) for SSCM in Plaxis. In order to make an appropriate fit between a Plaxis SoilTest and the oedometer test results, SSCM is chosen to model Eem clay and the corresponding C_r, C_c, and C_α are imported from the oedometer lab results. Note that the C_s input of the SSCM in Plaxis is the C_r index from the lab for these specific oedometer results and C_α in Plaxis as well as the lab is often denoted as $C_{\alpha\epsilon}$ in literature. These indices are visualised in Figure 3.19 and can be converted to SSCM parameters using the following correlations:

$$\lambda^* = \frac{C_c}{1 + e_0} \cdot \frac{1}{ln(10)} \tag{3.8}$$

$$\kappa^* = \frac{2 \cdot C_r}{1 + e_0} \cdot \frac{1}{ln(10)} \tag{3.9}$$

$$\mu^* = \frac{C_{\alpha\epsilon}}{1 + e_0} \cdot \frac{1}{ln(10)} \tag{3.10}$$

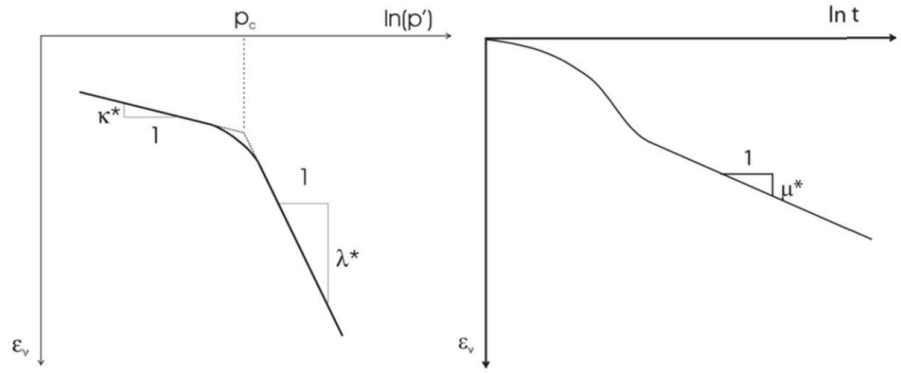

Figure 3.19: Visualisation of the SSCM parameters λ^*, κ^*, and μ^* (Waterman & Broere, 2004).

Using Eq. 3.8 - 3.10, the modified compression indices can be calculated and checked with the stiffness parameters calculated by Plaxis' SSCM to verify the correct inputs for the Eem clay samples, see Table 3.4 below. The table also lists the compression/creep ratio of the sample, which can be calculated by $CR/C_{\alpha\epsilon} = 2.3 \cdot \lambda^*/C_{\alpha\epsilon}$. For Eem clay, a ratio between 30 - 40 is considered reliable for use in design, meaning that the ratio for the samples in this research (20 - 25) are outside of the preferred range. Another method to determine the quality of the sample is described by $\Delta e/e_0$ and the OCR, so per load step or phase one can determine whether the quality is very poor, poor, average, or good. Based on these rules of thumb, the disturbance of the 'best' samples is still relatively high with an average sample quality common for Dutch soils.

Table 3.4: Modified compression indices and OCR for use of SSCM in Plaxis (SoilTest).

Sample	**OCR**	**OCR$_2$**	C_r	C_c	$C_{\alpha\epsilon}$	λ^*	κ^*	μ^*	$CR/C_{\alpha\epsilon}$	$\Delta e/e_0$
East	2.37	5.27	0.103	0.428	0.0076	0.0826	0.0398	0.0015	25.0	NA
North #1	2.02	2.62	0.079	0.580	0.0109	0.1067	0.0291	0.0020	22.5	0.068
North #2	1.64	2.07	0.126	0.776	0.0159	0.1410	0.0458	0.0029	20.4	0.062

A comparison (or fit) between the Plaxis SoilTest results and laboratory can be achieved by digitising and post-processing the oedometer test data (Appendix A.2) using void ratio and strain, see Eq. 3.11.

$$\epsilon_{yy} = \frac{\Delta h}{h} \tag{3.11}$$

where, h is the height of the sample and Δh is the change in height after 24 hours. In soil mechanics, the change in (volumetric) strain is often defined by the change in void ratio (e) for each load step. Using this relationship (see Eq. 3.12), the Plaxis modelled stress versus strain oedometer curve can be compared to the load versus void ratio graphs - also called virgin compression curve - in Figures A.5, A.7, and A.10 whith the option to optimise the Eem clay SSCM stiffness parameters (λ^*, κ^*, μ^*, ν'_{ur}, K_0^{nc}, and M).

$$\Delta\epsilon_v = -\frac{\Delta e}{1 + e_0} \tag{3.12}$$

where, e_0 is the initial void ratio (1.25, 1.36, and 1.39), Δe is the change in void ratio per load step, and $\Delta\epsilon_v$ is the resulting change in volumetric strain for each step (Verruijt, 2001). Since an oedometer test is a 1D compression test, the sign convention is negative and the change in vertical strain calculated by Plaxis (ϵ_{yy}) is the same as the change in volumetric strain (ϵ_v). Lastly, Δe for the Eem clay samples in northern Amsterdam can be retrieved from the virgin compression curves shown in Figures 3.20 and 3.21 below. Note that these graphs are a copy of the extensive test results in Appendix A.2. Modelling in Plaxis is only performed for the two samples taken from the North of Amsterdam to examine whether Plaxis is able to capture the soil behaviour of the Eem clay layer starting at NAP - 31 m in Figure 3.1 for use in the pile group model in Section 3.1.5.

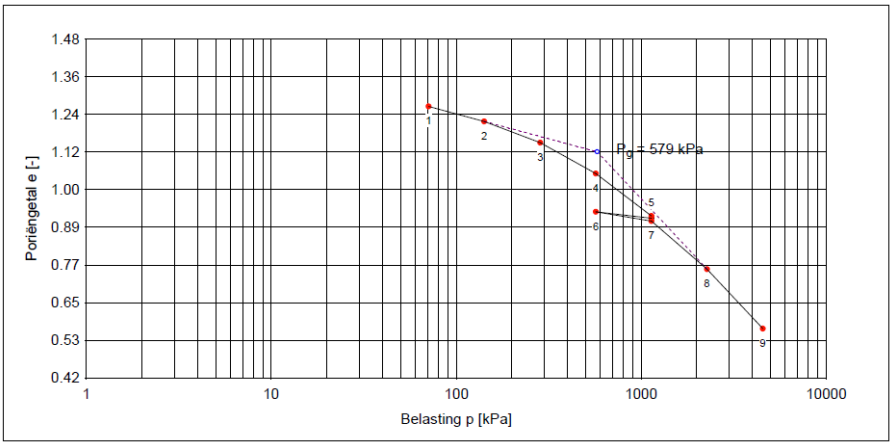

Figure 3.20: NEN-Bjerrum oedometer test results (void ratio versus applied load) performed by MOS for *Kavel Z1* in northern Amsterdam (sample North #1).

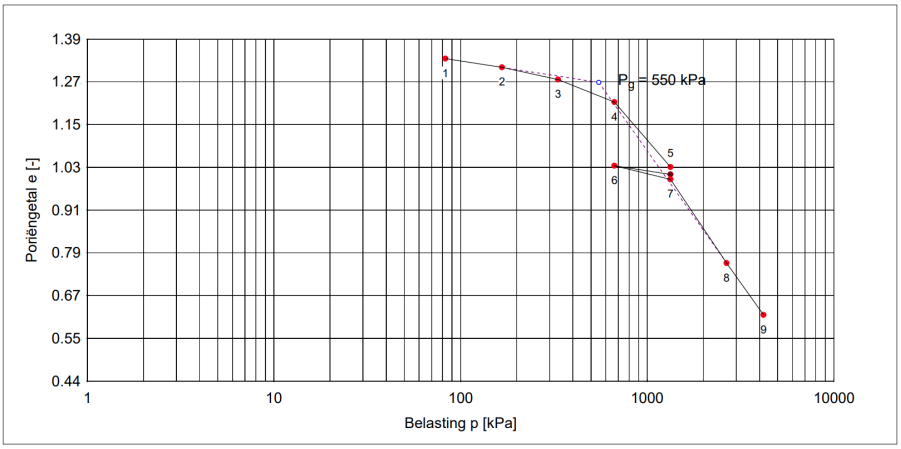

Figure 3.21: NEN-Bjerrum oedometer test results (void ratio versus applied load) performed by MOS for *Kavel Z1* in northern Amsterdam (sample North #2).

Figure 3.22 on the next page shows the unfitted results of the oedometer soil test modelled by Plaxis' SoilTest facility and the results retrieved from the lab using the soil properties and compression indices explained above.

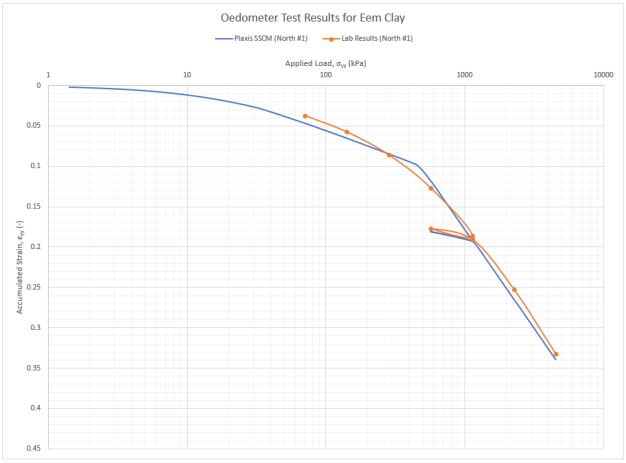

(a) North Sample #1.

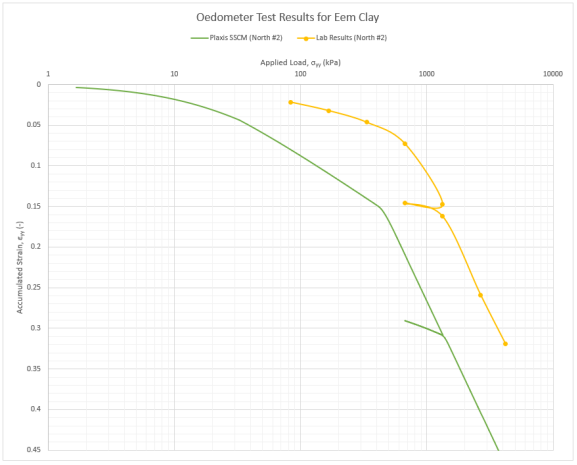

(b) North Sample #2.

Figure 3.22: Results of oedometer test for Eem clay between the lab data and a Plaxis FEM SoilTest as SSCM for a) North sample #1, and b) North sample #2 taken from northern Amsterdam.

To better understand the discrepancies between the lab data and the SSCM results from Plaxis found for sample #2 in Figure 3.22b, two additional samples at two shallower depths are modelled, see Appendix B.2 Figures B.6a and B.6b based on the laboratory data in Figures A.11 and A.12. A shallower depth was chosen as the sample disturbance was expected to be lower. Figure 3.23a below illustrates the digitised oedometer results from the laboratory for three of the four Eem clay samples (to reduce the untidiness of multiple plots in one chart). In addition, Figure 3.23b shows the combined load-strain results for the laboratory and Plaxis' SoilTest facility while Appendix B.2 Figure B.7b shows similar trends for all four samples retrieved at different depths from the North of Amsterdam.

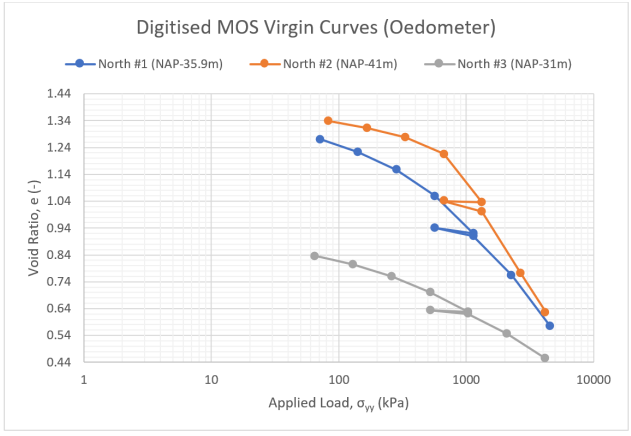

(a) Laboratory.

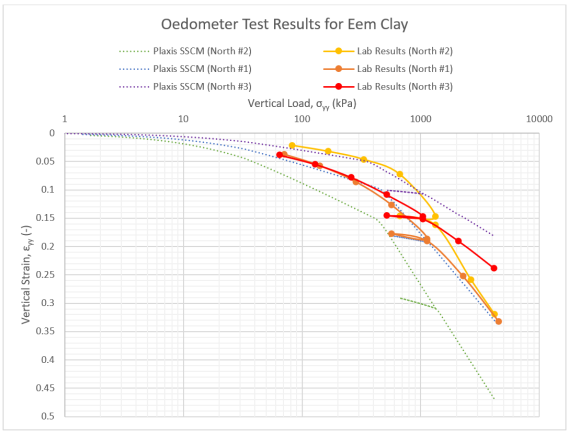

(b) Lab & Plaxis.

Figure 3.23: Combined results of oedometer test for three different Eem clay samples in northern Amsterdam a) from the laboratory, and b) between the lab data and a Plaxis FEM SoilTest as SSCM.

From the results, one can see that sample #1 (at NAP - 35.9 m) has a perfect fit between the oedometer Plaxis SoilTest for Eem clay as SSCM and the results from the laboratory. However, sample #2 at deeper depth (NAP - 41 m) shows a softer response in Plaxis while samples #3 (NAP - 31 m) and #4 (NAP - 34 m) show a stiffer response. Discrepancies may be a result of the measured initial void ratio and pre-consolidation stress in the laboratory, which are often unreliable and inaccurate (Brinkgreve, 2021), especially for deep soil samples. On top of that, C_r under primary compression (load steps 1-2) differs significantly from C_r under

reloading (steps 6-7) for samples #3 and #4. As a result, the pre-consolidation stress may be overestimated by 150-200 kPa resulting in stiffer Plaxis results. On the other hand, sample #2 shows some inconsistency with regards to C_r and C_s. These indices differ too much, leading to an apparent stiffer response of the oedometer test with regards to Plaxis. Based on trial-and-error of changing soil parameters, it was found that the cohesion and friction angle of the samples have a significant effect on the initial strain upon primary loading. Unfortunately, these strength parameters are not provided by MOS' oedometer test report and therefore kept constant for all samples based on the *Noord-Zuidlijn* subway database for Eem clay (i.e., c'_{ref} = 5 kPa and $\phi = 28°$). In foundation design, however, the analysis in Plaxis (3D) starts from a specified initial loading stage instead of 0 as in the SoilTest, which should neglect the small-strain sensitivity of soil stiffness for SSCM. On top of that, the factor 2.0 in Eq. 3.9 for κ^* is an overestimation of the reloading curve for OC soils such as Eem clay (Lengkeek, 2022). Therefore, Lengkeek (2022) recommends a factor between 1.0 and 2.0 instead. Applying this correlation in the SSCM results in a better fit between the stress-strain oedometer soil test results in Plaxis and the laboratory.

Furthermore, the SSCM does not include structure (bonding) while this often occurs in natural clays. However, the shape of the load-strain and corresponding stiffness behaviour appears to be satisfactory for all samples. Therefore, one may conclude that Plaxis' SSCM is able to capture the soil behaviour of Eem clay qualitatively well for use in the pile group model. Considering the CRUX database for Eem clay is based on careful calibration and an extensive probabilistic analysis of ≈ 150 samples that match well with the soil properties and model parameters of North sample #1 (see Appendix B.1 Tables B.5 and B.6), the SSCM parameters of CRUX are used herein.

Load Distribution to Eem Clay

To formulate a proper hypothesis for the effects of a EB-I pile group (and consolidation) on the stress distribution to the Eem clay layer at NAP - 31 m, Tomlinson's load spread method (described by Figure 2.28 in Section 2.3.2) is first used. Based on Tomlinson, a realistic SLS surface load of 382 kPa is spread by 1/4 over D_{tom} (NAP - 13.5 m to NAP - 19.8 m). The resulting surface load of **296 kPa** is then applied at z = -19.8 m in Plaxis 3D. The resulting effective stresses are shown in Figure 3.24. When you subtract the initial effective stress (**259 kPa**) due to the self weight (see Figure 3.24a) from the maximum effective stresses (**398 kPa**) after applying the load (t = 1 day) and 50 years of consolidation (see Figure 3.24b), a change in vertical effective stress of **139 kPa** is found due to the applied load and 50 years of consolidation. See Figure 3.25. When you compare the Plaxis 3D stresses acting on the Eem clay layer with the oedometer results from the laboratory, one can conclude that the Eem clay will still behave as an OC soil under high-rise building loads. A final OCR slightly above 1.0 is expected as the vertical effective stress (398 kPa) is less than the pre-consolidation pressure (≈ 443 kPa for North sample #3 at NAP - 31 m, see Figure A.11). Once the load and resulting stress go beyond this point on the (virgin) compression curve, the Eem clay is expected to respond as a NC soil. A NC soil will respond less stiff and result in larger settlements under the same load, as was explained by the theory in Section 2.4.1.

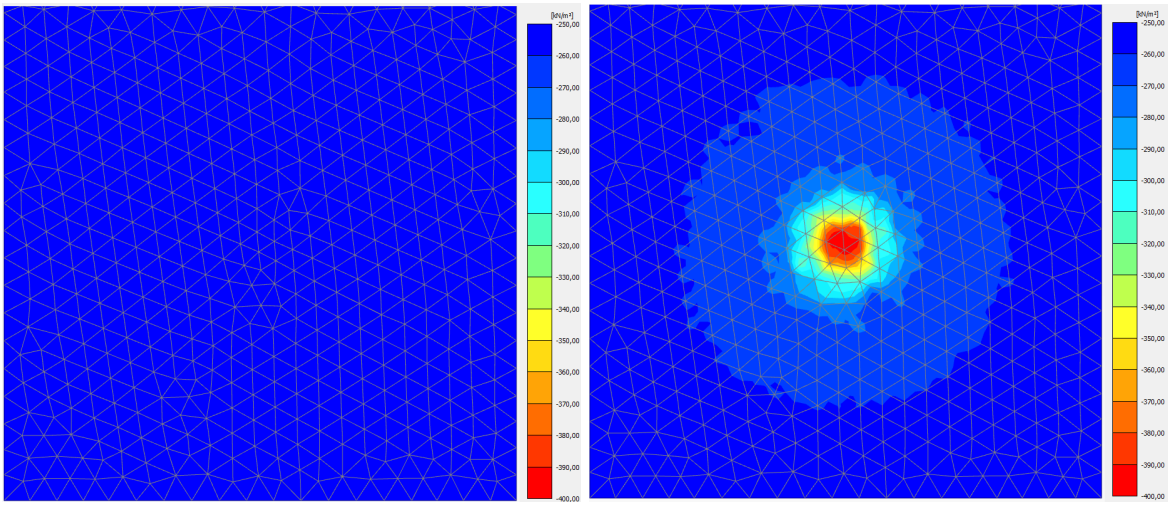

(a) Initial. (b) Consolidation.

Figure 3.24: Cartesian effective stresses (σ'_{zz}) calculated at top of Eem clay (= NAP - 31 m) by Plaxis 3D under SLS surface load (= 382 kPa) applied at Tomlinson depth (= NAP - 19.8 m) with 1/4 spread (= 296 kPa) for a) initial K_0 conditions, and b) after 50 years of consolidation.

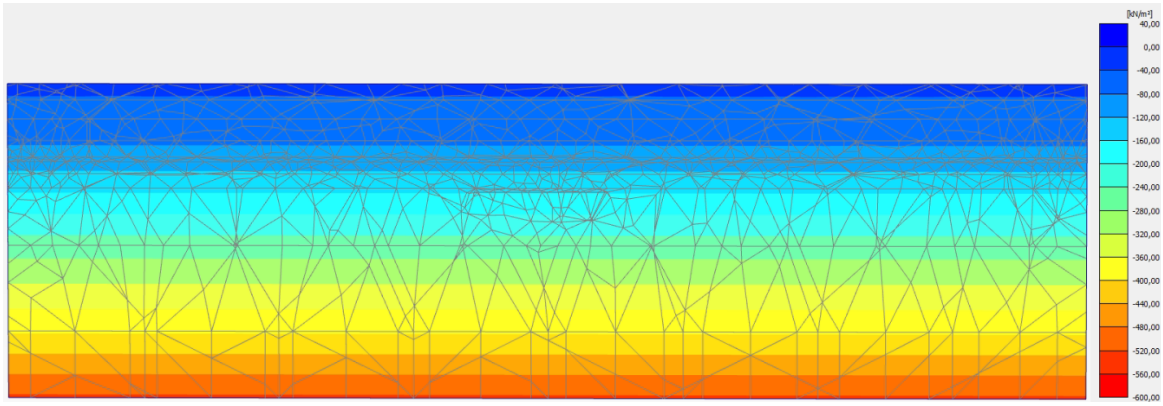

(a) Initial.

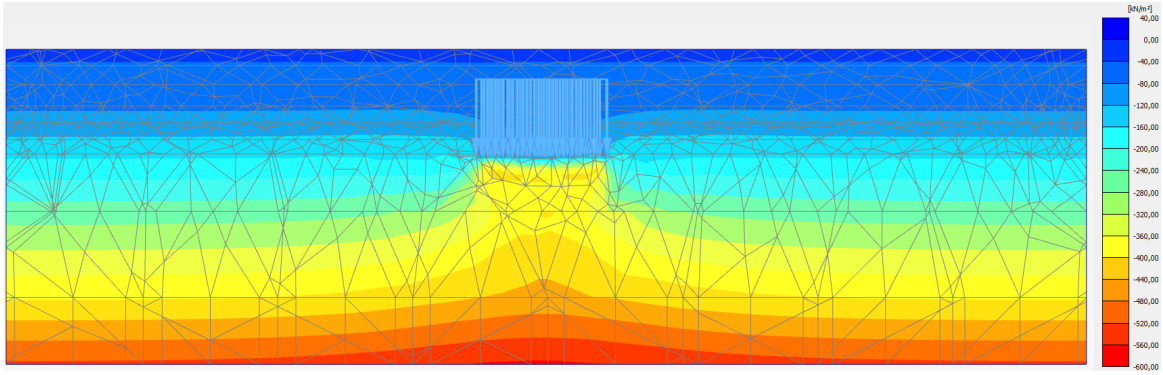

(b) Consolidation.

Figure 3.25: Cartesian effective stresses (σ'_{zz}) calculated for entire depth (= NAP + 2.85 m − NAP - 63 m) by Plaxis 3D under SLS surface load (= 382 kPa) applied at Tomlinson depth (= NAP - 19.8 m) with 1/4 spread (= 265 kPa) for a) initial K_0 conditions, and b) after 50 years of consolidation.

Instead of a stress analysis only, resulting settlements in different layers due to the SLS surface load representing a pile group are calculated and shown in Figure 3.26. The s_2 settlements will be compared (as

model verification) with the settlement trough of the EB-I pile group model in Section 3.1.5. In the pile group model, the settlement trough will be computed for a more realistic stress distribution due to the shaft and base resistance of a pile (group) for both BC methods while the SLS building load is applied as point loads (1,302 kN) on top of the individual EB-I piles. Based on Figure 3.26, one can see that the Eem clay layer as SSCM with CRUX' soil parameters still contributes to **63%** of the s_2 settlements ($= (80mm - 18mm)/99mm \cdot 100\%$) even when the clay behaves as an OC soil. The settlement contribution due to the Drenthe clay is negligible. Note that the orange curve represents the s_2 foundation settlements at 4D below PTL, which are send to the structural engineers and applied or fitted in their structural model(s). However, attention needs to be paid to the fitting of these curves as the SSCM over-predicts the width of the settlement trough based on the theory discussed in Sections 2.4.3 and 2.4.5. Thus, the actual settlement curves will be steeper and could be improved in a future stage of this research by the use of HSS for the deep clay layers where $\Delta\sigma'_v \leq 20\% \cdot \sigma'_{v0}$.

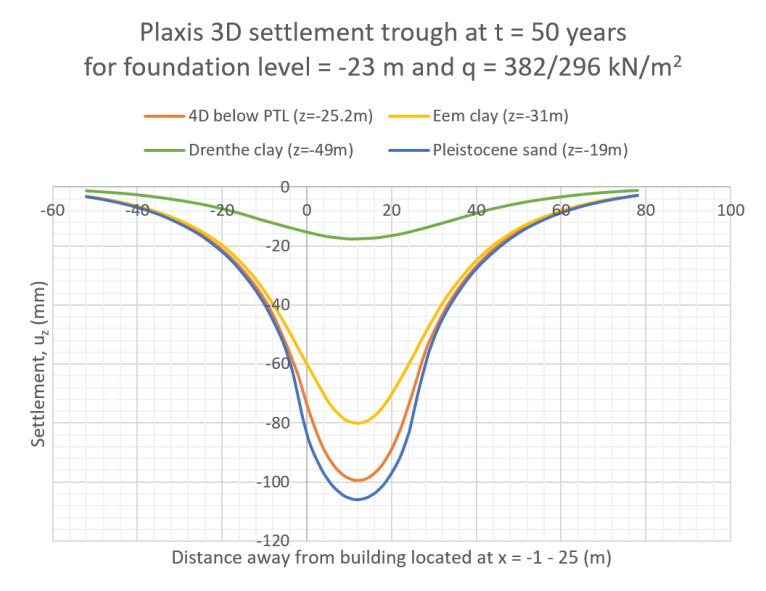

Figure 3.26: Preliminary (s_2) settlement curves at the top of each soil layer in Plaxis 3D using SSCM for Eem & Drenthe clays, HSS for other layers, and building load applied at Tomlinson depth (= - 19.8 m) with 1/4 spread.

3.1.5 Pile Group in Plaxis 3D

In order to better understand the soil and pile behaviour under realistic high-rise building loads, the next step in the research is to investigate the stress distribution of a EB-I pile group in Plaxis 3D with use of the CRUX Eem clay parameters discussed in Section 3.1.4. The analysis will be performed for both the NEN and Maasvlakte pile factors to investigate the load transfer (to the Eem clay) due to the shaft and due to the base for a pile group on top of the (s_1) results for a single pile (Section 3.1.3). The s_2 settlements computed at 4D below PTL (see Figure 3.27) and stress results can also be compared to the simplified pile group model using Tomlinson's equivalent raft approach as discussed in the previous sub-section and shown by the orange curve in Figure 3.26.

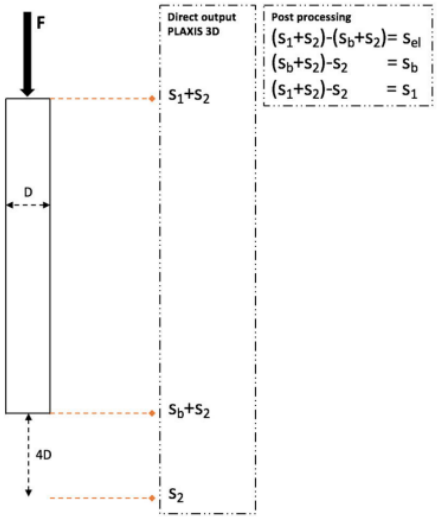

Figure 3.27: Visualisation of Plaxis post-processing for different foundation settlements due to pile group effects according to the NEN 9997-1 (Frissen, 2020).

It is expected that the shaft resistance between pile and soil may disappear when the center-to-center distance reduces to 4D ($= 4 * 0.560m = 2.24m$) or less. For such a small pile spacing, the soil volume between the piles is relatively small and may fail due to the reduced shaft capacity, which results in a downwards soil movement along (with) the piles. When this occurs, more load is transferred to the base of the pile which may be further distributed to the Eem clay causing additional settlements. This phenomena is expected to occur sooner for piles designed in accordance with the NEN pile factors due to the higher α_p (= 0.63) for the base capacity, R_{base}, in comparison to the updated (Maasvlakte) pile factors (= 0.35).

Increasing Foundation Width

Firstly, the effect of an increasing foundation area and therefore the number of piles will be investigated. For this, three different models are build and each model is ran twice; once with the multi-linear bearing capacity for the EB-I based on NEN pile factors and once with the Maasvlakte pile factors. For each scenario, the change in vertical effective stress ($\Delta\sigma'_{zz;Eem}$) distributed from PTL (= NAP - 23 m) to the top of the Eem clay layer (= NAP - 31 m) as a result of the SLS point loads (1,302 kN) acting on top of each EB-I pile and 50 years of consolidation is computed by Plaxis 3D, see Figures 3.29 (NEN method) and 3.30 (Maasvlakte method) for the largest pile group (169 piles). In addition, Figures 3.31a (initial), 3.31b (NEN) and 3.31c (Maasvlakte) show the change in vertical effective stress from GL to the bottom of the Drenthe clay layer. Appendix B.2 (Figures B.8 - B.9) show the horizontal cross-sections for the other four scenarios and Table 3.5 below summarises the results. In this table, one can also find the maximum change in vertical effective stress at PTL ($\Delta\sigma'_{zz;ptl}$), 4D below ($\Delta\sigma'_{zz;4D}$), and the resulting maximum settlements (s_2) for each of the six scenarios and the individual pile models. The s_2 settlements are also plotted in a combined settlement graph shown in Figure 3.28.

Table 3.5: Summary of maximum $\Delta\sigma'_{zz}$ at top of Eem clay (= NAP - 31 m), pile tip level (= NAP - 23 m), 4D below PTL (= NAP - 25.2 m) and s_2 settlements at NAP - 25.2 m after 50 years of consolidation for increasing foundation width and number of piles (as EB-I) with NEN or Maasvlakte pile factors under F = 1,302 kN.

Foundation Width (m)	**No. of Piles**	**Pile Factors**	$\Delta\sigma'_{zz;Eem}$ **(kPa)**	$\Delta\sigma'_{zz;ptl}$ **(kPa)**	$\Delta\sigma'_{zz;4D}$ **(kPa)**	s_2 **(mm)**
1 m x 1 m	1 pile	NEN	1.3	6.7	5.9	0.41
1 m x 1 m	1 pile	MV2	1.1	5.8	4.3	0.40
6 m x 6 m	16 piles	NEN	15.4	119	118	10.7
6 m x 6 m	16 piles	MV2	14.5	116	102	10.2
16 m x 16 m	81 piles	NEN	91	406	306	55.3
16 m x 16 m	81 piles	MV2	88	395	302	54.4
24 m x 24 m	169 piles	NEN	141	563	404	97.2
24 m x 24 m	169 piles	MV2	139	510	383	95.9

Based on the change in vertical effective stress shown by the horizontal cross-sections for each scenario at three different depths, the difference between the NEN and Maasvlakte design methods are negligible. The percent difference is highest at PTL ($\Delta\sigma'_{zz;ptl}$) and ranges from **2.5%** to **9.9%** for increasing foundation width and number of piles. This is significantly lower in comparison to individual piles where a difference of **14%** can be found at PTL. The difference can be explained by the effect of neighbouring piles. More piles will result in a larger stress bulb at the base of the pile group, which is distinguished more for the NEN method due to the higher α_p and resulting base resistance, R_{base}.

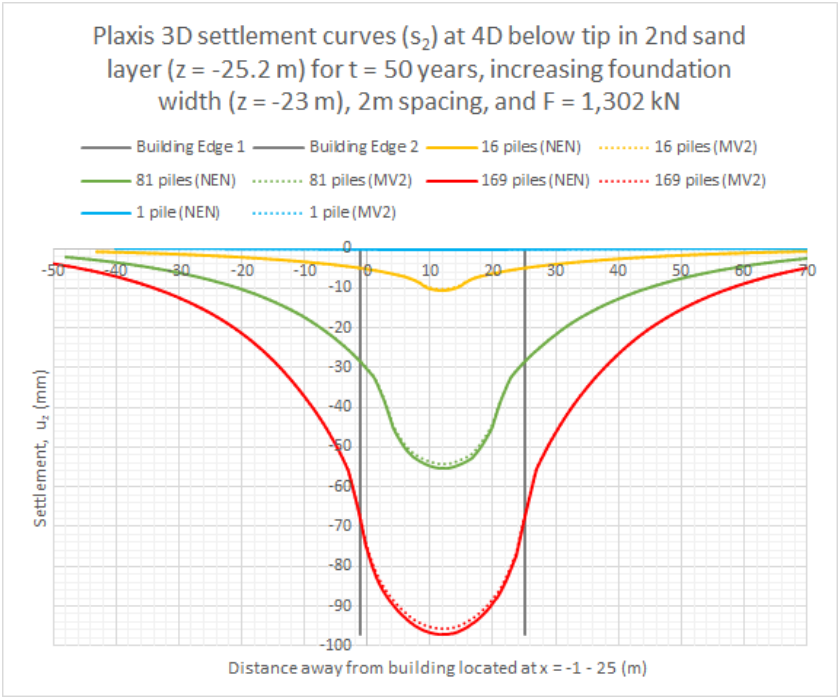

Figure 3.28: Combined settlement curves (s_2) 4D below pile tip (= NAP - 25.24 m) in Plaxis 3D for increasing foundation width and number of piles (as EB-I) with NEN or Maasvlakte pile factors.

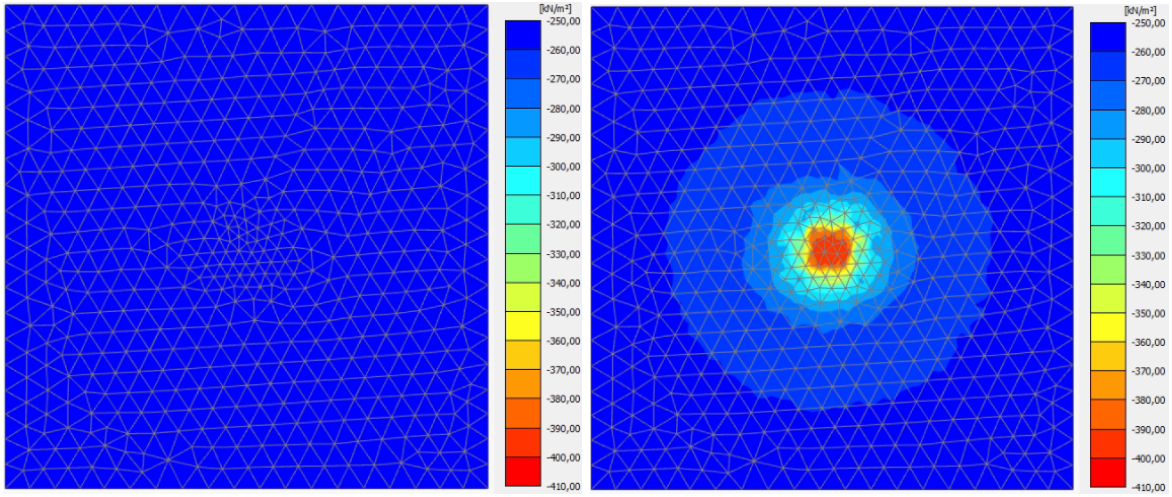

(a) Initial. (b) Consolidation.

Figure 3.29: Cartesian effective stresses (σ'_{zz}) calculated at top of Eem clay (= NAP - 31 m) by Plaxis 3D under SLS point loads (= 1,302 kN) applied at 169 pile heads (as EB-I) with **NEN** pile factors for a) initial K_0 conditions, and b) after 50 years of consolidation.

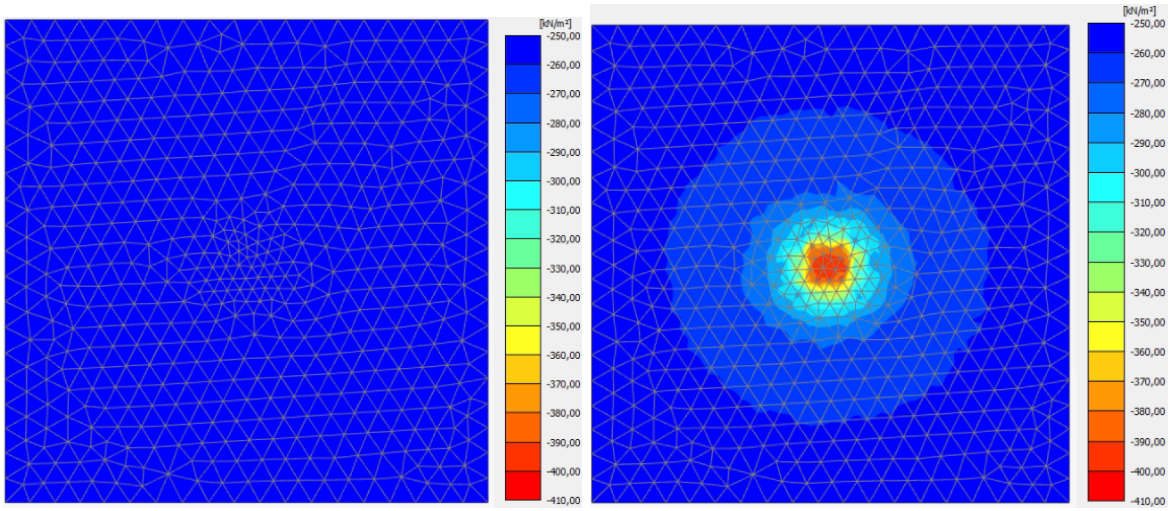

(a) Initial. (b) Consolidation.

Figure 3.30: Cartesian effective stresses (σ'_{zz}) calculated at top of Eem clay (= NAP - 31 m) by Plaxis 3D under SLS point loads (= 1,302 kN) applied at 169 pile heads (as EB-I) with **Maasvlakte** pile factors for a) initial K_0 conditions, and b) after 50 years of consolidation.

However, for s_2 settlements, the change in stress felt by the soil due to the applied SLS loads 4D below PTL is most important as this signifies the bottom of the stress bulb developed by pile groups (see Figure 2.23 in Section 2.3). At this depth, the percent difference ranges from **1%** to **14%**, which is much lower than **31%** for individual piles. Nonetheless, this effect on the s_2 values for pile groups falls within **5%** and is mostly controlled by the stress distribution to the layers below 4D where $\Delta\sigma'_{zz;Eem}$, for instance, only differs $\approx$ **1-6** %.

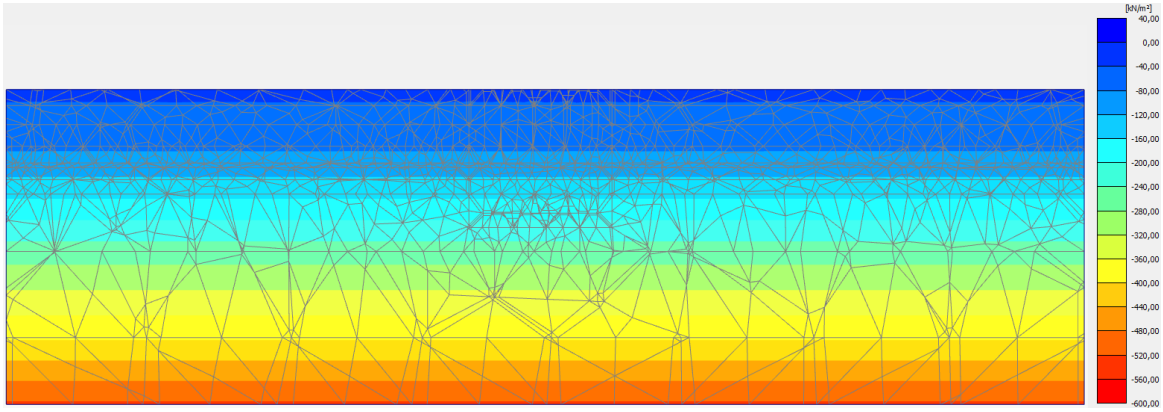

(a) Initial.

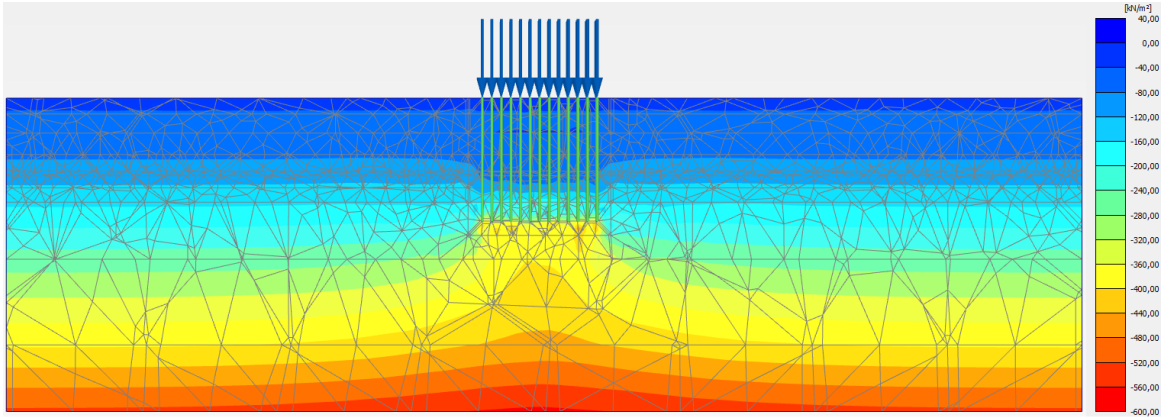

(b) Consolidation (NEN).

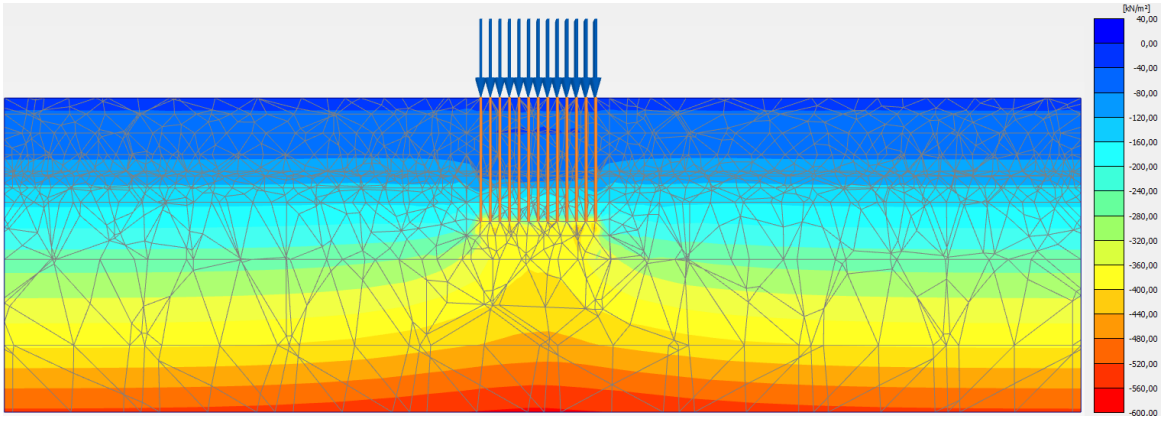

(c) Consolidation (MV2).

Figure 3.31: Cartesian effective stresses (σ'_{zz}) calculated for entire depth (= NAP + 2.85 m − NAP - 63 m) by Plaxis 3D under SLS point loads (= 1,302 kN) applied at 169 pile heads (as EB-I) for a) initial K_0 conditions, b) after 50 years of consolidation with NEN factors, and c) Maasvlakte factors.

The influence of the pile factors and consequent pile capacity on the s_2 settlement predictions after 50 years of consolidation is better illustrated by Figure 3.28. In this graph, one can see that the dashed lines (updated pile factors) follow the same trend as the corresponding, continuous line for the same pile group geometry. Based on this analysis, one may conclude that the s_2 settlements are controlled by the geometry of the problem more than the bearing capacity input of the embedded beams. Furthermore, one can see that pile group behaviour overrules the behaviour of a single pile for increasing foundation widths and number of piles ($s_2 \geq s_1$).

Increasing Pile Spacing

Secondly, the effect of pile spacing is analysed. To reduce the computation time, the new Plaxis feature "swept meshing" is used. According to the Plaxis manual, this new function can be applied to volumes for which a mesh is generated at the source face and 'swept' along the sweeping direction of the volume, see Figure 3.32. For this reason, a large difference ($\geq$ **21**%) can be found for the change in stresses caused by 169 piles (2 m spacing) in Table 3.6 below and the previously mentioned results in Table 3.5. This shows the mesh dependency of the embedded beam model on the stress distribution, even for the new formulation (EB-I). However, the s_2 settlements computed with or without swept meshing differ only by $\approx$ **1**%, so the method is still considered reliable for a quantitative comparison of the settlements as a result of differing pile spacing under the same foundation width (26 m x 26 m). Note that the foundation width is not the same as the surface load area used by Tomlinson's equivalent raft approach. The latter is based on the distance between the outer piles (24 m x 24 m), which are located 1 m from the edge of the foundation. This has no influence on the results for a pile foundation as the load is carried by the piles instead of (partially) by the slab.

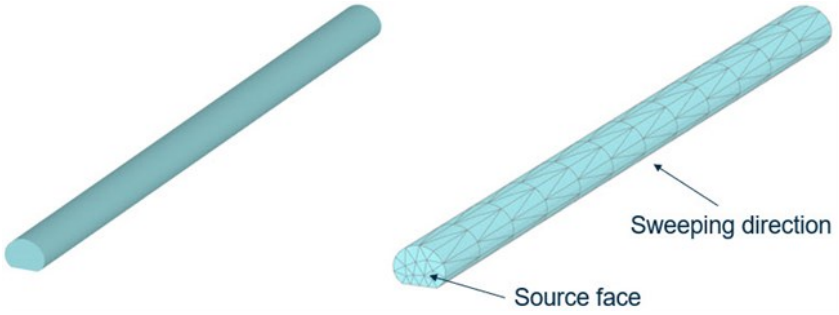

Figure 3.32: Swept meshing principles in Plaxis 3D (Brinkgreve, 2021).

Table 3.6: Summary of maximum $\Delta\sigma'_{zz}$ at top of Eem clay (= NAP - 31 m), pile tip level (= NAP - 23 m), 4D below PTL (= NAP - 25.2 m) and s_2 settlements at NAP - 25.2 m after 50 years of consolidation for increasing pile spacing and decreasing number of piles (as EB-I) with NEN or MV2 pile factors under F = 1,302 kN.

Pile Spacing (m)	**No. of Piles**	**Pile Factors**	$\Delta\sigma'_{zz;Eem}$ **(kPa)**	$\Delta\sigma'_{zz;ptl}$ **(kPa)**	$\Delta\sigma'_{zz;4D}$ **(kPa)**	s_2 **(mm)**
NA	1 pile	NEN	1.3	6.7	5.9	0.41
NA	1 pile	MV2	1.1	5.8	4.3	0.40
2 m	169 piles	NEN	114	241	336	95.3
2 m	169 piles	MV2	113	234	326	94.4
3 m	81 piles	NEN	46	80	107	36.6
3 m	81 piles	MV2	45	78	104	36.3
4 m	49 piles	NEN	25	39	47	19.3
4 m	49 piles	MV2	24	37	46	19.2

Similar to the increasing pile group and number of piles, Table 3.6 above shows a summary of the influence of the pile spacing under the same SLS point loads (= 1,302 kN) and 50 years of consolidation on the change in vertical effective stresses felt by the soils at the top of the Eem clay layer ($\Delta\sigma'_{zz;Eem}$), at the base of the pile ($\Delta\sigma'_{zz;ptl}$), and at 4D below ($\Delta\sigma'_{zz;4D}$). The effects on the s_2 settlements are also tabulated and in addition illustrated in Figure 3.33 below. For the pile spacing scenarios, a similar trend is observed for the NEN and updated design method for which the computed s_2 settlement results differ by less than 1%. One can also conclude that using less piles with a spacing $\geq$ 5D under the same point loads will result in significantly less settlements and a more economic design. Realistically, the SLS point loads acting on the piles should increase

when the number of piles is reduced under the same high-rise building (see Figure 3.37). However, this was only possible for the 2 m and 3 m pile spacing models as the building load acting on the individual piles would exceed its ultimate bearing capacity and fail. See Figure 3.40 (Section 3.1.6) for a more elaborated comparison between different centre-to-centre distances of piles. Nonetheless, the pile spacing has proved to be a key design parameter for an economic, sustainable, and safe high-rise building.

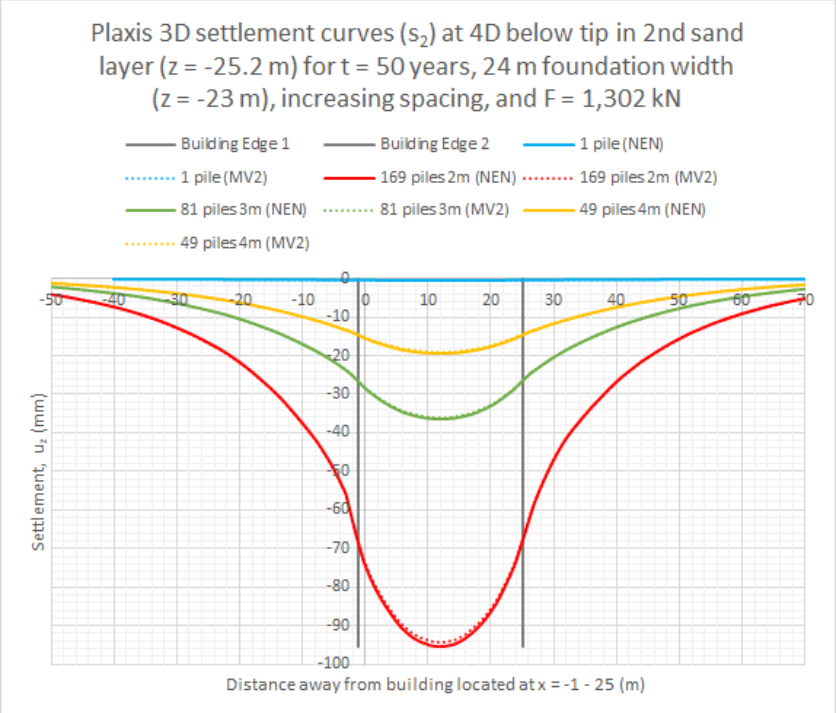

Figure 3.33: Combined settlement curves (s_2) 4D below pile tip (= NAP - 25.24 m) in Plaxis 3D for increasing pile spacing and decreasing number of piles (as EB-I) with NEN or Maasvlakte pile factors within 26 m x 26 m foundation dimensions.

Finally, the influence of the swept meshing function in Plaxis 3D on the change in $\sigma'_{zz;Eem}$ as a result of 169 axially loaded piles at 2 m spacing is illustrated by Figures 3.34 and 3.35. These horizontal cross-sections clearly show the effect of swept meshing on the mesh distribution below pile tip level when compared to Figure 3.29 and 3.30. Note that the legends do not have the same scale when used for a quantitative σ'_{zz} comparison. Figures B.10 and B.11 in Appendix B.2 illustrate the $\Delta\sigma'_{zz;Eem}$ for both pile design methods applied to a model with 81 piles at 3 m spacing (= 5D) and to 49 piles at 4 m spacing (= 7D), respectively.

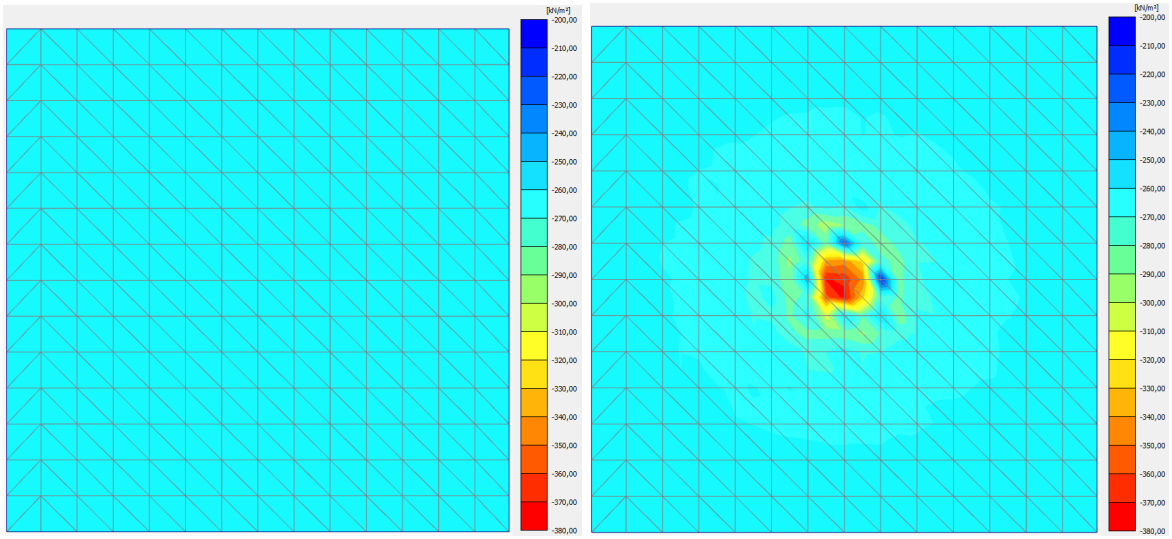

(a) Initial. (b) Consolidation.

Figure 3.34: Cartesian effective stresses (σ'_{zz}) calculated at top of Eem clay (= NAP - 31 m) by Plaxis 3D (swept meshing) under SLS point loads (= 1,302 kN) applied at 169 pile heads (as EB-I) at 2 m (= $3.5 \cdot D$) spacing with NEN pile factors for a) initial K_0 conditions, and b) after 50 years of consolidation.

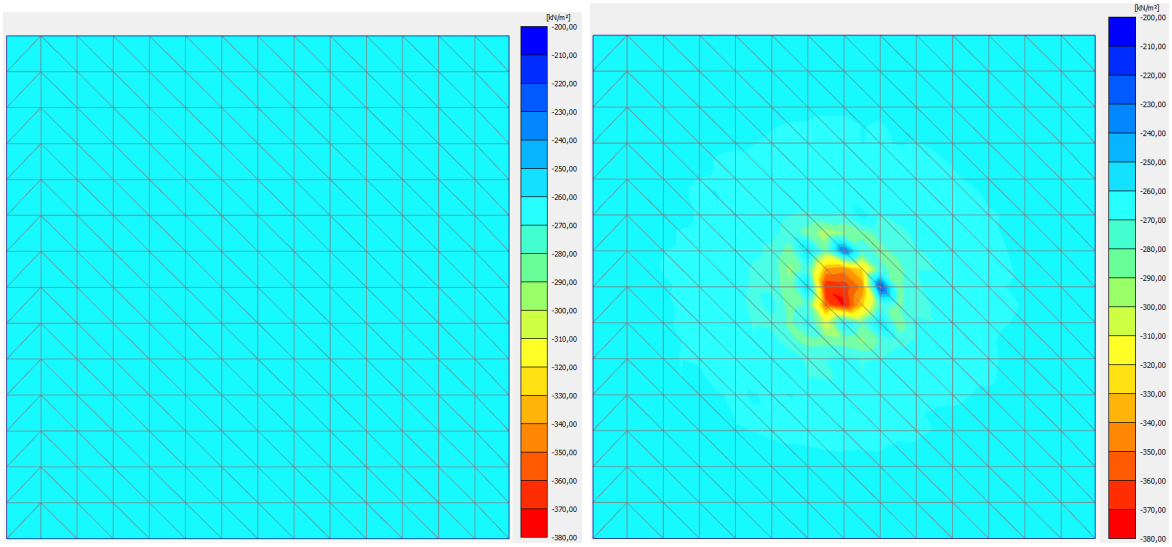

(a) Initial. (b) Consolidation.

Figure 3.35: Cartesian effective stresses (σ'_{zz}) calculated at top of Eem clay (= NAP - 31 m) by Plaxis 3D (swept meshing) under SLS point loads (= 1,302 kN) applied at 169 pile heads (as EB-I) at 2 m (= $3.5 \cdot D$) spacing with Maasvlakte pile factors for a) initial K_0 conditions, and b) after 50 years of consolidation.

In addition, Figures B.12, B.13, and 3.36 visualise the stress distribution from GL to the bottom of the Drenthe clay layer for a pile spacing of 2 m (169 piles), 3 m (81 piles), and 4 m (49 piles). Minor differences can be observed between the NEN and updated bearing capacity methods, however, a significant difference of the pile spacing on the load distribution to the deep, compressible clay layers can be noticed.

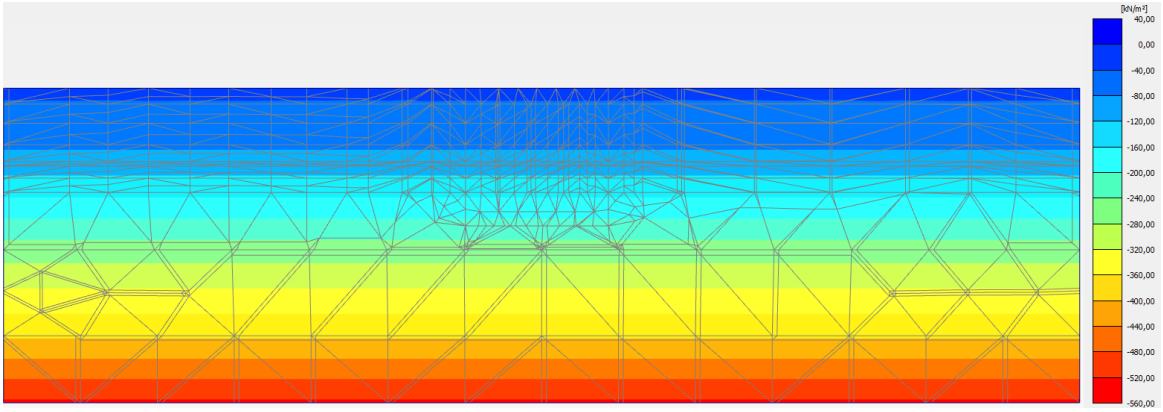

(a) Initial.

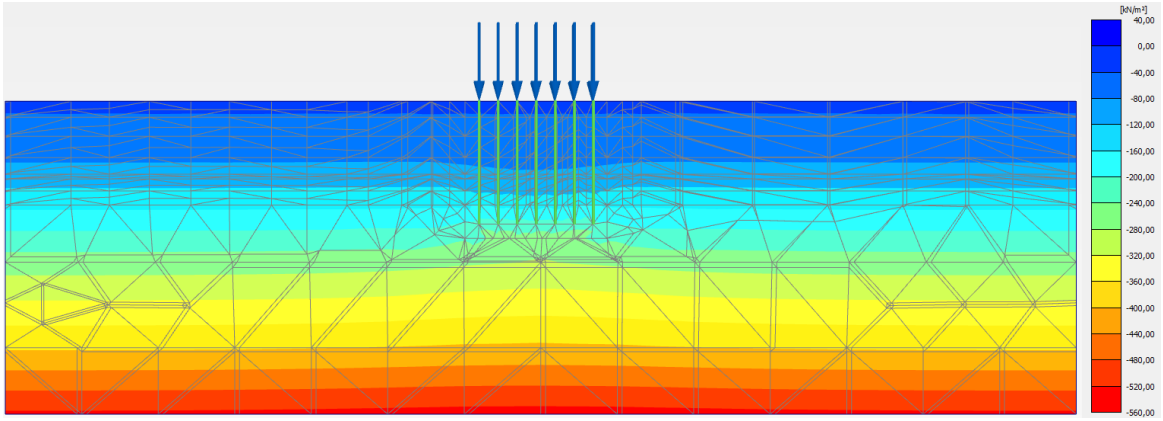

(b) Consolidation (NEN).

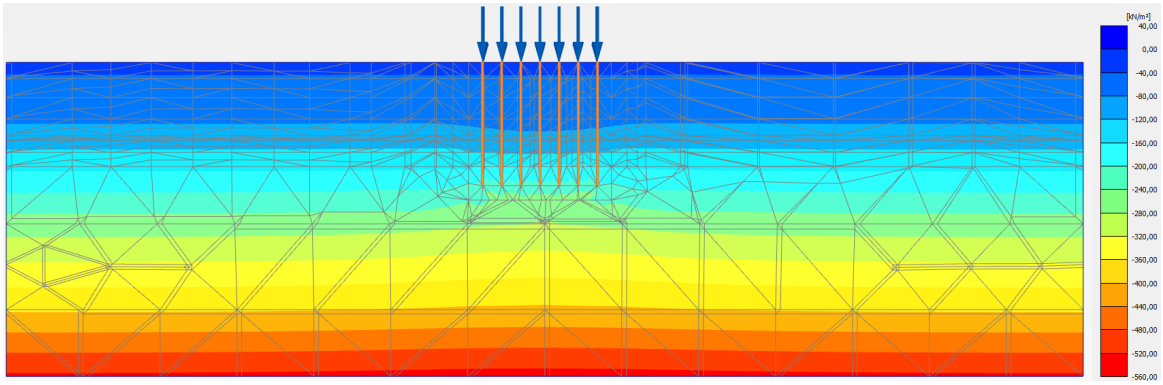

(c) Consolidation (MV2).

Figure 3.36: Cartesian effective stresses (σ'_{zz}) calculated for entire depth (= NAP + 2.85 m − NAP - 63 m) by Plaxis 3D under SLS point loads (= 1,302 kN) applied at 49 pile heads (as EB-I) at 4 m (= $7 \cdot D$) spacing for a) initial K_0 conditions, b) after 50 years of consolidation with NEN factors, and c) Maasvlakte factors.

Increasing Building Loads

Thirdly, the influence of the building loads on the pile group behaviour is investigated. In the previous analysis, only the SLS load is considered meaning that the stress distribution to the pile tip is only influenced by the linear elastic behaviour of the pile. In Figure 3.6 (Section 3.1.3), one can see that a pile designed with the NEN pile factors behaves in a similar way as a pile designed with the updated pile factors until the load exceeds the SLS capacity. For this reason, for the same pile group geometry (81 piles at 3 m spacing), the SLS load acting on the top of the EB-I piles is increased to ULS and beyond its ultimate capacity, R_{total}, for both design methods. Appendix B.2 Figures B.13 - B.15 show the change in vertical effective stress due to increasing building loads. For the scenario where the applied load equals the ultimate bearing capacity of the pile (without partial factors), one can see that the change in stresses felt at 4D below the base of the piles ($\sigma'_{zz;4D}$) differ by $\approx$ **150 kPa**. Most stresses are felt by the sand (4D) directly below the piles designed in accordance with the NEN and located at the edges of the pile group. In a realistic high-rise building design, the point loads acting on the piles will not be equal to each other and will increase towards the centre of the building making the piles in the centre carry more load than the outer piles. After load distribution within the superstructure due to the building stiffness will then result in higher pile loads at the edges of the building instead of the centre. However, the distribution down to the Eem clay layer is not significantly influenced by the different pile factors for this geometry. An SSI modelling approach in Section 3.2 will further investigate the pile group behaviour and resulting s_2 settlements under SLS high-rise building loads determined by SCIA.

Additionally, Figure 3.37 show the resulting s_2 settlement curves for both design methods as a result of the increasing point loads. One can see that the difference between the bearing capacity methods increase slightly (from **1%** to **4%**) when the applied load advances past the linear elastic portion of the load settlement curve for a Fundex 460/560.

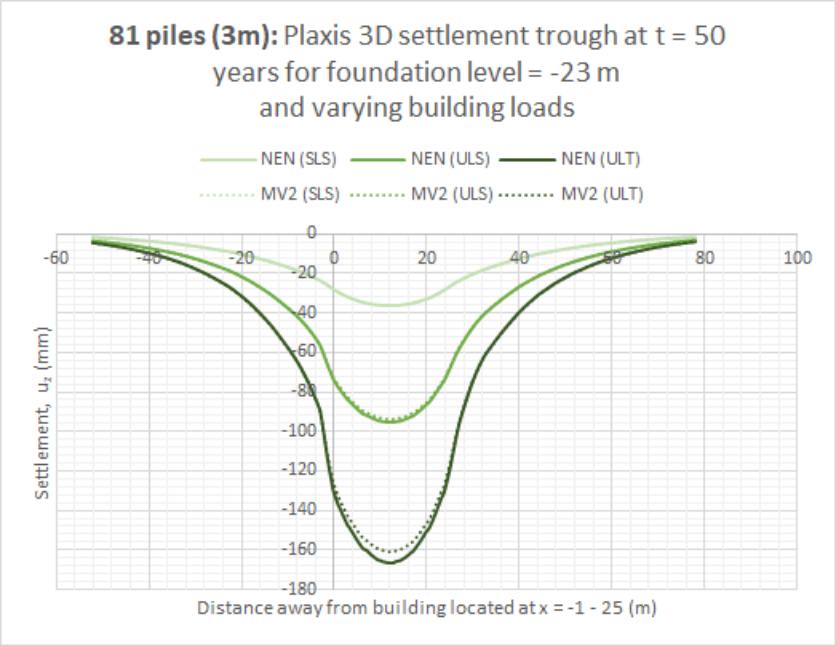

Figure 3.37: Combined settlement curves (s_2) 4D below pile tip (= NAP - 25.24 m) in Plaxis 3D for increasing pile loads applied at 81 pile heads (as EB-I) at 3 m ($= 5 \cdot D$) spacing with NEN or Maasvlakte pile factors within 26 m x 26 m foundation dimensions.

3.1.6 Conclusion: Influence of Pile Factors on Foundation Settlements

Even though it was expected to observe a difference in stress distribution and resulting settlements under a pile group designed by different pile factors, the analysis performed in Plaxis 3D showed otherwise.

Firstly, Figure 3.38 summarises the deterministic results of the s_1 settlement predictions for a Fundex 460/560 as type 1 (NEN) and type 2 (MV2) based on 1 CPT with the use of:

1. D-Foundations (2022) with limits on q_c (12-15 MPa) and pile factors according to the current daily practice (*NEN9997-1*) as described in Appendix A.4,
2. Analytical approximations without limited q_c values for the bearing capacity (*NEN9997-1**) as described in Section 3.1.1,
3. CEMS' PileCore (2022) without limited q_c values for the bearing capacity and the option to include multiple CPT's (*PileCore*) by a statistical analysis (ξ) as described in Section 3.1.3,
4. Improved FEM models in Brinkgreve (2021) with piles modelled as embedded beams with the new formulation (EB-I) and PileCore's bearing capacity input (*Plaxis 3D*) as described in Section 3.1.3.

Note that the methods do not include partial factors (i.e., γ_f or ξ) and the dashed line shows an average s_1 value based on all methods.

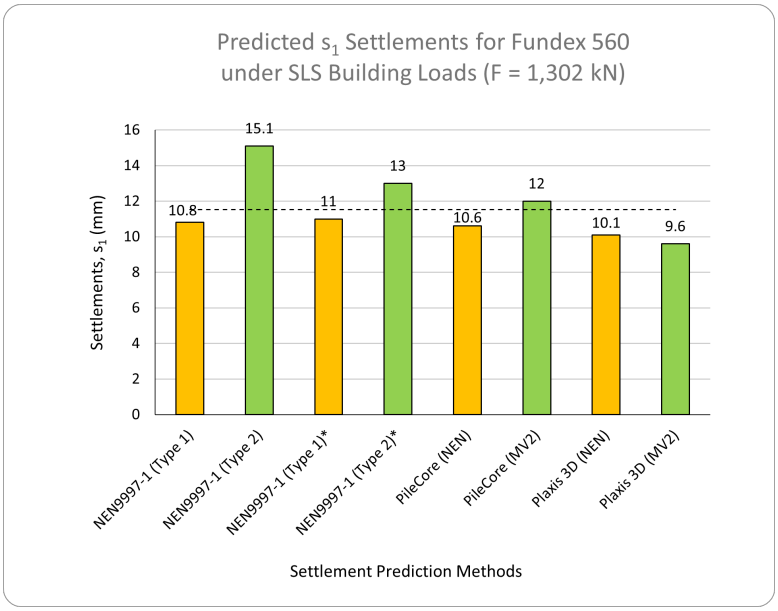

Figure 3.38: Predicted s_1 settlements for a Fundex 560 as type 1 (NEN) and type 2 (MV2) pile based on different methods and software under the same SLS building load.

One can see that the method currently used in daily practice (NEN9997-1) predicts the largests s_1 settlements for a Fundex 460/560 pile with type 2 load-settlement behaviour. This is because of the use of NEN9997-1 screwed pile factors and the limit on the q_c values (12 - 15 MPa) for the bearing capacity of a type 2 pile in D-Foundations. The influence of a higher shaft capacity versus base capacity for a type 2 pile based on updated pile factors (type 2 or MV2) is shown by the second (NEN9997-1*) and third (PileCore) green columns.

Considering s_2 settlements are significantly larger than s_1 settlements ($\approx$ 100 mm $\geq$ 10 mm), it was chosen to not fit the EB-I piles with NEN factors in Plaxis 3D to the type 1 normalised load displacement curve in the NEN9997-1 (Figure 2.1) as proposed by Frissen (2020). Neither was decided to fit the MV2 EB-I pile to the pile load tests performed at the *Maasvlakte* in Plaxis 3D (Gavin, 2020). On top of that, one can see in Figure 3.38 that even without fitting the load-settlement behaviour of the pile(s) in Plaxis 3D, the s_1 settlements for this specific pile design only differs by $\approx 6\%$ for the NEN pile factors and $\approx 20\%$ for the updated pile factors (MV2). The latter could be due to the lower α_p factor (0.35) versus the factor in the NEN (0.63) resulting in less stress at PTL and thus less pile tip settlements, s_b. Furthermore, Plaxis 3D does not include installation effects to properly model different pile type (1 or 2) behaviour.

Secondly, pile group behaviour and the effects of different pile factors and pile spacing was investigated in Plaxis 3D. Figure 3.39 shows the combined s_2 settlement results for a 26 m x 26 m foundation slab (with a 24 m center-to-center spacing of the outer piles) based on:

1. An analytical approximation (NEN9997-1) as described in Section 3.1.2,
2. A simplified FEM analysis in Brinkgreve (2021) according to Tomlinson's equivalent raft approach and a SLS surface load with 1/4 spread as described in Section 3.1.4,
3. A FEM analysis in Brinkgreve (2021) for 169 piles as EB-I spaced 2 m apart under equivalent SLS point loads as described in Section 3.1.5,
4. A FEM analysis in Brinkgreve (2021) for 81 piles as EB-I spaced 3 m apart under equivalent SLS point loads as described in Section 3.1.5.

Note that the methods do not include partial factors (i.e., γ_f or ξ) and the dashed line shows an average s_2 value based on the FEM methods (items 2 - 4) only.

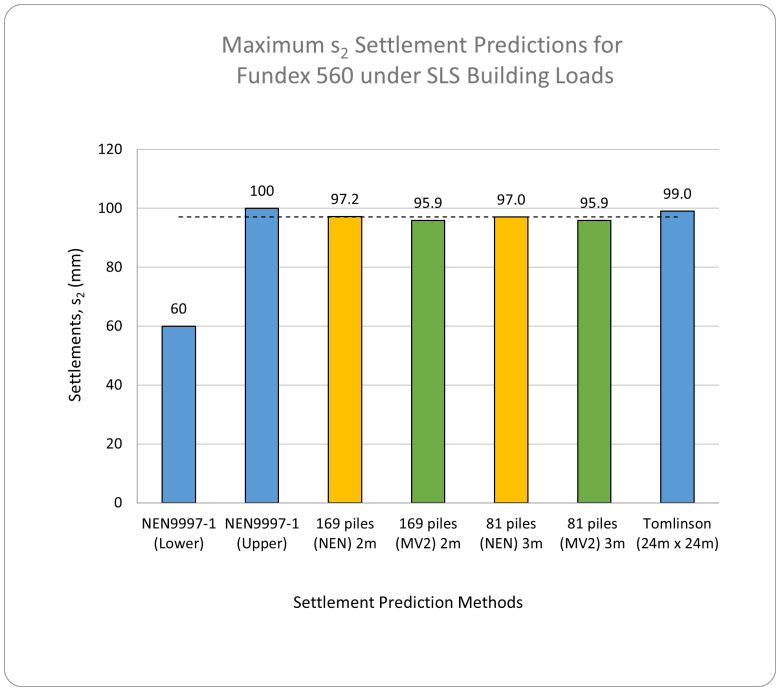

Figure 3.39: Predicted s_2 settlements for a Fundex 560 as type 1 (NEN) and type 2 (MV2) pile by hand and by Plaxis 3D under equivalent SLS building loads and a foundation width of 26 m x 26 m.

One can see that the upper analytical method is a relatively good approximation of the predicted s_2 settlements computed by either the simplified load spread method according to Tomlinson and the more elaborated embedded beams approach in Plaxis 3D. More importantly, one may conclude that the influence of pile factors and resulting bearing capacity input according to the NEN9997-1 (NEN) or updated pile design (MV2) is negligible for s_2 settlements computed 4D below PTL. For this reason, only the NEN pile factors will be considered in the remainder of this thesis to improve the current SSI design loop for a high-rise building. Nevertheless, after taking out the "swept meshing" effect, Figure 3.40 still shows a slight increase in change of vertical effective stresses felt by the top of the Eem clay layer for a pile group with a spacing of 3 m and NEN factors in comparison to Tomlinson or 2 m spacing. The difference may be due to a larger stress bulb development for a pile group with a larger pile spacing.

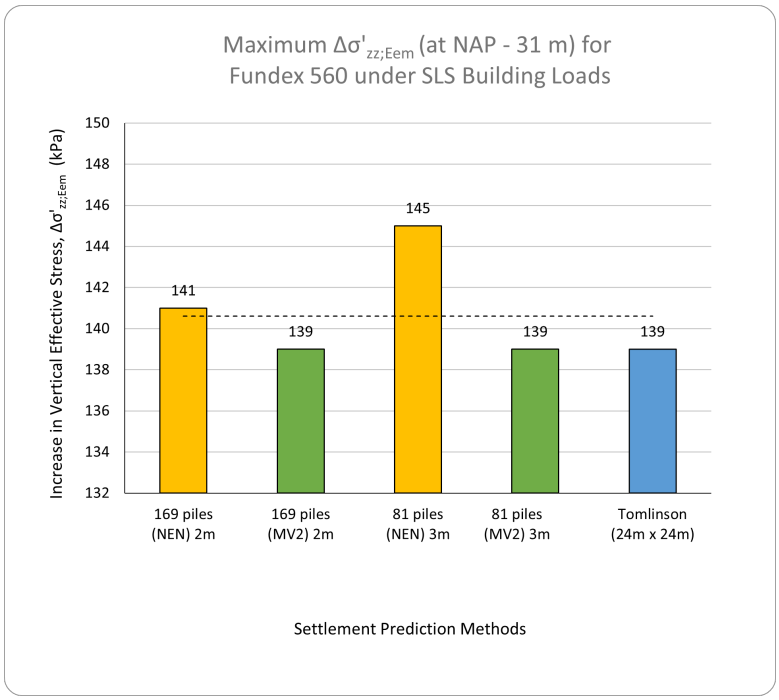

Figure 3.40: Computed change in vertical effective stress at top of Eem clay layer due to equivalent SLS building loads and 50 years of consolidation for a Fundex 560 as type 1 (NEN) and type 2 (MV2) by Plaxis 3D and a foundation width of 26 m x 26 m.

Furthermore, Figures B.16 - B.19 in Appendix B.2 shows the combined results with smaller pile groups for which a similar conclusion regarding pile factors and s_2 settlements applies.

Thirdly, the settlement contribution due to Eem clay layer for the pile group with 169 piles and 2 m spacing is found to be **66%**, see Figure 3.41. This is comparable with the computed **63%** for Tomlinson's equivalent raft approach. One can also state that the Eem clay layer will still respond relatively stiff (OC) to the applied building loads as the additional 139 kPa will not exceed the yield stress of the compressible clay layer.

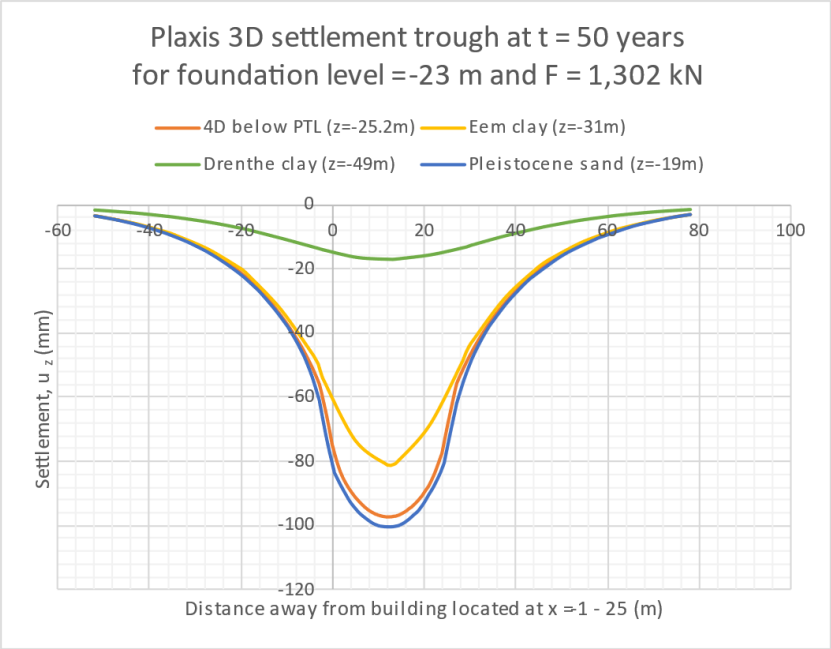

Figure 3.41: Settlement curves (s_2) at the top of each soil layer in Plaxis 3D using SSCM for Eem & Drenthe clays, HSS for other layers, and building load applied as SLS point loads on 169 piles spaced 2 m apart with NEN pile factors.

In the following sections of this chapter, the knowledge gained by the analytical settlement approximations and the parametric study of the numerical single pile, soil test, and pile group models described above will be applied to an improved version of the current SSI design methodology that was described in Section 2.1.3 of the previous chapter. An enhanced version of the simple SSI design loop based on VRI's mattress model approach will be practiced in Section 3.2 using Tomlinson's load spread method (Section 3.2.2) and the PileCore fitted embedded beam (EB-I) method with **NEN pile factors** (Section 3.2.4). Additional model variations and scenarios (see Figure 3.42) will be compared in Appendix B.2.1 to test the uncertainties and bandwidth of a streamlined approach for an updated, more complex and realistic SSI design methodology.

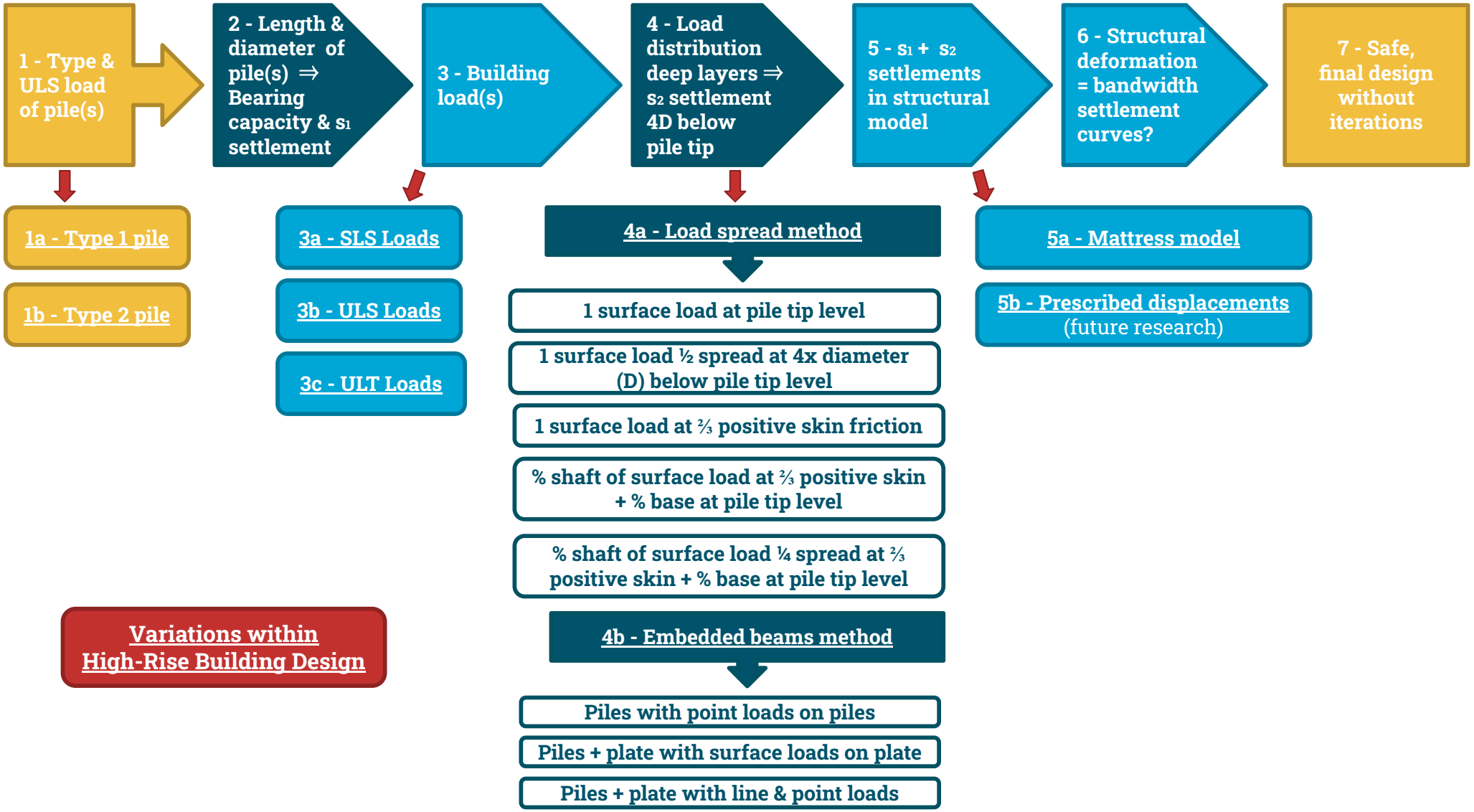

Figure 3.42: Proposed geotechnical and structural modelling variations (for use in Section 3.2 and Appendix B.2.1) based on literature review (Ch. 2).

3.2 Simple Soil-Structure Interaction Modelling

This section follows the general idea of the SSI modelling approach as described in Section 2.1.3. The design steps taken will be listed below alongside a short explanation of model assumptions and (numerical) results.

3.2.1 Model Setup

The numerical, design approach will not be applied to a real case study. Instead, a simple, symmetric high-rise building design of **69 m** (23 stories) will be used. As the tower height falls below 70 m, partial factors according to safety class **CC2** for residential buildings are used for the load classes. The building will be constructed in northern Amsterdam (see Figure 3.1 for the soil profile), as briefly mentioned in Section 3.1 for the parametric study of a similar foundation system.

Geometry (step 0)

In general, the structural design and geometry of the setup is governed by the architectural plans and preliminary drawings. The resulting structural plans for the simple tower were drawn in AutoCAD, see Figures C.1 and C.2 in Appendix C, but is more commonly modelled in Autodesk Revit and SCIA as part of BIM 3D, see Figure 3.43 below. The required strength and stiffness of the materials for the structural elements are calculated by the structural engineer, see Table C.1. Rules of thumb and basic assumptions are used for the initial dimensions of the structural elements and spacing or centre-to-centre distance between, see Table C.2.

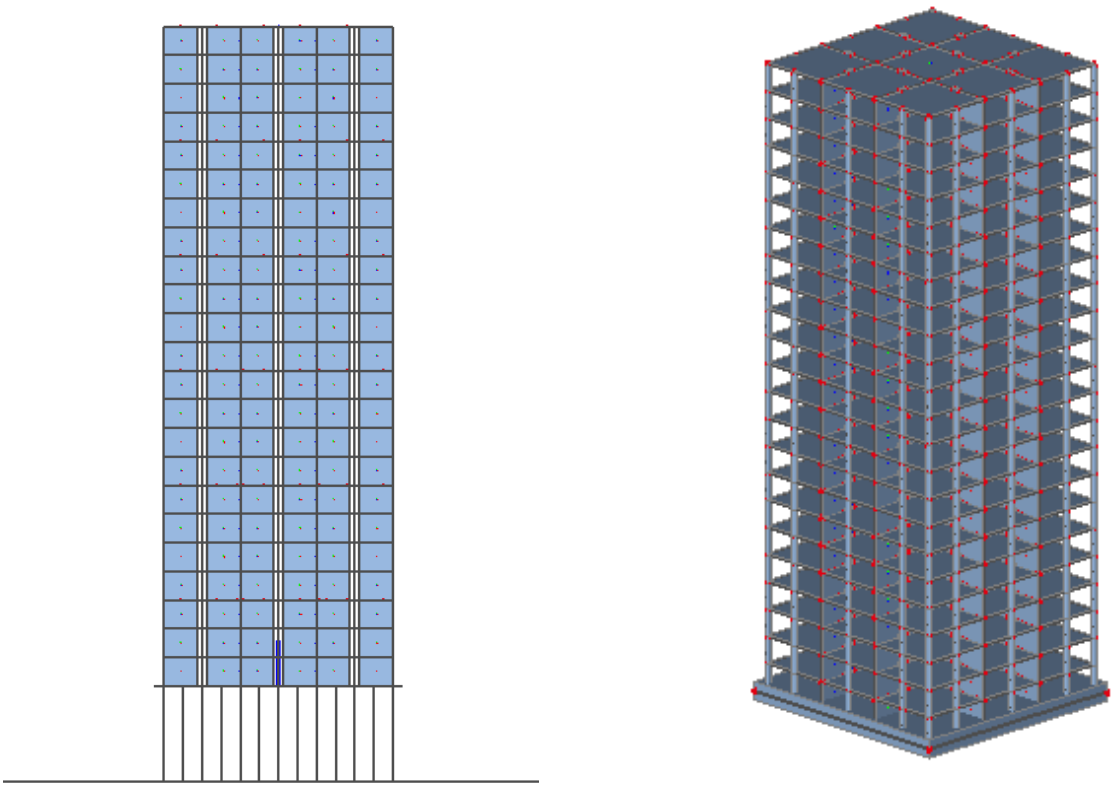

(a) 2D. (b) 3D.

Figure 3.43: Visualisation of simple, symmetric tower modelled in SCIA.

Initial pile plans are designed (by the structural engineer) and an appropriate foundation system (see Section 2.2.3) is chosen to carry the high-rise building load from the superstructure to the bearing layer. In this case, a pile foundation was chosen with a thick 2 m floor (i.e., ground floor or basement) to connect the pile heads instead of a pile cap. For this foundation design, a symmetric and simplified pile grid with a centre-to-centre distance of 2 m is chosen, see Figure 3.44. The coordinates of the corresponding piles in SCIA differ from the coordinates in Plaxis 3D as the axis origin of the SCIA model was determined for the centre of the tower. The total model domain of SCIA, however, corresponds well with the model domain of the subsurface in Plaxis 3D by an offset of 52 m in both the x- and y-directions. This way, the 3D model in Plaxis satisfies the domain needs for a foundation level in the second Pleistocene sand layer as described by Figure 2.2 in Section 2.1.1.

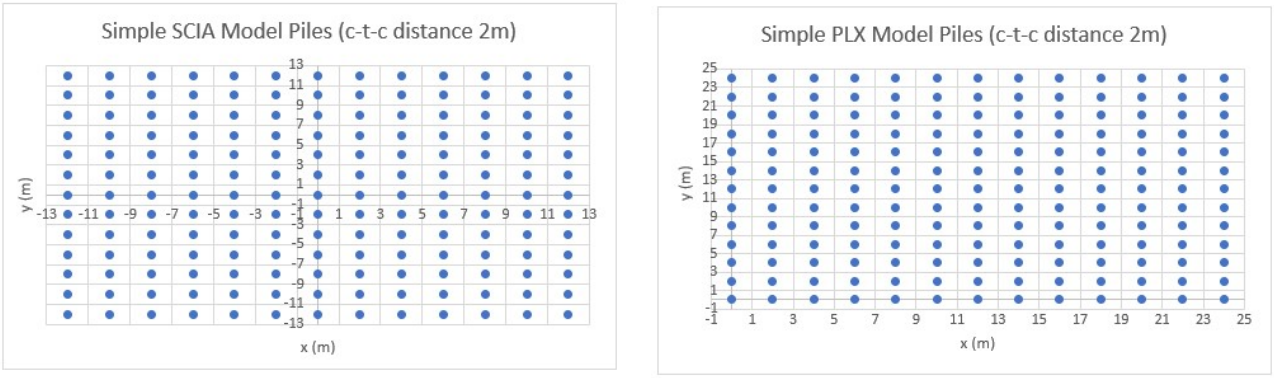

(a) Coordinates in **SCIA**.

(b) Coordinates in **Plaxis**.

Figure 3.44: Coordinates and center-to-center distance of piles in a) SCIA, and b) Plaxis for a 24 m x 24 m tower with a 26 m x 26 m foundation plate and pile spacing of 2 m for 169 piles.

Soil Parameters (step 0)

The soil stratigraphy for the Plaxis model is based on CPT data (see Figures A.1 - A.3) measured in the North of Amsterdam. The interpretation and following simplification of the data is the same as the soil profile used for the pile group model in Section 3.1.5, see (Figure B.2 and) soil layering below:

- **Sand fill** (NAP + 2.85 m – NAP - 0.5 m),
- **Peat** (NAP - 0.5 m – NAP - 4.5 m),
- **Clay** (NAP - 4.5 m – NAP - 9 m),
- **Sandy clay** (NAP - 9 m – NAP - 12.5 m),
- **Peat** (NAP - 12.5 m – NAP - 13.5 m),
- **First Pleistocene sand** (NAP - 13.5 m – NAP - 16 m),
- **Clayey sand** (NAP - 16 m – NAP - 19 m),
- **Second Pleistocene sand** (NAP -19 m – NAP - 31 m),
- **Eem clay** (NAP - 31 m – NAP - 49 m),
- **Drenthe clay** (NAP - 49 m – NAP - 63 m),
- **Third Pleistocene sand** (NAP - 63 m).

The constitutive model used for the Eem and Drenthe clay in Plaxis 3D was the SSCM as explained in Section 2.4.3. The soil parameters for this material model were verified in Section 3.1.4 and corresponded well with the CRUX database (Table B.6). For the other layers, the HSS material model was chosen as substantiated in Section 2.4.5. For these models, the soil parameters were retrieved from the CRUX database (Table B.3), which is partially based on standardised soil properties (i.e., Table 2b) from the NEN9997-1 (Eurocode 7, 2005). **Note:** instead of modelling the third Pleistocene sand layer, the boundary conditions of the bottom of the model domain (NAP - 63 m) in Plaxis 3D were specified as open for the ground water flow analyses.

Pile Loads (step 1)

For the pile foundation, a Fundex 460/560 pile was used, which is a common pile for high-rise building design for a typical, Dutch soil stratigraphy. This means that a concrete pile with casing and lost foot was used that has a shaft diameter (d_{eq}) of 460 mm and base diameter (D_{eq}) of 560 mm. Based on this information (from the contractor) along with the simple building geometry and pile plan described above, the maximum load in the pile was estimated by the structural engineer. For this specific tower design, the maximum ULS load in the pile was approximated as **1,805 kN**, which is used in the next step to determine the ultimate pile capacity and required pile tip level to carry the ULS load induced by the (self weight of the) high-rise building.

Pile Capacity (step 2)

In order to calculate the minimum foundation level and corresponding pile length of a pile group consisting of Fundex 560 to satisfy the ULS load equilibrium, a sample calculation in D-foundations for a different case study in northern Amsterdam was used as a first estimate. After trial and error, the resulting PTL for the pile group was found as **NAP - 23 m** for a pile length of $\approx$ 26 m to carry a ULS load of 1,805 kN, as was shortly explained in the previous section (3.1.3). The cone resistance (q_c) was limited to 15 MPa and NEN pile factors were used while commonly used partial factors (ξ, γ_f) for pile design were taken out of the equation. As a result, the FoS for the pile group design increased (from 1.2) to **2.3** with an ultimate bearing capacity (R_{ult}) of **4,119 kN**, see Table 3.1 in the previous section and Figure A.18 in Appendix A.5. The shaft capacity (R_{shaft}) of the total bearing capacity was found to be **1,369 kN** and positive skin friction was assumed to start from the first Pleistocene sand layer (NAP - 13.5 m) and linearly increased (with 144 kN/m) to the PTL at NAP - 23 m. The resulting base resistance (R_{base}) was then found to be **2,751 kN**, from which a significant portion was found to be distributed down to the 32 m thick clay layers 8 m below pile tip as was concluded in Section 3.1.6. For this reason, a s_2 settlement analyses (in Plaxis 3D) and mattress model approach (in SCIA) is needed to complete the final design of this particular high-rise building in Amsterdam.

Building Loads (step 3)

For the s_1 and s_2 settlement analysis, only the SLS quasi-permanent portion of the building loads are needed as was explained by Eq. 2.8 in Section 2.2.1. Based on the maximum SLS pile load and bearing capacity, a pile stiffness ($k_{v;1}$) was found as **123 kN/mm** for a pile head settlement (s_1) of **10.6 mm** of a Fundex 460/560 (see Table 3.1). The pile stiffness was implemented as linear springs in the SCIA model with a spacing of 2 m. As a result, the maximum SLS pile load was found as **1,302 kN** with a corresponding surface load of **339 kPa** for an outer c-to-c pile spacing of 24 m by 24 m based on a total SLS resultant force of **195,490 kN**.

3.2.2 Current Design Loop (step 4a): Load Spread Method

As was concluded in Sections 3.1.5 & 3.1.6, Tomlinson's equivalent raft approach can be used appropriately in Plaxis 3D to estimate stresses at depth and resulting s_2 settlements caused by the preliminary building loads for a simple tower as described above. However, Tomlinson did not seem adequate to calculate the change in vertical effective stresses caused by the loads and transferred to PTL and 4D below (see Figures B.18 and B.19). Instead, Tomlinson's load spread method (see Section 2.3.2 for the theoretical background) was only used to estimate the stresses distributed to the deep Eem clay layer (see Figure 3.45), which were found to be compressible and contribute to **62 %** of the total s_2 settlements of **84 mm** under 339 kPa applied at 2/3 positive skin friction (= NAP - 19.8 m) with a load spread of 1/4 (= **265** kPA). Note that s_2 settlements are computed at 4D depth below PTL, which is the orange line in Figure 3.46. Based on a s_1 settlement of $\approx$ 10 mm (see Section 3.1.1), the total settlements of the building after 50 years of consolidation are then estimated to be **94 mm**, which is in line with the expected settlements of other towers in Amsterdam according to the CRUX database, see Figure D.3. In addition, the consolidation and creep rate seem to fall within the bandwidth of the measured settlement rate by InSAR data, see Appendix D.

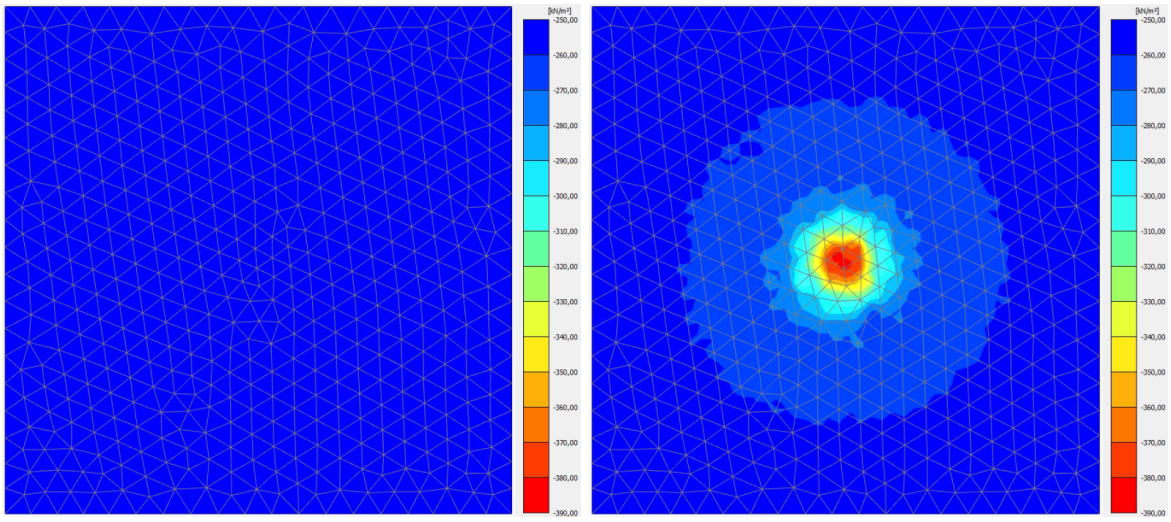

(a) Initial. (b) Consolidation.

Figure 3.45: Cartesian effective stresses (σ'_{zz}) calculated at top of Eem clay (= NAP - 31 m) by Plaxis 3D under SLS surface load (= 339 kPa) applied at Tomlinson depth (= NAP - 19.8 m) with 1/4 spread (= 265 kPa) for a) initial K_0 conditions, and b) after 50 years of consolidation.

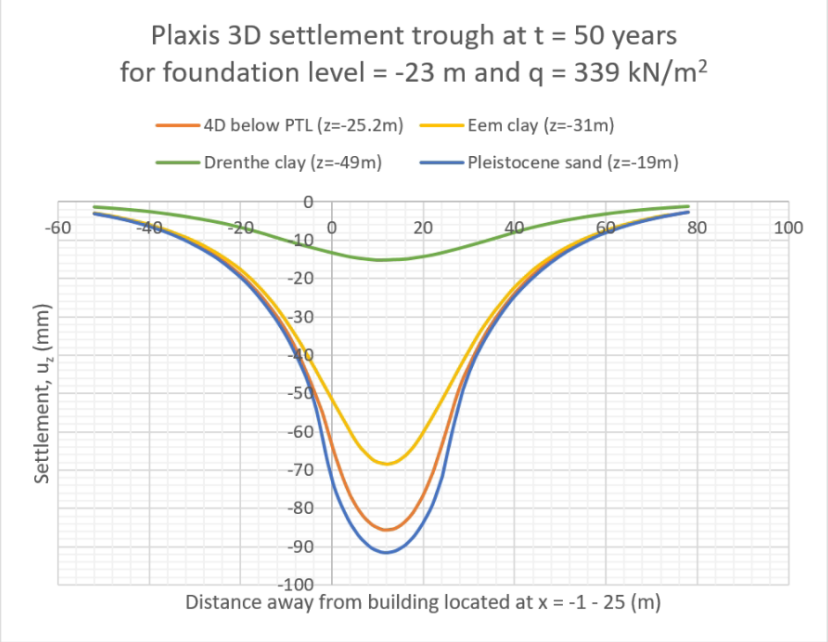

Figure 3.46: Preliminary (s_2) settlement curves at the top of each soil layer in Plaxis 3D using SSCM for Eem & Drenthe clays, HSS for other layers, and building load applied as surface load with 1/4 spread (= 265 kPa) at Tomlinson depth (D_{tom} = - 19.8 m).

3.2.3 Current Design Loop (step 5): Mattress Model

After finalising the preliminary settlement curves for the simple tower, the information is shared with the structural engineer as input for the mattress fit model in SCIA Engineer (2021). This model has the same dimensions as the Plaxis 3D model, but simplifies the subsurface to linear springs only, which are connected at the top by a plate of 1 m thick.

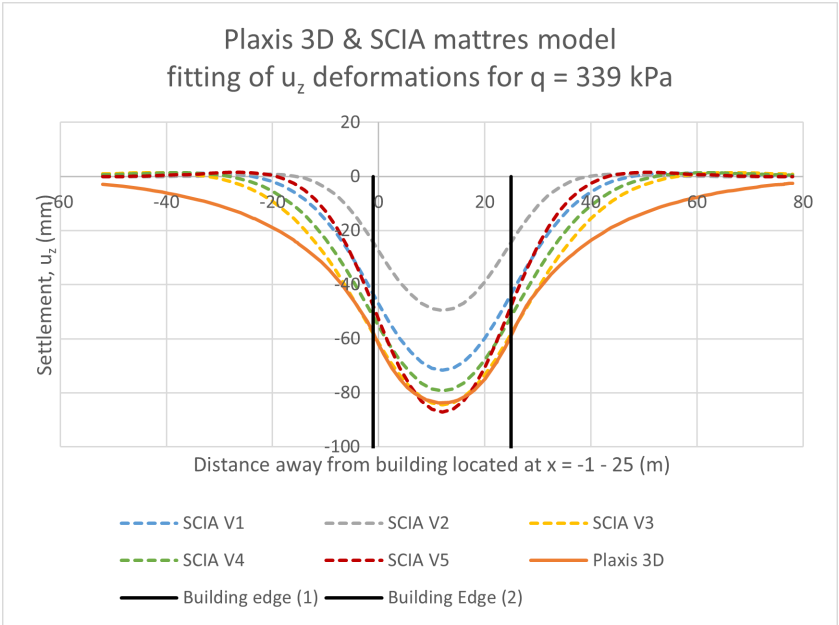

Figure 3.47: Fitting procedure of deformations (u_z) from SCIA's mattress model with Plaxis 3D settlements (s_2) for Tomlinson's load spread method without load redistribution within superstructure or iteration(s).

A surface load with the same dimensions (= 24 m x 24 m) and value (= 339 kPa) as the Plaxis analysis was applied to the top of the plate and a cross-section was drawn through the centre of the building, similar to the cross-section computed in Plaxis 3D. Then, the stiffness of the plate (E_{plate}) and springs ($k_{bedding}$) in SCIA were manually adjusted (with the help of Excel) to match the deformations of the mattress fit model (u_z) with the s_2 settlement curve at 4D below PTL from Plaxis 3D, see Figure 3.47 above. Table 3.7 below lists the values of the parameters illustrated by the SCIA curves V1 through V5. One can notice that increasing the $k_{bedding}$ results in a higher peak value, while increasing the E_{plate} in SCIA widens the deformation curve.

Table 3.7: Parameter combinations to fit the mattress model deformations to the Plaxis settlement curve.

Parameter	**SCIA V1**	**SCIA V2**	**SCIA V3**	**SCIA V4**	**SCIA V5**
E_{plate} (MN/m)	1.5 E^5	7.5 E^4	2.25 E^5	2.0 E^5	7.5 E^4
$k_{bedding}$ (MPa)	12.0	25.0	7.25	9.0	12.0
$u_{z;max}$ (mm)	71.7	49.5	84.4	79.3	87.2

Figure 3.48 elaborates on the fitting of this mattress model by showing a zoomed-in version of the settlement plot. It is important to match the settlement curves between the foundation or building limits, which are known as the differential settlements. The deformations outside of the building edges are not important for the structural analysis of the tower as those deformations only affect the surrounding buildings. Furthermore, Section 2.4.3 explained that the use of the SSCM (for the Eem & Drenthe clay layers) in Plaxis 3D results in a wider settlement curve in comparison to the HSS model or measured settlements (for tunnels). Therefore, this approach and the resulting SCIA model deformations should not be used to draw conclusions regarding the effects on surrounding structures, which is also outside of the scope of this thesis.

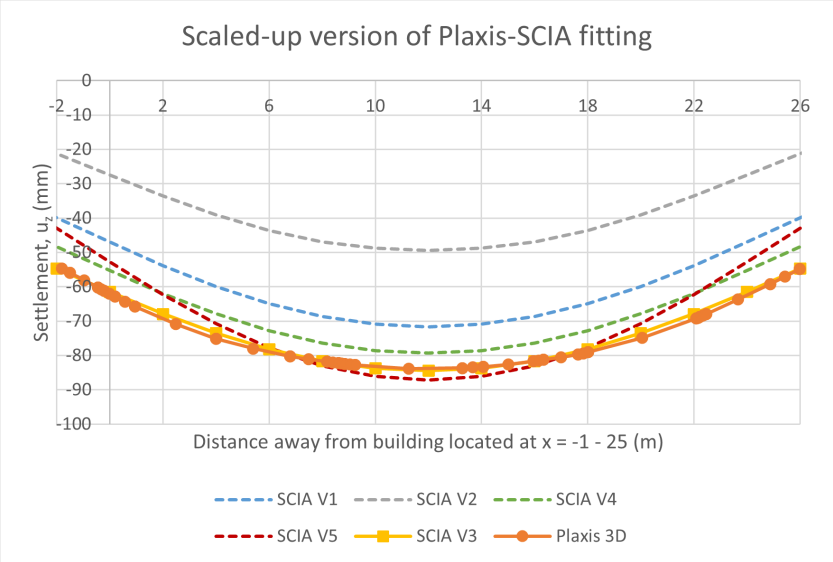

Figure 3.48: Zoomed in version of fitting procedure of deformations (u_z) from SCIA's mattress with Plaxis 3D settlements (s_2) for Tomlinson's load spread method without load redistribution within superstructure or iteration(s).

After finding the best fit for the two mattress model parameters (E_{plate} & $k_{bedding}$), the parameters are added to the total SCIA model that includes the actual tower and piles instead of the simplified surface load on top of the mattress consisting of the 1 m thick plate and linear springs. Note that the deformations of the mattress in the total SCIA model will be less than the s_2 settlements computed by the SCIA mattress fit

model (and Plaxis 3D) due to the effect of building stiffness and load redistribution within the superstructure. The latter will be explained next and the building stiffness will be clarified by Figure 3.52 in Section 3.2.6.

3.2.4 Current Design Loop (step 4b): Embedded Beams Method

To investigate the effects of load redistribution within the superstructure on the s_2 settlements, a new methodology will be proposed and explained herein.

As was shown by Figure 2.11 in Section 2.1.3, the adjusted force flow within the superstructure due to the long-term s_2 settlements results in a load redistribution from the centre of the building to the edges over time. For this particular high-rise building design, a significant increase of $\approx$ 800 kN was found for the SLS load or normal force of the outer piles (from 1,041 kN to 1,874 kN) when the s_2 settlements were applied as a fitted mattress underneath the superstructure in SCIA. To take this effect into account, many engineers claim that iteration of settlement curves between a geotechnical engineer and structural engineer is needed. To investigate this claim, the adjusted pile reactions were subtracted from the total SCIA model for each of the 169 piles and looped back to the Plaxis 3D model as updated building loads (= point loads) acting on 169 embedded beams, see Figure 3.49 for the s_2 settlement results. One can see that the maximum s_2 settlements decreased from **84 mm to 75 mm**, resulting in a reduction of differential settlements from **24 mm to 15 mm**. Thus, iteration with the use of EB-I and updated building loads translates to a foundation rotation of **1:867** (instead of 1:542), which meets the maximum rotation restriction of a CC2 structure (= 1:600) according to design codes.

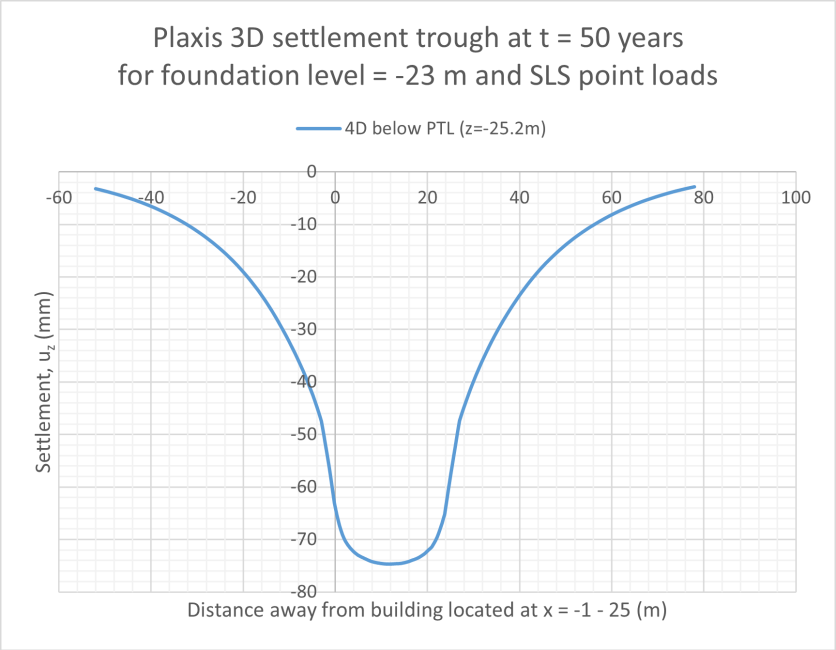

Figure 3.49: Updated (s_2) settlement curve computed by Plaxis 3D at 4D below PTL and building load applied as updated SLS point loads at EB-I piles with NEN pile factors.

The embedded beams were modelled in Plaxis 3D based on the new formulation (EB-I) using a similar pile fitting procedure as proposed by Frissen (2020), see Figure 3.2. For instance, the embedded beams were first fitted against the pile capacity calculated by PileCore. Note that the individual piles were not fitted for the correct (s_1) load-settlement behaviour (with the normalised NEN curves) or installation effects as this falls outside the scope of this research and was found to have no significant effect on the s_2 settlements below PTL.

3.2.5 Current Design Loop (step 6): Model Uncertainty & Iteration

To better picture the effects of iterating the building loads and resulting settlements, Figure 3.50 below shows the preliminary s_2 settlement curve based on a SLS surface load with Tomlinson's load spread method (orange) and the updated curve based on updated point loads (after redistribution) with the newly proposed EB-I method in Plaxis 3D. Based on this chart, the model uncertainty or potential error without iteration can be determined as $\approx$ **11** % difference (84 mm versus 75 mm). Even though this feedback loop to the geotechnical engineer takes into account the load redistribution within the superstructure, it does not adequately incorporate the effects of building stiffness. The stiffness of the foundation and superstructure of the high-rise building has a significant effect on the settlements, as was discussed in Section 2.5. For this reason, Section 3.2.6 will emphasize on how to properly implement the building stiffness in the s_2 settlement analysis as a final model verification for the SSI design methodology.

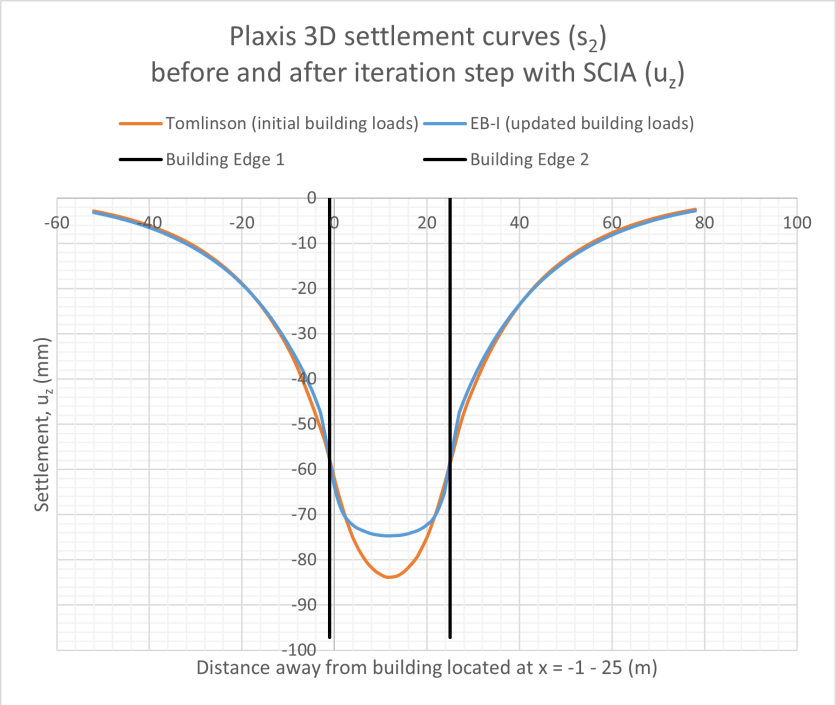

Figure 3.50: Combined (s_2) settlement curves computed by Plaxis 3D at 4D below PTL before (Tomlinson) and after (EB-I) load distribution in superstructure.

3.2.6 Current Design Loop (steps 7-8): Model Verification

As a first attempt to incorporate building stiffness, Tomlinson's load spread method is used in Plaxis 3D with a stiff plate instead of only a surface load at depth, which is equivalent to an infinitely flexible plate. This can be a first approach to determine the settlement bandwidth based on the two extreme building limits (see Figure 2.35 in Section 2.5). The settlement curve flattens out, resulting in less peak settlements and lower differential settlements, as seen in Figure 3.51. As expected, one can also see that the EB-I method falls perfectly within the two building stiffness extremes.

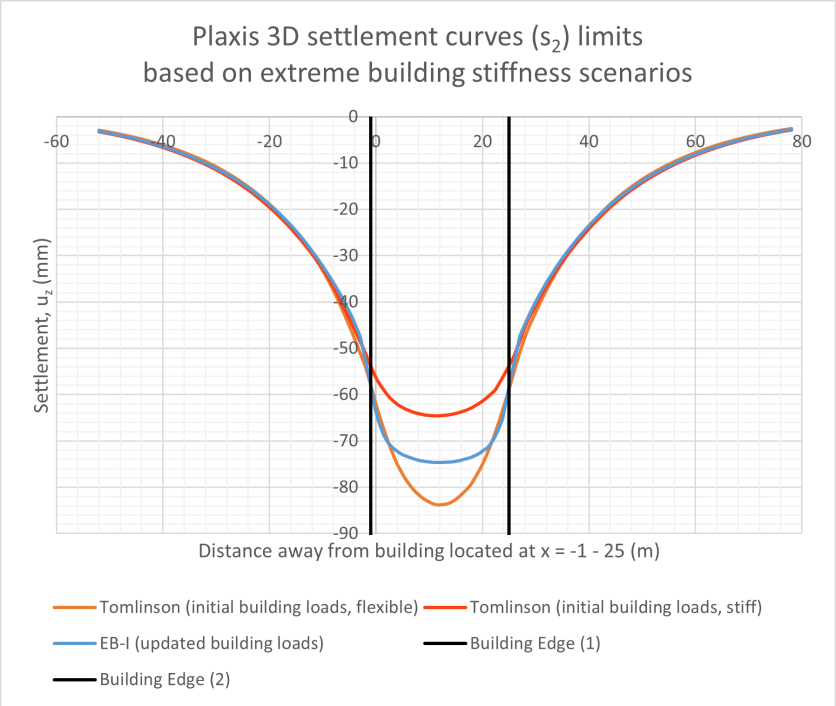

Figure 3.51: Initial (Tomlinson's load spread method) and updated (EB-I method) settlement curves (s_2) 4D below pile tip (= -25.2 m) in Plaxis 3D using an **elastic** and **stiff** plate representing building stiffness limits.

To better understand the effects of the actual stiffness of the superstructure on the settlements, the initial Tomlinson approach is plotted in Figure 3.52 (orange) along with the deformations of the SCIA mattress (yellow) after adding the two fitted mattress model parameters to the total SCIA model including the high-rise building structure.

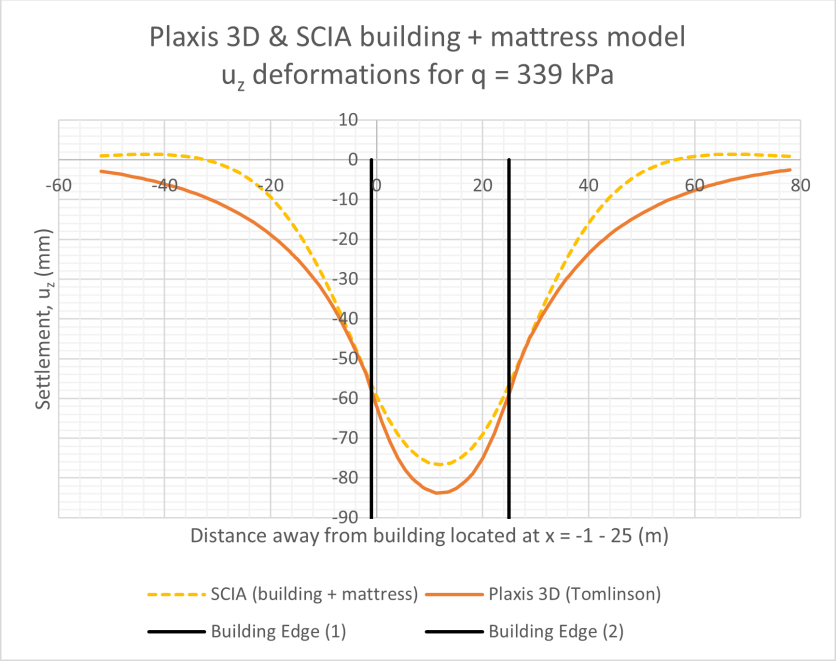

Figure 3.52: Settlement curves (s_2) in Plaxis 3D (Tomlinson) versus SCIA after adding fitted mattress model (E_{plate} & $k_{bedding}$) underneath piles (as $k_{v,1}$) and tower. **Note:** Plaxis 3D (Tomlinson) = SCIA (mattress)

Thus, the combined effect of load redistribution as a function of the realistic building stiffness of the superstructure results in a lower s_2 peak settlement (= **76 mm**), differential settlement (= **18 mm**), and rotation angle (= **1:722**) in comparison to Tomlinson's preliminary settlement analysis (84 mm, 24 mm, 1:542) without these building effects.

As final model verification, it was chosen to model the SCIA high-rise building structure as a simplified version in Plaxis 3D, on top of the EB-I model. As a first step, a simpler model scenario of only the foundation plate on top of the embedded beams was modelled in Plaxis (as was introduced in Figure 3.42) with the same SLS surface load on top of the plate. Then, the Plaxis model was extended with the use of plates and anchors with the same dimensions and stiffness of the structural elements in SCIA, see Tables B.11 and B.10. This way, the same superstructure was modelled in both SCIA (Figure 3.53a) and Plaxis 3D (Figure 3.53b).

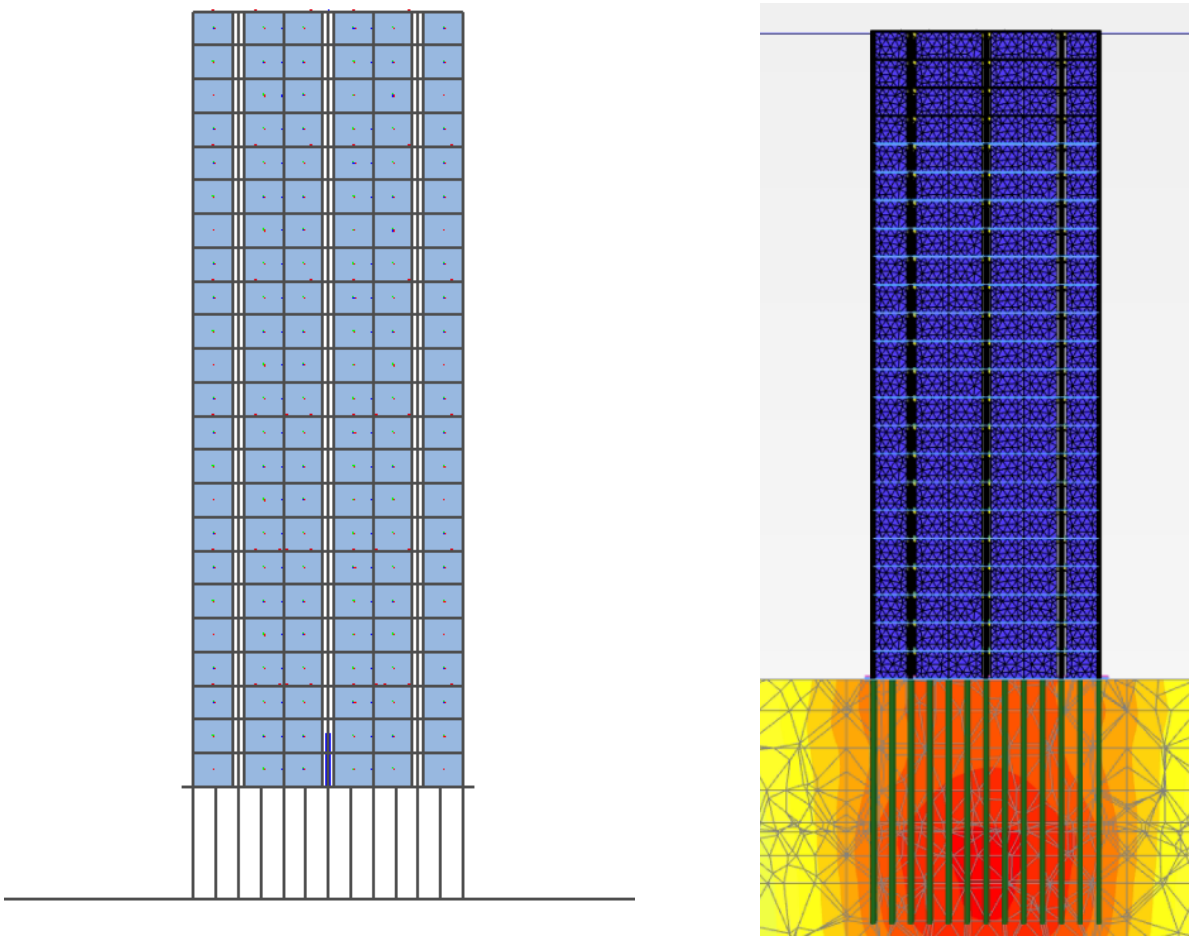

(a) SCIA.

(b) Plaxis 3D.

Figure 3.53: Vertical sections of simple tower design in a) SCIA, and b) Plaxis.

Initially, the building loads from SCIA were modelled in Plaxis 3D by overruling the self weight of the structural elements in Plaxis 3D by 0 kN/m^3 and implementing the SLS building loads as surface loads acting on each floor ($\approx$ 339 kPa / 23 floors). This approach resulted in the most reliable load transfer and resulting settlements. See Figure 3.54 for the s_2 settlement curve computed by Plaxis 3D for the piles and foundation plate with surface load (= EB-I + foundation plate) and for the model with the piles, foundation plate, and entire superstructure with surface loads at each floor (= EB-I + building).

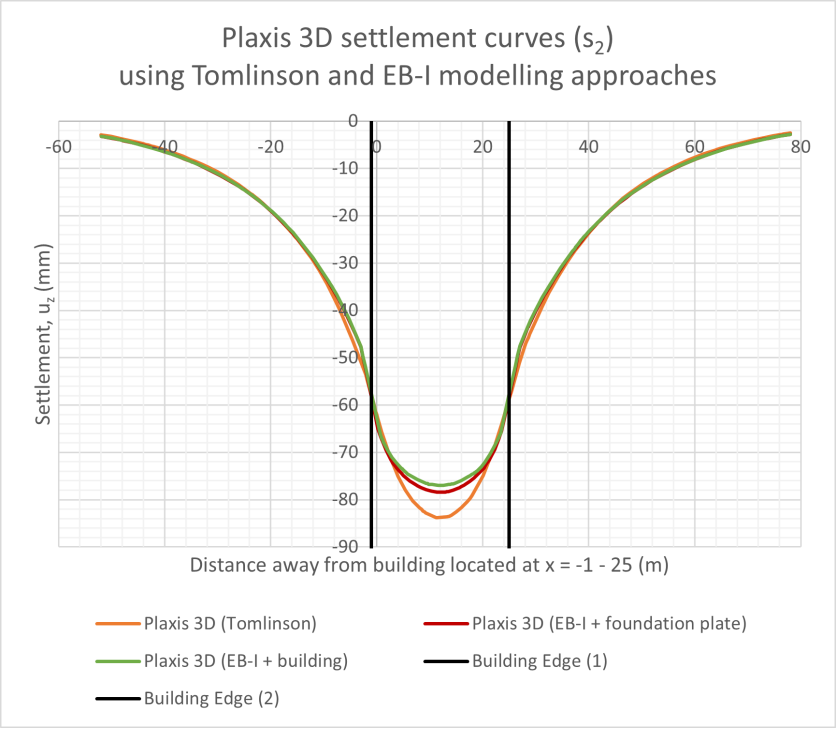

Figure 3.54: Initial settlement curves (s_2) 4D below pile tip (= -25.2 m) in Plaxis 3D embedded beam method using a realistic building stiffness as a) foundation plate or b) entire building and surface loads at each floor.

Note that the settlement results of EB-I + building have very similar peak and differential settlements results (**77 mm & 17 mm**) as EB-I + foundation plate (**78 mm & 18 mm**). However, the Plaxis model with only the foundation plate requires less computation time and costs and is therefore recommended over modelling the entire superstructure.

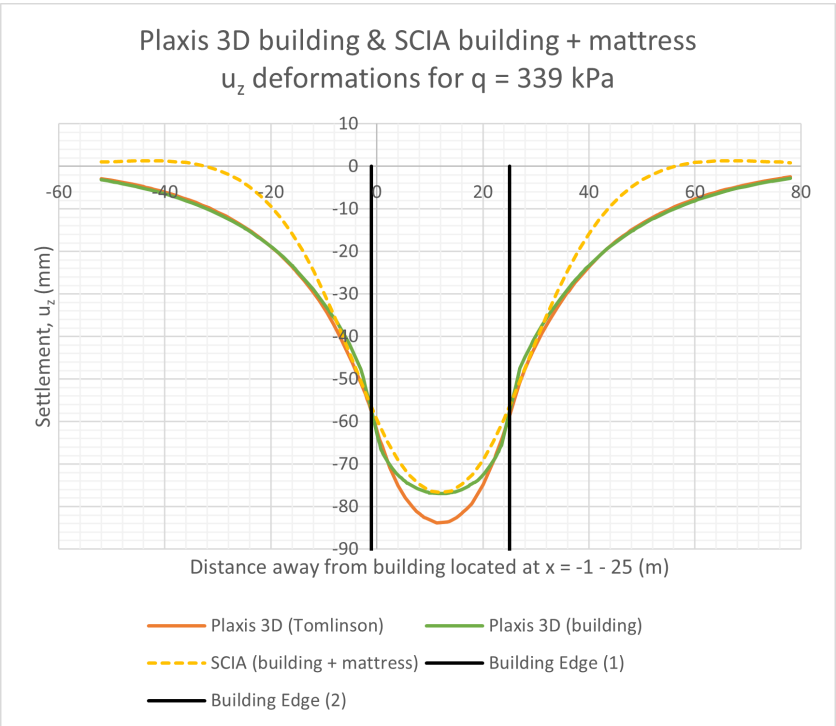

Figure 3.55: Comparison of settlement curves (s_2) 4D below pile tip (= -25.2 m) in Plaxis 3D and SCIA.

Finally, Figure 3.55 shows the similarities in (differential) settlements for the simplified tower in Plaxis 3D versus the simplified subsurface model in SCIA, which both meet design criteria. Figures 3.56 and 3.57 summarise the results. Thus, based on this specific case, the mattress model approach proposed in this thesis is found to be a safe and adequate design methodology making the old-fashioned iterative approach redundant.

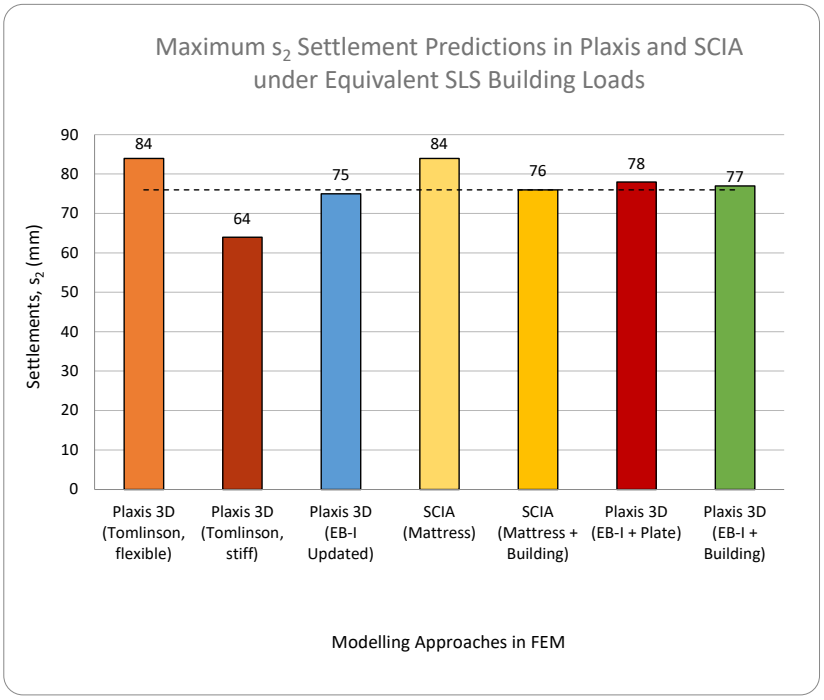

Figure 3.56: Summary of computed s_2 peak settlements for different modelling approaches.

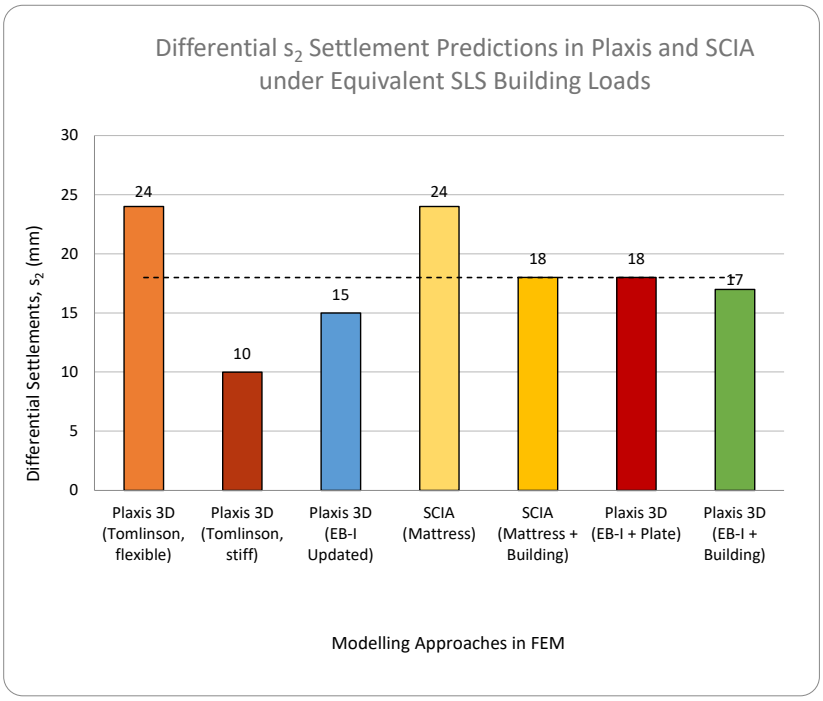

Figure 3.57: Summary of computed s_2 differential settlements for different modelling approaches.

3.3 Conclusions Research Question 2

This chapter provided insight on the following items and consequent sub-research questions to better understand possible improvements in foundation settlement prediction methods used in daily practice:

Sub-Question 2a:

"How does a pile (group) behave under high-rise building loads in soft soil deposits?"

Based on literature review, Frissen (2020) claims that the new embedded beam formulation (EB-I) in Plaxis 3D shows improved performance on mesh dependency without an increase in computational power. In addition, convergence was found between medium and fine mesh size distributions. For those reasons, the new formulation and a similar pile fitting procedure proposed by Frissen (2020) were used for the ultimate bearing capacity of the pile to predict pile head settlements (= s_1) for a Fundex 460/560. This was done by hand based on the NEN (type 1) and MV2 (type 2) pile design methods and compared with several other software packages (D-Foundations, PileCore, and Plaxis 3D). It was found that Plaxis 3D does not properly model the entire load-settlement response of a Fundex 560 for both design methods. However, for the NEN pile factors, Plaxis showed an almost exact fit with the predicted s_1 settlements in the linear SLS range of the individual pile response. The under-prediction of s_1 settlements for the type 2 (MV2) method can be explained by use of the EB-I, which contains a stiffer load-displacement curve compared to the current formulation in Plaxis 3D. However, the effect (of different pile factors) turned out to be negligible for the SLS load distribution down to the soil layers below pile tip level and resulting s_2 settlements for a pile group. Thus, the prediction and modelling of s_2 settlements appeared to be geometry driven instead of bearing capacity or pile factor governed.

Sub-Question 2b:

"What settlement mechanisms are contributing to the measured, absolute settlements of high-rise buildings?"

The article by Hoefsloot and Wiersema (2020) and additional InSAR data provided by SkyGEO (Appendix D), show that high-rise buildings in Rotterdam and Amsterdam start settling during and right after construction. Hoefsloot and Wiersema (2020) were able to fit the parameters of the SSCM for the Kedichem clays to the strain rate of the measured satellite data in Rotterdam, proofing consolidation and creep settlements of these layers below foundation level. In this thesis, SSCM parameters for four Eem clay samples were tested in Plaxis' SoilTest facility and resulted in a satisfactory load-strain response under 1D compression. Moreover, Plaxis 3D analysis showed that $\approx$ **65%** of the total s_2 settlements can be contributed to the compression of the $\approx$ 18 m thick Eem clay layer (in Amsterdam).

Question 2:

"What is the error margin of the current design practice and is it possible to streamline it by safely eliminating the iterative process between geotechnical and structural models while maintaining realistic SSI effects?"

When the SSI modelling approach summarised in Figure 2.37 - as answer to the first research question - is followed, an error of **11%** was found when the updated SLS building loads due to load redistribution in the superstructure from SCIA are not looped back to Plaxis 3D. However, both Tomlinson's load spread method as the embedded bean (EB-I) analyses in Plaxis do not take into account the realistic building stiffness of the foundation and/or superstructure. When this is implemented, an almost exact fit (= **1.3%**) of the maximum and differential s_2 settlements between the building edges is found without iterations while meeting the design criteria of 1:600 for foundation rotations.

Chapter 4

Discussion of Results

This chapter will seek to find an answer for the main research question to fulfill the research goal of this thesis:

Main Research Question:

"What integral design methodology can be followed by a geotechnical engineer to develop a joint, soil-structure interaction model that can be operated by a structural engineer to design a high-rise building structure in soft soil conditions?"

4.1 Summary of Literature Review & Research Results

This thesis provided insight on the prediction and modelling of long-term foundation settlements for high-rise buildings in soft soil deposits due to soil-structure interaction (SSI). Since the 1990's, towers have started to dominate the skyline of cities in the West of the Netherlands (Randstad), which is underlain by the compressible Kreftenheye, Drenthe and Eem formations. High-rise buildings are seen as a solution to accommodate for the ongoing housing shortage in the country. Many researchers and practitioners have been investigating settlement analysis since it became mandatory by Dutch municipalities for the design and contract phase of a tower structure. However, a uniform approach to model and communicate resulting (deep foundation) settlements from geotechnical to structural models appears to be missing. For this reason, this thesis report investigated, proposed and verified a SSI numerical modelling approach in Plaxis 3D and SCIA. This method allows structural engineers to incorporate pile head (s_1) and deep foundation settlements (s_2) into structural FEM models without the need to iterate the results for convergence of settlement curves.

Settlement Mechanisms

This research project also investigated underlying settlement mechanisms contributing to measured high-rise building subsidence. The Eurocode 7 (2005) divides foundation settlements into pile head settlements (s_1) and pile group settlements (s_2) due to compressible soil layers four pile base diameters (=4D) below foundation level. The contributory mechanisms to these foundations settlements are both short-term and long-term: pile tip settlement (short-term), elastic compression (short-term), immediate settlements as elastic compression of sand layers (short-term), primary and secondary consolidation settlements (long-term), and creep settlements (long-term) of cohesive soils. Building (foundations) also settle due to external influences such as cyclic unloading-reloading mechanisms (i.e., wind or earthquakes), surrounding structures (i.e., tunnels or deep excavations), pumping of nearby surface water, or fluctuating ground water tables due to seasonal change. The latter was considered out of scope for the settlement predictions in this research (as it influences the negative skin friction mostly). Absolute settlements for high-rise building structures can be measured by the use of InSAR satellite data. However, such measurements in the Netherlands can only be applied after construction of the tower and lack the influence of immediate and consolidation settlements during the ($\approx$ 2 year) construction period of such a building structure.

Individual Pile Behaviour in FEM

Proper modelling of pile (group) behaviour in Plaxis 3D was achieved for the linear SLS load-settlement range of a single pile using the new formulation of embedded beams (EB-I) and a medium size mesh distribution. The bearing capacity input of the EB-I was based on the ultimate bearing capacity calculations by PileCore for the NEN pile design method and corresponding pile factors for a Fundex 460/560 (type 1) installed at a typical soil profile in Amsterdam. Using updated pile factors - found by recent pile load tests performed on the Maasvlakte (MV2, type 2) for screw injection piles - resulted in a similar ultimate bearing capacity in PileCore, however, the Fundex pile responded less stiff and the contribution by the shaft friction was $\approx$ 60% higher in comparison to the base resistance. Even though the MV2 pile design resulted in a slight decrease in pile tip settlement (s_b), the resulting pile head settlement (s_1) was only $\approx$ 1 mm less than the NEN pile design under the same SLS load when the elastic compression (s_{el}) was considered. Thus, for the same SLS load, the pile head settlement was not very sensitive to the choice of design method and pile factors for this particular pile (Fundex 460/560) and soil stratigraphy (northern Amsterdam).

Soil Behaviour in FEM

On top of the research performed by Hoefsloot and Wiersema (2020), this thesis streghthens the claim that consolidation and creep settlements measured by InSAR data are caused by the dissipation of excess pore water pressure in compressible layers due to load distribution below pile tip. Hoefsloot and Wiersema (2020) were able to fit the soil parameters of Kedichem clay samples for the soft soil creep model (SSCM) in Plaxis to the InSAR measured strain rate for three high-rise building sites in Rotterdam. In addition, this thesis performed a 1D oedometer compression test in Plaxis' SoilTest facility on four different Eem clay samples taken from boreholes in northern Amsterdam. The load-strain results were found to have a reasonable fit with oedometer test results from the laboratory for the same samples. Similar SSCM parameters were used to model the Eem and Drenthe clay layers for the pile group model at the Amsterdam site in Plaxis 3D.

Pile Group Behaviour in FEM

The effect of different pile factors on the long-term (s_2) settlements was also investigated alongside other parameters. A different pile design results in a change in load and stress distribution from the foundation down to the compressible Eem and Drenthe clay layers below foundation (or pile tip) level. It was found that pile factors and more shaft friction versus base resistance in the linear SLS range did not have a significant effect on the s_2 settlements of a pile group. Furthermore, the spacing between piles in the same pile group under equivalent SLS point loads had a large effect on the change of vertical effective stress at pile tip level and slightly below (4D lower). Nonetheless, the stress (and load) distribution down to the Eem clay layer located 8 m below PTL was much lower and did not exceed the clay's pre-consolidation pressure due to significant load spread in the Pleistocene sand layer above. Therefore, the over-consolidated (OC) soil behaviour of the Eem clay layer was not influenced by the pile spacing or different pile factors and resulting change in load distribution under the same load conditions. On top of that, a simplified and much faster modelling approach was compared with the embedded beam pile group models. This load spread method or equivalent raft approach was invented by Tomlinson and Woodward (2008) and is mostly used for analytical methods. The similarities in results were defined by a slight change in maximum s_2 settlement values and curves for each model scenario in Plaxis 3D in comparison to Tomlinson's method.

Building Stiffness

To verify the state-of-the-art SSI mattress modelling approach in Plaxis 3D and SCIA, the effects of load redistribution within the superstructure - after adding the long-term settlement trough as a plate with coupled springs - as a function of the correct building stiffness were investigated. Load redistribution within the structural SCIA model can be analysed by implementing the redistributed building loads - from the centre to the edges of the building - as updated point loads acting on uncoupled embedded beams (no foundation plate) in the same Plaxis 3D subsurface model. Implementation of a more realistic building stiffness in a geotechnical model was achieved by modelling several structural scenarios in Plaxis 3D. The s_2 settlement results were then compared with the deformations from the total building model with mattress (= plate + linear springs) for the same Plaxis 3D cross-section in SCIA. The deformations of the mattress - representing deep compressible soil layers - were fitted to match the preliminary settlement curve computed by Tomlinson's load spread method in Plaxis 3D. The s_2 settlements computed by the Plaxis 3D model with the entire building structure on top of embedded beams (EB-I) and a foundation plate was found to only have a **1.3% difference** with the deformations of the mattress from SCIA without iterations.

4.2 Conclusions Main Research Question

This chapter provided insight on the following items and consequent main research question to verify and improve the contemporary design methodology for foundation settlements due to SSI effects:

Main Research Question:

"What integral design methodology can be followed by a geotechnical engineer to develop a joint, soil-structure interaction model that can be operated by a structural engineer to design a high-rise building structure in soft soil conditions?"

Summary of Verified Soil-Structure Interaction Approach in FEM:

1. **Step 1:** The contractor or structural engineer estimates the type(s) & ULS load of pile(s) and corresponding costs for the preliminary foundation design of a high-rise building structure,
2. **Step 2:** The geotechnical engineer calculates pile length & diameter and corresponding ultimate bearing capacity (R_{ult}) for a linear spring stiffness ($k_{v;1}$) and pile head settlements (s_1) at 70% of the ULS load,
3. **Step 3:** The structural engineer determines the SLS quasi-permanent (surface) building load(s) while adding individual pile stiffness ($k_{v;1}$) and several loading conditions to structural FEM model (in SCIA),
4. **Step 4(a):** The geotechnical engineer analyses the load distribution from the pile tip to the deep compressible layer(s) based on Tomlinson's equivalent raft approach (in Plaxis 3D) to compute the preliminary (s_2) settlement curve four diameters below foundation level due to the SLS building load(s),
5. **Step 5:** The structural engineer creates a mattress model in a separate FEM model (in SCIA) consisting of linear springs ($k_{bedding}$) connected at the top by a concrete plate with stiffness (E_{plate}). The SLS (surface) load from *step 3* is added to the top of the plate / mattress and the two mattress parameters are changed until a satisfying fit of the mattress deformations with the s_2 settlement curve is achieved,
6. **Step 6:** The SLS fitted mattress model ($k_{bedding}$ & E_{plate}) is added to the total structural model (in SCIA) including the superstructure and piles as line elements with $k_{v;1}$ springs at the bottom or top,
    - ***Optional Step 4(b):*** After adding the long-term s_2 settlements as deformable mattress underneath the building structure (in SCIA), load redistribution within the superstructure will result in a force flow from the centre piles of the building to the piles at the edges. To check and verify the effects on the s_2 settlements, updated SLS building loads as pile reactions can be retrieved from the structural model and transferred back to the geotechnical model as point loads acting on individual, uncoupled embedded beams (EB-I) in Plaxis 3D. One can then compute an updated s_2 settlement curve that includes the effect of redistribution of load, but not for building stiffness.
7. **Step 7:** The structural and geotechnical engineers determine convergence or a bandwidth of the mattress (s_2) deformations underneath the building structure (in SCIA). For the final design, the bandwidth could be verified by comparing the mattress deformations with the s_2 settlements from a geotechnical model (in Plaxis 3D) that includes the building stiffness as the entire structure or plate on top of embedded beams (EB-I) fitted for the ultimate bearing capacity (R_{ult}) from *step 2*,
8. **Step 8:** Do the consequent foundation rotations due to long-term differential settlements (= difference between building edge and centre) fall within design criteria (1:600)? Structural (SCIA) FEM model can then be used for contract phase and final design of structural elements without the need of iterations.

4.3 Final Discussion

The final to last section of this thesis will recap on the contribution to the social, scientific, and design relevancy initially stated in the research methodology (Ch. 1). Furthermore, possibilities for automation of the design flow and SSI approach to predict, model, and verify (long-term) foundation settlements will be discussed. Finally, limitations of the FEM models and overall approach will be stated and proposed as recommendations for future research in Section 4.4.

4.3.1 Research Relevancy

High-rise building structures are believed to fulfill the housing need in densely populated areas such as *the Randstad* in the Netherlands. This research proposed and verified an integral design methodology for a simple tower design of 23 building stories. Based on this geometry, the total height of the tower remains below 70 m and thus falls within the CC2 safety class of residential structures. As a result, housing costs will be more affordable due to the lower partial factors needed to calculate loading conditions for the structural model. Higher partial factors would have resulted in higher ULS loads and consequent pile head (s_1) settlements. However, the safety class does not influence the SLS quasi-permanent load(s) or resulting deep foundation (s_2) settlements. Structural dimensions are thus optimised more and result in a more sustainable design (lower CO_2 emissions) and less costs for the owner or renter of the dwelling.

Contribution to Scientific Relevance

This thesis performed a parametric study of different pile factors based on the NEN9997-1 (NEN, type 1) and updated pile factors based on recent Maasvlakte (MV2, type 2) pile load tests and the influence on both s_1 as s_2 settlements. This type of parametric study has not been performed yet in academia or practice and shows new insights on the effects of different pile design methods as part of a foundation settlement analysis.

Contribution to Engineering & Design Relevance

The main research goal of this thesis was to evaluate current design methodologies to predict and model foundation settlements of high-rise buildings in the Netherlands. By following an improved methodology of the mattress model SSI approach, a model verification was performed. This is a tremendous help in daily practice to ultimately enforce one uniform approach among structural designers and geotechnical engineers in the Netherlands, which can reduce tedious design steps and costs associated with old-fashioned analysis.

4.3.2 Possibilities for Automation

Fitting of s_2 settlements from a 3D geotechnical model (in Plaxis) to a 2D structural model (in SCIA) is still prone to tediousness and can be automated using manual input data (white boxes) by a geotechnical engineer (green boxes) and structural engineer (blue boxes), see Figure 4.1 on the next page. The flowchart is a more sophisticated version of a road map draft attached to the end of this thesis (Appendix D) as Figure D.5.

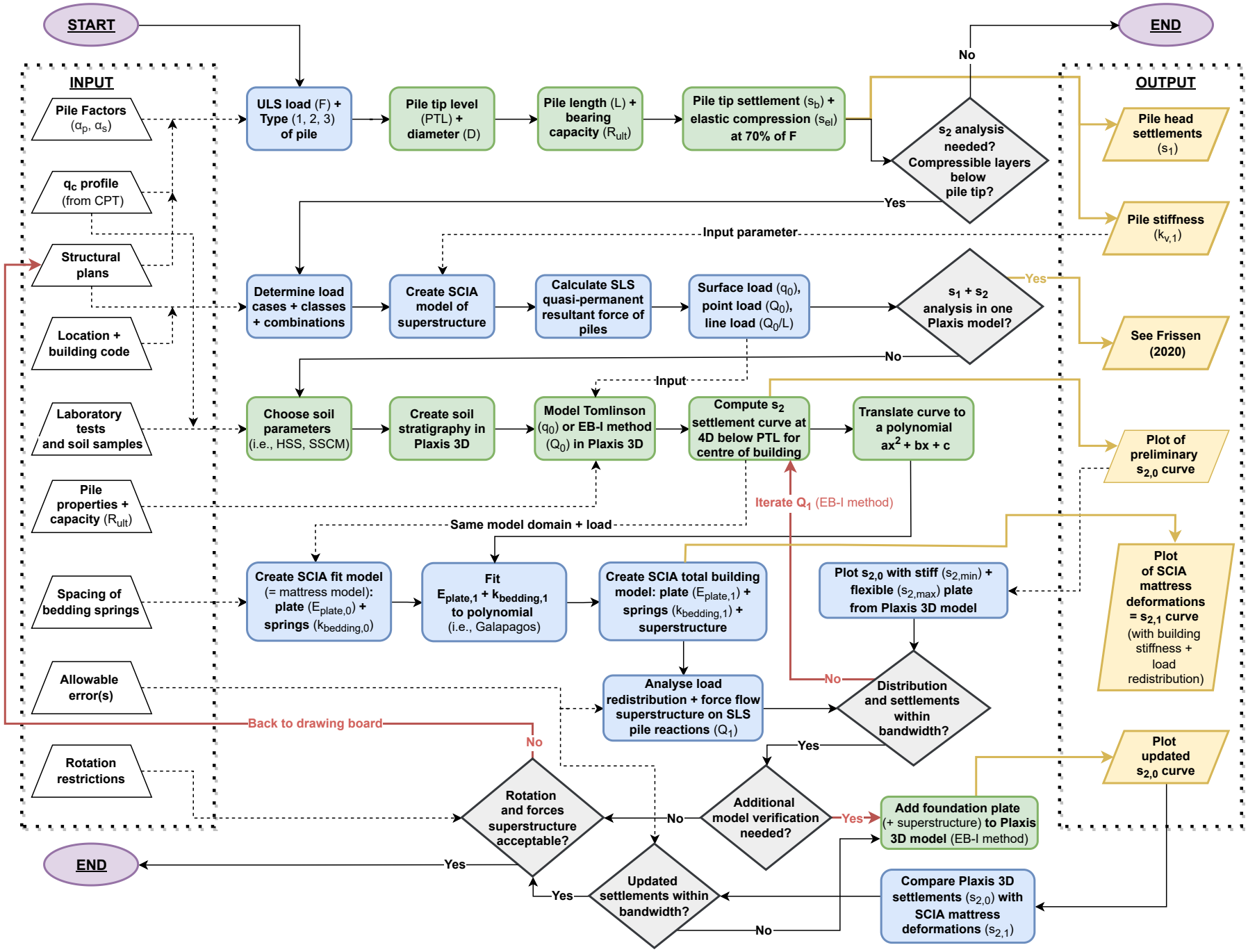

Figure 4.1: Proposed flowchart for automation of soil-structure interaction modelling between Plaxis 3D and SCIA. **Note:** the red paths should be avoided.

4.3.3 Model Limitations

Due to limitations in the scope of the research topic, the following modelling constraints should be considered:

- The new embedded beam formulation (EB-I) in Plaxis 3D is too stiff for modelling of type 2 piles beyond the linear SLS load-settlement range, however, the old formulation can be used instead,
- The modelling approach is only verified for a symmetric tower and a typical soil profile in Amsterdam,
- Tomlinson's load spread method is not reliable for prediction of the increase in vertical effective stresses due to the transfer of building loads directly at and below foundation level (= 4D),
- In the case of multiple SLS surface loads or zones from the structural engineer, Tomlinson's 1:4 load spread - starting from 2/3 positive skin friction - can only be applied to the outer surfaces due to otherwise numerical integration errors for overlapping surfaces in Plaxis 3D,
- The methodology still requires an iterative step (fitting of mattress), however, iteration is minimised and possibilities for automation are discussed,
- The SSI mattress model in SCIA should not be used for assessment of the effect on surrounding buildings and is only reliable within the foundation or building edges (where the settlement curve is fitted 1:1 to the curve from Plaxis). Instead, only the Plaxis 3D model should be used for adjacent structures.

4.4 Future Recommendations

As final part of the MSc thesis report, several recommendations for future research are proposed below to serve as the next step in the research process to achieve the meta goal "*To establish a more universal design procedure at a national level in which a simple, numerical soil modelling approach will be developed and validated for interactive use by geotechnical and structural engineers to include the effects of settlements caused by soft soil layers beneath the foundation level*". Most importantly, the SSI modelling approach needs more validation regarding a larger range of (varying) buildings loads for both symmetric and asymmetric tower structures that often contain. This is important as most high-rise building designs include a plinth or nearby smaller buildings that affect (the settlement trough of) one-another. The list of recommendations below propose the following next steps to conquer the meta goal and limitations for the research topic on modelling of high-rise building settlements including SSI effects:

- Better investigate the unloading and volumetric expansive behaviour shown by Plaxis 3D for a single pile model as EB-I and both pile factor methods at a depth of 4D below PTL and lower,
- Test if above unexpected, 'new' soil behaviour is realistic for the granular soil layers below a single pile and whether this can be measured during actual pile load tests on site,
- Include both shaft en base diameters (d_{eq} and D_{eq}) in the EB-I material model by splitting the geometry of the pile in two different constitutive models on top of each other and connecting both with a fixed node for a more realistic base response,
- Model a more appropriate type 2 load-settlement behaviour and softer stiffness for a Fundex 560 (EB-I) and compare with the old embedded beam formulation,

- Investigate and include more ways to numerically model s_1 and installation effects (in addition to s_2) settlements as part of the integral and interactive design method between geotechnical and structural engineers instead of using a deterministic approach based on most recent codes (i.e., NEN9997-1 or Eurocode 7),
- Model more oedometer test results for Eem and Drenthe clay (or Kedichem clay) samples in Plaxis' SoilTest facility for a more consistent fit with SSCM,
- Perform more oedometer tests on Eem and Drenthe clay (or Kedichem clay) samples for which the sample age (= time between sampling and testing) is restricted to 1 day or less,
- Capture the sensitivity of the current SSI approach in a settlement bandwidth by including the load spread (cases 4a) & embedded beam model variations (cases 4b) as briefly discussed in Appendix B.2.1,
- Investigate the effect of multiple surface building loads (i.e., a plinth at the base of a tower) and asymmetry of the loads (i.e., rectangular tower) on the effectiveness of the mattress model fit approach in the current SSI approach,
- Validate the current, integral design approach with the use of InSAR data for case studies of towers in Amsterdam and other locations in the Netherlands (i.e., Rotterdam),
- Compare the state-of-the art SSI design method with other design methods (i.e., prescribed displacements, PD) currently used in practice to implement a uniform design procedure as part of the appendix of the Dutch building code for high-rise buildings (= *Nationaal Covenant Hoogbouw*),
- Compare the new method with SSI design approaches beyond high-rise buildings (i.e., offshore) and methodologies abroad for (similar) subsurface conditions (i.e., Frankfurt or Dubai),
- Optimise the new, uniform SSI method from a structural and geotechnical engineering viewpoint. Examples of geotechnical topics to better investigate are **1)** mesh optimisation, **2)** varying pile lengths and PTL, **3)** other soil and q_c profiles, **4)** gradual loading construction phases, **5)** a linear elastic fill (for excavations), **6)** HS instead of HSS for the sand layers, **7)** HSS instead of SSCM for the deep clay layers to include small-strain behaviour, and **8)** permeability sensitivity for consolidation & creep of deep clay layers as SSCM (or HSS). Examples of structural topics are **1)** creep of concrete for the structural elements, **2)** cracked versus uncracked concrete, **3)** non-linear $k_{v,1}$ pile springs (s_1) or non-linear $k_{bedding}$ springs (s_2) in SCIA, and **4)** conversion of SCIA mattress model deformations to prescribed displacements (PD) as long-term load combination instead of permanent displacements as part of the total ULS building model.
- Automate the SSI design approach with the use of Python and an application programming interface (API) to communicate between FEM models (i.e., SCIA and Plaxis) of multiple stakeholders as illustrated in Figures 4.1 and D.5.

Bibliography

Abdel-Azim, O. A., Abdel-Rahman, K., & El-Mossallamy, Y. M. (2020). *Numerical investigation of optimized piled raft foundation for high-rise building in Germany.* Innovative Infrastructure Solutions, 5:11.

Abdelaziz, S. L. (2020). *Lecture notes MSc course CEE5544 Foundation Engineering II [Lecture].* Blacksburg (VA), USA: Virginia Polytechnic Institute; State University (Virginia Tech).

Andeweg, M. T., & Koopman, F. W. A. (2007). *Cost C16: Research in Architectural Engineering: Vol. 2. Improving the quality of existing urban building envelopes - state of the art.* IOS Press BV, 95-109.

Baas, B. (2001). *De geschiedenis van het funderen en heien.* Historische vereniging Golderake.

Ballast Nedam. (2018). *Galaxy tower.* Retrieved on 24-12-2021 from: https://www.ballast-nedam.nl/wat-we-doen/projectenoverzicht/2021/galaxy-tower.

Bartels, N. A. J., & van Gijn, F. J. (2020). *The BaanTower: Constructieve uitgangspunten omgevingsvergunning [Internal Document].* Van Rossum Raadgevende Ingenieurs BV.

Boomen, T. v. (2016). *De skyline van Amsterdam verandert in hoog tempo.* Het Parool.

Brassinga, H., & van Tol, A. F. (1991). *Deformation of a high-rise building adjacent to a strutted diaphragm wall.* 10th European Conference of Soil Mechanics; Foundation Engineering Florence, Balkema, 787-790.

Breeveld, B. J. S. (2013). *Modelling the Interaction between Structure and Soil for Shallow Foundations [Master Thesis].* Delft: Delft University of Technology (TU Delft).

Brinkgreve, R. B. J. (2014). *Efficient modelling of pile foundations in the Finite Element Method [Powerpoint Slides].* Plaxis, Delft University of Technology (TU Delft).

Brinkgreve, R. B. J. (2020a). *Lecture notes MSc course CIE4361 Behaviour of Soils & Rocks [Lecture].* Delft: Delft University of Technology (TU Delft).

Brinkgreve, R. B. J. (2020b). *Reader of MSc course CIE4361 Behaviour of Soils & Rocks [Reader].* Delft: Delft University of Technology (TU Delft).

Brinkgreve, R. B. J. (2021). *PLAXIS Manual (V21.01) [Software].* Plaxis BV Netherlands. Available from https://communities.bentley.com/products/geotech-analysis/w/wiki/46137/manuals---plaxis.

Camu, K. (2019). *Zo gaat de skyline van de toekomst eruit zien.* Vastgoedjournaal. Retrieved on 11-01-2022 from: https://vastgoedjournaal.nl/news/39960/zo-gaat-de-skyline-van-de-toekomst-eruit-zien.

Chortis, G., Hartmann, D., de Jong, F. K., & Meinhardt, G. (2021). *DO Zettingsanalyse kavel B10 Amsterdam [Internal Document].* CRUX Engineering BV.

Dao, T. P. T. (2011). *Validation of Plaxis embedded piles for lateral loading [Master Thesis].* Delft: Delft University of Technology (TU Delft).

De Gans, W. (2011). *De bodem onder Amsterdam.* De Geologische Dienst Nederland van TNO.

De Jong, F. K., & De Koning, M. (2021). *Paalgroep zakking (s2) hoogbouw [internal document].* Kern Document - CRUX Engineering BV.

De Jong, F. K., & Meinhardt, G. (2021). *DO Funderingsadvies kavel B10 Amsterdam [Internal Document].* CRUX Engineering BV.

Den Haan, E. J. (2008). *De intrinsieke tijd in het Isotachenmodel.* Vakblad Geotechniek.

D-Foundations. (2022). *Version 22.1.1 [Software]*. Deltares. Available from https://download.deltares.nl/en/download/geotechnical-software/.

Engin, H. K., & Brinkgreve, R. B. J. (2009). *Investigation of Pile Behaviour Using Embedded Piles*. Proceedings of the 17th International Conference on Soil Mechanics; Geotechnical Engineering, 1189–1192.

Eurocode 7. (2005). *Geotechnical design - Part 1: General rules. EN 1997-1*. Brussels: European Committee for Standardization.

Fleming, K., Weltman, A., Randolph, M., & Elson, K. (2009). *Piling Engineering*. Third edition. Taylor & Francis.

Frissen, M. J. L. (2020). *Determination of differential settlements of high-rise building foundations in soft soil conditions [master thesis]*. Delft: Delft University of Technology (TU Delft).

Gavin, K. G. (2020). *Updating Dutch national guidelines for determining the axial capacity of piles in sand*. IPA News Letter, Volume 5, Issue 3.

Gavin, K. G. (2021). *Lecture notes MSc course CIE4362 Soil Structure Interaction [Lecture]*. Delft: Delft University of Technology (TU Delft).

Granitzer, A., & Tschuchnigg, F. (2021). *Practice-Oriented Validation of Embedded Beam Formulation in Geotechnical Engineering*. Graz University of Technology.

Hoefsloot, F., & Wiersema, W. (2020). *Evaluatie en voorspellen zettingen hoogbouw op basis van satellietdata*. Geotechniek, jaargang 24 (nummer 1), 28-35.

Jacobs, D. H. J. E. (2021). *The influence of negative skin friction on the bearing capacity of timber piles in Amsterdam [Master Thesis]*. Delft: Delft University of Technology (TU Delft).

Lengkeek, H. (2022). *Testing and modeling of sheet pile reinforced dikes on organic soils: Insights from the Eemdijk full-scale failure test [PhD Dissertation]*. Delft: Delft University of Technology (TU Delft).

Meinhardt, G., & de Koning, M. (2021). *Theorie paalgroepzakking [internal document]*. Kern Document - CRUX Engineering BV.

Modder, J. (2016). *Nederlands perspectief op hoogbouw*. Stichting Hoogbouw. Retrieved on 23-12-2021 from https://www.cementonline.nl/artikel/nederlands-perspectief-op-hoogbouw.

Odijk, T. (2017). *Structural behaviour of a high-rise building on compressible soil [Master Thesis]*. Delft: Delft University of Technology (TU Delft).

Omgevingswet. (2018). *Landelijke richtlijn bouw- en sloopveiligheid*. Vereniging Bouw- & Woningtoezicht Nederland.

PileCore. (2022). *Version 2.0.0 [Software]*. CRUX Engineering Microservices BV (CEMS). Available from https://nuclei.cemsbv.io/#/pilecore/compression/app.

Poulos, H. G., & Davis, E. H. (1968). *The Settlement Behaviour of Single Axially Loaded Incompressible Piles and Piers*. Géotechnique, 18(3), 351–371.

Sadek, M., & Shahrour, I. (2004). *A three dimensional embedded beam element for reinforced geomaterials*. International Journal for Numerical; Analytical Methods in Geomechanics, 28(9), 931–946.

Schippers, R. J., Bijnagte, J., & van Tol, A. F. (2021). *Geotechnisch ontwerp van de Zalmhaven te Rotterdam (deel 1)*. Geotechniek.

Schippers, R. J., & Broekens, R. R. (2022). *Geotechnisch ontwerp van de Zalmhaven te Rotterdam (deel 2)*. Geotechniek.

Schoenmakers, S. (2020). *Sluishuis Amsterdam [Internal PowerPoint slides]*. Van Rossum Raadgevende Ingenieurs BV.

SCIA Engineer. (2021). *Version 22.1.5019 [Software]*. Nemetschek Company. Available from https://www.scia.net/en/scia-engineer/downloads#scia-engineer-21.

Skau, K. S. e. a. (2018). *Reducing cost in offshore wind by integrated structural and geotechnical design*. J. Phys.: Conf. Ser. 1104 012029.

SkyGeo. (2022). *Interactive maps for InSAR data [Internal]*. Retrieved on 28-09-2022 from https://maps.skygeo.com/maps/.

Smulders, C. M. (2018). *An improved 3D embedded beam element with explicit interaction surface [Master Thesis]*. Delft: Delft University of Technology (TU Delft).

Stichting Bouwresearch. (1995). *Handboek funderingen (Deel A & B)*. Ten Hagen & Stam B.V.

Ter Steege, F. B. (2022). *Screw and Screw-Injection Piles Classification of the load-settlement response and improving the design process [Master Thesis]*. Delft: Delft University of Technology (TU Delft).

Terzaghi, K., & Peck, R. B. (1967). *Soil Mechanics in Engineering Practice*. John Willey & Sons, NY, 729.

Tomlinson, M., & Woodward, J. (2008). *Pile Design and Construction Practice*. Fifth edition (Vol. 5). Taylor & Francis.

Tschuchnigg, F. (2013). *3D Finite Element Modelling of Deep Foundations Employing an Embedded Pile Formulation [PhD Dissertation]*. Graz University of Technology.

Turello, D. F., Pinto, F., & Sánchez, P. J. (2016). *Embedded beam element with interaction surface for lateral loading of piles*. International Journal for Numerical; Analytical Methods in Geomechanics, 40, 568–582.

Van den Eijnden, A. P. (2022). *Lecture notes MSc course CIE4366 Numerical Modelling in Geo-Engineering [Lecture]*. Delft: Delft University of Technology (TU Delft).

Van der Sluis, A. G. (2017). *Galaxy Tower te Utrecht: Constructieve omschrijving en uitgangspunten t.b.v. omgevingsvergunning [Internal Document]*. Van Rossum Raadgevende Ingenieurs BV.

Van Wessel, C. (2016, March 4). *Hoogbouw in Amsterdam / Skyline Amsterdam / Het Parool [Video]*. YouTube. Retrieved on 23-12-2021 from: https://www.youtube.com/watch?v=YRqtiz0gFNU&t=11s.

Verruijt, A. (2001). *Soil Mechanics*. Delft: Delft University of Technology (TU Delft).

Vesic, A. S. (1977). *Design of pile foundations*. Transportation Research Board, National Research Council.

Visser, G. T., & Gutter, H. H. (1999). *Zettingsanalyse voor Amsterdamse hoogbouw*. Geotechniek, jaargang 3 (nummer 3), 5-15.

Waterman, D., & Broere, W. (2004). *PRACTICAL APPLICATION OF THE SOFT SOIL CREEP MODEL - PART III*. Plaxis BV Netherlands.

Yengar, Y., & Olgun, M. (2017). *Evaluation of Design Methods of Piled Raft Foundations under Vertical Loadings*. Conference: 2nd International Conference on Civil; Environmental Engineering, Nevsehir, Turkey.

Zoidi, E. (2015). *Prediction of settlements for high-rise buildings on deformable subsoil [Master Thesis]*. Delft: Delft University of Technology (TU Delft).

Appendix A

Appendix: CPT Profiles, Lab tests, D-Foundations & PileCore

This Appendix contains lab tests and CPT plots for representative soil profiles along with summary tables from D-Foundations and CRUX's program PileCore (invented by CEMS) used for the pile load test, pile group model, soil test and simple & complex modelling approaches.

A.1 CPT Profiles

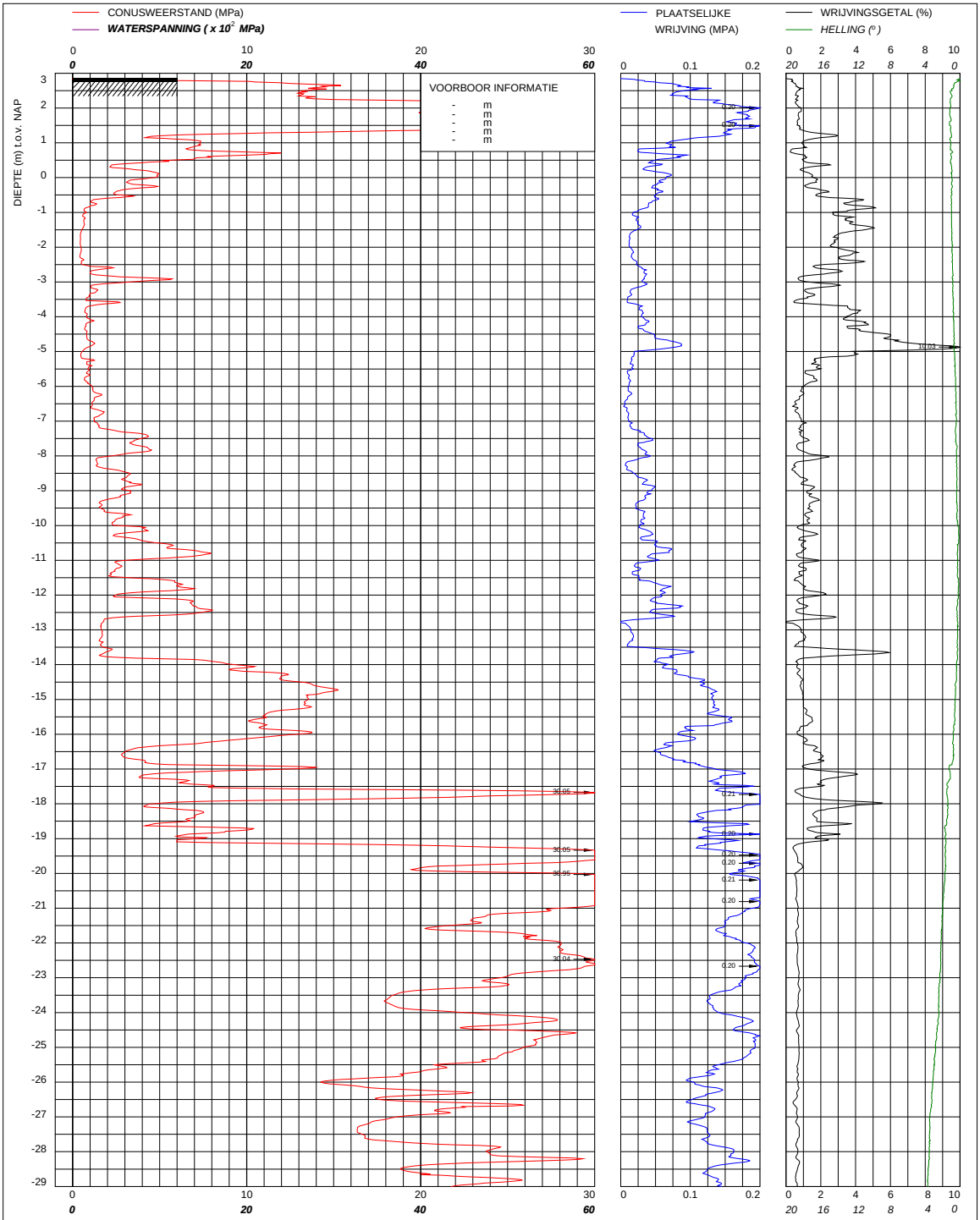

Figure A.1: Page 1 (out of 3) of cone penetration test data retrieved by Multiconsult in northern Amsterdam (2019).

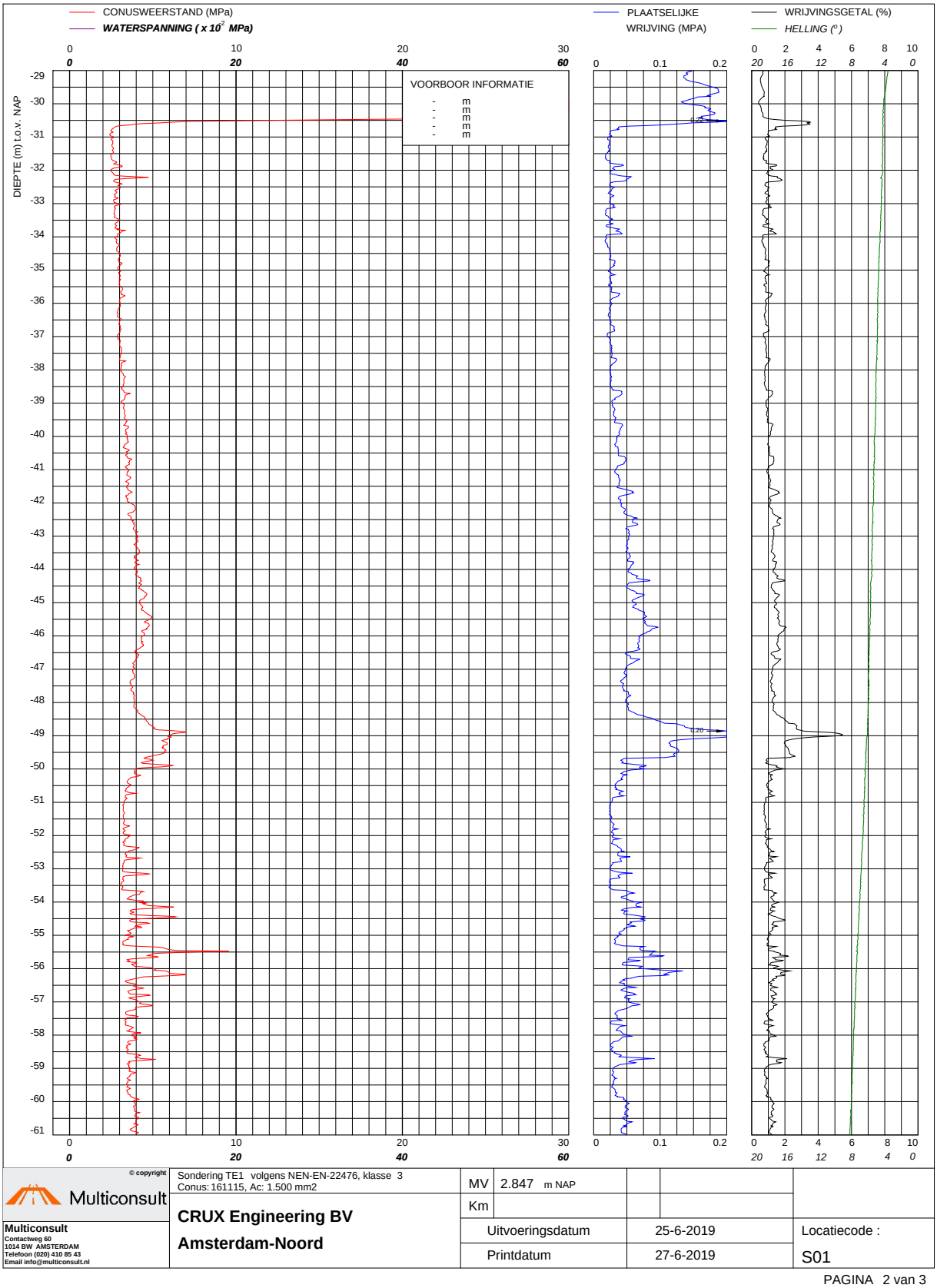

PAGINA 2 van 3

Figure A.2: Page 2 (out of 3) of cone penetration test data retrieved by Multiconsult in northern Amsterdam (2019).

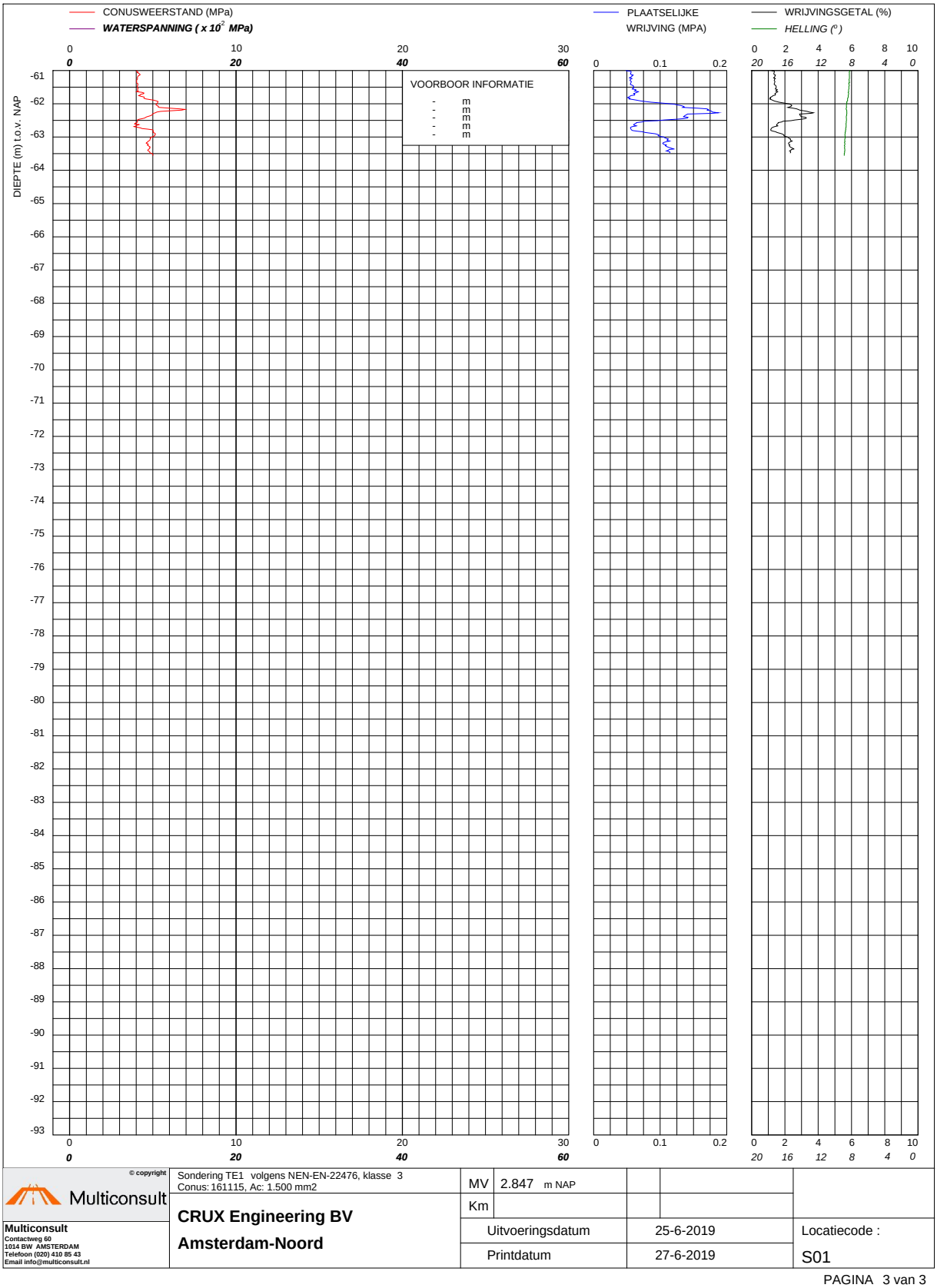

Figure A.3: Page 3 (out of 3) of cone penetration test data retrieved by Multiconsult in northern Amsterdam (2019).

A.2 Lab Results

SAMENDRUKKINGSPROEF

Plaats : Amsterdam

NEN / Bjerrum (NEN5118)

Boring	:	B01	Startdatum	:	05-06-2018	Diepte :	NAP -27.24 / -27.29 m.
Monster	:	29	Einddatum	:	15-06-2018	Initieel vol.gew.	γ : 16.85 kN/m^3
Bus	:	22399	Hoogte monster	:	19.00 mm	Droog vol.gew.	γ_{dr}: 11.44 kN/m^3
Apparaat	:	14	Zetting (24u)	:	0.593 mm	Watergehalte	W : 47 %
Soort monster	:	Ongeroerd	e_0	:	1.25	Grondsoort :	Klei, matig siltig, grijs

Belastingtrappen:	**Trap1**	**Trap2**	**Trap3**	**Trap4**	**Trap5**	**Trap6**	**Trap7**
Belasting	210	315	399	840	1260	840	1260
$C_{c/r/sw} = \Delta e / \Delta \log p$		0.130	0.160	0.306	0.428	0.050	0.103
$C_\alpha^* = \Delta \varepsilon / \Delta \log t$				0.0076			

* Berekening C_α gebaseerd op de proefstukhoogte aan het begin van de trap

C_r = 0.103	C_c = 0.428	C_{sw} = 0.050	C_α = 0.0076
Trap 6 - 7	Trap 4 - 5	Trap 5 - 6	Trap 4

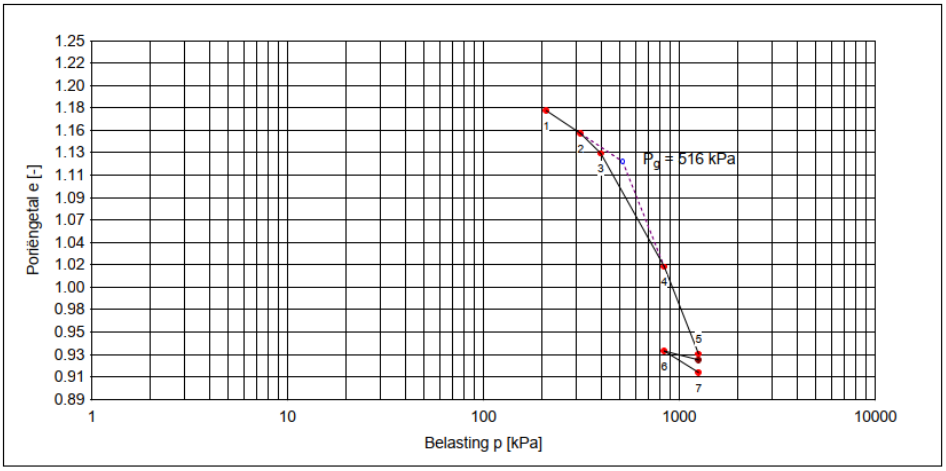

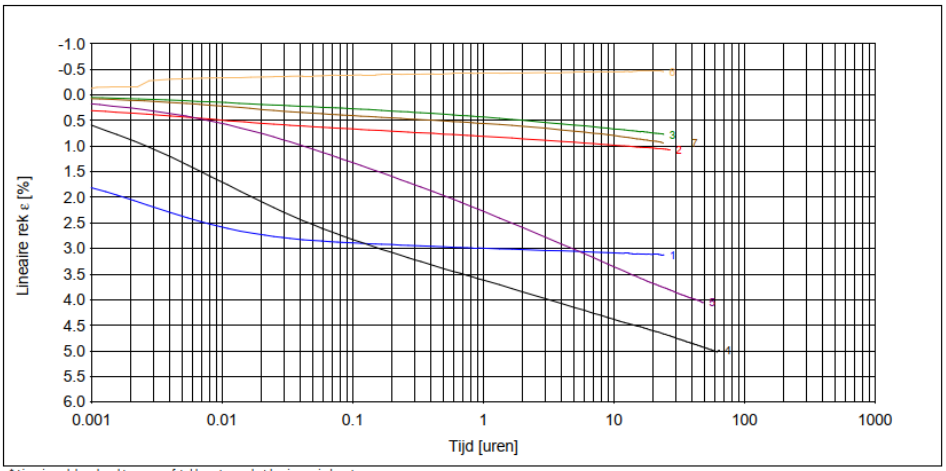

* Lineaire rek berekend t.o.v. proefstukhoogte aan het begin van iedere trap

MOS GRONDMECHANICA B.V. Postbus 801, 3160 AA Rhoon - Tel: 088 51 30 200 - www.mosgeo.com

MOS GRONDMECHANICA

Figure A.4: Oedometer lab test performed by MOS Grondmechanica BV on Eem clay in eastern Amsterdam (2018) using Koppejan (NEN5118).

SAMENDRUKKINGSPROEF

Plaats : Amsterdam

Koppejan (NEN5118)

Boring	: B01	Startdatum	: 05-06-2018	Diepte	:	NAP -29.26 / -29.31 m.	
Monster	: 31	Einddatum	: 15-06-2018	Initieel vol.gew.	γ :	16.44	kN/m^3
Bus	: 219	Hoogte monster	: 19.00 mm	Droog vol.gew.	γ_{dr}:	10.68	kN/m^3
Apparaat	: 13	Zetting (24u)	: 0.993 mm	Watergehalte	W :	54	%
Soort monster	: Ongeroerd	h (24u)	: 18.007 mm	Grondsoort :		Klei, matig siltig, grijs	

Belastingtrappen:	**Trap1**	**Trap2**	**Trap3**	**Trap4**	**Trap5**	**Trap6**	**Trap7**
Belasting [kN/m^2]	227	341	432	910	1365	910	1365
C_p	24.6	23.0	12.2	10.4	51.7	41.4	
C_s	153.7	93.9	116.6	53.4	111.5	201.8	
$C_{10}4$	15.0	11.6	8.6	5.8	18.1	22.7	

Grensspanning p_g	**Voor p_g**	**Na p_g**	**Ontlasten**	**Herbelasten**	**Ontlasten(2)**	**Herbelasten(2)**
533 [kN/m^2]	C_p = 24.6	C_p' = 10.4	C_p = 51.7	C_p = 41.4		
	C_s = 153.7	C_s' = 53.4	C_s = 111.5	C_s = 201.8		
	$C_{10}4$ = 15.0	$C_{10}4'$ = 5.8	$C_{10}4$ = 18.1	$C_{10}4$ = 22.7		

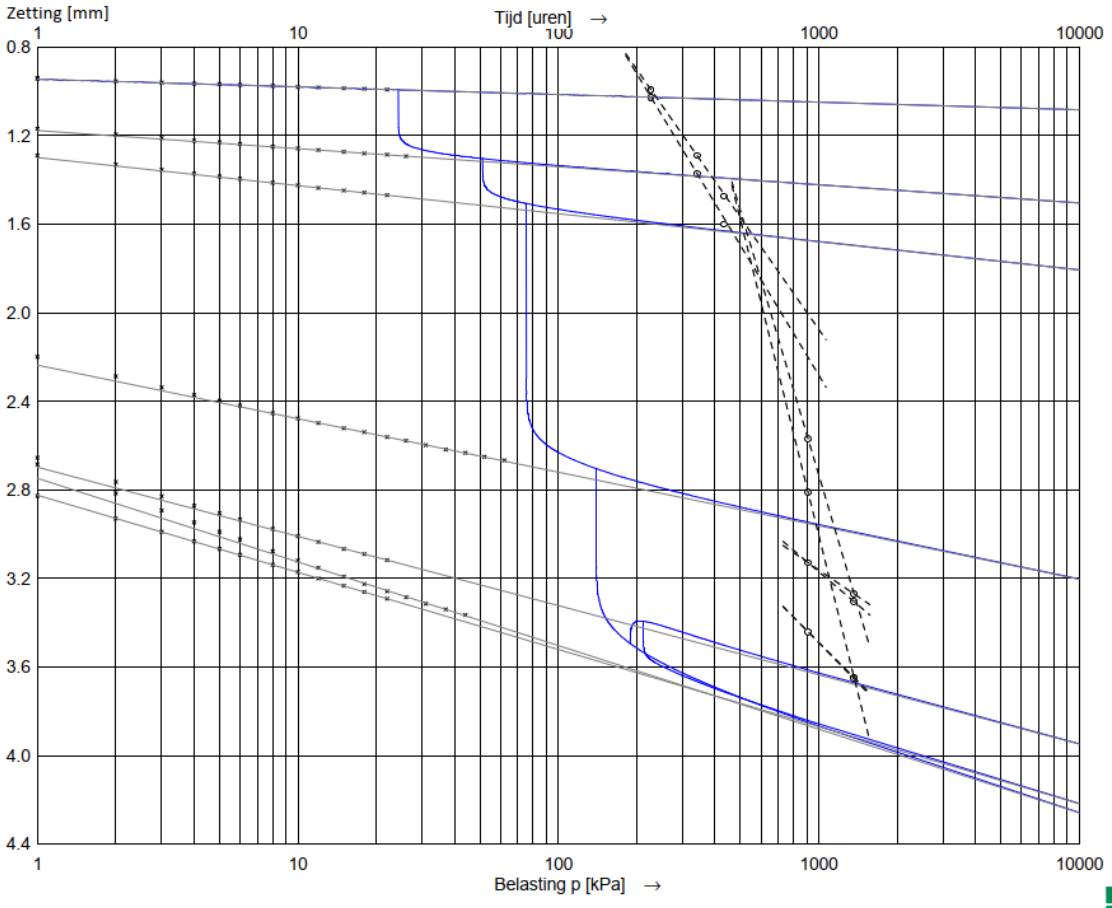

MOS GRONDMECHANICA

MOS GRONDMECHANICA B.V. Postbus 801, 3160 AA Rhoon - Tel: 088 51 30 200 - www.mosgeo.com

Figure A.5: Oedometer lab test performed by MOS Grondmechanica BV on Eem clay in eastern Amsterdam (2018) using NEN / Bjerrum (NEN5118).

SAMENDRUKKINGSPROEF

Plaats : Amsterdam

Koppejan (NEN5118)

Boring	: 15	Startdatum	: 25-1-2019	Diepte	:	NAP -35.92 / -35.96 m.	
Monster	: 6	Einddatum	: 11-2-2019	Initieel vol.gew.	γ :	16.16	kN/m^3
Bus	: 7602	Hoogte monster	: 19.00 mm	Droog vol.gew.	γ_{dr} :	10.86	kN/m^3
Apparaat	: 18	Zetting (24u)	: 0.751 mm	Watergehalte	W :	49	%
Soort monster	: Ongeroerd	h (24u)	: 18.249 mm	Grondsoort :		Klei, matig siltig, grijs	

Belastingtrappen:	**Trap1**	**Trap2**	**Trap3**	**Trap4**	**Trap5**	**Trap6**	**Trap7**	**Trap8**	**Trap9**
Belasting [kN/m^2]	71	142	285	569	1138	569	1138	2276	4552
C_p		34.2	24.7	16.9	12.6	64.4	55.5	10.6	9.0
C_s		371.2	277.2	132.3	132.7	243.9	308.2	95.1	177.0
$C_{10}4$		25.0	18.2	11.2	9.1	31.3	32.3	7.3	7.5

Grensspanning p_g	**Voor p_g**	**Na p_g**	**Ontlasten**	**Herbelasten**	**Ontlasten(2)**	**Herbelasten(2)**
397 [kN/m^2]	C_p = 34.2 C_s = 371.2 $C_{10}4$ = 25.0	C_p' = 10.4 C_s' = 127.9 $C_{10}4'$ = 7.9	C_p = 64.4 C_s = 243.9 $C_{10}4$ = 31.3	C_p = 55.5 C_s = 308.2 $C_{10}4$ = 32.3		

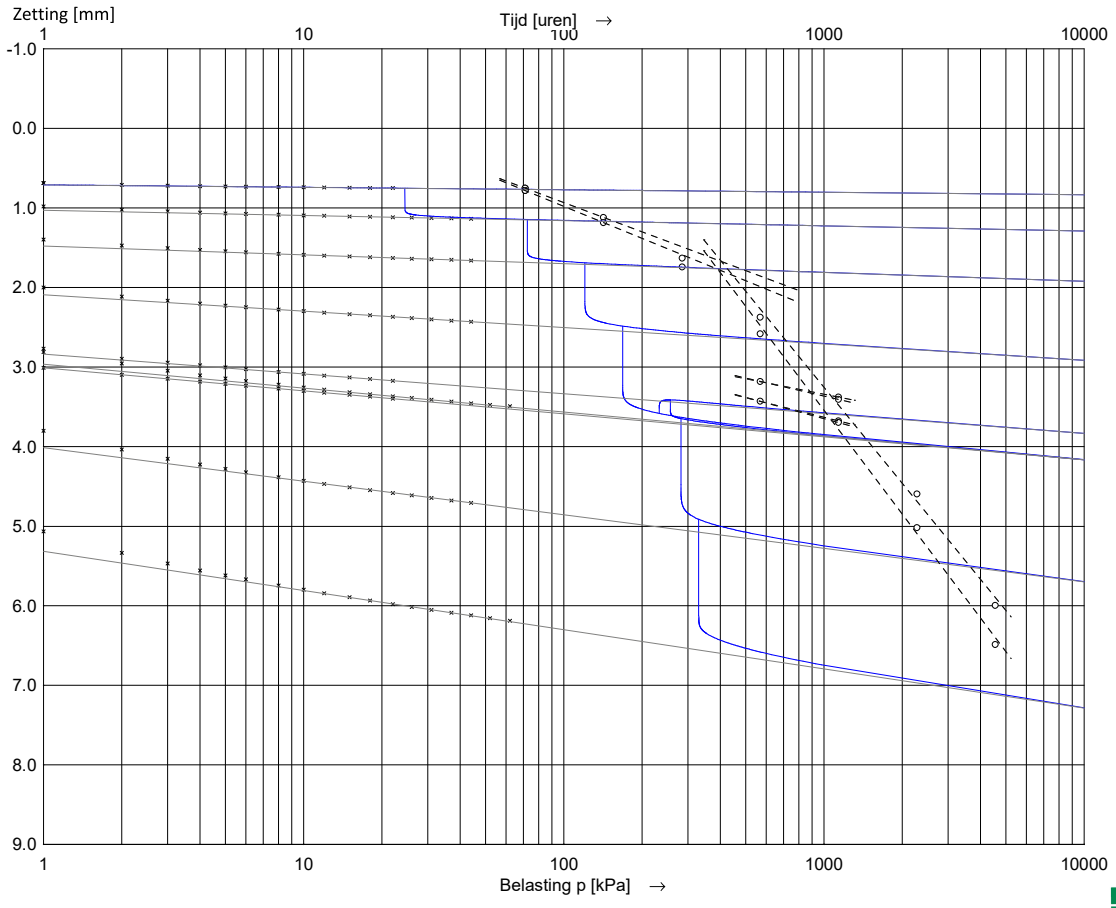

MOS GRONDMECHANICA B.V. Albert Plesmanweg 47, 3088 GB Rotterdam - Tel: 088-5130200 - www.mosgeo.com

Figure A.6: Oedometer lab test performed by MOS Grondmechanica BV on Eem clay in northern Amsterdam (2019) using Koppejan (NEN5118).

SAMENDRUKKINGSPROEF

Plaats : Amsterdam

NEN / Bjerrum (NEN5118)

Boring	: 15	Startdatum	: 25-1-2019	Diepte	:	NAP -35.92 / -35.96 m.	
Monster	: 6	Einddatum	: 11-2-2019	Initieel vol.gew.	γ :	16.16	kN/m^3
Bus	: 7602	Hoogte monster	: 19.00 mm	Droog vol.gew.	γ_{dr}:	10.86	kN/m^3
Apparaat	: 18	Zetting (24u)	: 0.751 mm	Watergehalte	W :	49	%
Soort monster	: Ongeroerd	e_0	: 1.36	Grondsoort :		Klei, matig siltig, grijs	

Belastingtrappen:	**Trap1**	**Trap2**	**Trap3**	**Trap4**	**Trap5**	**Trap6**	**Trap7**	**Trap8**	**Trap9**
Belasting	71	142	285	569	1138	569	1138	2276	4552
$C_{c/r/sw} = \Delta e / \Delta \log p$		0.156	0.188	0.282	0.402	0.066	0.079	0.467	0.580
C_α^* $= \Delta\varepsilon / \Delta \log t$			0.0037	0.0067	0.0086		0.0024	0.0116	0.0101

* Berekening C_α gebaseerd op de proefstukhoogte aan het begin van de trap

C_r = 0.079	C_c = 0.580	C_{sw} = 0.066	C_α = 0.0109
Trap 6 - 7	Trap 8 - 9	Trap 5 - 6	Trap 8, 9

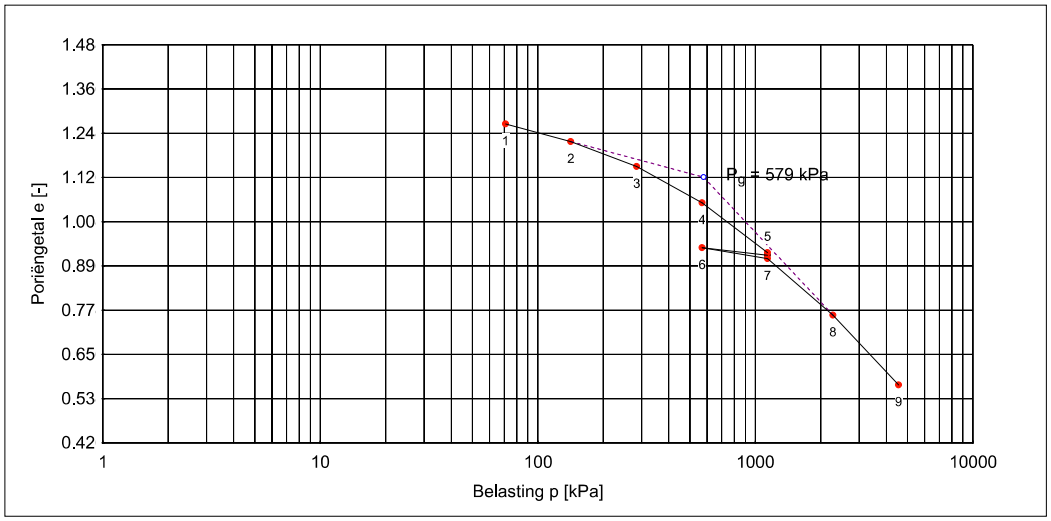

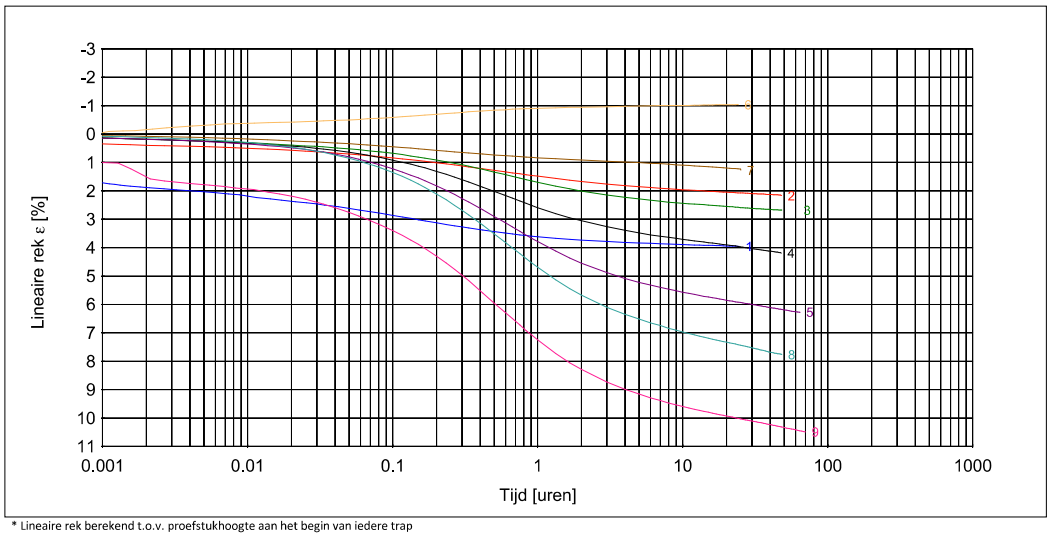

* Lineaire rek berekend t.o.v. proefstukhoogte aan het begin van iedere trap

MOS GRONDMECHANICA B.V. Albert Plesmanweg 47, 3088 GB Rotterdam - Tel: 088-5130200 - www.mosgeo.com

Figure A.7: Oedometer lab test performed by MOS Grondmechanica BV on Eem clay (North #1) in northern Amsterdam (2019) using NEN / Bjerrum (NEN5118).

SAMENDRUKKINGSPROEF

Plaats : Amsterdam

Isotachen

Boring	:	15	Startdatum	:	25-1-2019	Diepte :	NAP -35.92 / -35.96 m.
Monster	:	6	Einddatum	:	11-2-2019	Initieel vol.gew.	γ : 16.16 kN/m^3
Bus	:	7602	Hoogte monster	:	19.00 mm	Droog vol.gew.	γ_{dr}: 10.86 kN/m^3
Apparaat	:	18	Zetting (24u)	:	0.751 mm	Watergehalte	W : 49 %
Soort monster	:	Ongeroerd	h (24u)	:	18.249 mm	Grondsoort :	Klei, matig siltig, grijs

Belastingtrappen:	**Trap1**	**Trap2**	**Trap3**	**Trap4**	**Trap5**	**Trap6**	**Trap7**	**Trap8**	**Trap9**
Belasting	71	142	285	569	1138	569	1138	2276	4552
a, b	0.0302	0.0375	0.0584	0.0880	0.0150	0.0178	0.1112	0.1522	
c							0.0011	0.0056	0.0048

Grensspanning P_g =	725.9kPa	**a =** 0.0178	**b =** 0.1522	**c =** 0.00386
		Trap 6 - 7	Trap 8 - 9	Trap 7, 8, 9

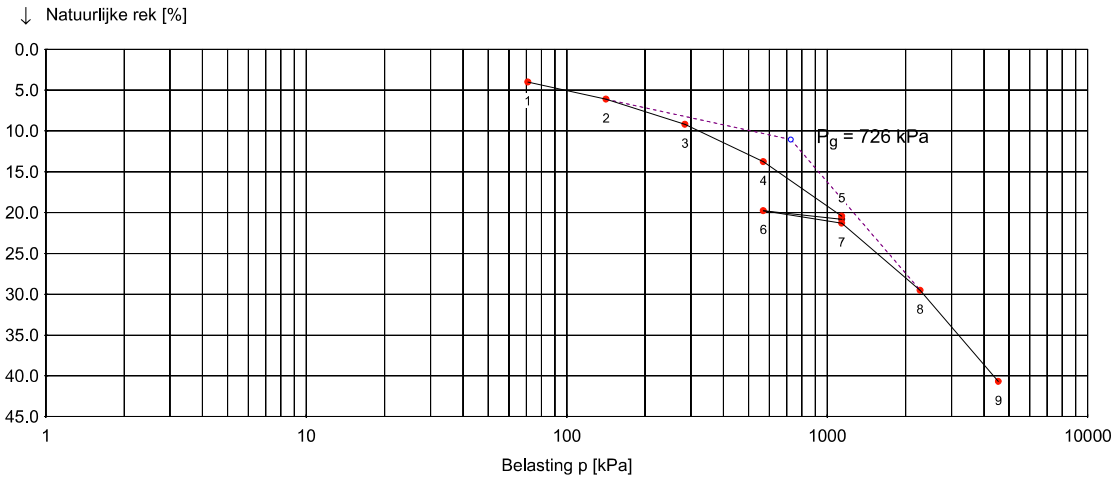

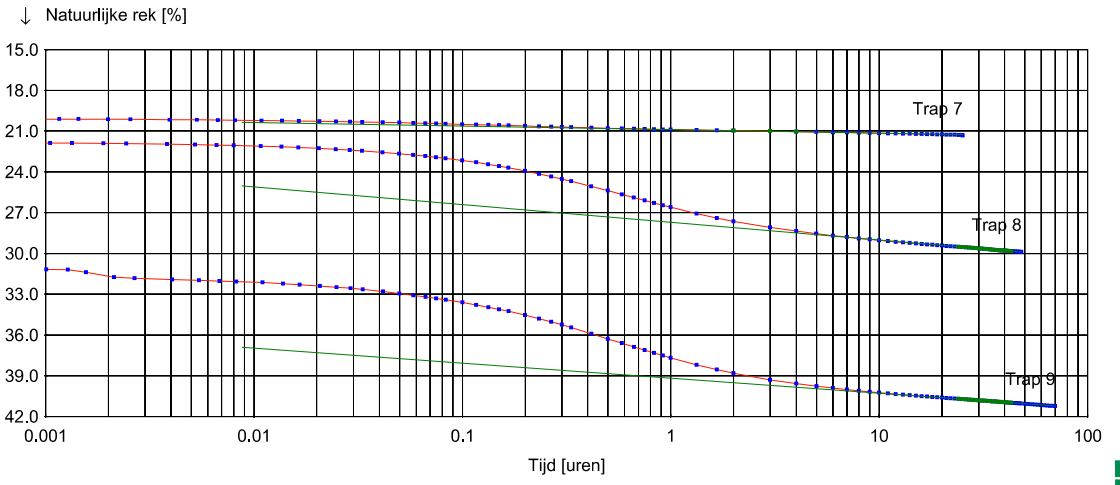

MOS GRONDMECHANICA B.V. Albert Plesmanweg 47, 3088 GB Rotterdam - Tel: 088-5130200 - www.mosgeo.com

Figure A.8: Oedometer lab test performed by MOS Grondmechanica BV on Eem clay in northern Amsterdam (2019) using Isotachen.

SAMENDRUKKINGSPROEF

Plaats : Amsterdam

Totaaloverzicht proefresultaten

MOS GRONDMECHANICA

Boring	: 15	Startdatum	: 25-1-2019	Diepte	:	NAP -35.92 / -35.96 m.	
Monster	: 6	Einddatum	: 11-2-2019	Initieel vol.gew.	γ :	16.16	kN/m^3
Bus	: 7602	Hoogte monster	: 19.00 mm	Droog vol.gew.	γ_{dr}:	10.86	kN/m^3
Apparaat	: 18	Zetting (24u)	: 0.751 mm	Watergehalte	W :	49	%
Soort monster	: Ongeroerd	e_0	: 1.36	Grondsoort :		Klei, matig siltig, grijs	

Bepaling parameters per trap

Belasting p [kPa]		71	142	285	569	1138	569	1138	2276	4552
NEN / Bjerrum	**Trap**	**1**	**2**	**3**	**4**	**5**	**6**	**7**	**8**	**9**
$C_{c/r/sw} = \Delta e / \Delta \log p$		0.1559	0.1883	0.2820	0.4017	0.0664	0.0788	0.4673	0.5802	
$CR/RR/SR = C_x / (1 + e_0)$		0.0661	0.0798	0.1195	0.1703	0.0281	0.0334	0.1981	0.2460	
$C_\alpha = \Delta\varepsilon / \Delta \log t$				0.0037	0.0067	0.0086		0.0024	0.0116	0.0101
KoppeJan	**Trap**	**1**	**2**	**3**	**4**	**5**	**6**	**7**	**8**	**9**
C_p		34.2	24.7	16.9	12.6	64.4	55.5	10.6	9.0	
C_s		371.2	277.2	132.3	132.7	243.9	308.2	95.1	177.0	
$C_{10}4$		25.0	18.2	11.2	9.1	31.3	32.3	7.3	7.5	
Taylor / Casagrande	**Trap**	**1**	**2**	**3**	**4**	**5**	**6**	**7**	**8**	**9**
c_v [10^{-8} m^2/s] (Taylor)				1.21	1.21	1.05		4.86	0.81	0.73
m_v [1/MPa]				0.13	0.10	0.08		0.01	0.05	0.03
k_{10} [10^{-11} m/s]				1.50	1.22	0.81		0.52	0.41	0.21
c_v [10^{-8} m^2/s] (Casagrande)				0.86	0.96	0.76		3.32	0.64	0.57
Isotachen	**Trap**	**1**	**2**	**3**	**4**	**5**	**6**	**7**	**8**	**9**
a, b		0.0302	0.0375	0.0584	0.0880	0.0150	0.0178	0.1112	0.1522	
c								0.0011	0.0056	0.0048

Bepaling P_g en parameters op basis van geselecteerde trappen

NEN / Bjerrum	**Trap 6 - 7**	**Trap 8 - 9**	**Trap 5 - 6**	**Trap 8, 9**
P_g = 578.6	C_r = 0.0788 RR = 0.0334	C_c = 0.5802 CR = 0.2460	C_{sw} = 0.0664 SR = 0.0281	C_α = 0.0109
KoppeJan	**Trap 1 - 2**	**Trap 4 - 5, 8 - 9**	**Trap 5 - 6**	**Trap 6 - 7**
P_g = 396.7	C_p = 34.2 C_s = 371.2 C_{10^4} = 25.0	C_p' = 10.4 C_s' = 127.9 C_{10^4}' = 7.9	A_p = 64.4 A_s = 243.9 A_{10^4} = 31.3	$C_{p(r)}$ = 55.5 $C_{s(r)}$ = 308.2 $C_{10^4(r)}$ = 32.3
Isotachen	**Trap 6 - 7**	**Trap 8 - 9**	**Trap 7, 8, 9**	
P_g = 725.9	a = 0.0178	b = 0.1522	c = 0.0039	

Figure A.9: Summary of (oedometer) lab tests performed by MOS Grondmechanica BV on Eem clay in northern Amsterdam (2019) using Koppejan (NEN5118), NEN / Bjerrum (NEN5118), and Isotachen.

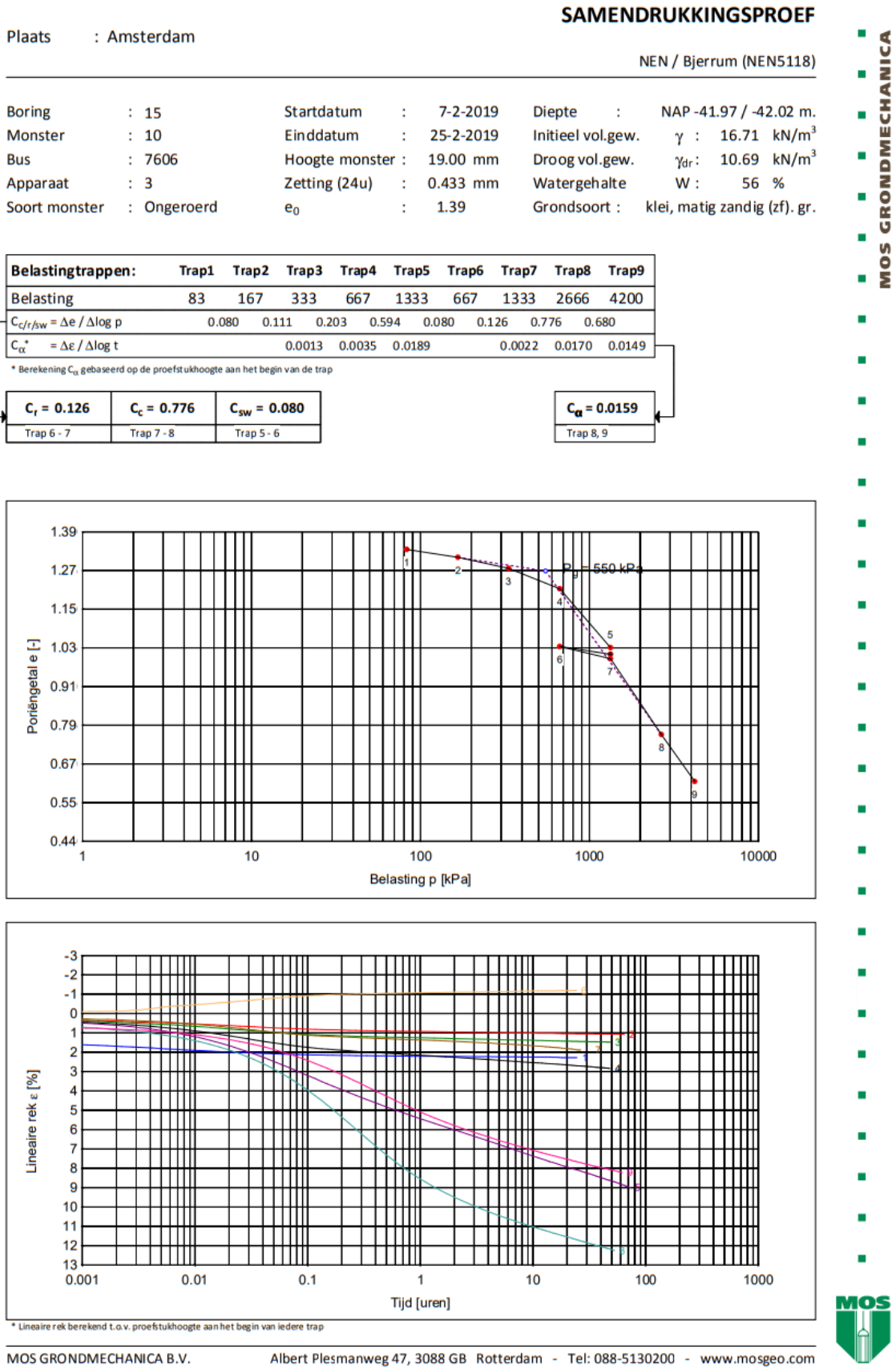

Figure A.10: Oedometer lab test performed by MOS Grondmechanica BV on Eem clay (North #2) in northern Amsterdam (2019) using NEN / Bjerrum (NEN5118).

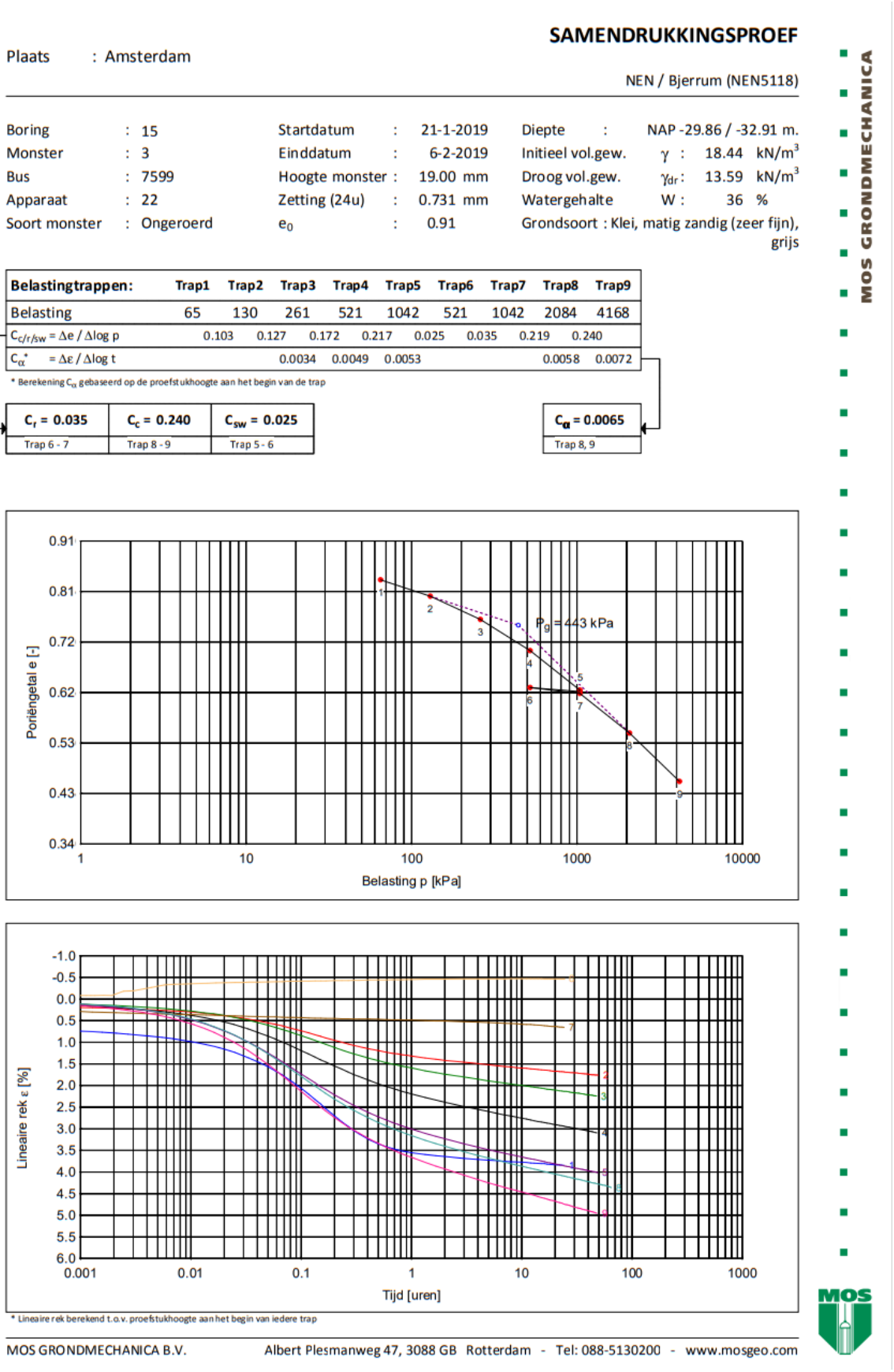

Figure A.11: Oedometer lab test performed by MOS Grondmechanica BV on Eem clay (North #3) in northern Amsterdam (2019) using NEN / Bjerrum (NEN5118).

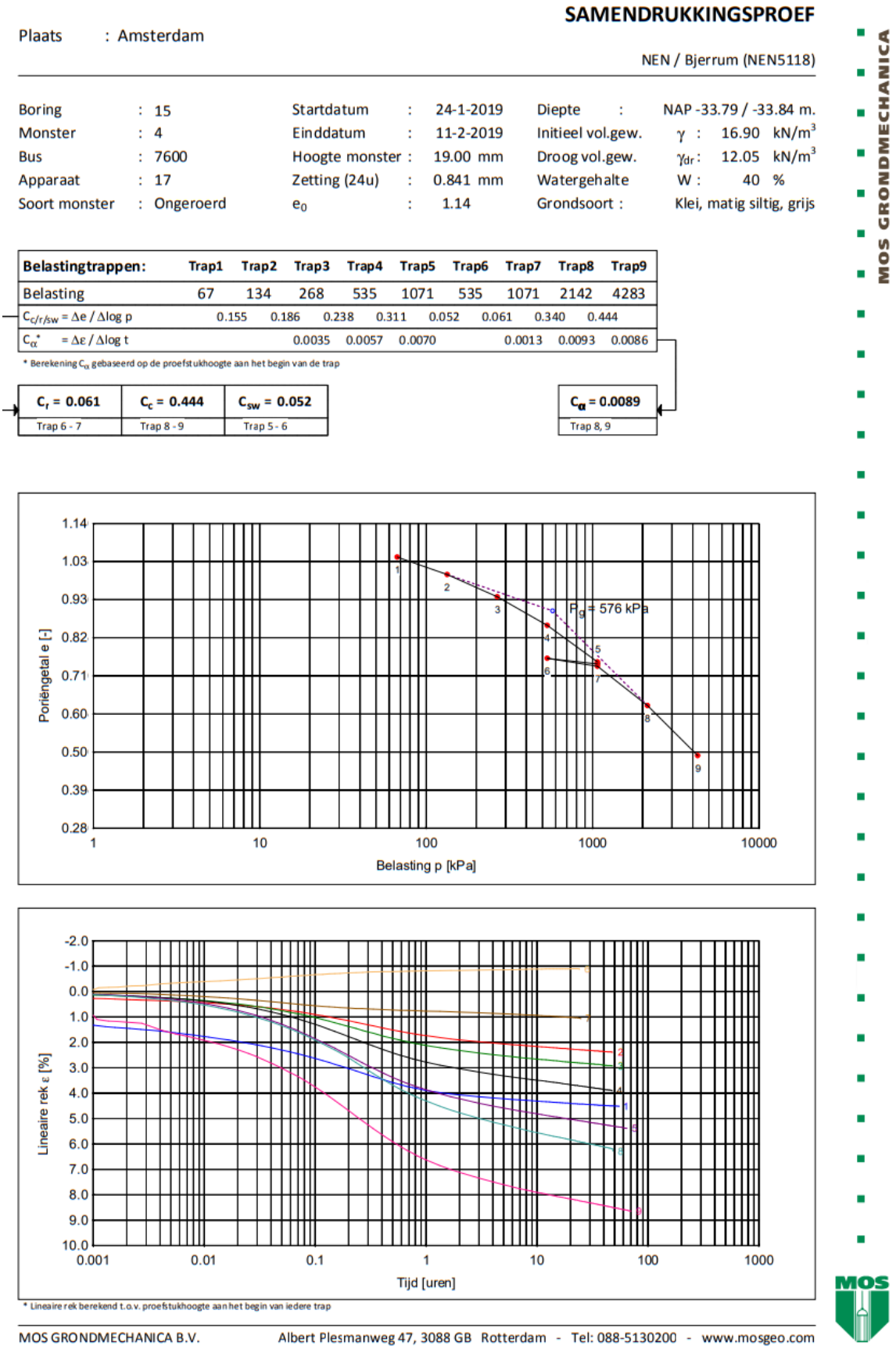

Figure A.12: Oedometer lab test performed by MOS Grondmechanica BV on Eem clay (North #4) in northern Amsterdam (2019) using NEN / Bjerrum (NEN5118).

A.3 D-foundations (Inputs)

Table A.1: Additional input data for soil profile in D-foundations.

Input	Value
Phreatic level (m)	0.75
Pile tip level (m)	-23.0
Overconsolidation ratio of bearing layer (-)	1.0
Top of positive skin friction zone (m)	13.5
Bottom of negative skin friction zone (m)	2.85
Expected ground level settlement (m)	0.11

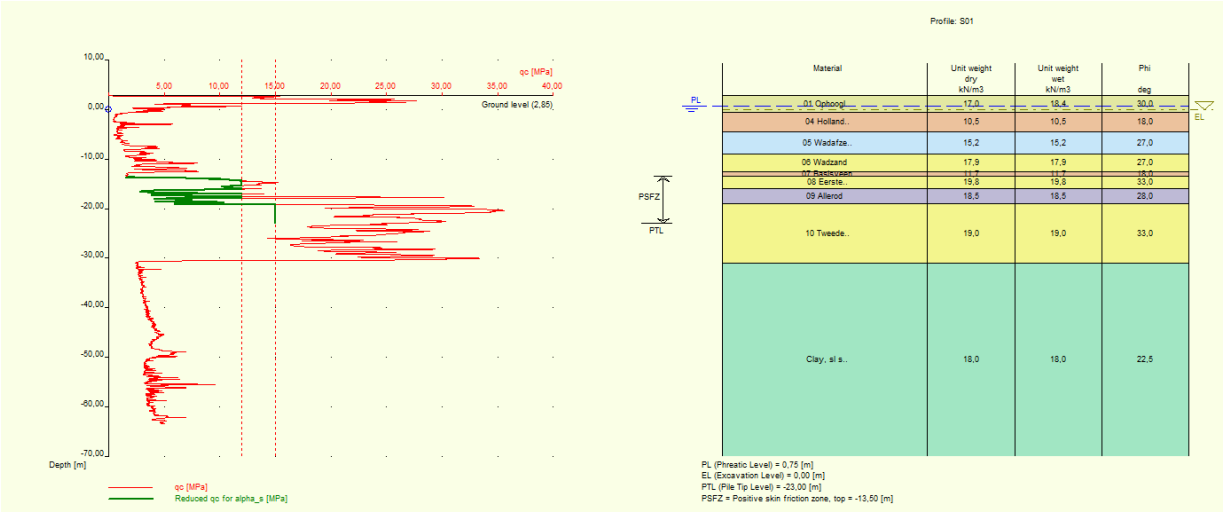

Figure A.13: Simplified soil stratigraphy for northern Amsterdam in D-foundations.

A.4 D-foundations (Outputs)

Table A.2: Summary table of ultimate bearing capacity and s_1 settlement calculated by D-Foundations for a Fundex 560 as NEN **type 1** load-settlement pile used to determine pile tip level by the NEN design method.

PPN m NAP	Min Rc;net;d indiv. kN	Rc;k groep kN	Rc;d groep kN	Rc;net;d groep kN	V	Maatg. Rc;net;d kN	u.c. -	Maatg. ξ -	Fs;tot;k kN	w_punt mm	kv;punt MN/m	w_el mm	kv;1 MN/m
-21	1143	1883	1570	1570	12%	**1570**	1,16	ξ3=1,25	1518	19,0	80	6,0	61
-21,5	1189	1983	1653	1653	12%	**1653**	1,10	ξ4=1	1518	13,8	110	6,0	77
-22	1237	2063	1719	1719	11%	**1719**	1,06	ξ4=1	1518	10,2	149	6,1	93
-22,5	1261	2103	1753	1753	12%	**1753**	1,04	ξ4=1	1518	7,7	197	6,2	109
-23	1323	2206	1838	1838	12%	**1838**	0,99	ξ4=1	1518	6,3	239	6,3	120
-23,5	1609	2589	2157	2157	9%	**2157**	0,84	ξ3=1,25	1518	5,1	298	6,4	132
-24	1748	2676	2230	2230	8%	**2230**	0,82	ξ3=1,25	1518	4,5	336	6,5	138
-24,5	1874	2841	2367	2367	8%	**2367**	0,77	ξ3=1,25	1518	3,8	400	6,6	146
-25	1973	2945	2454	2454	6%	**2454**	0,74	ξ3=1,25	1518	3,3	454	6,7	152

Table A.3: Summary table of ultimate bearing capacity and s_1 settlement calculated by D-Foundations for a Fundex 560 as NEN **type 2** load-settlement pile to determine pile tip level by the NEN design method.

PPN m NAP	Min Rc;net;d indiv. kN	Rc;k groep kN	Rc;d groep kN	Rc;net;d groep kN	V	Maatg. Rc;net;d kN	u.c. -	Maatg. ξ -	Fs;tot;k kN	w_punt mm	kv;punt MN/m	w_el mm	kv;1 MN/m
-21	1143	1883	1570	1570	12%	**1570**	1,16	ξ3=1,25	1518	38,3	40	6,0	34
-21,5	1189	1983	1653	1653	12%	**1653**	1,10	ξ4=1	1518	28,8	53	6,0	44
-22	1237	2063	1719	1719	11%	**1719**	1,06	ξ4=1	1518	22,4	68	6,1	53
-22,5	1261	2103	1753	1753	12%	**1753**	1,04	ξ4=1	1518	17,7	86	6,2	63
-23	1323	2206	1838	1838	12%	**1838**	0,99	ξ4=1	1518	14,8	102	6,3	72
-23,5	1609	2589	2157	2157	9%	**2157**	0,84	ξ3=1,25	1518	12,1	126	6,4	82
-24	1748	2676	2230	2230	8%	**2230**	0,82	ξ3=1,25	1518	10,9	139	6,5	87
-24,5	1874	2841	2367	2367	8%	**2367**	0,77	ξ3=1,25	1518	9,4	161	6,6	95
-25	1973	2945	2454	2454	6%	**2454**	0,74	ξ3=1,25	1518	8,6	177	6,7	100

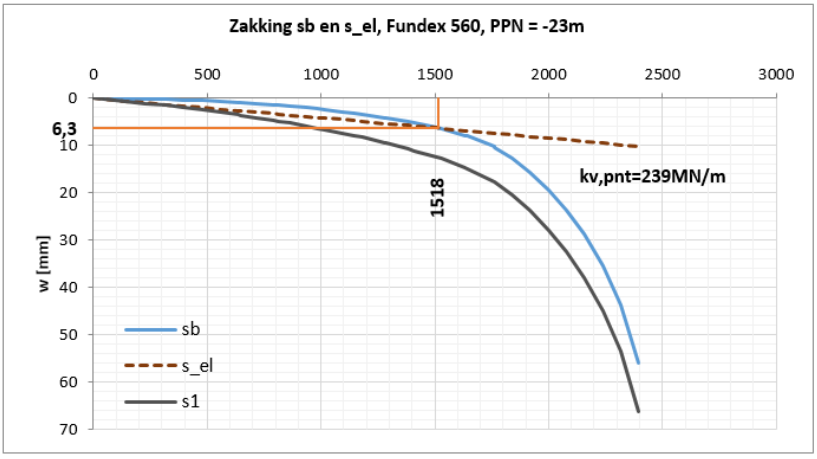

Figure A.14: Load settlement curve (s_1) for type 1 pile (Fundex) calculated by D-Foundations using the NEN design method for a ULS load of 1,825 kN.

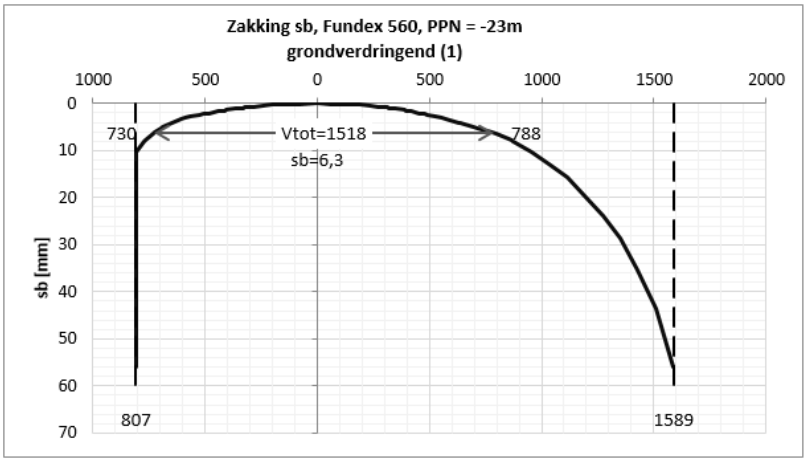

Figure A.15: Load settlement curves (s_b) based on shaft resistance (left) and base resistance (right) for a Fundex 560 as type 1 pile calculated by D-foundations using the NEN design method for a ULS load of 1,825 kN.

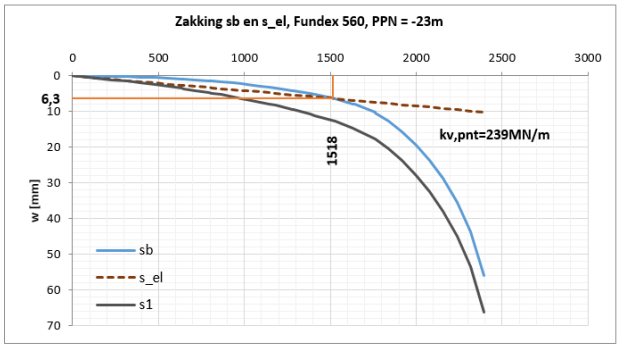

(a) Fundex as **Type I** pile.

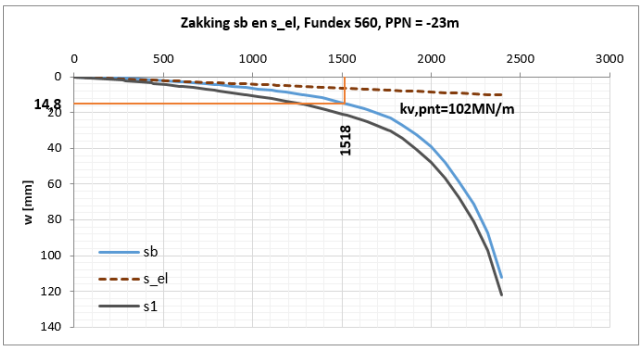

(b) Fundex as **Type II** pile.

Figure A.16: Load settlement curves (s_1) for a Fundex 560 as a) type 1, and b) type 2 pile calculated by D-Foundations using the NEN design method for a ULS load of 1,825 kN.

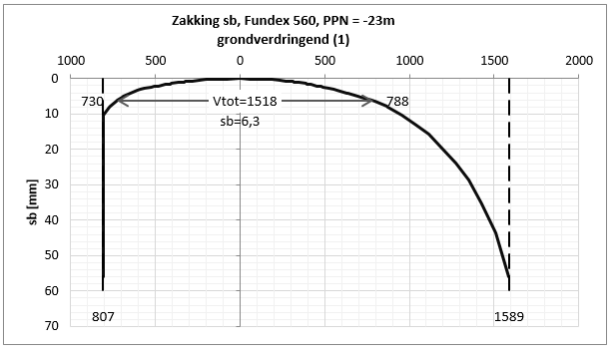

(a) Fundex as **Type I** pile.

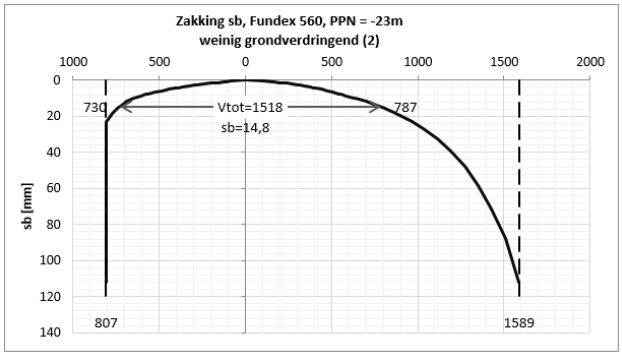

(b) Fundex as **Type II** pile.

Figure A.17: Load settlement curves (s_b) based on shaft resistance (left) and base resistance (right) for a Fundex 560 as a) type 1, and b) type 2 pile calculated by D-Foundations using the NEN design method for a ULS load of 1,825 kN.

A.5 PileCore

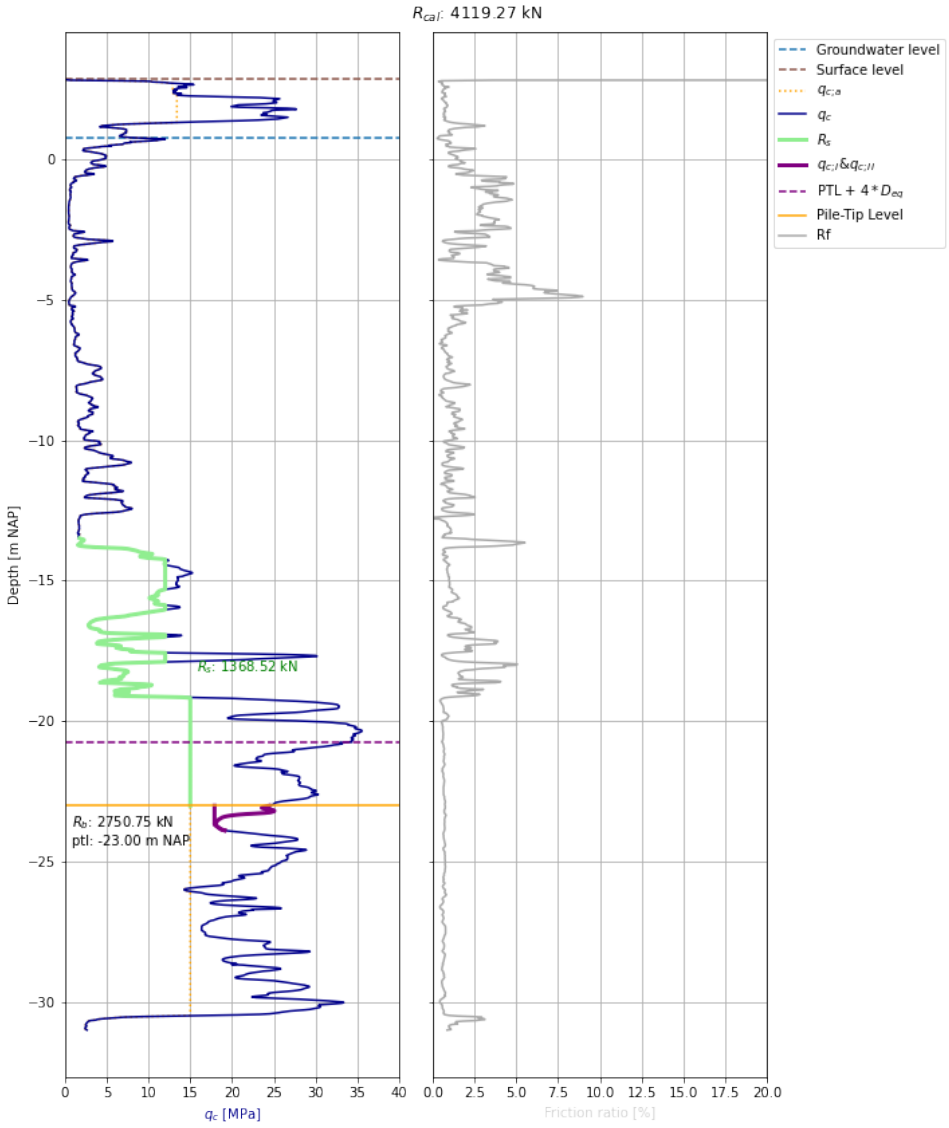

Figure A.18: CPT averaging technique and friction ratio determined by PileCore for a Fundex 460/560 with NEN pile factors, type 1 behaviour, and limited q_c.

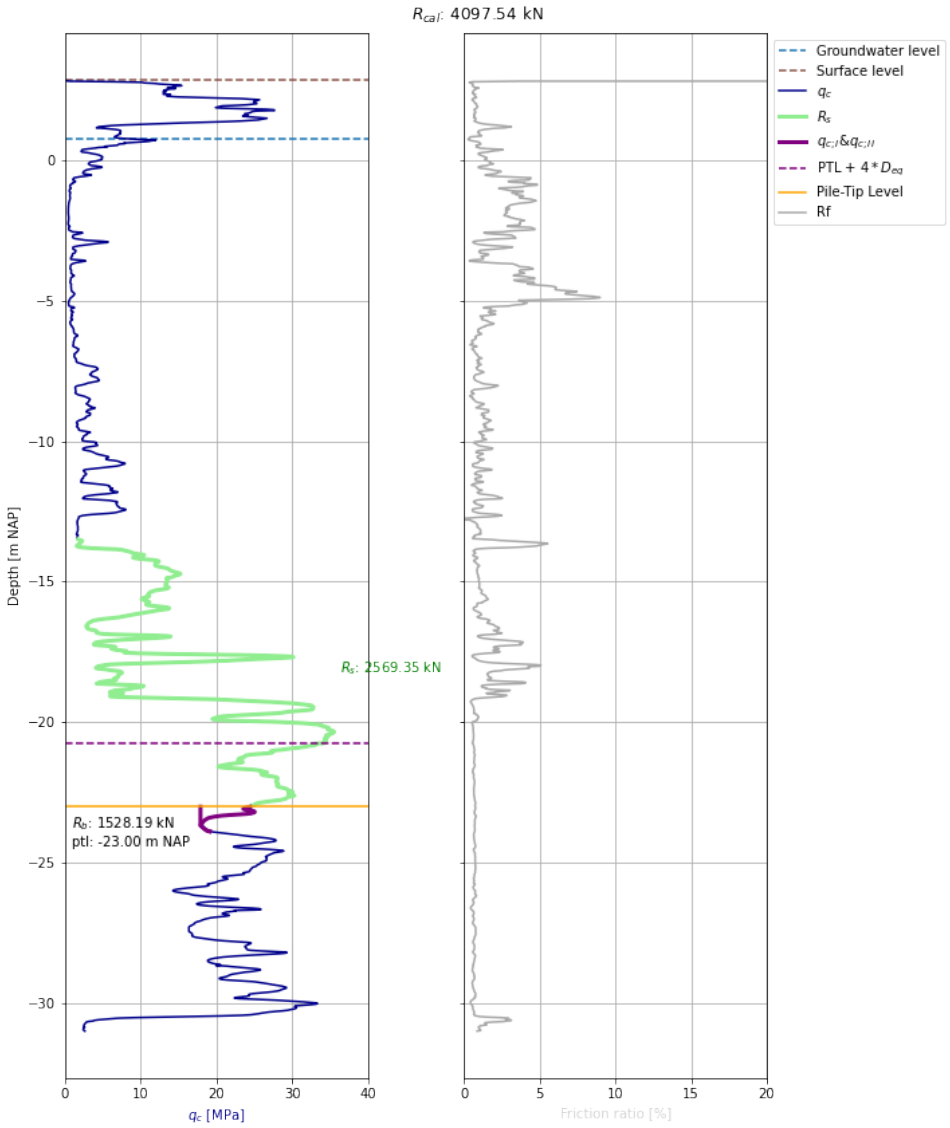

Figure A.19: CPT averaging technique and friction ratio determined by PileCore for a Fundex 460/560 with Maasvlakte pile factors, type 2 behaviour, and no limit on q_c.

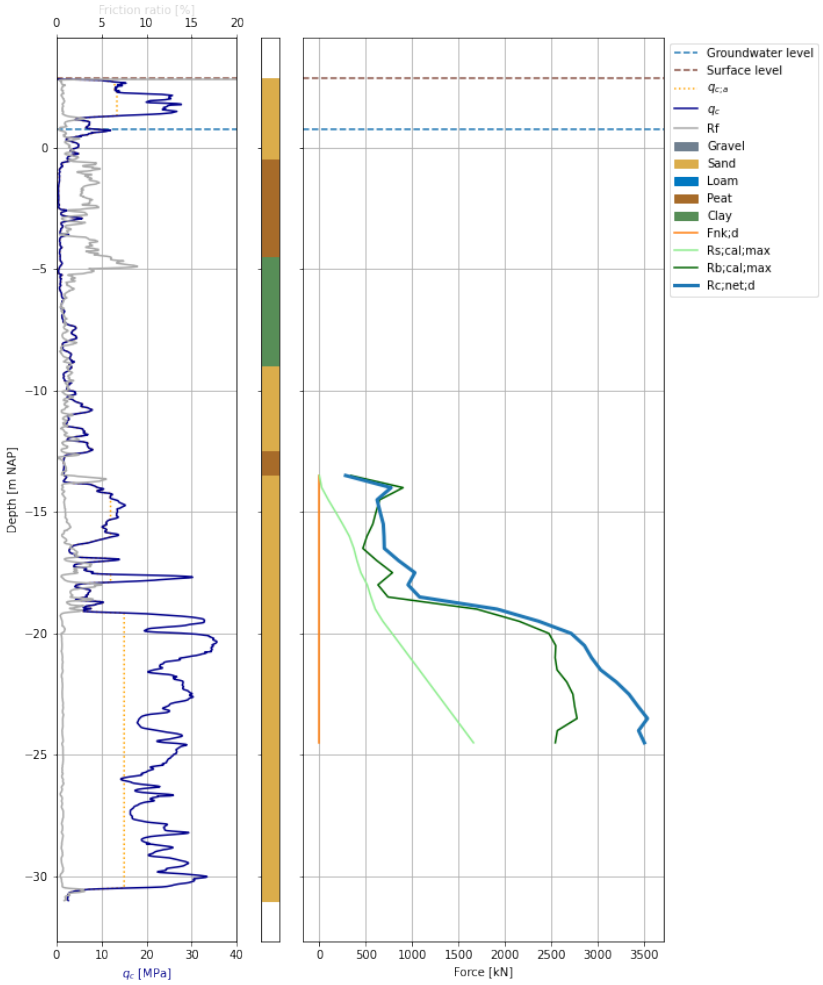

Figure A.20: CPT input (S01) and (maximum) bearing capacity calculated by PileCore for a Fundex 460/560 with NEN pile factors, type 1 behaviour, and limited q_c.

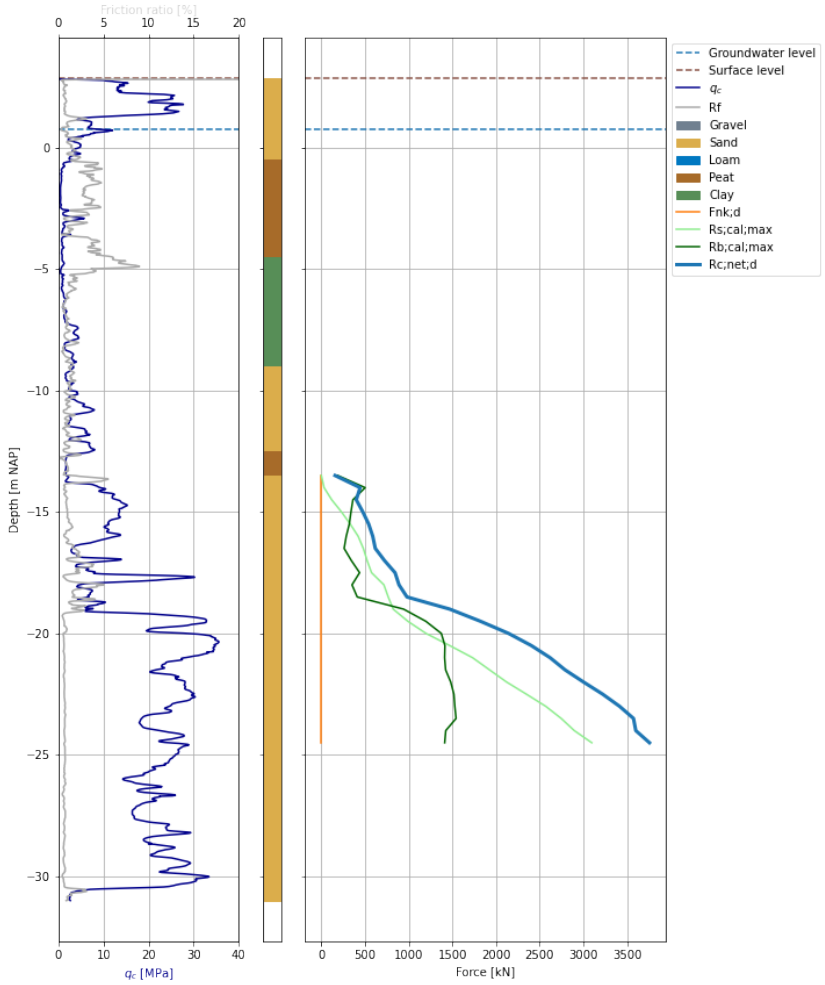

Figure A.21: CPT input (S01) and (minimum) bearing capacity calculated by PileCore for a Fundex 460/560 with updated pile factors (Maasvlakte test), type 2 behaviour, and no limit on q_c.

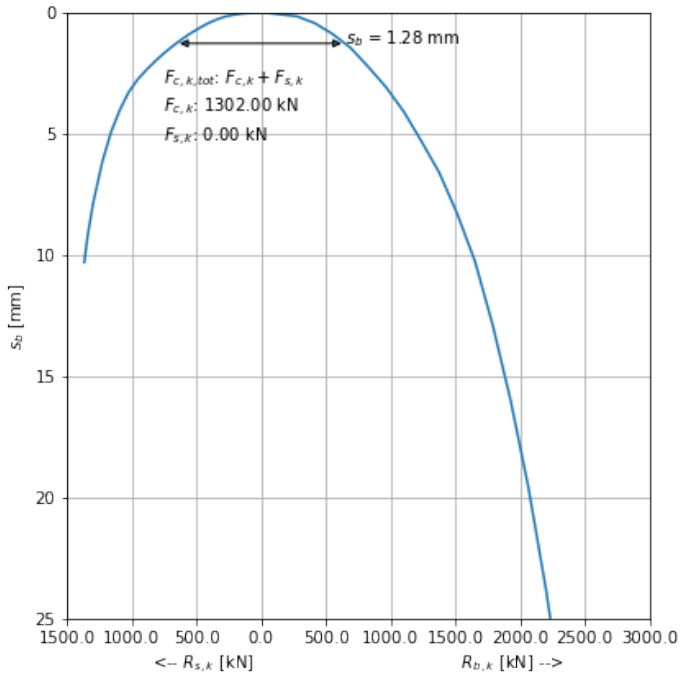

Figure A.22: Resulting (minimum) pile tip settlement calculated by PileCore for a Fundex 460/560 with NEN pile factors, type 1 behaviour, and limited q_c.

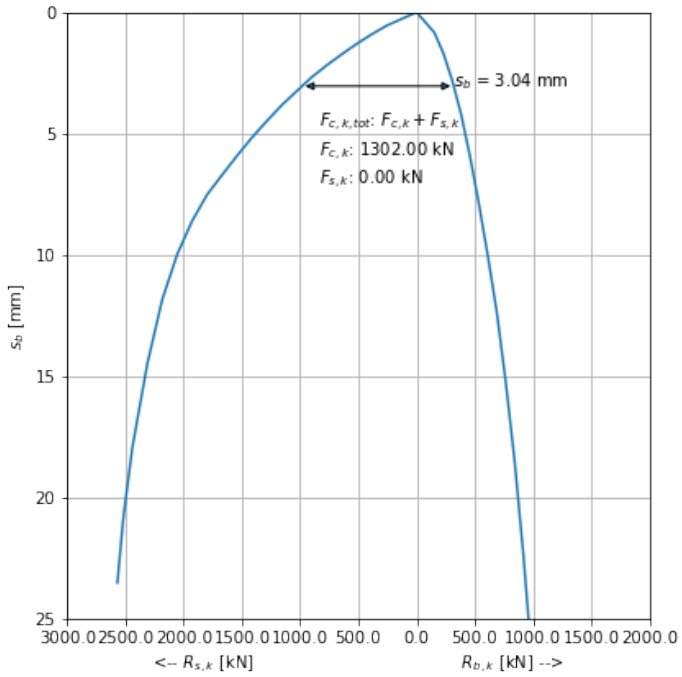

Figure A.23: Resulting (maximum) pile tip settlement calculated by PileCore for a Fundex 460/560 with Maasvlakte pile factors, type 2 behaviour, and no limit on q_c.

Appendix B

Appendix: Plaxis 3D

This Appendix contains inputs and numerical results of simple and complex geotechnical models in Plaxis 3D.

B.1 Inputs

Below follow the soil model parameters and corresponding constitutive models used for the pile load test, pile group model, soil test, simple and complex (model variations) SSI approach for a symmetric tower described in Chapter 3.

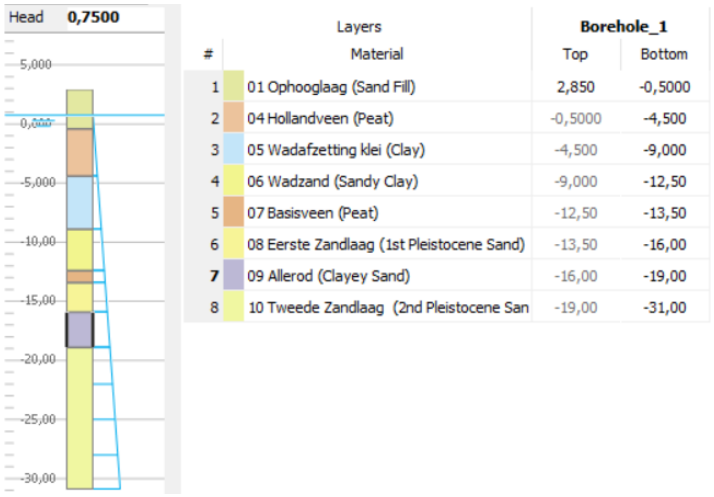

#	Layers: Material	Borehole_1: Top	Bottom
1	01 Ophooglaag (Sand Fill)	2,850	-0,5000
2	04 Hollandveen (Peat)	-0,5000	-4,500
3	05 Wadafzetting klei (Clay)	-4,500	-9,000
4	06 Wadzand (Sandy Clay)	-9,000	-12,50
5	07 Basisveen (Peat)	-12,50	-13,50
6	08 Eerste Zandlaag (1st Pleistocene Sand)	-13,50	-16,00
7	09 Allerod (Clayey Sand)	-16,00	-19,00
8	10 Tweede Zandlaag (2nd Pleistocene San	-19,00	-31,00

Figure B.1: Simplified soil stratigraphy in Plaxis 3D for the North of Amsterdam (pile load test).

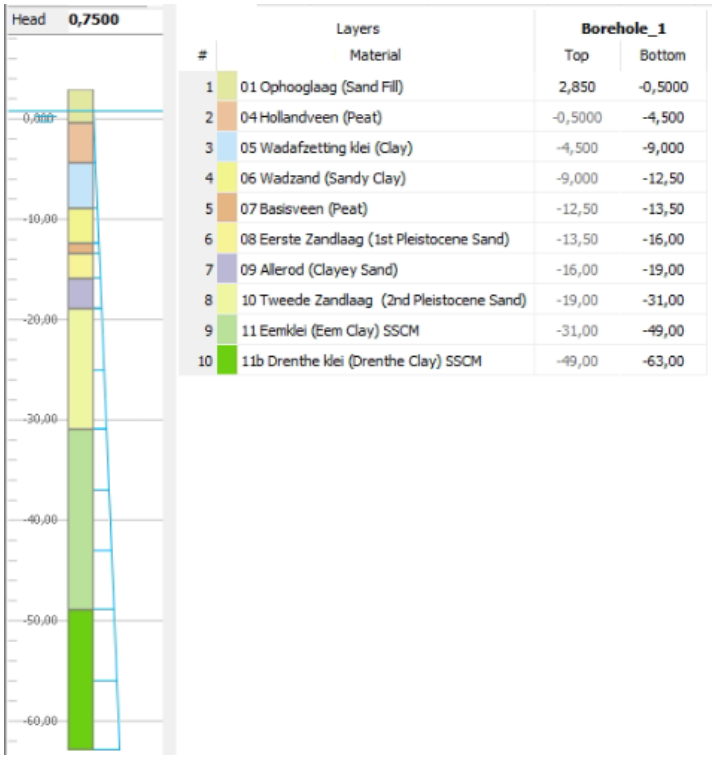

#	Layers: Material	Borehole_1: Top	Bottom
1	01 Ophooglaag (Sand Fill)	2,850	-0,5000
2	04 Hollandveen (Peat)	-0,5000	-4,500
3	05 Wadafzetting klei (Clay)	-4,500	-9,000
4	06 Wadzand (Sandy Clay)	-9,000	-12,50
5	07 Basisveen (Peat)	-12,50	-13,50
6	08 Eerste Zandlaag (1st Pleistocene Sand)	-13,50	-16,00
7	09 Allerod (Clayey Sand)	-16,00	-19,00
8	10 Tweede Zandlaag (2nd Pleistocene Sand)	-19,00	-31,00
9	11 Eemklei (Eem Clay) SSCM	-31,00	-49,00
10	11b Drenthe klei (Drenthe Clay) SSCM	-49,00	-63,00

Figure B.2: Simplified soil stratigraphy in Plaxis 3D for the North of Amsterdam (pile group model).

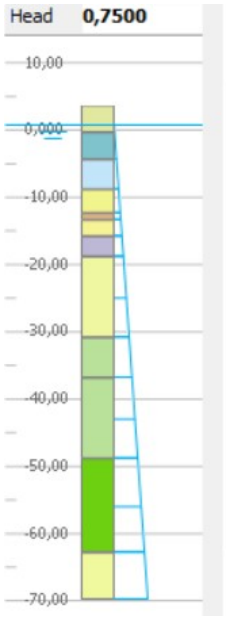

	Layers	Borehole_1	
#	Material	Top	Bottom
1	01 Ophooglaag	3,500	-0,5000
2	Geul klei met zand	-0,5000	-4,500
3	05 Wadafzetting klei	-4,500	-9,000
4	06 Wadzand	-9,000	-12,50
5	07 Basisveen	-12,50	-13,50
6	08 Eerste Zandlaag	-13,50	-16,00
7	09 Allerod	-16,00	-19,00
8	10 Tweede Zandlaag	-19,00	-31,00
9	11 Eemklei - var. 1d	-31,00	-37,00
10	11 Eemklei - var. 1d	-37,00	-49,00
11	11b Drenthe klei 1d	-49,00	-63,00
12	12 Derde zandlaag	-63,00	-70,00

Figure B.3: Detailed soil stratigraphy in Plaxis 3D for the North of Amsterdam (load spread variations).

The input parameters listed in Table B.1 can be changed in a sensitivity analysis to quantify the effects on the output of the soil model. The output of Plaxis 3D for settlement analysis is normally one (symmetric building) or two (asymmetric building) displacement (u_z) curves taken from a line cross-section at 4D below PTL over the length of the FEM domain.

Table B.1: List of input parameters for commonly used constitutive models in Plaxis 3D.

Constitutive Model	**Input Parameters**
Soft Soil (SSM)	λ^*, κ^*, ν_{ur}, c', ϕ', ψ, K_0^{NC}, e_0, OCR, k_x, k_y, k_z
Soft Soil Creep (SSCM)	λ^*, κ^*, μ^*, ν_{ur}, c', ϕ', ψ, K_0^{NC}, e_0, OCR, k_x, k_y, k_z
Hardening Soil (HS)	E_{50}^{ref}, E_{oed}^{ref}, E_{ur}^{ref}, m, p^{ref}, ν_{ur}, c', ϕ', ψ, R_f, K_0^{NC}, e_0, OCR, k_x, k_y, k_z
HS Small (HSS)	E_{50}^{ref}, E_{oed}^{ref}, E_{ur}^{ref}, G_0^{ref}, $\gamma_{0.7}$, m, p^{ref}, ν_{ur}, c', ϕ', ψ, R_f, K_0^{NC}, e_0, OCR, k_x, k_y, k_z

Table B.2: Constitutive model parameters of LE material for soil layers in Plaxis based on the modified *Noord-zuidlijn* subway database (load spread variations).

Identification		01 Ophooglaag LE	Geulvulling, veen met klei LE	Geul klei met zand LE	04 Hollandveen LE	05 Wadafzetting klei LE	Aanvullen zand LE
Identification number		2	14	15	16	17	18
Material model		Linear elastic	Linear elastic	Linear elastic	Linear elastic	Linear elastic	Linear elastic
Drainage type		Drained	Drained	Drained	Drained	Drained	Drained
γ_unsat	kN/m³	17	12,1	16,9	10,5	15,2	18
γ_sat	kN/m³	18,4	12,1	16,9	10,5	15,2	20
Rayleigh α		0	0	0	0	0	0
Rayleigh β		0	0	0	0	0	0
E	kN/m²	41670	7500	20830	8333	12500	20830
E_inc	kN/m²/m	0	0	0	0	0	0

Table B.3: Constitutive model parameters of HSS material for soil layers in Plaxis based on the modified *Noord-zuidlijn* subway database (pile load test & pile group model & load spread method).

Identification		01 Ophooglaag (Sand Fill)	04 Hollandveen (Peat)	05 Wadafzetting klei (Clay)	06 Wadzand (Sandy Clay)	07 Basisveen (Peat)	08 Eerste Zandlaag (1st Pleistocene Sand)	09 Allerod (Clayey Sand)	10 Tweede Zandlaag (2nd Pleistocene Sand)
Identification number		2	3	4	5	6	7	8	9
Material model		HS small	HS small	HS small	HS small	HS small	HS small	HS small	HS small
Drainage type		Drained	Drained	Drained	Drained	Drained	Drained	Drained	Drained
γ_unsat	kN/m^3	17	10,5	15,2	17,9	11,7	19,8	18,5	19
γ_sat	kN/m^3	18,4	10,5	15,2	17,9	11,7	19,8	18,5	19
e_init		0,5	0,5	0,5	0,5	0,5	0,5	0,5	0,5
E_50^ref	kN/m^2	17000	2000	7500	10000	2000	35000	15000	85700
E_oed^ref	kN/m^2	15000	1023	3665	5627	1023	20000	9140	85700
E_ur^ref	kN/m^2	50000	10000	15000	25000	7000	100000	30000	257100
power (m)		0,5	0,8	0,9	0,5	0,8	0,5	0,5	0,5
C_c		0,023	0,3372	0,09413	0,06131	0,3372	0,01725	0,03775	0,004026
C_s		0,00621	0,03105	0,0207	0,01242	0,04436	0,003105	0,01035	0,001208
c_ref	kN/m^2	1	3	3	2	2	0	0	0
φ (phi)	°	30	18	27	27	18	33	28	33
ψ (psi)	°	0	0	0	0	0	3	0	3
γ_0.7		0,00016	0,00037	0,00036	0,00025	0,00037	0,00013	0,00023	0,000064
G_0^ref	kN/m^2	80120	28900	41520	54200	28900	122600	59900	231000
ν_ur		0,2	0,2	0,2	0,2	0,2	0,2	0,2	0,2
K_0^nc		0,5	0,691	0,546	0,546	0,691	0,4554	0,5305	0,4554
R_f		0,9	0,9	0,9	0,9	0,9	0,9	0,9	0,9
Stiffness		Standard	Standard	Standard	Standard	Standard	Standard	Standard	Standard
Strength		Manual	Manual	Manual	Manual	Manual	Rigid	Rigid	Rigid
R_inter		0,67	0,5	0,5	0,5	0,5	1	1	1
K_0 determination		Automatic	Automatic	Automatic	Automatic	Automatic	Automatic	Automatic	Automatic
OCR		1	1	1	1	1	1	1	1
k_x	m/day	1	1	1	1	1	5	5	5
k_y	m/day	1	1	1	1	1	5	5	5
k_z	m/day	1	1	1	1	1	5	5	5
c_k		1E+15	1E+15	1E+15	1E+15	1E+15	1E+15	1E+15	1E+15

Table B.4: Constitutive model parameters of HSS material for soil layers in Plaxis based on the modified *Noord-zuidlijn* subway database (load spread variations).

Identification		01 Ophooglaag	04 Hollandveen	05 Wadafzetting klei	06 Wadzand	07 Basisveen	08 Eerste Zandlaag	09 Allerod	10 Tweede Zandlaag	12 Derde zandlaag	Geul klei met zand	Geulvulling, veen met klei	11 Eemklei HSS	11b Drenthe klei HSS
Identification number		1	3	4	5	6	7	8	9	11	12	13	20	21
Material model		HS small	HS small	HS small	HS small	HS small	HS small	HS small	HS small	HS small	HS small	HS small	HS small	HS small
Drainage type		Drained	Drained	Drained	Drained	Drained	Drained	Drained	Drained	Drained	Drained	Drained	Drained	Drained
γ_unsat	kN/m^3	17	10,5	15,2	17,9	11,7	19,8	18,5	19	19	16,9	12,1	17,1	18,5
γ_sat	kN/m^3	18,4	10,5	15,2	17,9	11,7	19,8	18,5	19	21	16,9	12,1	17,1	18,5
Rayleigh α		0	0	0	0	0	0	0	0	0	0	0	0	0
Rayleigh β		0	0	0	0	0	0	0	0	0	0	0	0	0
E_50^ref	kN/m^2	17000	2000	7500	10000	2000	35000	15000	85700	100000	10000	2000	8000	12000
E_oed^ref	kN/m^2	15000	1023	3665	5627	1023	20000	9140	85700	100000	4547	1071	3289	4402
C_s		0,00621	0,03105	0,0207	0,01242	0,04436	0,003105	0,01035	0,001208	0,001035	0,01242	0,0621	0,01035	0,00621
e_init		0,5	0,5	0,5	0,5	0,5	0,5	0,5	0,5	0,5	0,5	0,5	0,5	0,5
c_ref	kN/m^2	1	3	3	2	2	0	0	0	0	5	5	5	0
φ (phi)	°	30	18	27	27	18	33	28	33	33	26	20	28	32,5
ψ (psi)	°	0	0	0	0	0	3	0	3	3	0	0	0	0
G_0^ref	kN/m^2	80120	28880	41520	54190	28880	122600	59870	231000	300000	49000	37200	61840	83470
R_f		0,9	0,9	0,9	0,9	0,9	0,9	0,9	0,9	0,9	0,9	0,9	0,9	0,9
Stiffness		Standard	Standard	Standard	Standard	Standard	Standard	Standard	Standard	Standard	Standard	Standard	Standard	Standard
K_0,x		0,5	0,691	0,546	0,546	0,691	0,4554	0,5305	0,4554	0,4554	0,5616	0,658	0,7914	0,6222
K_0,y		0,5	0,691	0,546	0,546	0,691	0,4554	0,5305	0,4554	0,4554	0,5616	0,658	0,7914	0,6222

Table B.5: Constitutive model parameters of SSCM material for Eem clay layers in Plaxis based on oedometer test results (soil test).

Identification		Sample 1 *North #1* (SSC)	Sample 2 *North #2* (SSC)	Sample 3 *North #3* (SSC)	Sample 4 *North #4* (SSC)
Identification number		14	15	16	17
Material model		Soft soil creep	Soft soil creep	Soft soil creep	Soft soil creep
Drainage type		Drained	Drained	Drained	Drained
γ_unsat	kN/m^3	16,16	16,71	18,44	16,9
γ_sat	kN/m^3	16,16	16,71	18,44	16,9
e_init		1,36	1,39	0,91	1,14
λ* (lambda*)		0,1069	0,1412	0,05463	0,09021
κ* (kappa*)		0,02911	0,04584	0,01593	0,02479
μ*		0,002008	0,002892	0,00148	0,001808
Use alternatives		No	No	No	No
C_c		0,58	0,776	0,24	0,444
C_s		0,079	0,126	0,035	0,061
C_α		0,0109	0,0159	0,0065	0,0089
c_ref	kN/m^2	5	5	5	5
φ (phi)	°	28	28	28	28
ψ (psi)	°	0	0	0	0
Set to default values		Yes	Yes	Yes	Yes
ν_ur		0,15	0,15	0,15	0,15
K_0^nc		0,5305	0,5305	0,5305	0,5305
M		1,459	1,429	1,448	1,457
Skempton-B		0,989	0,989	0,989	0,989
Tensile strength	kN/m^2	0	0	0	0
Stiffness		Standard	Standard	Standard	Standard
R_inter		0,67	0,67	1	1
Consider gap closure		Yes	Yes	Yes	Yes
Drainage conductivity_2, dk	$m^3/day/m$	0	0	0	0
K_0 determination		Automatic	Automatic	Automatic	Automatic
K_0,x = K_0,y		Yes	Yes	Yes	Yes
K_0,x		1,104	0,9094	0,9802	1,171
OCR		2,62	2,07	2,27	2,81
POP	kN/m^2	0	0	0	0
k_x	m/day	0,0001	0,0001	0,0001	0,0001
k_y	m/day	0,0001	0,0001	0,0001	0,0001
k_z	m/day	0,0001	0,0001	0,0001	0,0001
c_k		1E+15	1E+15	1E+15	1E+15

Table B.6: Constitutive model parameters of SSCM material for soil layers in Plaxis based on the modified *Noord-zuidlijn* subway database (pile group model & load spread method).

Identification		11 Eemklei (Eem Clay) SSC	11b Drenthe klei (Drenthe Clay) SSC
Identification number		11	12
Material model		Soft soil creep	Soft soil creep
Drainage type		Drained	Drained
γ_unsat	kN/m^3	17,1	18,5
γ_sat	kN/m^3	17,55	19,4
e_init		0,5	0,5
λ* (lambda*)		0,0911	0,0619
κ* (kappa*)		0,0252	0,0292
μ*		0,0023	0,0013
Use alternatives		No	No
C_c		0,3143	0,2136
C_s		0,04347	0,05037
C_α		0,007935	0,004485
c_ref	kN/m^2	5	0
φ (phi)	°	28	32,5
ψ (psi)	°	0	0
Set to default values		Yes	Yes
ν_ur		0,15	0,15
K_0^nc		0,5305	0,4627
M		1,456	1,547
Skempton-B		0,989	0,989
Tensile strength	kN/m^2	0	0
Stiffness		Standard	Standard
R_inter		1	1
Consider gap closure		Yes	Yes
Drainage conductivity_2, dk	$m^3/day/m$	0	0
K_0 determination		Automatic	Automatic
K_0,x = K_0,y		Yes	Yes
K_0,x		0,9943	1,218
OCR		2,31	3,64
POP	kN/m^2	0	0
k_x	m/day	0,00004	0,00004
k_y	m/day	0,00004	0,00004
k_z	m/day	0,00004	0,00004
c_k		1E+15	1E+15

Table B.7: Constitutive model of embedded beam for a ≈ 26 m Fundex 460/560 pile (type 1, NEN pile factors) in Plaxis 3D. **Note:** E is modified for an equivalent EA of $d_{eq} = 460$ mm to better predict s_{el}.

Identification		Fundex460 /560 (NEN)
Identification number		1
Material type		Elastic
E	kN/m²	1,30E+07
γ	kN/m³	5
Beam type		Predefined
Predefined beam type		Massive circular beam
Diameter	m	0,56
A	m²	0,2463
I_2	m⁴	4,827E-3
I_3	m⁴	4,827E-3
Axial skin resistance		Multi-linear
Multi-linear axial resistance		Axial skin resistance table
F_max	kN	2751

#	Distance [m]	Axial skin resistance [kN/m]
1	0,000	0,000
2	16,35	0,000
3	25,85	288,2

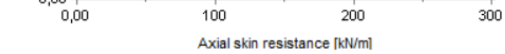

Table B.8: Constitutive model of embedded beam for a ≈ 26 m Fundex 460/560 pile (type 2, Maasvlakte pile factors) in Plaxis 3D. **Note:** E is modified for an equivalent EA of $d_{eq} = 460$ mm to better predict s_{el}.

Identification		Fundex460/ 560 (MV2)
Identification number		2
Material type		Elastic
E	kN/m²	1,30E+07
γ	kN/m³	5
Beam type		Predefined
Predefined beam type		Massive circular beam
Diameter	m	0,56
A	m²	0,2463
I_2	m⁴	4,827E-3
I_3	m⁴	4,827E-3
Axial skin resistance		Multi-linear
Multi-linear axial resistance		Axial skin resistance table
F_max	kN	1528

#	Distance [m]	Axial skin resistance [kN/m]
1	0,000	0,000
2	16,35	0,000
3	25,85	540,8

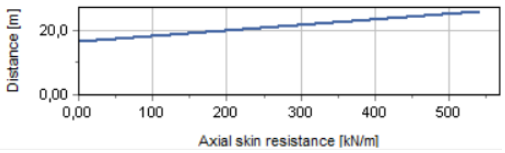

Table B.9: Constitutive model of 1m thick elastic and stiff plates for building stiffness lower and upper limits using s_2 load spread method & variations in Plaxis 3D.

Identification		Plate (flexible)	Plate (stiff)
Identification number		1	2
Comments			
Material type		Elastic	Elastic
γ	kN/m³	0	0
Isotropic		Yes	Yes
E_1	kN/m²	1	1E+09
E_2	kN/m²	1	1E+09
ν_12		0	0
G_12	kN/m²	0,5	5E+08

Table B.10: Material input of 2D concrete, structural plate elements in Plaxis 3D (based on SCIA). **Note:** $\gamma = 0$ with a (surface) load equal to the dead load resulted in a better match with SCIA.

Element	**Material Type**	**Thickness, d (m)**	**Weight, γ (kN/m^3)**	**Stiffness, E_1 (kN/m^2)**
Wall (2D)	Elastic	0.25	25.0	20.0 E^6
Floor (2D)	Elastic	0.25	25.0	1.0 E^6
Foundation Plate (2D)	Elastic	2.0	25.0	15.0 E^6

Table B.11: Material input of 1D concrete, structural (anchor) elements in Plaxis 3D (based on SCIA). **Note:** $\gamma = 0$ with a (surface) load equal to the dead load resulted in a better match with SCIA.

Element	**Material Type**	**Dimensions, (m)**	**Stiffness, E (kN/m^2)**	**Stiffness, EA (kN)**
Lintel (1D)	Elastic	0.3 x 0.53	10.0 E^6	1.6 E^6
Column (1D)	Elastic	0.6	30.0 E^6	8.5 E^6
Foundation Pile (1D)	Elastic	See Table B.7	See Table B.7	See Table B.7

Table B.12: Numerical control parameters in Plaxis 3D (pile load test & pile group).

Numerical Control Parameters	**Value**
Solver type	Picos (multicore iterative)
Max. cores to use	1
Max. number of steps stored	1
Use compression for result files	*Unchecked*
Use default iter parameters	*Unchecked*
Max. steps	1000
Tolerated error	0.02
Max. unloading steps	5
Max. load fraction per step	0.5
Over-relaxation factor	1.2
Max. number of iterations	80
Desired min. number of iterations	20
Desired max. number of iterations	60
Arc-length control type	*On*
Use subspace accelerator	*Unchecked*
Use line search	*Unchecked*
Use gradual error reduction	*Unchecked*

Table B.13: Mesh information for 10-noded tetrahedral elements in Plaxis 3D (pile load test).

Plaxis Element	**Mesh Coarseness**
General element distribution	Medium
Global scale factor	1.2
Min. element size factor	5E-3
Embedded beam (line) element & point (load)	0.5
Polygon surface (top of pile)	0.5
Soil volume 1 (9 m x 9 m x 25.85 m around pile)	0.25
Soil volume 2 (40 m x 40 m x 33.85 m general)	1.0

Table B.14: Example of construction phases in Plaxis 3D (pile load test).

ID	**Phase**	**Point Load (kN)**	**Start from**	**Type**	**Loading**	**Pore Pressure**	**Reset $\|u\|$ & $\|\epsilon\|$**
Initial	1	NA	NA	K0	Staged	Phreatic	Ignore suction
Add pile	2	NA	Initial	Plastic	Staged	Phreatic	*Unchecked*
Add load	3	50	Add pile	Plastic	Staged	Phreatic	*Checked*
Add load	4	150	Add pile	Plastic	Staged	Phreatic	*Checked*
Add load	5	250	Add pile	Plastic	Staged	Phreatic	*Checked*
Add load	6	500	Add pile	Plastic	Staged	Phreatic	*Checked*
Add load	7	750	Add pile	Plastic	Staged	Phreatic	*Checked*
Add load	8	1250	Add pile	Plastic	Staged	Phreatic	*Checked*
Add load	9	1500	Add pile	Plastic	Staged	Phreatic	*Checked*
Add load	10	1750	Add pile	Plastic	Staged	Phreatic	*Checked*
Add load	11	2000	Add pile	Plastic	Staged	Phreatic	*Checked*
Add load	12	2250	Add pile	Plastic	Staged	Phreatic	*Checked*
Add load	13	2500	Add pile	Plastic	Staged	Phreatic	*Checked*
Add load	14	2750	Add pile	Plastic	Staged	Phreatic	*Checked*
Add load	15	3000	Add pile	Plastic	Staged	Phreatic	*Checked*
Add load	16	3250	Add pile	Plastic	Staged	Phreatic	*Checked*
Add load	17	3500	Add pile	Plastic	Staged	Phreatic	*Checked*
Add load	18	3750	Add pile	Plastic	Staged	Phreatic	*Checked*
Add load	19	4000	Add pile	Plastic	Staged	Phreatic	*Checked*
Add load	20	4250	Add pile	Plastic	Staged	Phreatic	*Checked*
Max. load	21	*Total bearing capacity*	Add pile	Plastic	Staged	Phreatic	*Checked*
SLS load	22	1302	Add pile	Plastic	Staged	Phreatic	*Checked*
ULS load	23	1805	Add pile	Plastic	Staged	Phreatic	*Checked*

B.2 Outputs

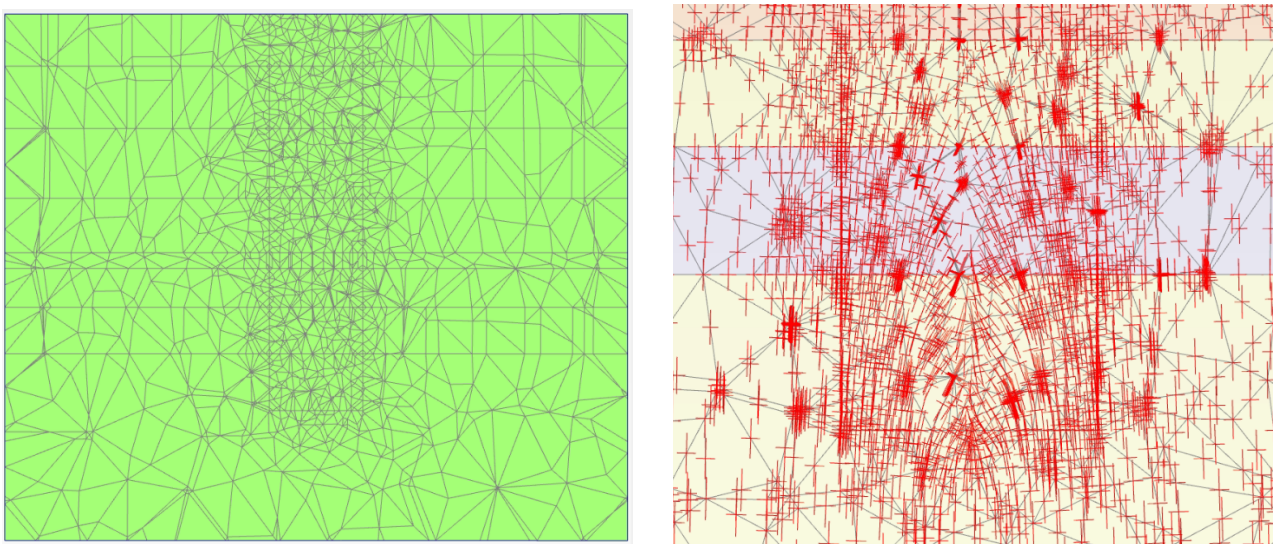

(a) Excess pore pressures.

(b) Principal effective stresses.

Figure B.4: Vertical changes of 1 pile under SLS load (= 1,302 kN) calculated for entire depth (= NAP + 2.85 m − NAP - 31 m) by Plaxis 3D for a) excess pore pressures (p_{excess}), and b) principal stress rotations (within D_{pos}).

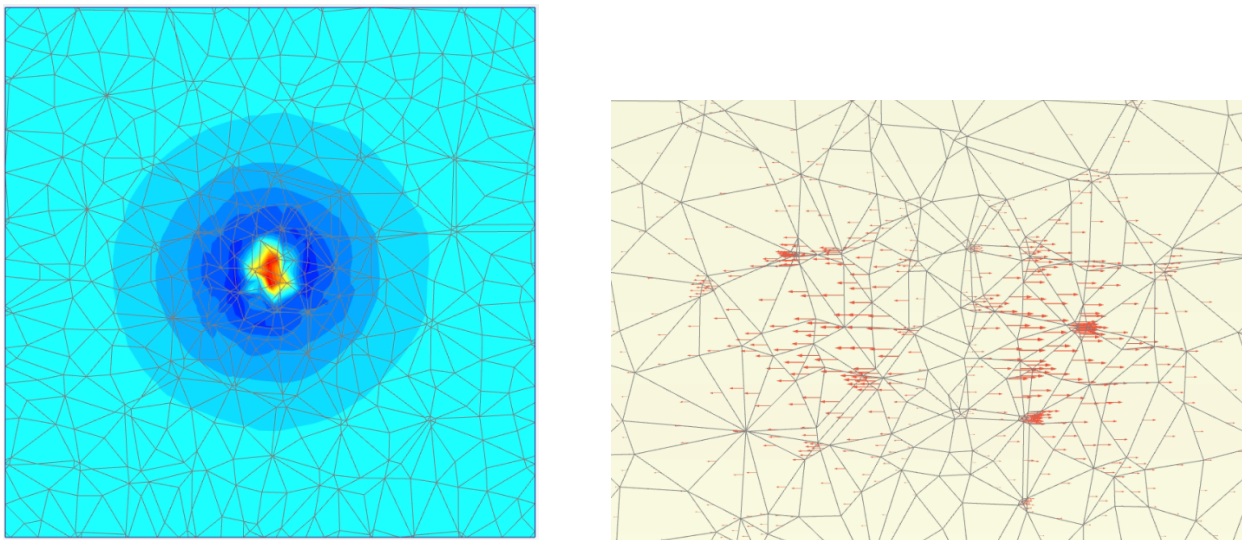

(a) Incremental strains.

(b) Horizontal displacements.

Figure B.5: Horizontal changes of 1 pile under SLS load (= 1,302 kN) calculated at 4D below pile tip level (= NAP - 25.24 m) by Plaxis 3D for a) incremental strains (ϵ_v), and b) horizontal displacements (u_x) within 6 m of pile.

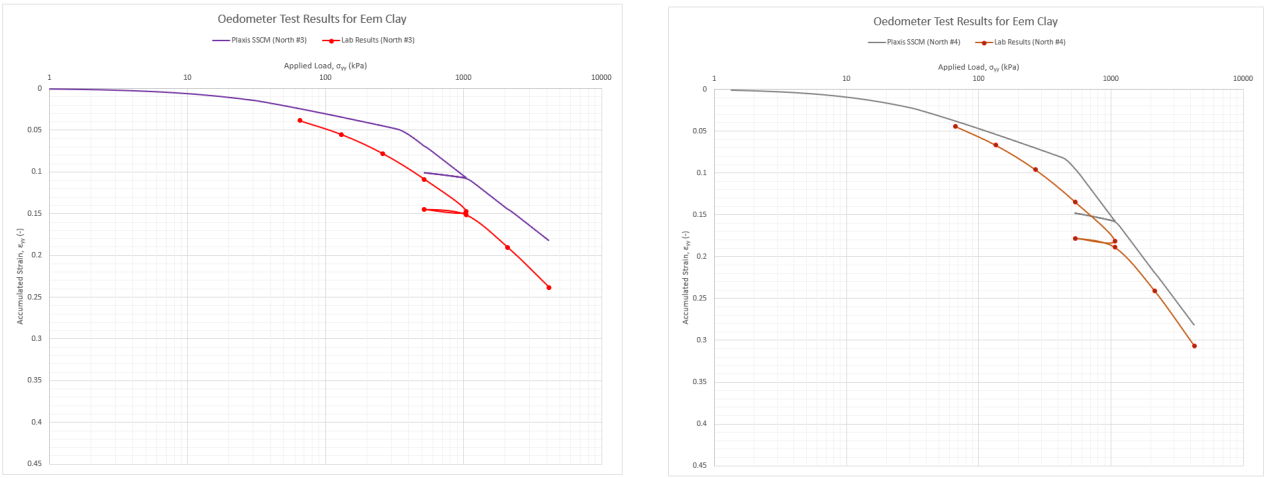

(a) Sample #3. (b) Sample #4.

Figure B.6: Results of oedometer test for Eem clay between the lab data and a Plaxis FEM soil test as SSCM for a) sample #3, and b) sample #4 taken from northern Amsterdam.

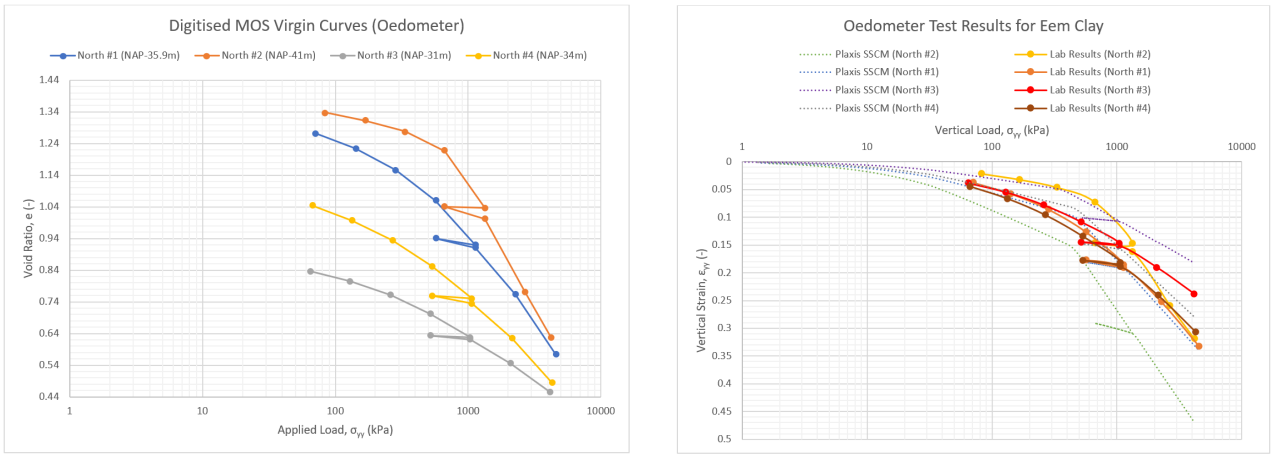

(a) Laboratory. (b) Lab & Plaxis.

Figure B.7: Combined results of oedometer test for four different Eem clay samples in northern Amsterdam a) from the laboratory, and b) between the lab data and a Plaxis FEM soil test as SSCM.

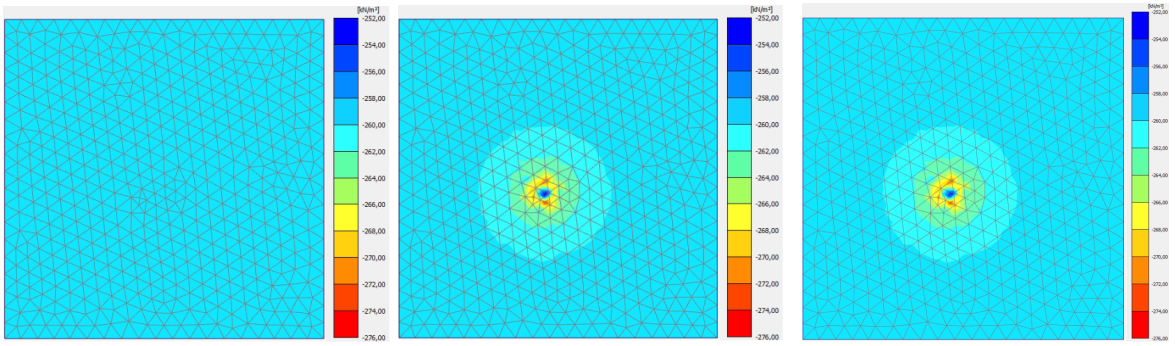

(a) Initial. (b) Consolidation (NEN). (c) Consolidation (MV2).

Figure B.8: Cartesian effective stresses (σ'_{zz}) calculated at top of Eem clay (= NAP - 31 m) by Plaxis 3D under SLS point loads (= 1,302 kN) applied at **16 pile heads (as EB-I) at 2 m (= 3.5 · D) spacing** for a) initial K_0 conditions, b) after 50 years of consolidation with NEN factors, and c) with Maasvlakte pile factors.

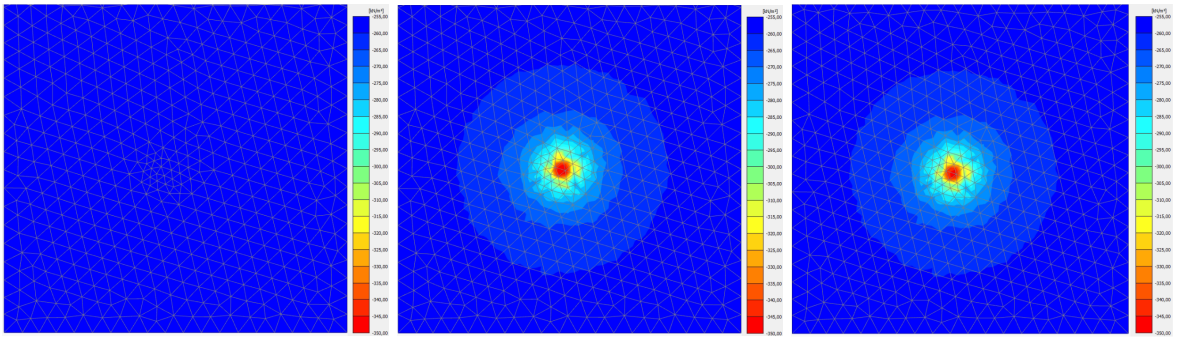

(a) Initial. (b) Consolidation (NEN). (c) Consolidation (MV2).

Figure B.9: Cartesian effective stresses (σ'_{zz}) calculated at top of Eem clay (= NAP - 31 m) by Plaxis 3D under SLS point loads (= 1,302 kN) applied at **81 pile heads (as EB-I) at 2 m (= $3.5 \cdot D$) spacing** for a) initial K_0 conditions, b) after 50 years of consolidation with NEN factors, and c) with Maasvlakte pile factors.

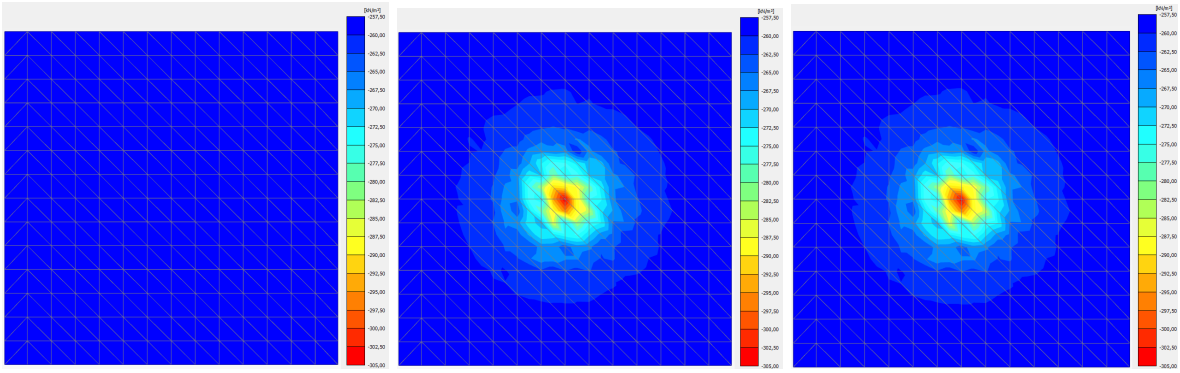

(a) Initial. (b) Consolidation (NEN). (c) Consolidation (MV2).

Figure B.10: Cartesian effective stresses (σ'_{zz}) calculated at top of Eem clay (= NAP - 31 m) by Plaxis 3D (swept meshing) under SLS point loads (= 1,302 kN) applied at **81 pile heads (as EB-I) at 3 m (= $5 \cdot D$) spacing** for a) initial K_0 conditions, b) after 50 years of consolidation with NEN factors, and c) with Maasvlakte pile factors.

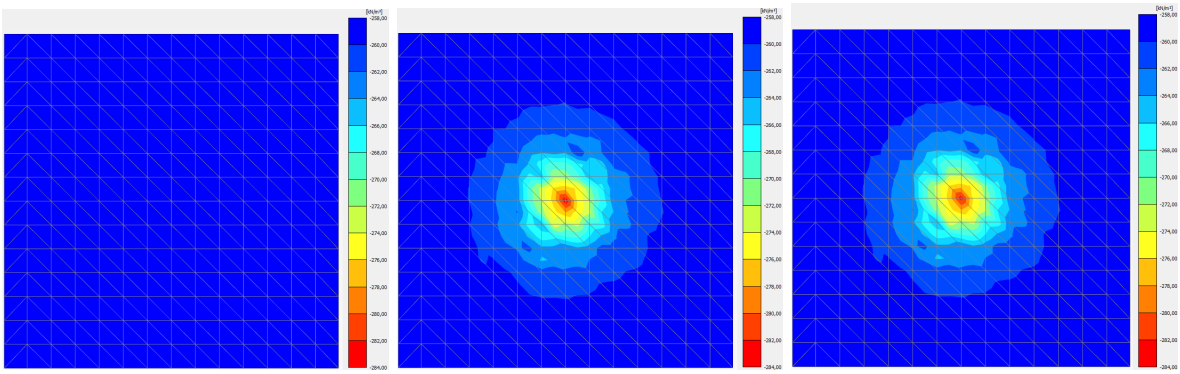

(a) Initial. (b) Consolidation (NEN). (c) Consolidation (MV2).

Figure B.11: Cartesian effective stresses (σ'_{zz}) calculated at top of Eem clay (= NAP - 31 m) by Plaxis 3D (swept meshing) under SLS point loads (= 1,302 kN) applied at **49 pile heads (as EB-I) at 4 m (= $7 \cdot D$) spacing** for a) initial K_0 conditions, b) after 50 years of consolidation with NEN factors, and c) with Maasvlakte pile factors.

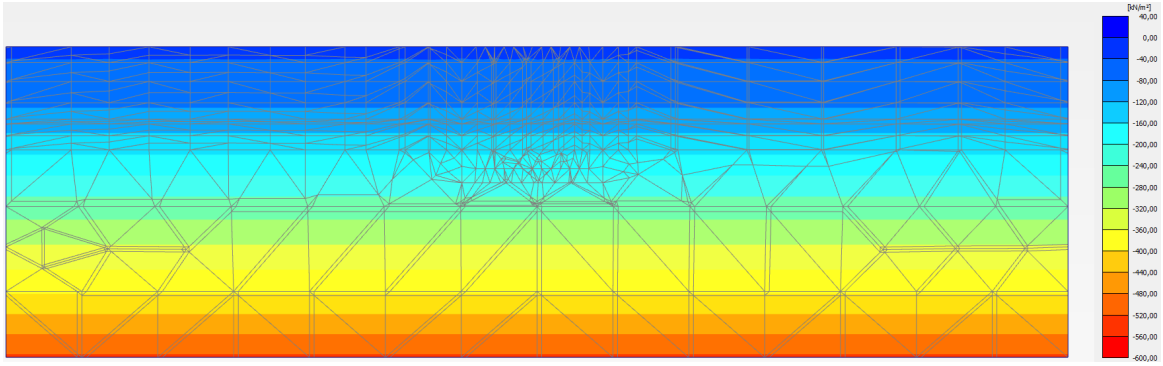

(a) Initial.

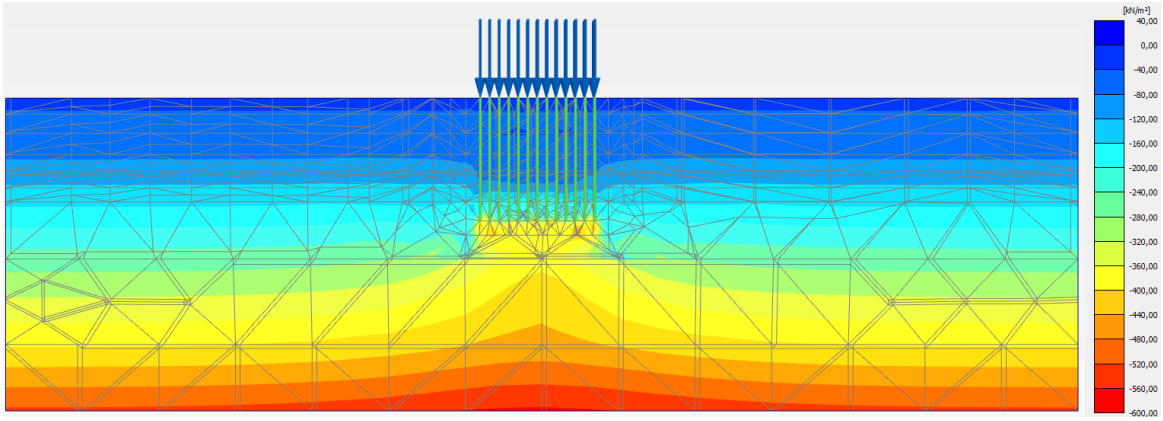

(b) Consolidation (NEN).

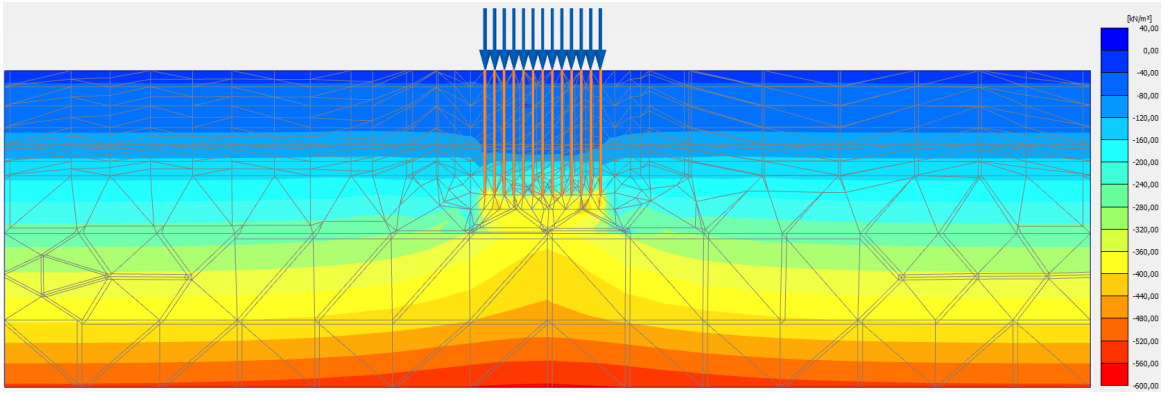

(c) Consolidation (MV2).

Figure B.12: Cartesian effective stresses (σ'_{zz}) calculated for entire depth (= NAP + 2.85 m − NAP - 63 m) by Plaxis 3D (swept meshing) under SLS point loads (= 1,302 kN) applied at **169 pile heads (as EB-I) at 2 m (**$= 3.5 \cdot D$**) spacing** for a) initial K_0 conditions, b) after 50 years of consolidation with NEN factors, and c) Maasvlakte factors.

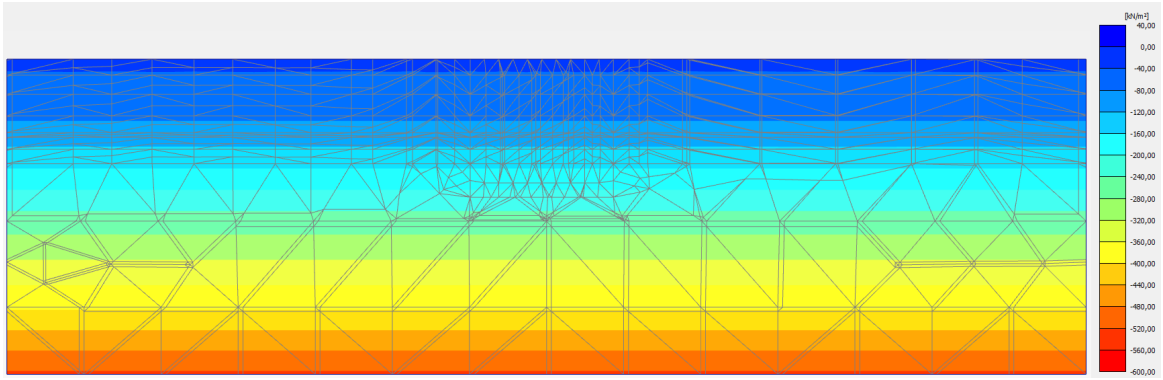

(a) Initial.

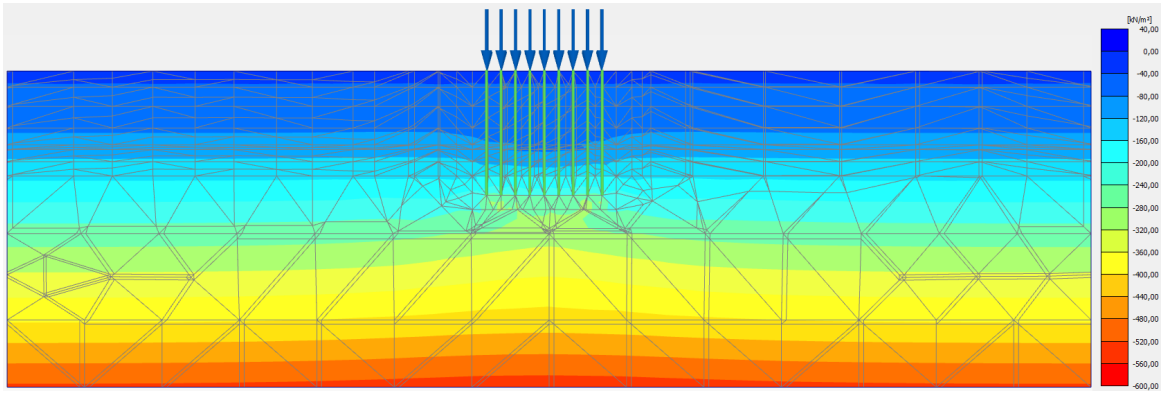

(b) Consolidation (NEN).

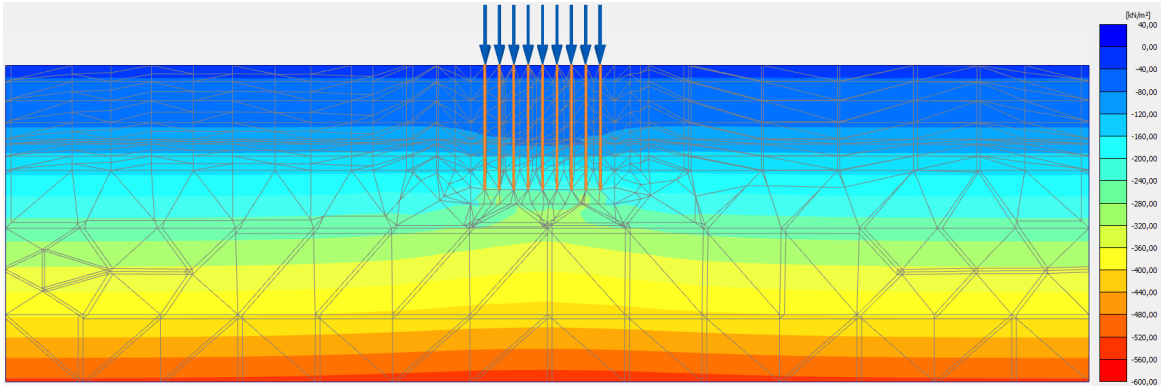

(c) Consolidation (MV2).

Figure B.13: Cartesian effective stresses (σ'_{zz}) calculated for entire depth (= NAP + 2.85 m − NAP - 63 m) by Plaxis 3D under **SLS** point loads (= 1,302 kN) applied at **81 pile heads (as EB-I) at 3 m (**$= 5 \cdot D$**) spacing** for a) initial K_0 conditions, b) after 50 years of consolidation with NEN factors, and c) Maasvlakte factors.

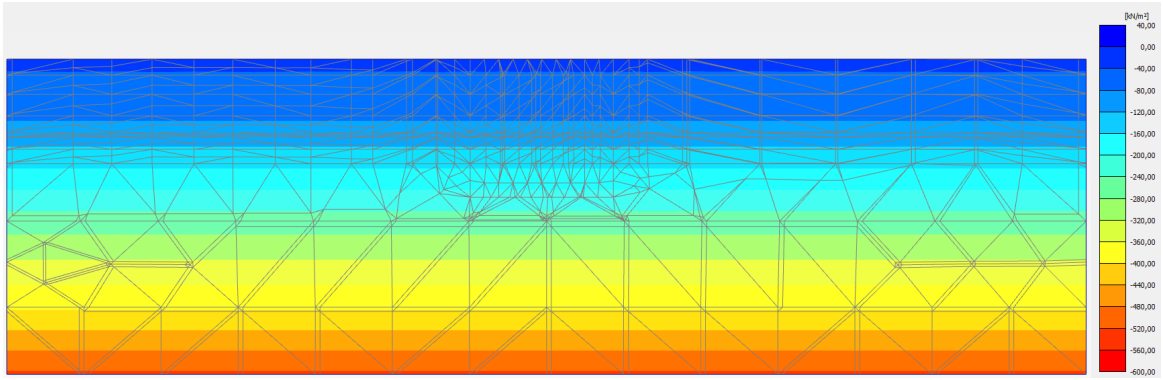

(a) Initial.

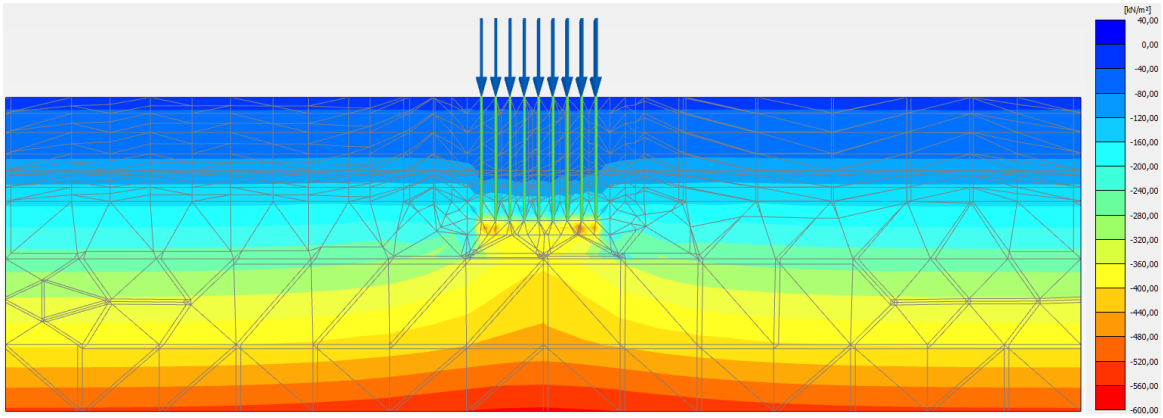

(b) Consolidation (NEN).

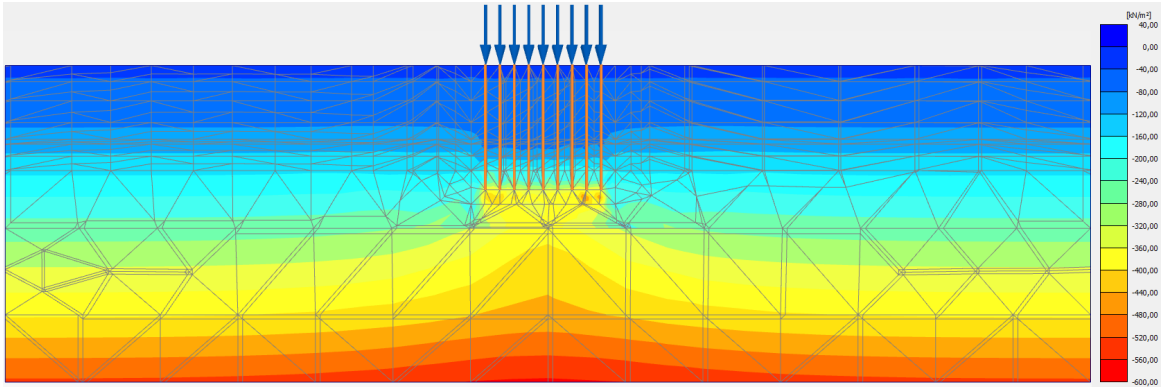

(c) Consolidation (MV2).

Figure B.14: Cartesian effective stresses (σ'_{zz}) calculated for entire depth (= NAP + 2.85 m − NAP - 63 m) by Plaxis 3D under ≈ 70% pile capacity (= **ULS**) point loads (= 2,717 kN) applied at **81 pile heads (as EB-I) at 3 m (**$= 5 \cdot D$**) spacing** for a) initial K_0 conditions, b) after 50 years of consolidation with NEN factors, and c) Maasvlakte factors.

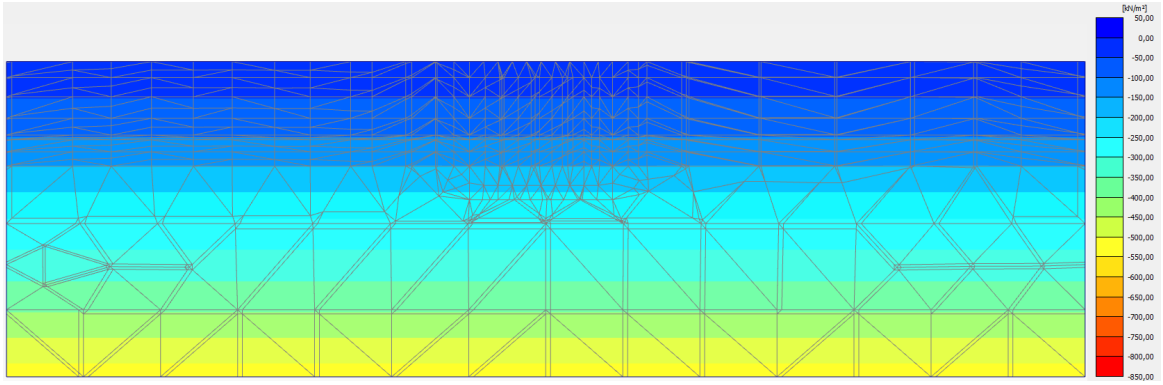

(a) Initial.

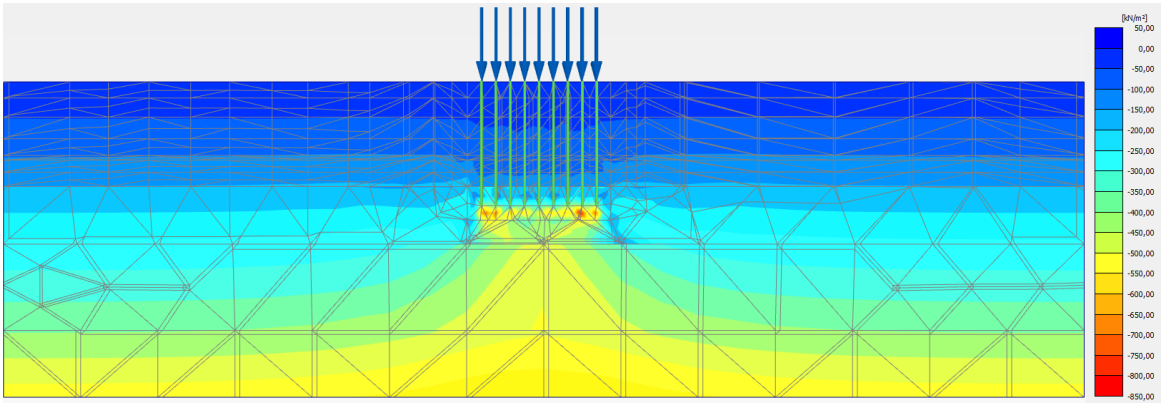

(b) Consolidation (NEN).

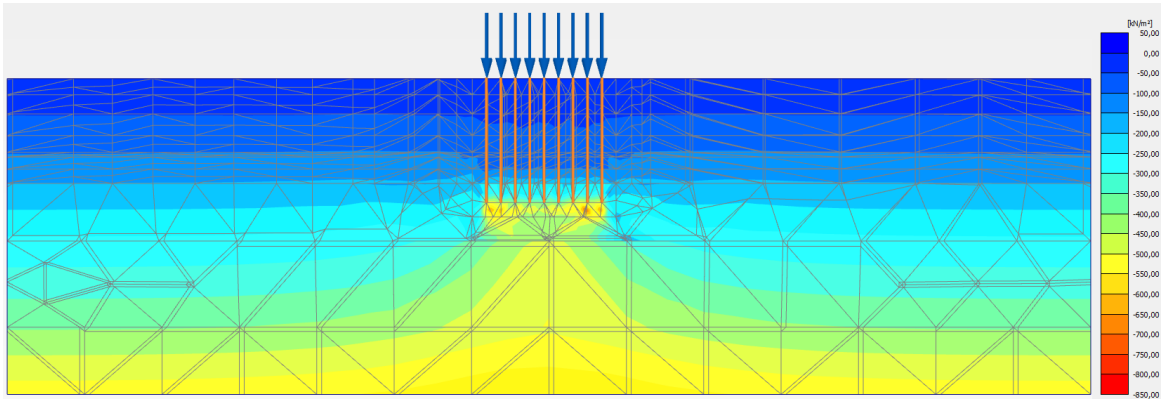

(c) Consolidation (MV2).

Figure B.15: Cartesian effective stresses (σ'_{zz}) calculated for entire depth (= NAP + 2.85 m − NAP - 63 m) by Plaxis 3D under ≈ **100% pile capacity** (= R_{total}) point loads applied at **81 pile heads (as EB-I) at 3 m** (= $5 \cdot D$) **spacing** for a) initial K_0 conditions, b) after 50 years of consolidation with NEN factors (R_{total} = 4,119 kN), and c) Maasvlakte factors (R_{total} = 4,098).

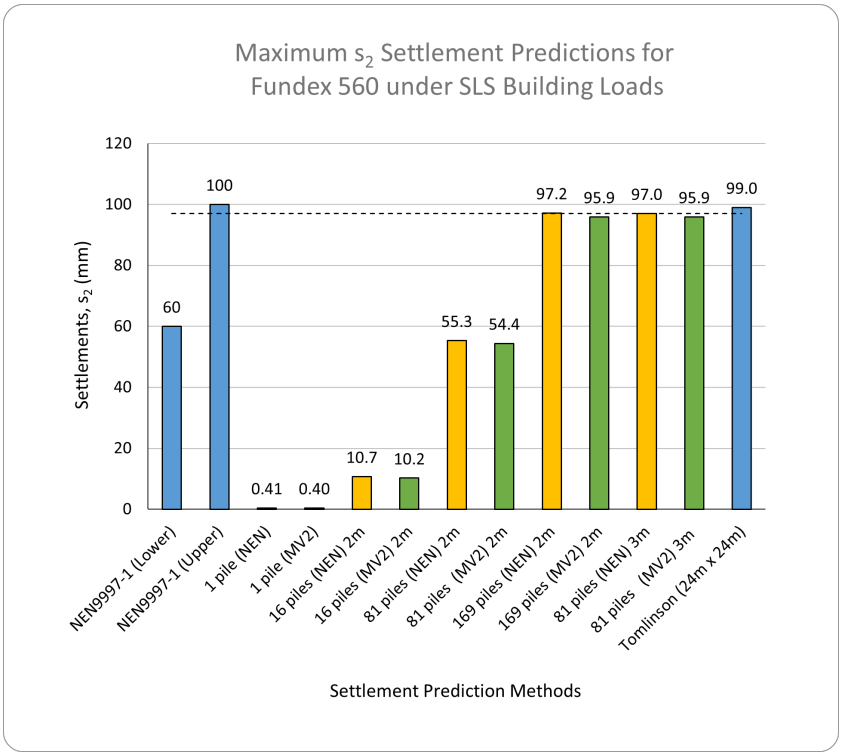

Figure B.16: Predicted s_2 settlements for a Fundex 560 as type 1 (NEN) and type 2 (MV2) pile based on different pile group configurations by hand and by Plaxis 3D under equivalent SLS building loads.

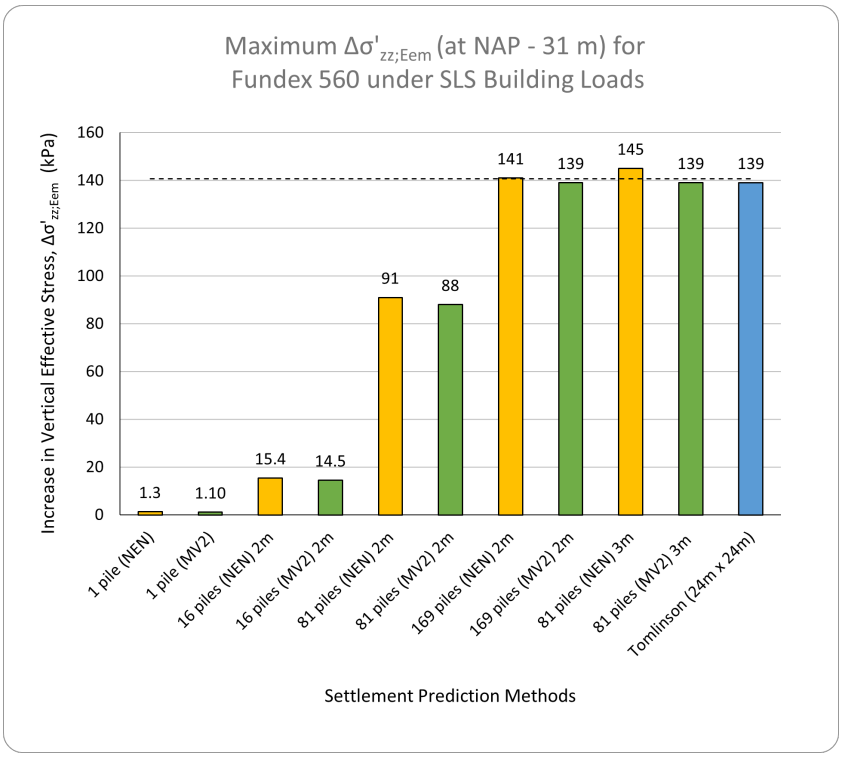

Figure B.17: Computed change in vertical effective stress at top of Eem clay due to SLS building loads and 50 years of consolidation for a Fundex 560 as type 1 (NEN) and type 2 (MV2) pile based on different pile group configurations in Plaxis 3D.

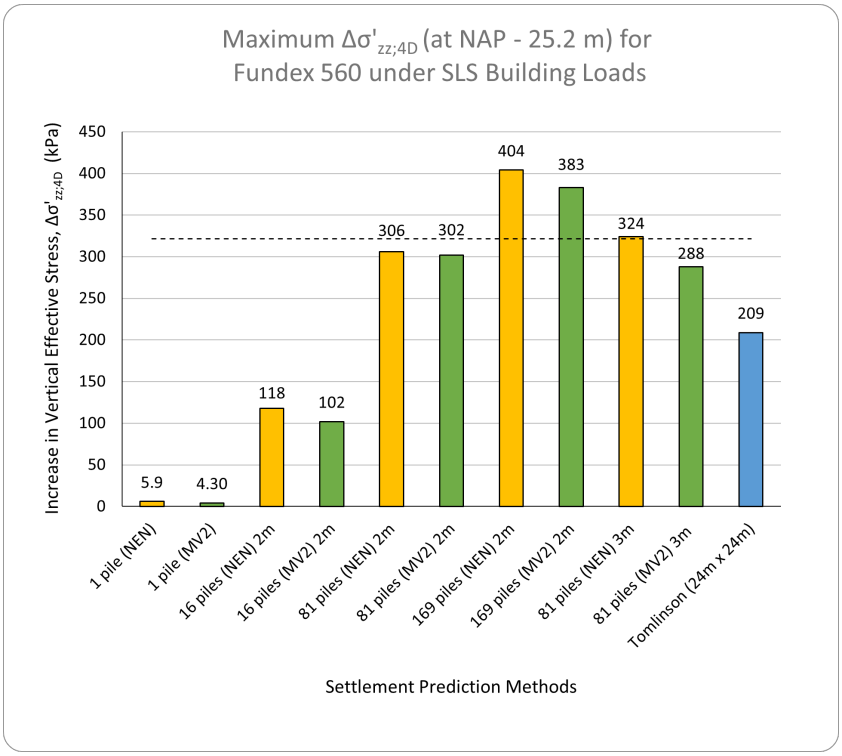

Figure B.18: Computed change in vertical effective stress 4D below PTL due to SLS building loads and 50 years of consolidation for a Fundex 560 as type 1 (NEN) and type 2 (MV2) pile based on different pile group configurations in Plaxis 3D.

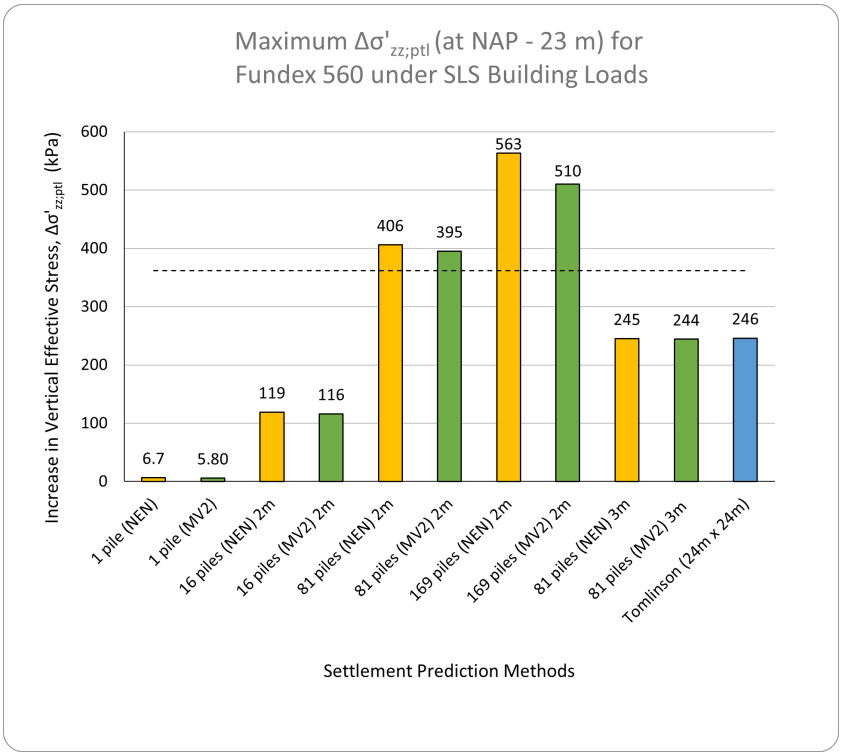

Figure B.19: Computed change in vertical effective stress at PTL due to SLS building loads and 50 years of consolidation for a Fundex 560 as type 1 (NEN) and type 2 (MV2) pile based on different pile group configurations in Plaxis 3D.

B.2.1 Additional Model Scenarios

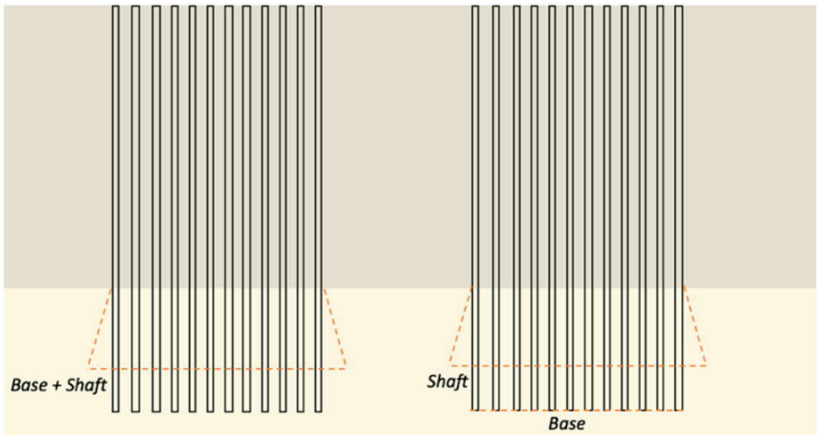

Figure B.20: Visualisation of Tomlinson's equivalent raft approach (left) as case 4a3 and an updated version used by CRUX (right) as case 4a4 in this thesis (Frissen, 2020).

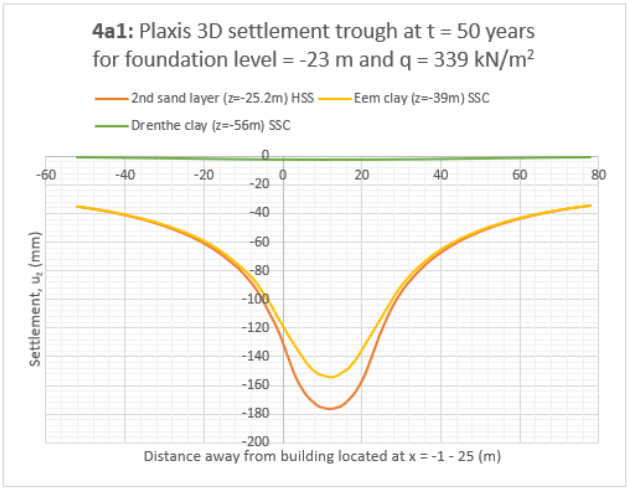

(a) Contribution per soil layers.

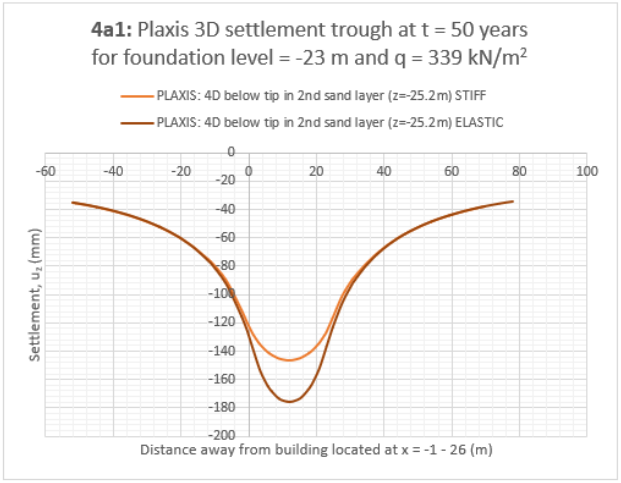

(b) Influence of stiffness.

Figure B.21: Settlement curves (s_2) 4D below pile tip (= -25.2 m) in Plaxis 3D for a) different soil layers, and b) different foundation stiffness for case 4a1: 1 surface load at pile tip level.

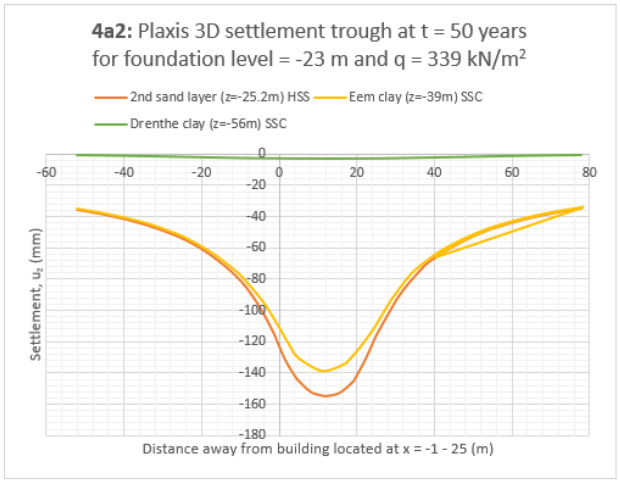

(a) Contribution per soil layers.

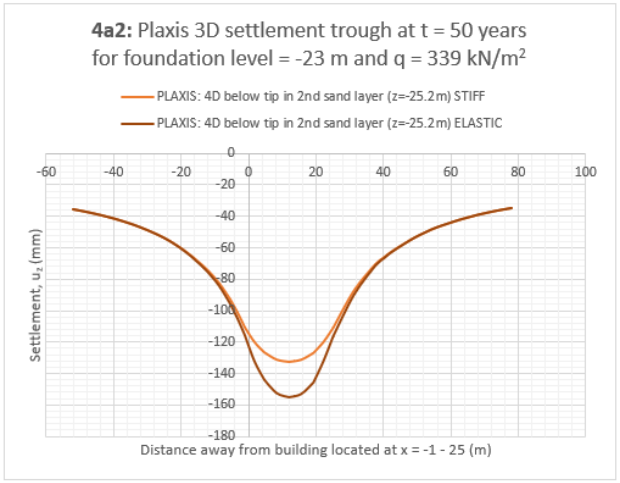

(b) Influence of stiffness.

Figure B.22: Settlement curves (s_2) 4D below pile tip (= -25.2 m) in Plaxis 3D for a) different soil layers, and b) different foundation stiffness for case 4a2: 1 surface load 1/2 increased at 4D below pile tip level.

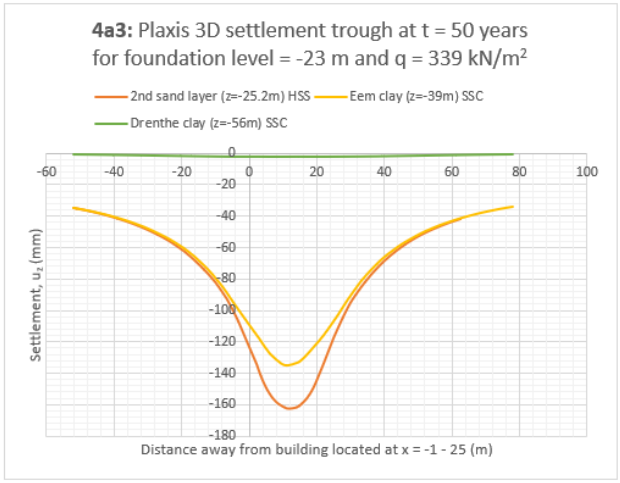

(a) Contribution per soil layers.

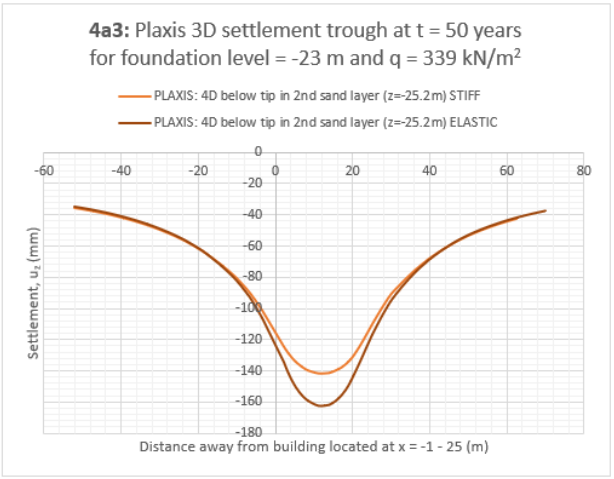

(b) Influence of stiffness.

Figure B.23: Settlement curves (s_2) 4D below pile tip (= -25.2 m) in Plaxis 3D for a) different soil layers, and b) different foundation stiffness for case 4a3: 1 surface load at 2/3 positive skin friction (= D_{tom}).

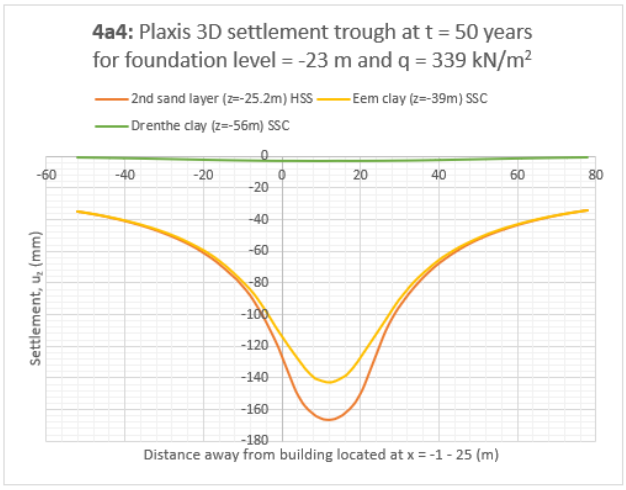

(a) Without load spread.

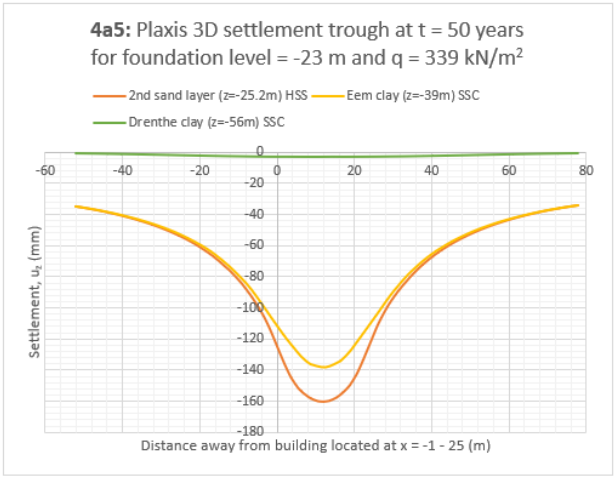

(b) With load spread.

Figure B.24: Settlement curves (s_2) 4D below pile tip (= -25.2 m) in Plaxis 3D at the top of different soil layers (without foundation stiffness) for a) case 4a4 (% shaft of surface load at D_{tom} + % base at pile tip level), and b) case 4a5 (% shaft of surface load 1/4 spread from top positive skin friction to D_{tom} + % base at pile tip level).

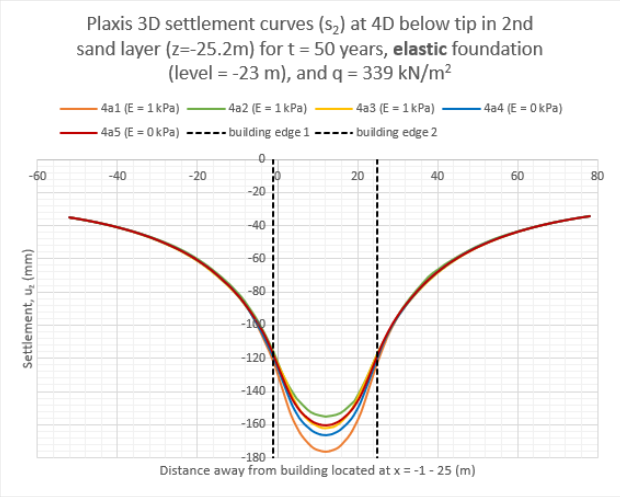

(a) **elastic** foundation plate.

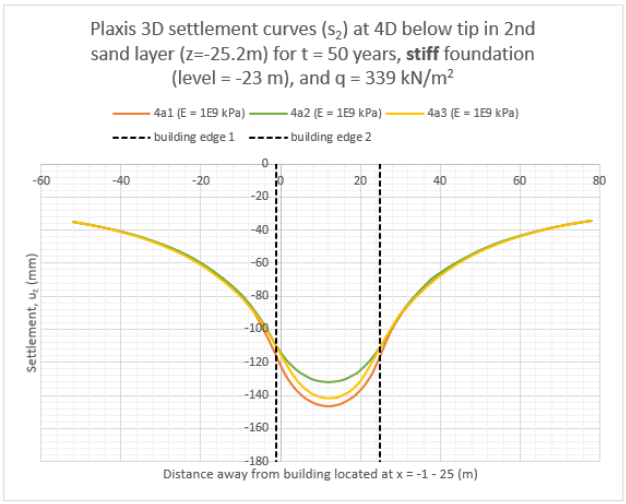

(b) **stiff** foundation plate.

Figure B.25: Settlement curves (s_2) 4D below pile tip (= -25.2 m) in Plaxis 3D using a) an **elastic**, and b) a **stiff** foundation plate for different cases.

Table B.15: Summary and percent difference for maximum settlements after 50 years for different load spread cases using an elastic and stiff foundation material.

Cases	$u_{z,max}$ (elastic) mm	$u_{z,max}$ (stiff) mm	Difference (%)
4a1	176	147	18
4a2	155	132	16
4a3	162	142	13
4a4	167	NA	NA
4a5	160	NA	NA

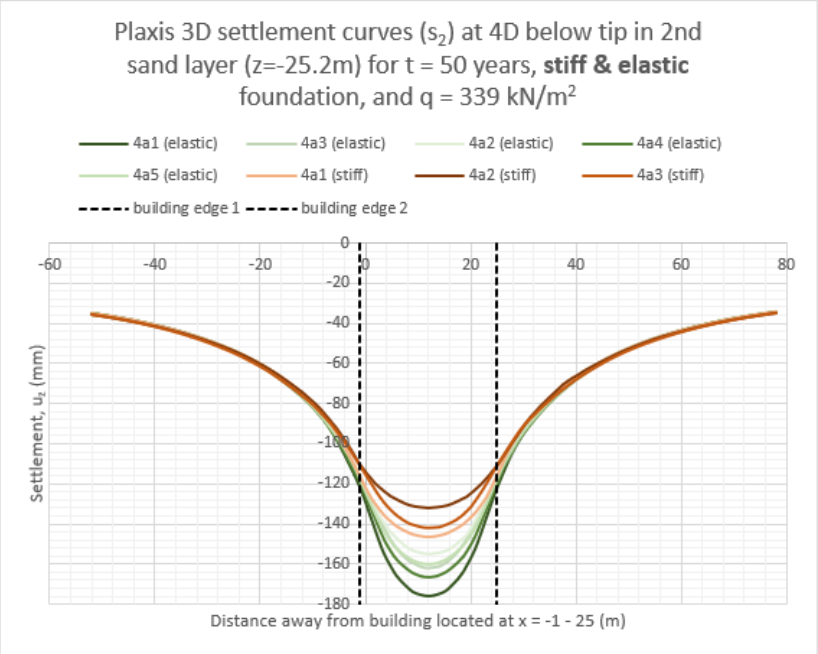

Figure B.26: Combined settlement curves (s_2) 4D below pile tip (= -25.2 m) in Plaxis 3D using an **elastic** and a **stiff** foundation plate for different load spread cases.

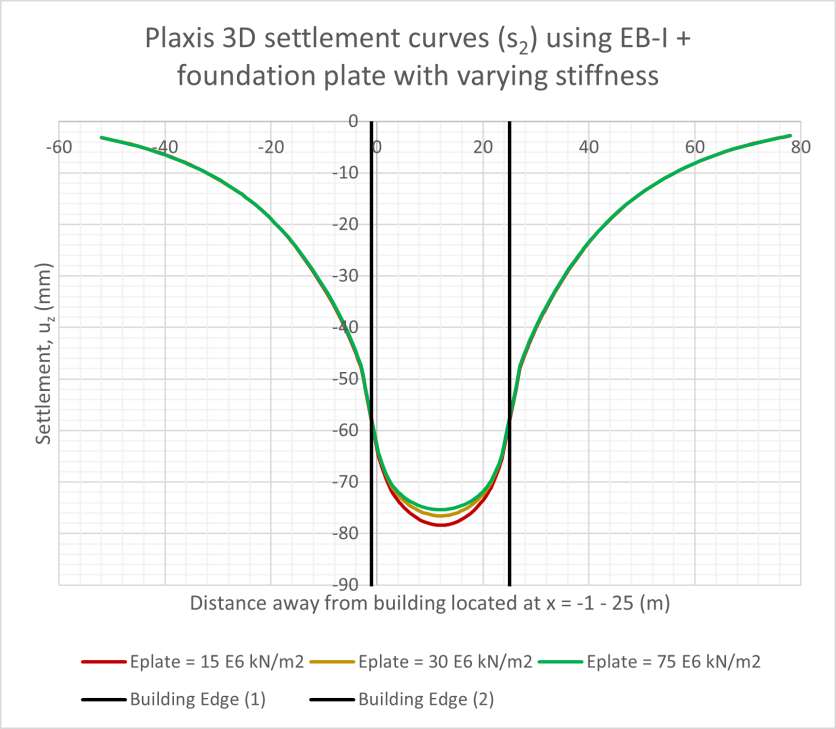

Figure B.27: Settlement curves (s_2) 4D below pile tip (= -25.2 m) in Plaxis 3D using EB-I + foundation plate for three different plate stiffness ($1 \cdot E$, $2 \cdot E$, and $5 \cdot E$). The results of $2 \cdot E$ correspond well with the settlement curve the total building model in Plaxis 3D and SCIA (Section 3.2.6).

Appendix C

Appendix: SCIA Engineer

This Appendix contains inputs and numerical results of simple and complex structural models in SCIA.

C.1 Inputs

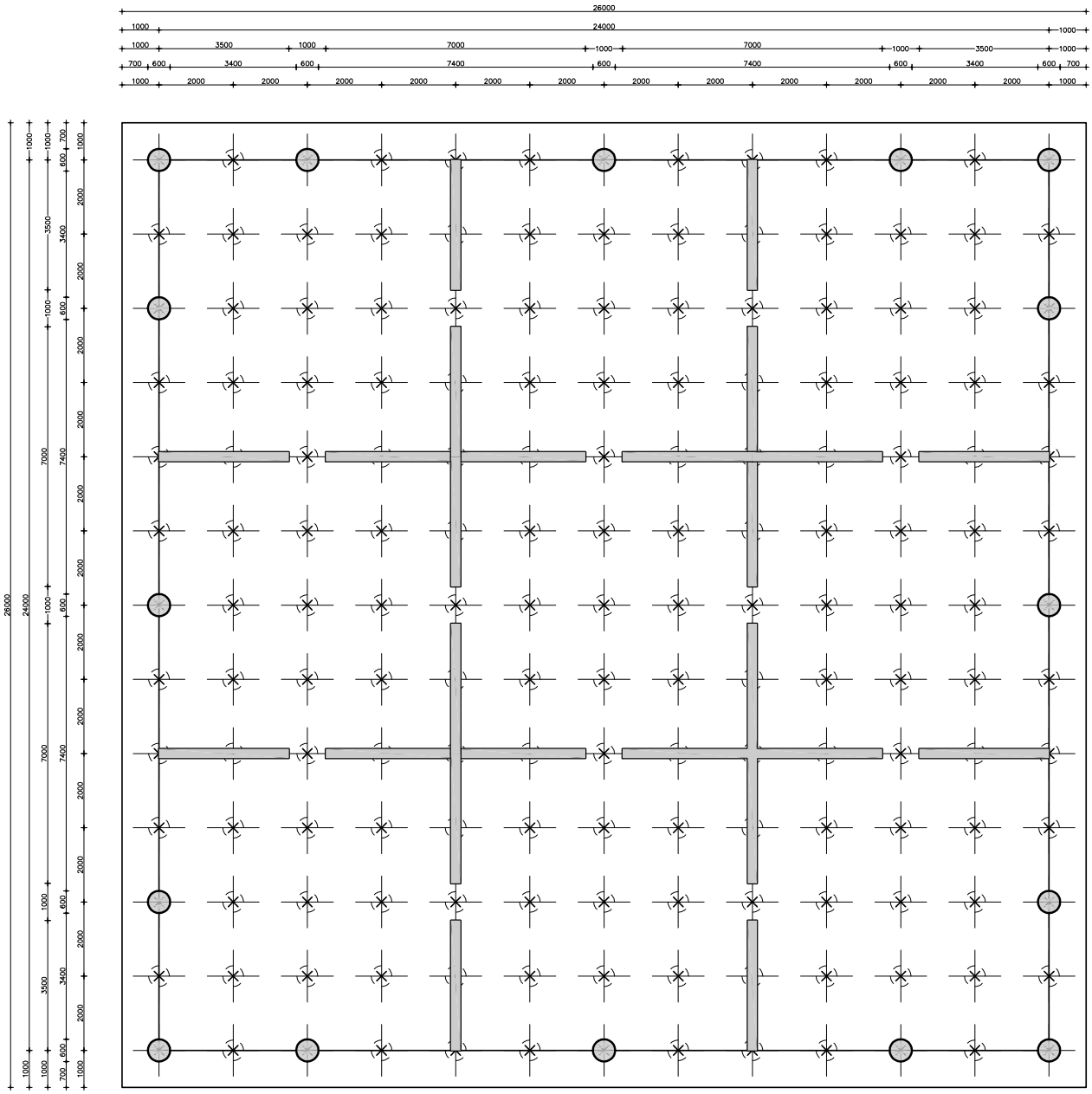

Figure C.1: Plan view of simple tower modelled in SCIA and Plaxis 3D (in Section 3.2).

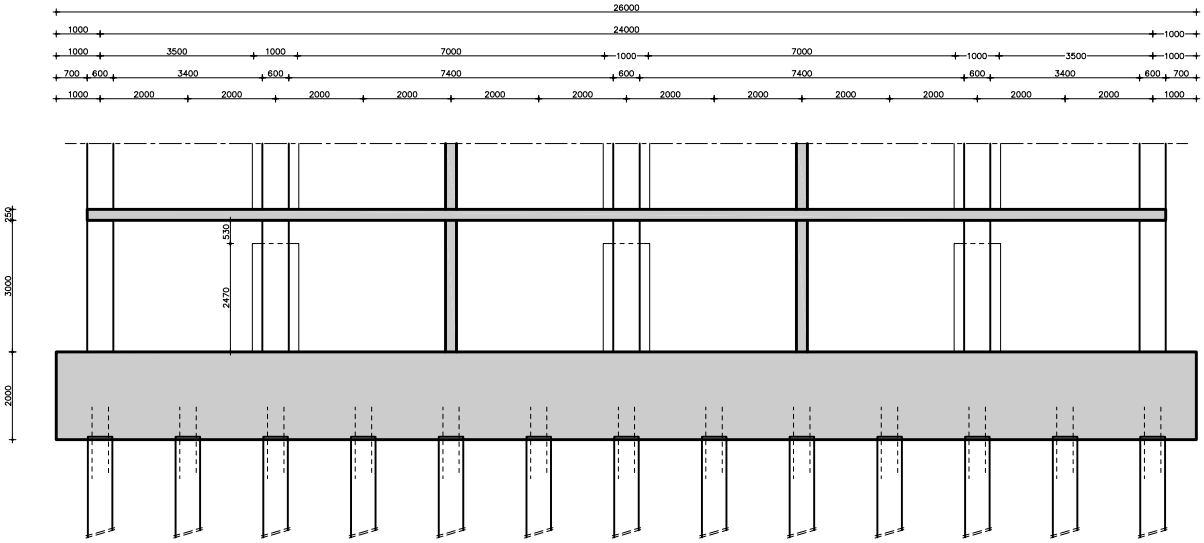

Figure C.2: Vertical view of simple tower modelled in SCIA and Plaxis 3D (in Section 3.2).

Table C.1: Material input of concrete, structural elements in SCIA.

Element	**Weight (kg/m^3)**	**Stiffness (MPa)**	**Poisson Coefficient (-)**
Lintel (1D)	2,500	1.0 E^4	0.2
Column (1D)	2,500	3.0 E^4	0.2
Wall (2D)	2,500	2.0 E^4	0.2
Floor (2D)	2,500	1.0 E^3	0.2
Foundation Plate (2D)	2,500	1.5 E^4	0.2
Foundation Pile (1D)	0	1.0 E^9*	0.2
Soil (Mattress Model, 2D)	0	E_{plate}	0.2

**1.0 E ^{9} considered infinitely stiff. Actual pile stiffness modelled as spring element with linear stiffness ($k_{v,1}$).*

Table C.2: Geometry of concrete, structural elements in SCIA.

Element	**Dimensions (mm)**	AE **(kN)**
Lintel (1D)	530 (h)	NA
Column (1D)	600 (d)	8.5 E^6
Wall (2D)	250 (b)	NA
Floor (2D)	250 (h)	NA
Foundation Plate (2D)	2000 (h)	NA
Foundation Pile (1D)	500 (d)	1.9 E^{11}*

Table C.3: Input data for load cases in SCIA. **Note:** BG401 not used in this thesis.

Name	**Description (NLD)**	**Action (NLD)**	**Direction**	**Value**
BG101: Self weight	*Eigen gewicht*	*Permanent*	-Z	Varies
BG102: Screed & facade	*Afwerking & gevel*	*Permanent*	-Z	1.4 kN/m^2 + 3.0 kN/m
BG201: Live	*Veranderlijk*	*Veranderlijk*	-Z	2.55 kN/m^2
BG301: Wind, X-direction	*Wind*	*Veranderlijk*	+/- X	See $q_{w;verd}$ in Tables C.5 & C.6
BG302: Wind, Y-direction	*Wind*	*Veranderlijk*	+/- Y	See $q_{w;verd}$ in Tables C.5 & C.6
BG401: Prescribed displacements	*Opgelegde vervormingen*	*Permanent*	-Z	Plaxis s_2 contours

Table C.4: NEN (or calculated) load factors for linear SLS and ULS load combinations as input data for SCIA. **Note:** SLS7 is the most important combination for (s_2) settlement analysis.

Name of Combination	**BG101**	**B102**	**BG201**	**BG301**	**BG302**
SLS1 Characteristic	1.00	1.00	$\psi_0 = 0.40$	0.00	0.00
SLS2 Characteristic & Wind +X	1.00	1.00	0.40	1.00	0.00
SLS3 Characteristic & Wind -X	1.00	1.00	0.40	-1.00	0.00
SLS4 Characteristic & Wind +Y	1.00	1.00	0.40	0.00	1.00
SLS5 Characteristic & Wind -Y	1.00	1.00	0.40	0.00	-1.00
SLS6 Frequent	1.00	1.00	$\psi_1 = 0.50$	0.00	0.00
SLS7 Quasi-permanent	1.00	1.00	$\psi_2 = 0.30$	0.00	0.00
ULS1 DL Extreme	1.35	1.35	$0.4 \cdot 1.5 = 0.60$	0.00	0.00
ULS2 LL Extreme	1.20	1.20	1.5 (2 stories) 0.60 (others)	0.00	0.00
ULS3 Max. Wind +X	1.20	1.20	0.60	$1.5 \cdot 1.1 \cdot 1.1 = 1.82$*	0.00
ULS4 Max. Wind -X	1.20	1.20	0.60	-1.82	0.00
ULS5 Max. Wind +Y	1.20	1.20	0.60	0.00	1.82
ULS6 Max. Wind -Y	1.20	1.20	0.60	0.00	-1.82
ULS7 Min. Wind +X	0.90	0.90	0.00	1.82	0.00
ULS8 Min. Wind -X	0.90	0.90	0.00	-1.82	0.00
ULS9 Min. Wind +Y	0.90	0.90	0.00	0.00	1.82
ULS10 Min. Wind -Y	0.90	0.90	0.00	0.00	-1.82

**1.1 for geometrical imperfection and another partial factor of 1.1 for second order effect due to wind.*

Table C.5: Spreadsheet (1) used to calculate wind loads (WL) for simple tower in SCIA.

VAN ROSSUM RAADGEVENDE INGENIEURS

Optredende windbelasting
X en Y -richting

order:
bladnummer:
berekeningnr:
datum: 15-7-2022

h_{geb} =	69,0	m	$v_{b,o}$ =	27,0	m/s	Terrein cat =	II
b_{geb} =	24,0	m	windgebied =	II		c_{dir} =	1,00
d_{geb} =	24,0	m	ρ =	1,25	kg/m^3	c_{season} =	1,00

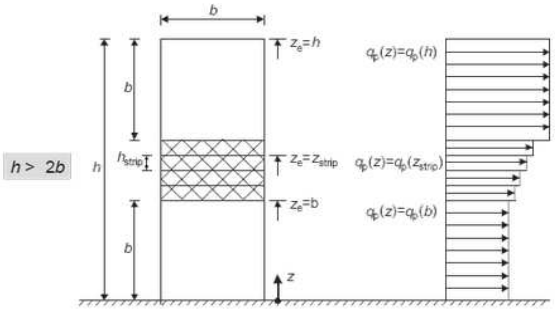

Hoogte = 69 m

Basiswindsnelheid

$v_b = c_{dir} \cdot c_{season} \cdot v_{b,0}$
v_b = 1,00 x 1,00 x 27,0
v_b = 27,0 m/s

Gemiddelde windsnelheid

$v_m(z) = c_r(z) \cdot c_o(z) \cdot v_b$
$v_m(z)$ = 1,22 x 1,00 x 27
$v_m(z)$ = 33,0 m/s

$$c_r(z) = k_r \cdot \ln\left(\frac{z}{z_0}\right)$$
$$c_r(z) = 0{,}21 \text{ x } \ln\left(\frac{69{,}0}{0{,}2}\right)$$
$c_r(z)$ = 1,22

k_r = 0,19 x $(z_0 / 0{,}05)^{0{,}07}$
k_r = 0,19 x $(0{,}2 / 0{,}05)^{007}$
k_r = 0,21

Stuwdruk

$q_p(z) = (1 + 7 \cdot I_v(z)) \cdot ½ \cdot \rho \cdot v_m^2(z)$
$q_p(z) = (1 + 7 \cdot 0{,}17) \cdot ½ \cdot 1{,}25 \cdot 33{,}03^2$
$q_p(z)$ = 1,50 kN/m²

$$I_v(z) = \frac{k_I}{c_o(z) \text{ x } \ln(z/z_0)}$$
$$I_v(z) = \frac{1{,}00}{1{,}0 \text{ x } \ln(69/0{,}2)}$$
$I_v(z)$ = 0,171

Hoogte = 24 m

Basiswindsnelheid

$v_b = c_{dir} \cdot c_{season} \cdot v_{b,0}$
v_b = 1,00 x 1,00 x 27,0
v_b = 27,0 m/s

Gemiddelde windsnelheid

$v_m(z) = c_r(z) \cdot c_o(z) \cdot v_b$
$v_m(z)$ = 1,00 x 1,00 x 27
$v_m(z)$ = 27,1 m/s

$$c_r(z) = k_r \cdot \ln\left(\frac{z}{z_0}\right)$$
$$c_r(z) = 0{,}21 \text{ x } \ln\left(\frac{24{,}0}{0{,}2}\right)$$
$c_r(z)$ = 1,00

k_r = 0,19 x $(z_0 / 0{,}05)^{0{,}07}$
k_r = 0,19 x $(0{,}2 / 0{,}05)^{007}$
k_r = 0,21

Stuwdruk

$q_p(z) = (1 + 7 \cdot I_v(z)) \cdot ½ \cdot \rho \cdot v_m^2(z)$
$q_p(z) = (1 + 7 \cdot 0{,}21) \cdot ½ \cdot 1{,}25 \cdot 27{,}06^2$
$q_p(z)$ = 1,13 kN/m²

$$I_v(z) = \frac{k_I}{c_o(z) \text{ x } \ln(z/z_0)}$$
$$I_v(z) = \frac{1{,}00}{1{,}0 \text{ x } \ln(24/0{,}2)}$$
$I_v(z)$ = 0,209

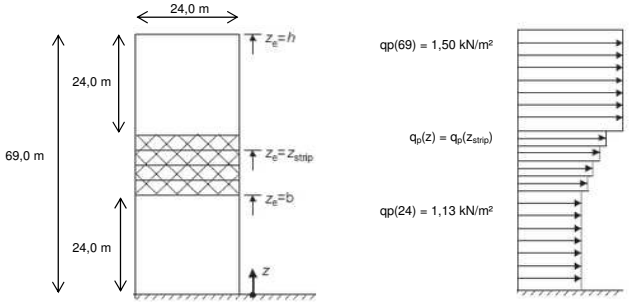

Table C.6: Spreadsheet (2) used to calculate wind loads (WL) for simple tower in SCIA.

VAN ROSSUM RAADGEVENDE INGENIEURS

Optredende windbelasting per verdieping
X en Y -richting

order:
bladnummer:
berekeningnr:
datum: 15-7-2022

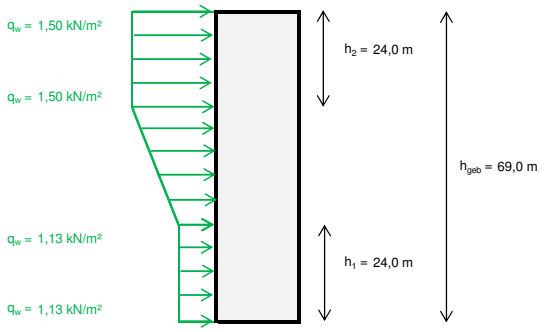

$c_s c_d$ = 1,1

Druk + Zuiging

Verdieping	h_{verd} [mm]	h_{vloer} [mm]	q_w [kN/m²]	q_w x $c_s c_d$ [kN/m²]	$q_{w;verd}$ [kN/m¹]	$q_{w;verd}$ x $c_s c_d$ [kN/m¹]	$q_{w;verd}$ x $c_s c_d$ x c_f [kN/m¹]
bg	3000	0	1,13	1,24	1,69	1,86	2,20
1e	3000	3000	1,13	1,24	3,38	3,72	4,41
2e	3000	6000	1,13	1,24	3,38	3,72	4,41
3e	3000	9000	1,13	1,24	3,38	3,72	4,41
4e	3000	12000	1,13	1,24	3,38	3,72	4,41
5e	3000	15000	1,13	1,24	3,38	3,72	4,41
6e	3000	18000	1,13	1,24	3,38	3,72	4,41
7e	3000	21000	1,13	1,24	3,38	3,72	4,41
8e	3000	24000	1,13	1,24	3,38	3,72	4,41
9e	3000	27000	1,18	1,30	3,46	3,81	4,51
10e	3000	30000	1,23	1,36	3,62	3,98	4,72
11e	3000	33000	1,29	1,42	3,78	4,16	4,93
12e	3000	36000	1,34	1,47	3,94	4,33	5,13
13e	3000	39000	1,39	1,53	4,10	4,51	5,34
14e	3000	42000	1,45	1,59	4,26	4,68	5,55
15e	3000	45000	1,50	1,65	4,42	4,86	5,76
16e	3000	48000	1,50	1,65	4,50	4,95	5,86
17e	3000	51000	1,50	1,65	4,50	4,95	5,86
18e	3000	54000	1,50	1,65	4,50	4,95	5,86
19e	3000	57000	1,50	1,65	4,50	4,95	5,86
20e	3000	60000	1,50	1,65	4,50	4,95	5,86
21e	3000	63000	1,50	1,65	4,50	4,95	5,86
22e	3000	66000	1,50	1,65	4,50	4,95	5,86
23e		69000	1,50	1,65	2,25	2,47	2,93
24e		69000	1,50	1,65	0,00	0,00	0,00
25e		69000	1,50	1,65	0,00	0,00	0,00
26e		69000	1,50	1,65	0,00	0,00	0,00
27e		69000	1,50	1,65	0,00	0,00	0,00
28e		69000	1,50	1,65	0,00	0,00	0,00
29e		69000	1,50	1,65	0,00	0,00	0,00
30e		69000	1,50	1,65	0,00	0,00	0,00
31e		69000	1,50	1,65	0,00	0,00	0,00
32e		69000	1,50	1,65	0,00	0,00	0,00
33e		69000	1,50	1,65	0,00	0,00	0,00
34e		69000	1,50	1,65	0,00	0,00	0,00
35e		69000	1,50	1,65	0,00	0,00	0,00
36e		69000	1,50	1,65	0,00	0,00	0,00
37e		69000	1,50	1,65	0,00	0,00	0,00
38e		69000	1,50	1,65	0,00	0,00	0,00
39e		69000	1,50	1,65	0,00	0,00	0,00
40e		69000	1,50	1,65	0,00	0,00	0,00
dak		69000	1,50	1,65	0,00	0,00	0,00

C.2 Outputs

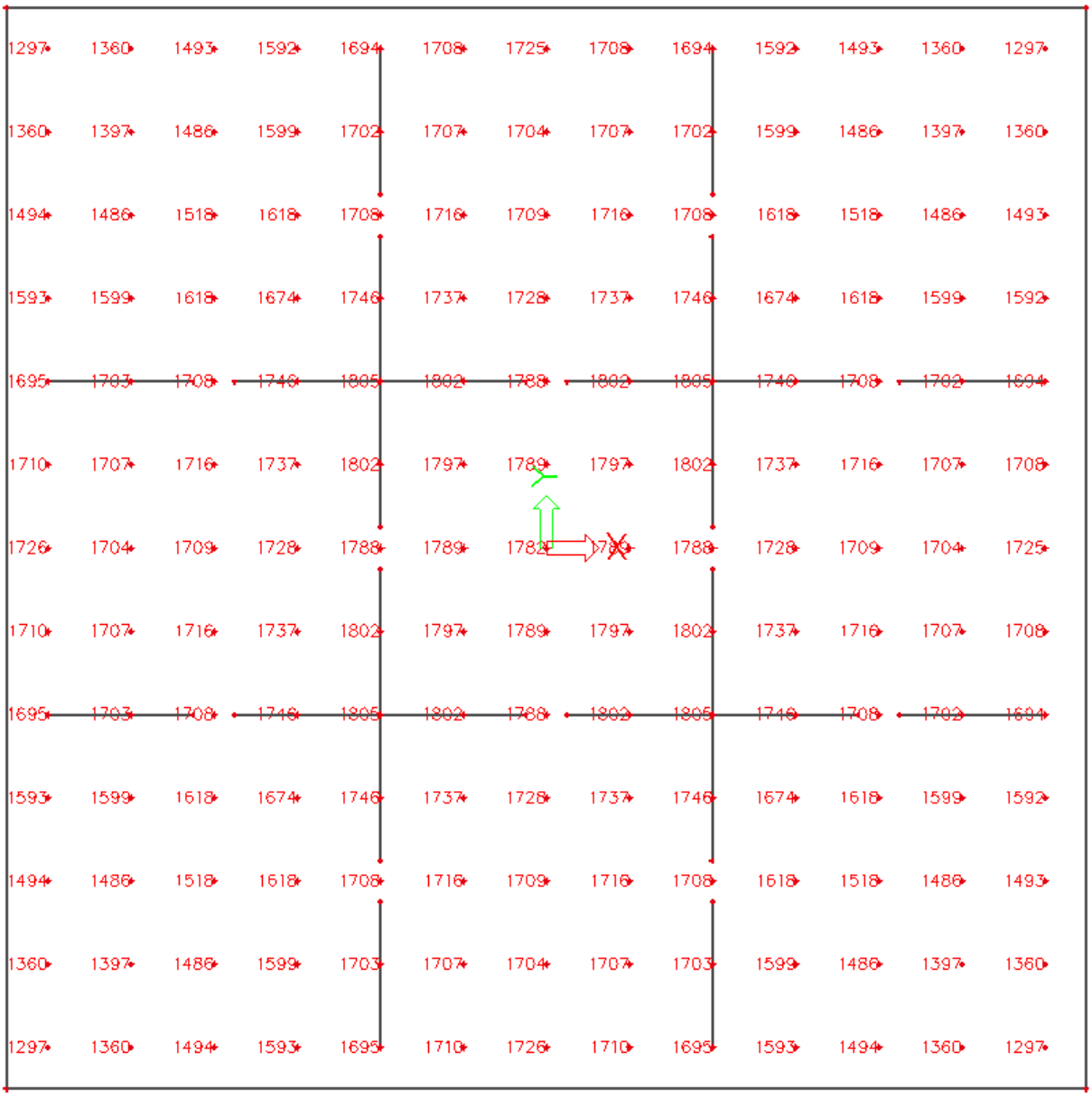

Figure C.3: **ULS** pile reactions in kN **without** redistribution of forces in superstructure due to s_2 settlements as mattress model in SCIA.

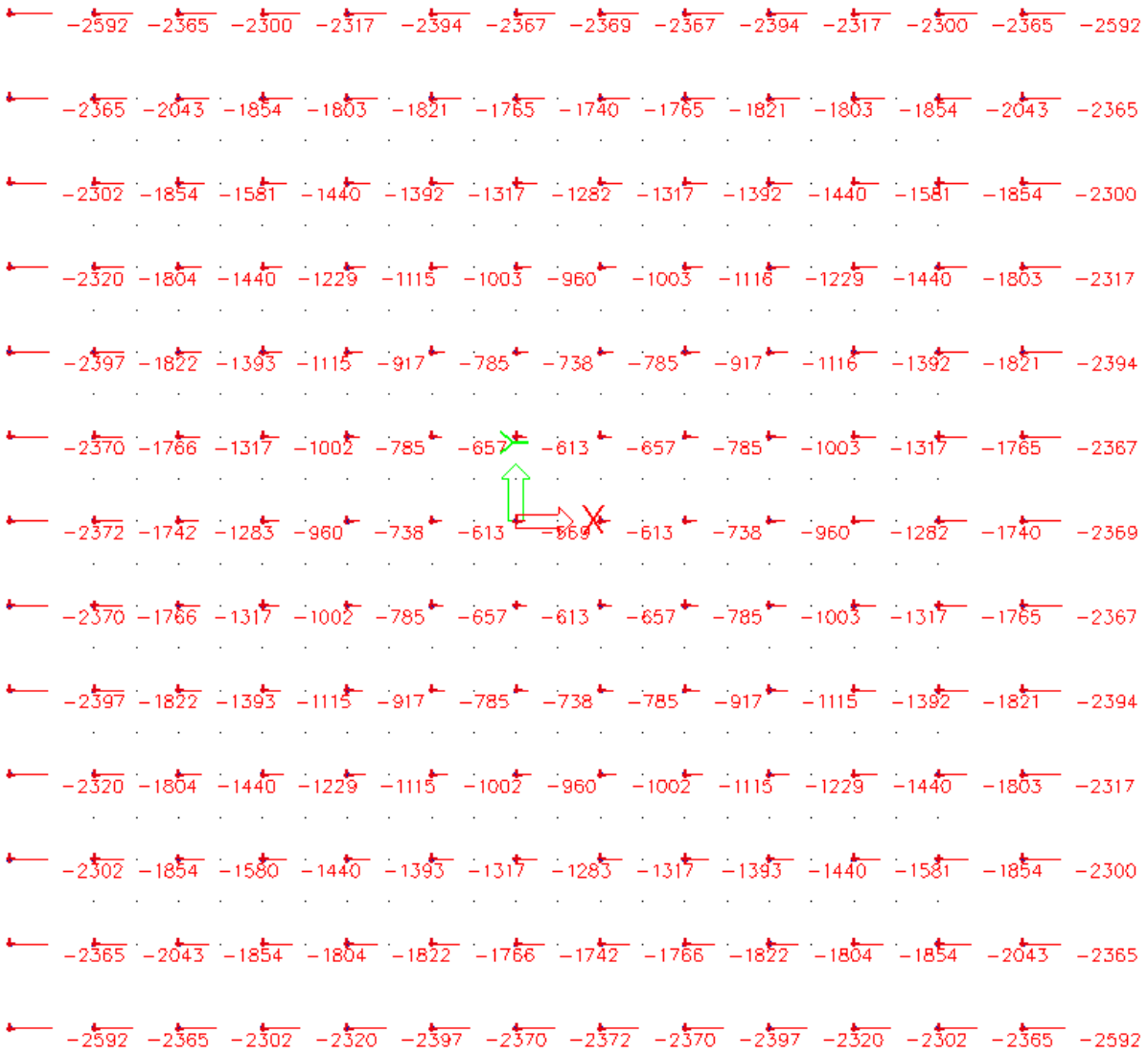

Figure C.4: **ULS** pile reactions in kN **with** redistribution of forces in superstructure due to s_2 settlements as mattress model in SCIA.

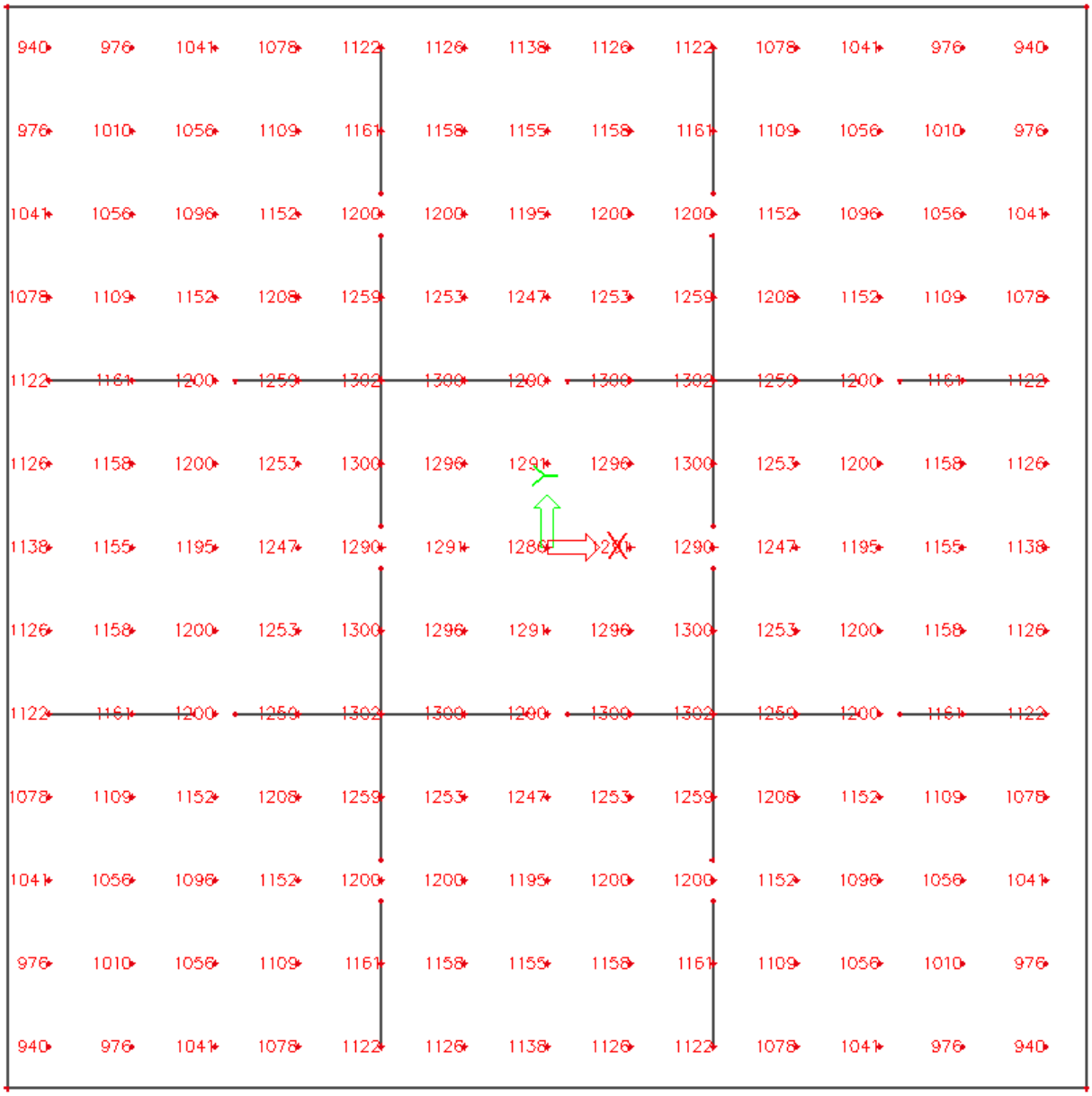

Figure C.5: **SLS** pile reactions in kN **without** redistribution of forces in superstructure due to s_2 settlements as mattress model in SCIA.

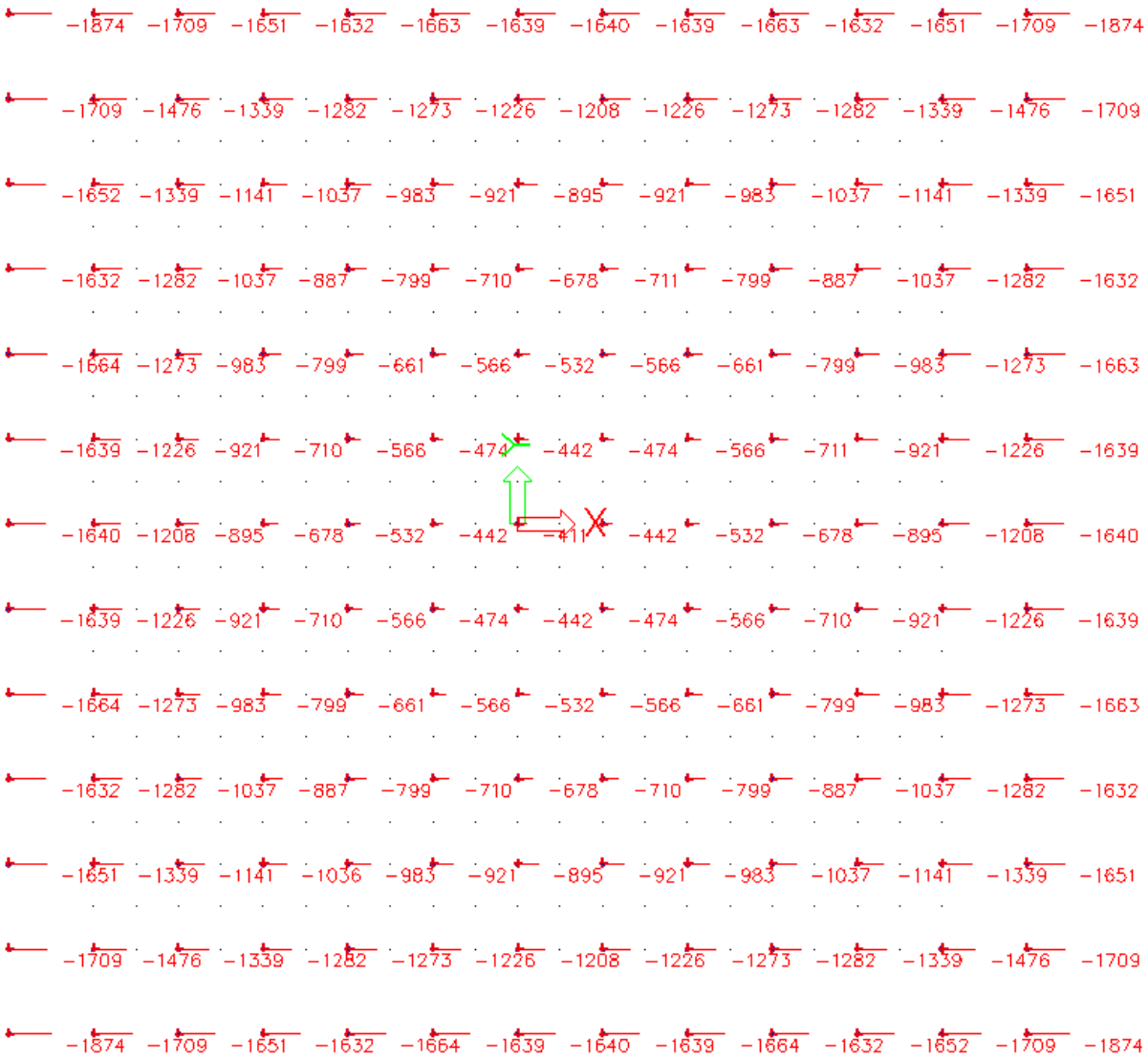

Figure C.6: **SLS** pile reactions in kN **with** redistribution of forces in superstructure due to s_2 settlements as mattress model in SCIA.

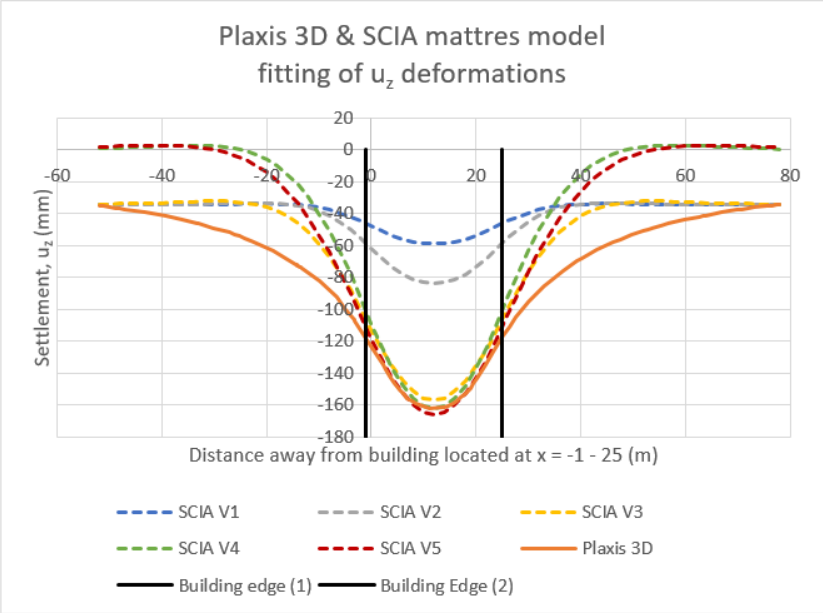

Figure C.7: Example of fitting procedure of (s_2) settlement curves from Plaxis 3D to SCIA.

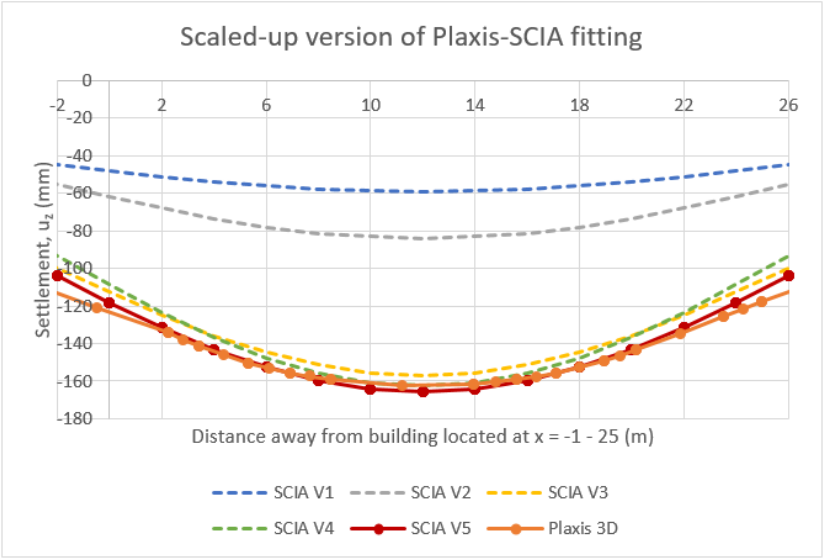

Figure C.8: Zoomed in version of fitting procedure of (s_2) settlement curves from Plaxis 3D to SCIA.

Appendix D

Appendix: (InSAR) Settlement Data and Design Flowcharts

This Appendix contains measured InSAR and predicted settlement data to be used for verification of the state-of-the-art design methodology in future research.

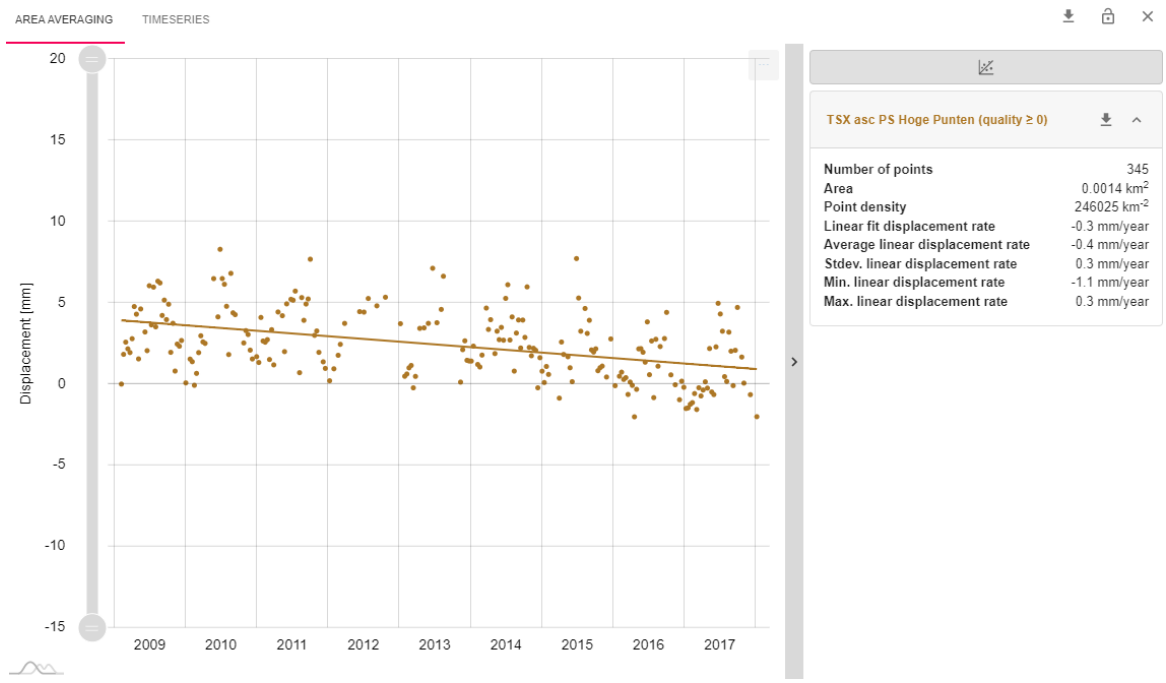

Figure D.1: Vertical displacement data and rate for the Breitnertoren in Amsterdam provided by InSAR data (SkyGeo, 2022).

Figure D.2: Amstel Map for the Breitnertoren in Amsterdam provided by InSAR data (SkyGeo, 2022).

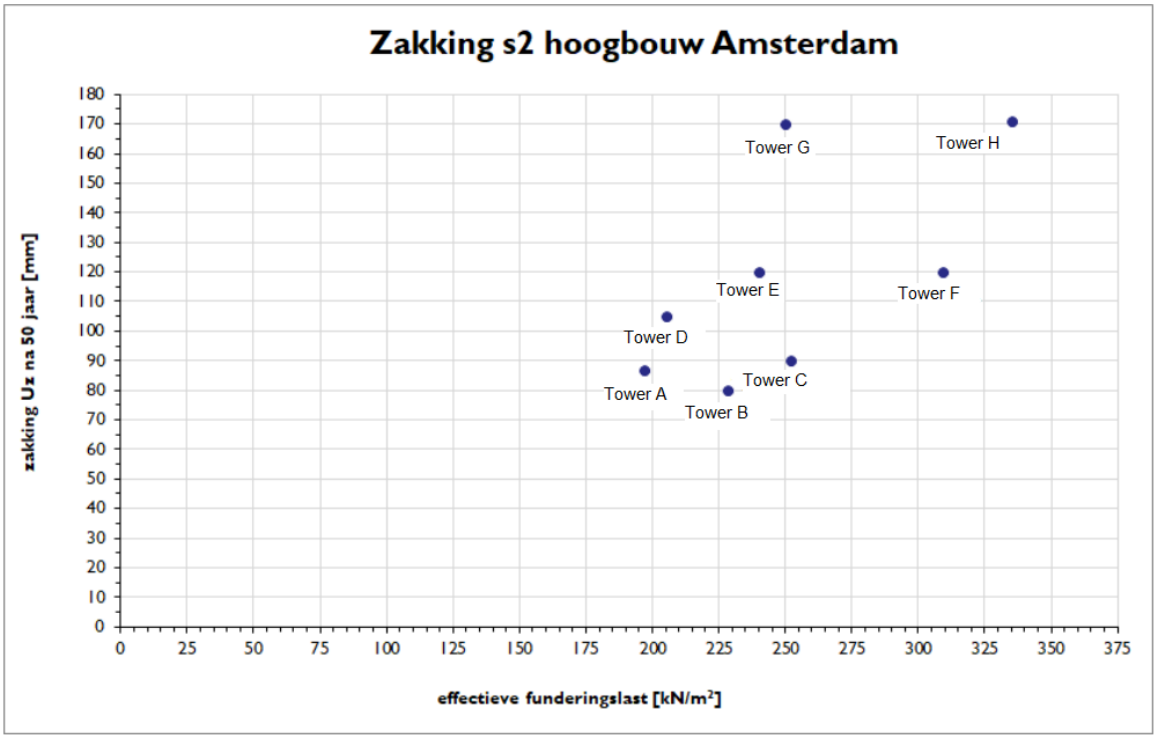

Figure D.3: Predicted s_2 settlements (by CRUX in Plaxis 3D) for towers ($\leq$ 70 m) in Amsterdam.

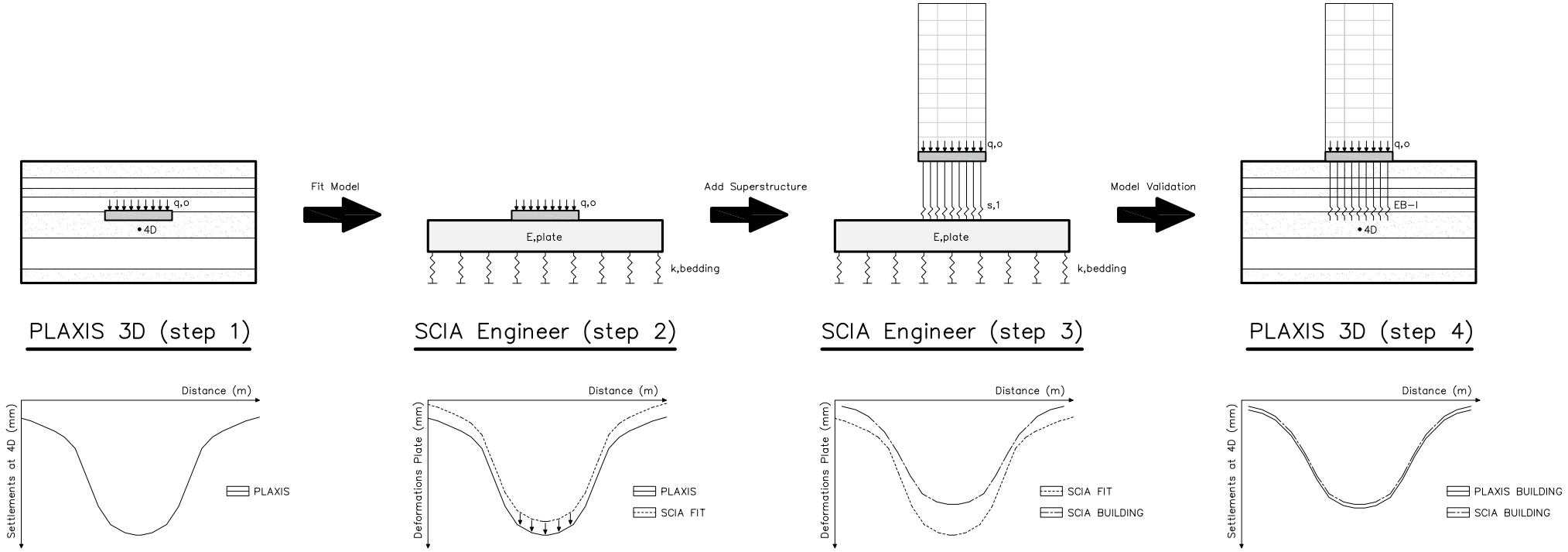

Figure D.4: Proposed design flow for verification of soil-structure interaction modelling in Plaxis 3D and SCIA Engineer.
(Enlarged version of Figure 1 in Abstract)

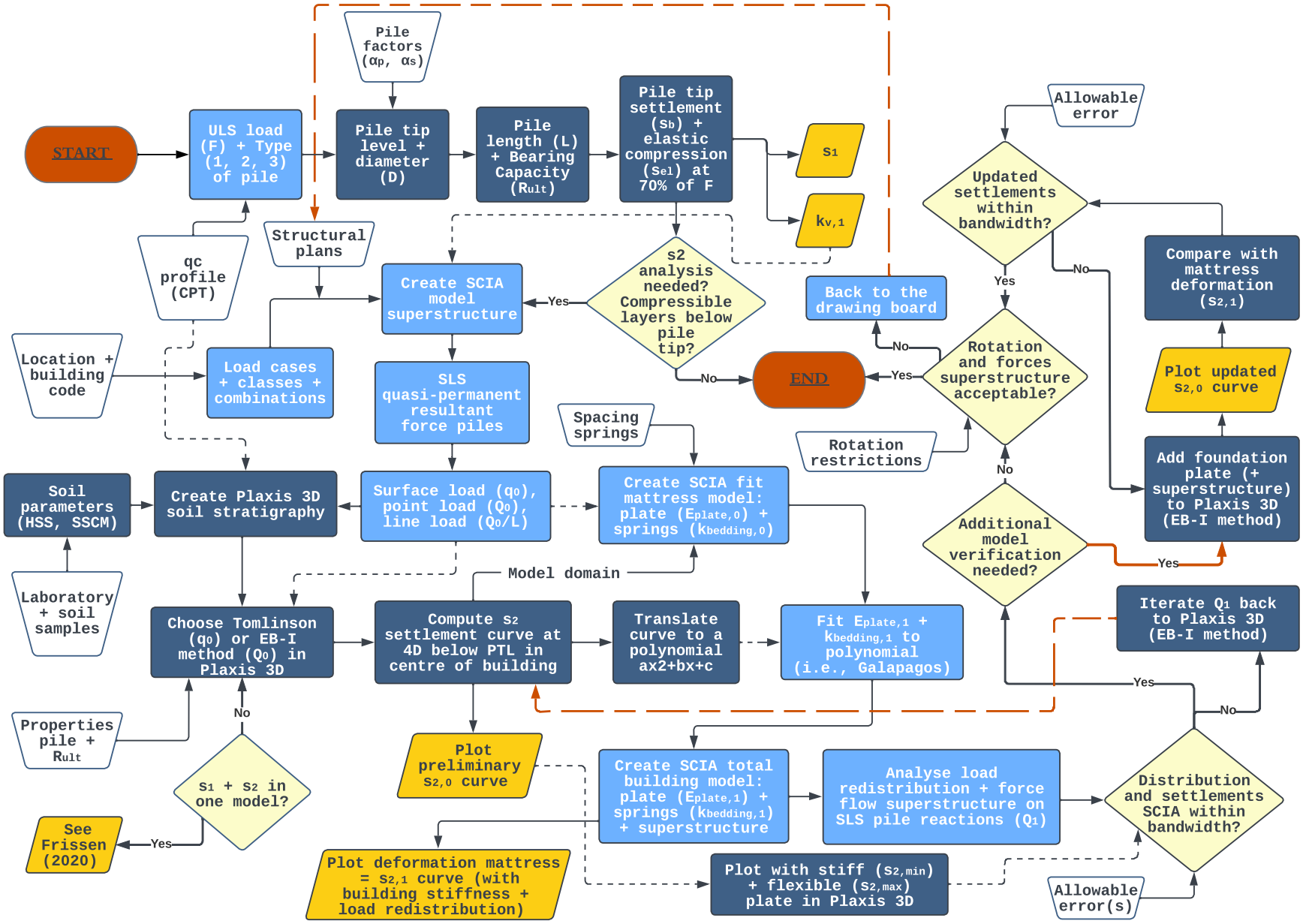

Figure D.5: Road map (as sketch for the finalised flow chart in Figure 4.1) for automation of soil-structure interaction modelling between Plaxis 3D and SCIA. **Note:** the red paths should be avoided.